
THE UNIVERSITY *of* EDINBURGH

# An Investigation into Taxane Resistant Breast Cancer

**Juliet Kenicer**

**A thesis submitted for the degree of Doctor of Philosophy**

**In the College of Medicine and Veterinary Medicine**

**The University of Edinburgh**

**October 2011**

# Declaration

The work presented in this thesis was carried out at the Edinburgh Cancer Research Centre. The Experimental work and interpretation of results were undertaken by the author. Contributions to this work in this thesis by colleagues are fully acknowledged in the text.

This work has not been, nor is currently being submitted for candidature for any other degree.

Juliet Kenicer
Edinburgh Cancer Research Centre
October 2011

# Acknowledgements

I would like to thank my supervisors Professor John Bartlett and Dr. Charlie Gourley for all their guidance and support and I am grateful to the Medical Research Council for funding my research.

Thank you to all my friends in the Endocrine Cancer Research Group, particularly Karen, Carrie, Alison, Vicky and Mel for all their help and advice – you have been fantastic.

I am also grateful to Professor Jorge Reis-Filho and Mr. Maryou Lambros MSc. at Breakthrough Breast Cancer Research in London for their collaboration and allowing me loose in their lab to conduct my aCGH experiments.

Thank you to Dr. Andy Sims for helping me analyse my gene expression data, to Elisabeth Freyer at the MRC for conducting some of my FACS analysis and to Morwenna Muir and Dr. Val Brunton for all their help in my mouse xenograft work.

To Dr. Vera Cerqueira thank you for your friendship and understanding.

Mum and Dad, you have instilled in me a curiosity and a desire to work hard that have proven to be invaluable for getting though my PhD, thank you for all your love, kindness and support.

Finally, I would like to thank George for being simply magnificent.

# Abstract

One group of chemotherapeutics that are used successfully to treat breast cancer, alone or in combination with other agents, are the taxanes; paclitaxel and docetaxel. They act by interfering with the spindle microtubule dynamics of the cell causing cell cycle arrest. However, the complexities underlying the mechanism of action are yet to be fully elucidated. Arguably, one of the most significant problems with taxanes is chemoresistance. Unfortunately, some patients are intrinsically resistant to taxanes and others acquire resistance to taxanes as treatment advances. This problem is exacerbated by a lack of understanding of the mechanisms underlying taxane resistance.

Isogenic breast cancer cell lines that were taxane resistant were generated to use as an experimental model. Paclitaxel resistant (PACR) MDA-MB-231, paclitaxel resistant ZR75-1 and docetaxel resistant (DOCR) ZR75-1 cell lines were successfully generated by incrementally increasing taxane dose in respective native cell lines *in vitro*. An extensive characterisation of each of the resistant cell lines was conducted, focussing primarily on the 25nM resistant cells which were determined to be the most clinically relevant dose of taxane. A suboptimal dose of 5nM, a "superoptimal" dose of 50nM and the native, taxane sensitive cells was included.

Dose response cell count experiments were performed that confirmed taxane resistant cells had been generated. It was shown that MDA-MB-231 native cells were more sensitive to paclitaxel than the ZR75-1 native cells, suggesting that ZR75-1 cells may already have low level inherent resistance. The MDA-MB-231 25nM PACR cells were tested to determine whether they retained PACR when maintained in media containing no paclitaxel. MDA-MB-231 25nM PACR cells were maintained in a taxane free environment for six months and then rechallenged with taxane. When rechallenged, the PACR cells previously maintained in the absence of paclitaxel mirrored the pattern of growth of corresponding PACR cells that had been maintained in the presence of paclitaxel. This proved that in the absence of paclitaxel, PACR cells did not revert to parent phenotype. This meant that experiments could be designed to grow cell lines as xenografts in mice, (in the absence of paclitaxel) & bring in vitro experiments into an *in vivo* setting. Effects of taxane treatment on both native and resistant cells were analysed using flow cytometry. Paclitaxel treatment exerted G2/M block in native MDA-MB-231 cells but when PACR cells were treated with the same dose of paclitaxel no G2/M block was observed, suggesting that PACR cells had developed a mechanism for escaping G2/M block. ZR75-1 native lines were also investigated and we established that treatment with paclitaxel also exerted a G2/M block in these lines. In future studies this process will be repeated to investigate the effect of taxane treatment on the ZR75-1 PACR and DOCR lines.

CD 1 nude mice were injected with cells from all five cell lines to grow xenografts, unfortunately MDA-MB-231 PACR cells failed to grow so they could not be used for further xenograft experiments. PACR, DOCR and Native ZR75-1 cells did successfully grow as xenografts in mice and confirmed that all 3 groups showed very similar growth patterns. A cross resistance experiment was conducted and it was determined that the DOCR xenografts maintained a taxane resistant phenotype to docetaxel, and not paclitaxel and the PACR xenografts may be perpetuate the paclitaxel resistant phenotype in xenografts and that there may be cross resistance to docetaxel in the paclitaxel resistant xenografts. This is the first time that taxane resistant cell lines grown in this way have been established as xenografts in mice. These cross resistance experiments represent novel findings and merit further investigation.

Extensive genomic and transcriptomic analyses were carried out on the cell lines to help identify potential taxane resistance markers. aCGH experiments were carried out to compliment the illumina experiments. The first set of experiments used DNA from pooled whole female blood as ref sample and DNA from each of the native and taxane resistant cell lines as test samples. The second set of experiments used DNA from native cells as a ref sample and DNA from their respective taxane resistant cells as a test, which allowed areas of loss or gain to be tracked in the genome as resistance increased. In the MDA-MB-231 cell lines the following areas of loss extended with increasing resistance: 1p36.13-q44, 6p25.3-q12, 8p, 10p, 19q, X Chr and the following areas of gain 2p25.3-23.3, 3p24.3-q13.3, 4p16.1-q12, 5q14.3-q31.1, 8q21.13-24.3, 11q15.1-q25, centromeric 12, and centromeric 14. In the ZR75-1 PACR and DOCR cell lines the areas of loss extended with increasing resistance in the following regions: 7q, 12p and 16q.

For gene expression analysis RNA was extracted from the MDA-MB-231 cell lines, labelled and hybridised them to illumina human ref 8 vs. 2 chips. Data showed a progressive increase in mRNA dysregulation as paclitaxel resistance increased. Eleven genes were dysregulated across all resistance levels in the PACR MDA-MB-231 cells when compared to the relative cell lines; RGS16, CLDN1, IL7R, P&PP1R14C, COBL, TRPV4, TSPAN8, CD33, NLRP2, P13, and PAGE5. The experiment was repeated using MDA-MB-231 PACR, ZR75-1 PACR and DOCR cells and resulting data was analysed to determine genes commonly dysregulated across resistance levels, between MDA-MB-231 PACR and ZR75-1 PACR and between ZR75-1 PACR and DOCR cell lines. An extensive literature search was conducted and established four genes of interest in the context of our genomic and transcriptomic experiments including AURKA, Mdr-1, Stathmin and YY1.

The novel biomarkers identified in the illumina experiments were validated with complimentary qPCR gene expression experiments looking at expression levels of the eleven commonly dysregulated genes identified and a panel of 19 other genes with significantly increased or decreased expression as resistance increased including AURKA, Mdr-1, Stathmin

and YY1. Western blots were performed with lysates from the cell lines using a standard panel of predictive breast cancer markers and AURKA, Mdr-1, Stathmin and YY1. Combining the data from the genomic study, the gene expression profile, qPCR and Western blotting it was established that Mdr-1 had increased expression in the taxane resistant ZR75-1 lines and YY1 had increased expression in the MDA-MB-231 PACR line.

Material from the LAPATAX trial was used to observe any transcriptomic changes occurring in tumours following treatment with docetaxel and to compare them to changes identified in our *in vitro* and xenograft models, this allowed the final step to be taken into a translational environment. LAPATAX (EORTC 10054) is a phase I-II study of Lapatanib and Docetaxel as neoadjuvant treatment for HER-2 +ve locally advanced/inflammatory or large operable breast cancer. Tumour material from eighteen core biopsies pre and post treatment was obtained, the mRNA was extracted, labelled and hybridised to the illumina array. This allowed the changes in gene expression pre and post docetaxel treatment to be tracked. The gene expression data from the LAPATAX trial was combined with gene expression data from our cell line panel and identified two novel putative markers of taxane resistance DUSP1 and FOS. Although sample size is small this has provided extremely valuable evidence directly from the clinic. These two novel putative biomarkers are extremely intriguing and certainly merit further investigation, ideally using additional taxane treated breast tumour tissue.

Ultimately, an isogenic *in vitro* model of taxane resistance was developed in two different cell lines and with two different taxanes within one cell line. The cell lines were characterised and the effect of the taxanes on the cell cycle was determined in the native and taxane resistant lines. Selected cell lines were grown as xenografts in mice and performed successful cross resistance studies upon them. A large transcriptomic and genomic analysis was conducted and has identified a panel of potential taxane resistance markers and areas of loss and gain in the genome perpetuated by increasing taxane resistance. This analysis was validated using qPCR and Western blotting. This allowed a panel of novel taxane resistance markers to be identified. In future studies it is hoped that these targets will be knocked down with shRNA to observe if the taxane resistant cell lines revert to the parental phenotype. I*n vitro* studies will be conducted to find agents that may be used to reduce expression of these markers and restore sensitivity to taxanes and consequently restore the efficacy of these drugs in a clinical setting. As far as the author is aware this is the first time that isogenic taxane resistant cell lines have been generated and investigated in this way.

# Abbreviations

aCGH – Array Comparative Genomic Hybridisation
ACS grade – American Chemical Society
ADP – Adenosine diphosphate
AI – Aromatase Inhibitor
AIPC – Androgen independent Prostate Cancer
AMPS – Ammonium Persulphate
ANOVA – Analysis of Variance
AP-1 – Activator Protein 1
ATF – Activating transcription factor
ATM – ataxia telangeictasia mutated
AURKA – Aurora Kinase A
AWS - adaptive weights smoothing

BAC – Bacterial Artificial Chromosome
BCIRG – Breast Cancer International Research Group
Bp – Base Pair
BRF – Biomedical Research Facility
°C – Degrees Centigrade

CASP8 – Caspase 8
CBS – Circular Binary Segmentation
CIN – Chromosomal Instability
CK – Creatine Kinase
COBL – Cordon Bleu protein
CRBC – Chicken Red Blood Cells
CST – Cell signalling Technology
CV – Coeffecient of Variation
Cy3 – Cyanine 3
Cy5 – Cyanine 5
CYP450 – Cytochrome p450

DAVID – Database for Annotation Visualisation and Integrated Discovery
DCIS – Ductal Carcinoma *In Situ*
DF – Degrees of Freedom
DFS – Disease Free Survival

DMSO – Dimethyl sulfoxide
DMEM – Dulbecco's Modified Eagle Medium
DOCR – Docetaxel Resistant Cells
DCIS – Ductal Carcinoa *In Situ*
DLT – Dose Limiting Toxicity
DSB – Double Strand Break

E1 - Estrone
E2 - Estradiol
E3 - Estriol
EGR – Early Growth Response Protein 1
EGFR - Epithelial derived growth factor receptor
EMT - Epithelial mesenchymal transition
ER - Oestrogen receptor
ERE – Oestrogen Response Elements
ERK - extracellular signal-regulated kinase-1
ETOH – Ethanol

FACS – Fluorescence Activated Cell Sorting
FCS – Foetal Calf Serum
FGFR2 – Fibroblast growth factor receptor
F – F Test
F Crit – F critical
FDR – False Discover Rate

GAGE – G Antigen Family E
GCSF - Granulocyte colony stimulating factor
GM-CSF - Granulocyte Macrophage Colony Stimulating Factor

HCB – Humidity Control Buffer
HCl – Hydrochloric Acid
HDAC – Histone Deacetylase
HERA – Herceptin adjuvant
Hr – hour
HYB – Hybridisation Buffer

IBC – Inflammatory Breast Cancer
IDC – Invasive Ductal Carcinoma

IGF-1 – Insulin Like Growth Factor 1
ILC – Invasive Lobular Carcinoma
ILR7 – Interleukin 7 Receptor
IVT – *In Vitro* Transcription

K - Thousand
Kb – Kilobase
KEGG – Kyoto Encyclopaedia of Genes and Genomes

LCIS – Lobular Carcinoma in Situ
L-Glut – L-Glutamine
LH – Lutenising Hormone
LSP1 – Lymphocyte specific protein

MAF – Musculoaponeurotic fibrosarcoma
MAPs – Microtubule Associated Proteins
MAPK – Mitogen Activated Protein Kinase
MAP3K1 - Mitogen-activated protein kinase kinase kinase 1
MBC – Metastatic Breast Cancer
Mdr-1 – Multidrug Resistance 1
MDS – Multidimensional scaling
MEK - Mitogen activated protein kinase kinase 1
Mg – Milligram(s)
Min – Minute
MKP-1 – Mitogen-Activated Protein Kinase (MAPK) Phospahatase
Ml – Millilitre(s)
MMP – Matrix Metaloproteases
MRD – Minimum Residual Dose
MS – Mean of Squares
MTD – Maximum Tolerated Dose
MTOC – Microtubule Organising Centre

NaOAc – Sodium Acetate
NaCl – Sodium Chloride
NCCTG N9831 – North Central Cancer Treatment Group
NEB – New England Biosciences
NSAIDs – Non-steroidal anti-inflammatory drug
NSPABP B31 – National Adjuvant Breast and Bowel Project

NSCLC – Non Small Cell Lung Carcinoma
OCT – Optimal Cutting Temperature
O/N – Overnight
ORR – Overall response rate
OS – Overall Survival

PACR – Paclitaxel Resistant
PAGE – P antigen family E
PALB2 - Partner and localizer of BRCA2
PARP – Poly (ADP Ribose) Polymerase
PBS – Phosphate Buffered Saline
pCR – Pathologic Complete Response
PCR – Polymerase Chain Reaction
PDGFRs - Platelet-Derived Growth Factor Receptors
Pen/Strep – Penicillin Streptomycin
PFS – Progression Free Survival
PI3K – Phosphoinositide 3-Kinase
PMSF - Phenylmethanesulfonylfluoride
PTEN – Phosphatase and Tensin Homologue
P – Val – P Value

QBA - quaternary benzo[c]phenanthridine alkaloids
qPCR – quantitative real time PCR
PVDF - Polyvinylidine fluoride

RCF – Relative Centrifugal Force
RGS16 - Retinally abundant regulator of G protein signalling
RNA – Ribonucleic acid
RPM – Revolutions per Minute
RT – Room Temperature
RT-PCR – Reverse Transcription Polymerase Chain Reaction

SAC – Spindle Assembly checkpoint
SAM – Significance analysis of Microarrays
SDS – Sodium Dodecyl Sulphate
Ser – Serine
SERD – Selective oestrogen Receptor Downregulator
SERM - Selective oestrogen Receptor Modulator

SPIA - Single Primer Isothermal Amplification
SS – Sum of Squares
SSC – Saline Sodium Citrate Buffer

TEMED – Tetramethylethylenediamine
TGF-β – transforming growth factor β1
Thr - Threonine
TKI – Tyrosine Kinase Inhibitors
TOPO II – Topoisomerase II
TRBC – Trout Red Blood Cells
TRPV4 – transient receptor cation channel Vanilloid, member 4.

UF – Ultra Filtered
UHRR – Universal Human RNA Reference
UNG – Uracil DNA Glycosylase
UTR – Untranslated Region

V – Volts
VEGF – Vascular Endothelial Growth Factor

Wt – Wild type
WTCRF – Welcome Trust Clinical Research Facility

YY1 – Ying Yang 1

# List of Figures

# List of Tables

# Table of Contents

M Spears, J Kenicer, A F Munro, JMS Bartlett. Type I RTKs as predictive or prognostic markers in early breast cancer. Biomarkers in Medicine (2008.) 2: 397-407.

# Chapter 1

## Introduction

## 1.1. Breast Cancer: Incidence and mortality.

### 1.1a Breast Cancer Incidence and Mortality.

It is a sobering fact that today women in Britain have a 1 in 9[309] risk of developing breast cancer over a life time. Breast Cancer is currently the most common Cancer in the UK (excluding non melanoma skin cancer) and although recently incidence has steadily increased, in the last two decades mortality rates have fallen (http://cancerhelp.cancerresearchuk.org/.)

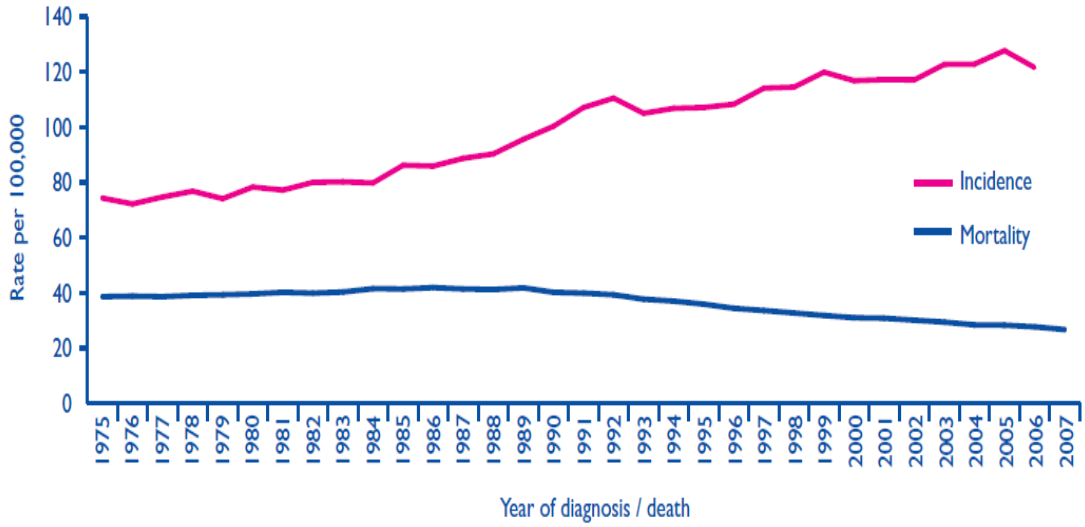


**Figure 1.1** European age-standardised incidence and mortality rates for female breast Cancer, Great Britain 1975-2007.org/.)

This encouraging fall in mortality rate has occurred as a result of a number of important factors which will be discussed in the following sections. There are significant differences in survival rates across Europe and the world. One of the key factors in the variation from country to country is late stage at diagnosis [1]. Low awareness of cancer has been shown to contribute to delay in presentation for cancer symptoms[2]. Late stage at diagnosis has also been shown to vary from rich and poor and black and white patients[3,4].

## 1.2. Breast cancer pathology: diagnosis.

Breast cancer is a complex collection of diseases, with a variety of symptoms. Early diagnosis is the key to successful treatment. Although controversy exists about the relative benefit to patients of breast screening compared with screening programmes of other types of Cancer, they are currently implemented in the UK using mammography to tumours in all women between the ages of 50 and 70 years old and those with symptoms of breast Cancer[5,6]. A number of factors have to be taken into consideration before beginning treatment for breast cancer. These factors can be assigned to three broad groups: key tumour features, key molecular

features and key patient features. Important tumour features include size, grade, type and nodal status. Molecular features such ER, PgR and HER2 status all play an important role in determining the correct treatment for breast cancer patients. Finally the individual characteristics of the patient like age, menopausal status and family history are all important factors to consider when deciding how to treat the patient.

### 1.2.a Key tumour features: Tumour type.

Which type of breast cancer the patient is diagnosed with is extremely important. Table 1.1 shows the percentage of different breast cancers diagnosed in the UK (data adapted from CRUK website: http://www.cancerhelp.org.uk/type/breast-cancer/about/types.) Invasive ductal and invasive lobular are the two most commonly diagnosed breast cancers, accounting for around nine out of ten diagnoses. Invasive Lobular Carcinomas have significantly better prognosis than ductal[7]. Ductal Carcinomas are sometime referred to as NST or NOS; **N**o **S**pecial **T**ype or **N**ot **O**therwise **S**pecified. Lobular invasive and rarer types of breast cancer are often categorised as ST; **S**pecial **T**ypes.

| Type of Breast Cancer | % or Proportion of Total Breast Cancers Diagnosed |
|---|---|
| Invasive Ductal | 70-80% |
| Invasive Lobular | 10% |
| Inflammatory | 1-2% |
| Paget's disease | 1-2% |
| Rare/special Types | 5-10% |
| Male Breast Cancer | 300 diagnosed each year |

**Table 1.1** Types of Breast Cancer diagnosed.

### 1.2ai Preinvasive forms of breast cancer

Some breast tumours are harmless like fibroadenomas and intraductal papillomas. More serious preinvasive cancers include DCIS (Ductal Carcinoma In Situ) and LCIS (Lobular Carcinoma In Situ) which are non invasive so have not spread to surrounding tissues. As their names suggest, DCIS is found in the ducts of the breasts whereas LCIS is confined solely to the breast lobules. DCIS can present in different subtypes e.g. comedo, papillary, micropapillary, solid and cribiform which reflect the morphological appearance of cells in the duct. Patients with DCIS can be treated with breast conserving surgery followed up by radiotherapy and sometimes Tamoxifen.

DCIS of the breast and LCIS are thought to be direct precursors of several subgroups of invasive breast cancer, in addition, it has been shown that most DCIS and LCIS cases share a common clonal origin with the associated invasive breast cancer[8,9]. DCIS has also been shown to evolve along more than one path[10]. However, some DCIS have been shown to be associated with

invasive lobular carcinomas and a small proportion of LCIS may give rise to invasive carcinomas of the ductal subtype[11]. This reiterates the finding that less severe forms of breast cancer may evolve along one of multiple pathways to become a more complex severe and invasive form of disease.

### 1.2aii Invasive Breast Cancers

One important hallmark of invasive breast cancer is its diversity and it is this aspect that can make it often more difficult to comprehend and ultimately treat. Patients with other aggressive forms of disease like inflammatory breast cancer must be treated with a more aggressive regime of therapies and will be given neoadjuvant chemotherapy, followed by surgery and perhaps radiotherapy followed by hormone therapy[12]. Patients with invasive breast cancer will have a much worse prognosis than those with DCIS or LCIS[13]. Invasive or infiltrating, breast cancer is diagnosed when DCIS or LCIS spread to, or invade, healthy surrounding tissue. Invasive breast cancer has the potential to metastasise to other parts of the body via the bloodstream or lymphatic system[14]. Breast cancer can spread by one of three methods; direct infiltration, via lymphatic system or through, haematogenous spread and sites of breast cancer metastasis are bone, lung, liver, pleura and the CNS[14]. The bones are the most common site of breast cancer first distant metastasis. Breast cancer metastases can relapse many years later; this is especially common in low grade hormone sensitive tumours[15].

There are many different types of invasive breast cancer. The most common type of invasive breast cancer is invasive ductal carcinoma (IDC) (re. Table 1.1.) Subtypes of invasive ductal carcinoma include inflammatory breast Cancer (IBC) which is an advanced aggressive form of the disease. IBC can be hard to diagnose as it is not characterised by the presence of a breast lump and it accounts for roughly 1-2% of breast tumours diagnosed (re table 1.1). Symptoms include breast pain and changes in the skin such as dimpling and an “orange peel” appearance which can often be mistaken for other conditions such as eczema and mastitis[12]. The majority of cases are detected using mammogram or ultrasound[12].

Medullary carcinoma of the breast is named for its resemblance to the medulla tissue in the brain; and accounts for around 5% of new breast cancer diagnoses. This generally has a good prognosis[16].

Inflammatory breast cancer is usually a very aggressive form of breast cancer and represents 1-2% of new cases (re. table 1.1.) It presents differently from most other forms. Common symptoms include swelling/enlargement of one breast, with features of inflammation; the breast may be warm to the touch, itchy and tender. Sometimes the skin in dimpled with an orange peel appearance[17].

Metaplastic carcinoma is a very rare type of invasive ductal cancer. These tumours include cells that are normally not found in the breast, such as cells that look squamous cells or osteoblasts. Metaplastic carcinoma has a poorer prognosis and is treated aggressively like invasive ductal cancer[18]. Paget's disease of the nipple, although not cancerous itself, can signal the presence of breast cancer beneath the skin. It starts in the breast ducts and spreads to the nipple and then the areola. Paget's disease is rare occurring in only 1-2% of breast cancers diagnosed (re. table 1.1.) The disease is almost always associated with DCIS and often with IDC[19]. It is often treated by mastectomy but if after the mastectomy there is only DCIS and no IDC found then there is a very good prognosis[19]. Tubular carcinomas are so called because of their tubular appearance under the microscope and represent about 2% of newly diagnosed cases. They are treated like IDC, have a good prognosis and rarely metastasise[20].

ILC generally originates in the lobes of the breast and goes on to infiltrate fatty tissue and other breast tissue[13], hence becoming invasive. Around 10% of breast cancers diagnosed are ILCs (re. table 1.1.)

Papillary carcinoma is rarely invasive and often considered to be a type of DCIS. Papillary cancer cell are often arranged in small, finger-like projections in layers when viewed under the microscope[21]. In rare cases when papillary carcinoma is invasive, it is treated like invasive ductal carcinoma, although generally the outlook better. Papillary carcinomas are more frequently diagnosed in older women, and they make up no more than 1% or 2% of all breast cancers[21].

Less common types of invasive breast cancer account around 5-10% (table 1.1) of the total of all breast cancers diagnosed. Cells of Adenoid cystic carcinoma resemble glandular or cystic cells under the microscope. This type of cancer often has a good prognosis and is not usually aggressive. As the name suggests mucinous carcinoma (sometimes referred to as colloid carcinoma) secrete mucous. They often have a good prognosis after treatment[22].

### 1.2aiii Sarcomas

Sarcomas are relatively rare in the breast and form in the connective tissue such as muscle, fat and blood vessels. The majority of breast cancers are carcinomas which form in the epithelial cells. Sarcomas of the breast are very rare. Angiosarcomas are highly proliferative and metastasise quickly. They occur rarely in the breast and originate from cells that line blood vessels or lymph vessels under the arm. Angiosarcoma usually occurs as a complication of previous radiation treatment, occurring 5 to 10 years after treatment[23-30]. Angiosarcoma has also been known to develop in the arm of women who have lymphedema as a result of radiation therapy of lymph node surgery to treat breast cancer (www.cancer.org/Cancer/BreastCancer/DetailedGuide.) Phyllodes are cytosarcomas and are

often large leaf-shaped, fast growing tumours that occur in periductal stromal cells of the breast. These tumours can often be benign, and can be treated by removing the tumor along with a margin of normal breast tissue[31-36]. Surgery for a malignant phyllodes tumour will remove a larger margin of normal tissue, these tumours generally do not benefit from chemotherapy or radiotherapy (www.cancer.org/Cancer/BreastCancer/DetailedGuide.)

Tumours can be composed of different types of cancer cells such as IDC and lobular: these are referred to as "mixed tumours." This reiterates the point that cancer is a complex of heterogeneic diseases.

## 1.2b Diagnosis

### 1.2.b.i Tumour Grade.

Grade and stage of tumours are also fundamental factors to consider when considering what treatment a patient will receive. Tumour grade reflects how tumour cells are growing and what they look like under magnification. Low grade tumours are slow growing whereas high grade ones grow rapidly.

Histological grade is reported using the "Bloom Richardson Scale[37]" or "Nottingham Score[38]. It is a combination of nuclear grade, mitotic rate, and tubule formation which are characteristics of the tumour cells seen under a microscope that predict its aggressiveness. In general, high grade tumours are more likely to recur when compared to low grade tumours.

**Nuclear Grade**: a score is given from 1 to 3 based on the appearance of the nuclear of the cancer cells. 1 is the most similar to normal cells (better) and 3 the least similar (worse.)
**Mitotic Rate**: describes how quickly the cancer cells are multiplying or dividing, again using a 1 to 3 scale with 1 being the slowest and 3 the quickest.
**Tubule Formation**: represents the percentage of cancer cells that are forming tubules. If 75% or more of cancer cells are forming tubules then a score of 1 is attributed, which is a good prognosis. A score of 2 is attributed if tubule formation is between 10 and 75%, which suggests a moderate prognosis and a score of 3 is attributed if tubule formation is less than 10%, suggesting a poor prognosis.

The three scores are combined to get a total score between 3 and 9 which translates to histological grade.

**Low grade**, (grade 1), well differentiated: Score of 3, 4 or 5.
**Intermediate grade**, (grade 2), moderately differentiated: score of 6 or 7.
**High grade**, (grade 3), poorly differentiated: score of 8 and 9.

### 1.2.b.ii. Tumour Stage.

After breast cancer is diagnosed it is important for clinicians to accurately stage the cancer so that they can decide accurately which treatment the patient should receive. One way of staging breast Cancer is by using the TNM method. The TNM method takes into account three aspects; **T**umour size, whether the lymph **N**odes have been affected and whether the cancer has **M**etastasised to another part of the body. Each of these three groups is divided into further subgroups, allowing a detailed analysis of the tumour.

**T Stage**

**Tx**: Tumour cannot be assessed.

**T0**: No evidence of tumour is seen.

**Tis**: Carcinoma *in situ*.

**T1**: Tumour is 2cm or less.

**T2**: Tumour is greater than 2 cm but less than 5 cm.

**T3**: Tumour is greater than 5cm.

**T4**: Tumour of any size but extends to the chest wall or skin, or is inflammatory breast cancer.

**N Stage** – The N stages below are based on a pathologist staging of lymph nodes following surgery. Lymph node status which may also be assessed by the physician prior to surgery termed clinical lymph node staging.

**Nx:** Node status cannot be assessed.

**N0:** No tumour is seen.

**N1:** regional lymph node metastasis present; (at some sites: tumor spread to closest or small number of regional lymph nodes.)

**N2:** tumor spread to an extent between N1 and N3 (N2 is not used at all sites.)

**N3:** tumor spread to more distant or numerous regional lymph nodes (N3 is not used at all sites.)

**M Stages**

**Mx:** Spread of the cancer has not been evaluated.

**M0**: Cancer does not appear to have spread to other organs such as lung liver and bone.

**M1:** The cancer has spread to other organs such as lung liver and bone (distant metastases.)

These ratings are combined with stage for the cancer.

**Stage 0:** Carcinoma in situ (Tis, NO, MO)

**Stage I:** T1, N0, M0.

**Stage IIA:** T0-1, N1 M0 or T2, N0, M0.

**Stage IIB:** T2, N1, M0 or T3, N0, M0.

**Stage IIIA:** T0-2, N2, M0 or T3, N1-2, M0**.**

**Stage IIIB:** T4, N0-2, M0.

**Stage IIIC: A**ny T, N3, M0.

**Stage IV:** any T, any N, M1.

The **N**ottingham **P**rognostic **I**ndex (NPI) is used for prognostication of early breast cancer, widely in the UK. The NPI takes into account three factors. How large the cancer is, if the cancer has spread to the lymph nodes, and the grade of the Cancer. The lymph node stage can be designated into three categories. Stage 1 is where no nodes are affected, stage 2 is where 1 or 2 nodes are affected and stage 3 is where 3 or more nodes are affected[39].

NPI Calculated as follows:

NPI = (0.2 x tumour diameter in cms) + lymph node stage + tumour grade.

Patients with an NPI of between zero and 2.4 have a low risk of relapse. Patients with a NPI of below 4 tend to have a moderate prognosis and a moderate risk of relapse. Patients with an NPI of over 5.4 have a poor prognosis and higher risk of relapse.

### 1.2.b.iii Molecular markers of breast cancer.

Molecular biomarkers are valuable tools for breast cancer prognosis and predicting response to therapy and a number of molecular markers can be used in the diagnosis of breast cancer.

ER is a steroidal hormone receptor and DNA binding transcription factor located on 6q25.1. Between 70 and 80% of all breast tumours are ER positive. Low grade tumours are more frequently ER positive and high grade tumours are more frequently ER negative. ER positive tumours have a better prognosis than ER negative tumours. One study looked at nearly 27,000 patients across all ages, they found that the proportion of ER+ve tumours increased over age 51 to 82%[40]. They conducted a large multivariate analysis and found that patients who were ER+ve had a significantly positive prognosis across all age group and this was limited to the first five years after diagnosis, $p<0.0001$[40]. After the first five years, prognosis was found to be slightly better for ER negative patients $p=0.049$. In addition the steroidal hormone progesterone

receptor can be used as a surrogate marker of oestrogen receptor activity to help predict clinical outcome[41,42].

Her2 is a 185kD proto-oncogene located on 17q21-22 and is a transmembrane surface bound RTK which plays a role in signal transduction pathways. Her2 plays a role in cell growth and differentiation and roughly 15-20% of breast cancer are amplified Her2 for it (EntrezGene), these cancers have a worse prognosis and increased risk of recurrence[43]. In one study patients whose tumours carried more than five copies of the erbB2/neu gene were far more prone to experience a relapse in the first 18 months after treatment than patients who lacked this amplification[44].

Ki67 is a protein thought play an important role in cell division and is located on 10q25-ter[45]. Ki67 is gradually being used a prognostic and predictive factor in breast cancer and may help predict benefit from specific treatment in particular subtypes of breast cancer[45]. However, it is still absent from the American Society of Clinical Oncology guidelines for required routine biological markers[46].

Breast tumour cells that lack oestrogen receptors and progesterone receptors, and do not have an excess of the HER2 protein on their surfaces are called triple negative breast cancers; these tend to be invasive ductal carcinomas (re.www.cancer.org). Triple negative breast cancers tend to proliferate and metastasise more quickly than other cancers and tend to be found more often in younger women[47,48]. Women with these cancers have a poor prognosis, because triple negative cancers lack receptors to target using endocrine and biological therapies. They tend to be managed using chemotherapy[49, 50].

### 1.3. Breast Cancer Risk Factors.

It is always pertinent to consider that, as with all cancers, breast cancer is not to be regarded as one disease but a complex of often diverse and heterogeneous diseases that have evolved and are evolving within an individual. It is also important to distinguish the terms hereditary and genetic in terms of cancer. Essentially all cancer is "genetic" as it occurs as a result of the changes in not one but many genes in the cell. Only a small proportion of breast cancers, roughly 3% are caused by inheriting a mutation in a known gene.

#### 1.3a. Age.

The causality of breast cancer is complex issue. The incidence of breast cancer increases with age, doubling every 10 years until the onset of menopause when the rate of increase begins to slow[51]. Roughly 25% of breast cancers occur in women under the age of 50, 50% occurs in women between the ages of 50 and 69 and 25% occurs in women aged 70 and over

(cancerhelp.org.uk.) The estimated risk of developing cancer by age in female in the UK from 2001-2005 is shown in table 1.2.

| Estimated risk at birth up to and including | UK (2001- 2005) |
|---|---|
| **Age 24** | 1 in 15,300 |
| **Age 29** | 1 in 2,300 |
| **Age 39** | 1 in 200 |
| **Age 49** | 1 in 52 |
| **Age 59** | 1 in 22 |
| **Age 69** | 1 in 14 |
| **Age 79** | 1 in 10 |
| **Age 84** | 1 in 10 |
| **Lifetime risk** | 1 in 9 |

**Table 1.2.** Estimated risk of developing breast cancer in the UK 2001-2005 (adapted from infocancerresearchuk.org.)

**1.3b. Family History and hereditary forms of breast cancer.**

A strong family history of breast cancer also increases the risk of developing the disease. The National Institute for Health and Clinical Excellence categorises women into one of three categories in terms of their risk of developing breast cancer, low, moderate and high, based upon their family history (www.nice.org.uk/nicemedia/live/10993/30233/30233.pdf).

Women who have one or more of the following family histories will have an increase chance of developing breast cancer; a mother or sister diagnosed with breast cancer before the age of 40, 2 close relatives from the same side of the family diagnosed with breast cancer - at least one must be a mother, sister or daughter, 3 close relatives diagnosed with breast cancer at any age, A father or brother diagnosed with breast cancer at any age, A mother or sister with breast cancer in both breasts - the first cancer diagnosed before the age of 50, 1 close relative with ovarian cancer and 1 with breast cancer, diagnosed at any age - at least one must be a mother, sister or daughter (http://www.cancerhelp.org.uk.) These familial breast cancers are almost certainly caused by the presence of a heritable genetic mutation[51].

Both the BRCAs are identified tumour suppressor genes. Women with BRCA1 or 2 mutations have an 85% risk of developing breast cancer in their lifetime, and an increased incidence of ovarian cancer[52]. Both the BRCAs are tumour suppressor genes. BRCA1 is located on chromosome 17q21 at BP 38,530,994. It is a large gene on which over 250 disease mutations occur. BRCA1 mutations account for around 40% of identified hereditary mutations. BRCA1 protein is involved in repairing DNA DSBs, transcription and transcriptional regulation,

ubiquitination and interacts with HDACs. It combines with other tumor suppressors, DNA damage sensors, and signal transducers to form a large multi-subunit protein complex known as the BRCA1-associated genome surveillance complex (BASC[53].) Different mutations in BRCA1 are common to different ethnic groups for example; 185delAG, 188del11, 5382insC are found in the Ashkenazi Jewish population[54,55]. BRCA2 is located on chromosome 13q12.3 at bp 31,787,616 it is also involved in the repair of DSBs and homologous recombination. Mutations in BRCA2 have also been shown to increase risk of other cancers including ovarian, pancreatic cancers and malignant melanoma. People with a biallelic mutation in BRCA2 suffer from a type of Fanconi anaemia a condition which predisposes sufferers to leukaemias, some solid tumours and exerts myelotoxicity[56]. Both BRCA1 and BRCA2 interact with the protein Rad51 which plays an important role in homologous recombination and the repair of DSBs[57].

Patients with Li Fraumeni syndrome have germline mutations in the p53 tumour suppressor gene and have an increased risk of developing a number of cancers including breast cancer, brain tumours and leukaemia[58]. Similarly, Cowden syndrome is an autosomal inherited disease in which patients have sufferers have germline mutations in the tumour suppressor gene PTEN and increased risk of developing breast, thyroid and other cancers[59]. Mutations in the tumour suppressor p53 and PTEN can also be tested for in breast cancer but are much rarer than BRCA mutations and are rarer in breast cancer than they are in many other cancers.

More common, low penetrance gene changes that individually increase breast cancer risk by a very small amount include CASP8, FGFR2, TNRCP, MAP3K1, rs4973768 and LSP1. There are also high penetrance genes that occur rarely and increase breast cancer risk, including CHEK2, ATM, BRIP1, and PALB2 (www.cancerhelp.org).

At present the only genes that are tested for in breast cancer patients are BRCA1 and BRCA2, p53 and PTEN.

### 1.3c Previous history of breast cancer, benign disease, LCIS and DCIS.

Women who have previously had cancer in one breast are at increased risk of developing the disease in the other breast. As discussed in previous sections, women with DCIS or LCIS have an increased risk, roughly double, of developing invasive breast cancer in the same or the other breast.

Studies show that women with a diagnosis of DCIS or LCIS have a risk of invasive breast cancer in the same or other breast that is approximately double that of women in the general population. Other types of DCIS and LCIS are less likely to develop into invasive breast cancer than high grade DCIS and pleomorphic LCIS (www.cancerhelp.cancerresearchuk.org).

Women with non proliferative benign breast disease do not usually have an increased risk of developing breast cancer unless they have a strong family history of the disease. Breast lumps with an overgrowth of cells (proliferation) but without abnormal (atypical) cells increase the risk of breast cancer by between 1.5 and 2 times the average risk. About 1 in 20 breast lumps (5%) show 'atypical hyperplasia'. This means the cells are not cancer, but are growing abnormally. Atypical hyperplasia increases risk of breast cancer by more than 4 times the average (www.cancerhelp.cancerresearchuk.org.)

### 1.3d Other risk factors for breast cancer:

### 1.3di Childbearing and Breastfeeding.

The age at menarche and menopause are both influence the likelihood of developing breast cancer. Girls who are younger at menarche have an increased risk of breast cancer and women who begin and natural menopause at 55 have twice the risk of women that start the menopause at 45[60]. In 1713 the Italian Physician Bernadino Ramazzini described breast cancer as "an occupational disease of nuns" as he had observed that a high proportion of nuns suffered from breast cancer[61]. Although Ramazzini mistakenly attributed this high frequency to the nun's sexual abstinence, this early epidemiological finding provided some important clues for future study.

Findings from the Collaborative Group on Hormonal Factors in Breast Cancer, the precursor to million women study have suggested that women who are younger at the when they have their first child have a lower risk of developing breast cancer. The risk of breast cancer in women who have their first child after the age of 30 is about twice that of women having their first child before the age of 20([51]. Women who are over the age of 35 when they have their first child and those that have no children are at the highest risk of breast cancer[51], which explains in part why Ramazzini perceived breast cancer to be "a disease of nuns." Breast feeding also has an impact on breast cancer risk, for every year of breast feeding during a woman's life there is a 4.3% reduction in risk of developing breast cancer, in addition for every child born there is a 7% reduction in risk[60]. It has been postulated that this protective effect occurs as during breast feeding the levels of circulating oestrogen are low.

### 1.3dii. Hormonal levels, HRT and contraceptive pill use.

Postmenopausal women with high levels of oestrogen and testosterone have 2 or 3 times greater risk of developing breast cancer than those with very low levels of both hormones. In premenopausal women the picture is much less clear[62]. However, premenopausal women with high levels of IGF-1 have an increased risk of breast cancer.

HRT has also been found to be associated with an increased risk of developing breast cancer: the Million Women Study found that current use of HRT is associated with an increased risk in incident and fatal breast cancer; the effect is substantially greater for oestrogen-progesten combinations than with other forms of HRT[62]. However, past users of HRT did not have an increased risk of developing breast cancer with their risk returning to normal after 5 years following cessation of use[63]. Data from the same study looking at the use of oral contraceptives found that women who were currently using combined oral contraceptives or have used the in the last ten years are at a slightly increased risk of having breast cancer diagnosed, although the additional cancers diagnosed tend to be localised to the breast[64]. There is no evidence of an increased risk of having breast cancer diagnosed ten or more years after cessation of use, and the cancers diagnosed are less advanced clinically than the cancers of never users[64].

### 1.3diii Breast Density.

A large meta-analysis of MRI scans looking at the density of women's breast looked at aggregate data for >14,000 cases and 226,000 non-cases from 42 studies showed that women with the most dense breast tissue had five times the risk of developing breast cancer than those with the least dense breast tissue[312].

### 1.3div Dietary Factors and Alcohol Consumption.

As with many neoplasms, diet has a strong influence on the risk of developing breast cancer which may account for some of the geographical variation in risk from developing and developed countries. Women in developed countries tend to have higher body mass indices than those in developing countries. The million women study found the effect of body mass index on risk differed significantly according to menopausal status and HRT use[66]. They found that risk of breast cancer among premenopausal women decreases with increasing BMI whereas the risk increases with BMI among postmenopausal women who have never used hormone replacement therapy[66]. Post menopausal women with increased BMI are more likely to have increased concentrations of circulating sex hormones which may explain the increased likelihood of developing breast cancer as fat is the major source of circulating oestrogen in post menopausal women[67].

The million women study also found that low to moderate alcohol consumption in women increases the risk of certain cancers. For every additional drink regularly consumed per day, the increase in incidence up to age 75 years per 1000 for women in developed countries is estimated to be about 11 for breast cancer[68].

### 1.3dv Geographical Variation.

There is also a geographical variation in the incidence of breast cancer. Women in developing countries tend to have much lower incidences of breast cancer than in more developed countries. This may be explained in part by the fact that women in developing countries tend to have more children at an earlier stage in their life and they tend to breast feed them for a longer period of time.

Interestingly, Japanese women also tend to have low levels of breast cancer, although Japan is undoubtedly a highly developed country. However, Japanese women have very high rates of breast feeding, up to 90%. There may also be dietary factors that contribute to this low level of incidence, which may explain why Japanese women who move from Japan to Western countries have much higher levels of the disease than Japanese women living in Japan[51].

## 1.4. Breast Cancer: Current Therapies

### 1.4a Surgery.

Surgery is often curative and provides the most important means for controlling breast cancer. Modern surgical approaches seek to balance cosmesis with disease control. Therefore for breast cancers confined to the breast, either "wide local excision" or lumpectomy, which preserve the breast are frequently used[69]. This approach requires careful pathological survey of the excision margins to ensure all the cancer is removed. For more advanced cancers mastectomy is often required[70]. The primary site of metastasis, the axillary lymph nodes is usually sampled using different approaches (e.g. sentinel lymph node biopsy, node sample[71]) with an axillary clearance performed when nodes containing cancer are identified.

### 1.4b Radiotherapy.

Radiation has been used to treat Cancer since the early twentieth century. Adjuvant radiotherapy is standard therapy used to improve local control after breast conserving surgery to reduce the risk of local recurrence[69], in a adjuvant setting to complement chemotherapy or to help control symptoms and improve quality of life in terminal cancer[70]. Cancer cells are rapidly dividing cells that are particularly sensitive to radiotherapy. In addition to standard radiotherapy that is applied externally. An internal form of radiotherapy can be applied using radioactive "seeds" which are placed directly at the site of the tumour. This method is term brachytherapy taking the word brachys from the Greek meaning "short distance."

### 1.4c. Endocrine Therapies.

Roughly eight out of ten breast cancers rely on oestrogen to grow: these are known as hormone sensitive or hormone receptor positive cancers a number of therapies exploit this fact. These

tumours can be treated by suppressing the bodies' production of oestrogen or by inhibiting the action of oestrogen receptors using tamoxifen.

There are three naturally occurring oestrogens, all three are produced as the result of an enzymatic conversion of on androgens. Estrone (E1) is a weaker form of estrogen and is the predominant form in postmenopausal women, Estradiol (E2) is the predominant form in non pregnant premenopausal post menarche females and estriol is the primary estrogen during pregnancy [72] .

Nearly 50 years ago Jensen and Jacobsen[73] came to the conclusion, based on the specific binding of estradiol 17-β (E2) in the uterus, that the biological effects of oestrogen had to be mediated by a receptor protein[74]. The function of oestrogen is mediated via the oestrogen receptor. There are two types of ER: ERα and ERβ, both ERα and ERβ are activated by oestrogen and inhibited by the anti-oestrogen tamoxifen. There is a great deal of homology between the two receptors. ERα is located on chromosome 6 and ERβ is located on chromosome 14. A lot less is understood about ERβ than ERα. Oestrogen receptors are transcription factors and members of the steroid/thyroid/retinoid nuclear receptor super-family. Conformational changes occur in the oestrogen receptor when oestrogen is bound leading to transcriptional activation of a panel of oestrogen related genes. On the promoter regions of these genes lie oestrogen response elements (EREs: small palindromic DNA sequences)) which bind to dimerised pairs of ligand bound oestrogen receptors. This sequence of events triggers conformational changes in the receptor and this leads, via a number of events, to changes in the rate of transcription of oestrogen-regulated genes, the recruitment and interaction of a number of co-activators and ultimately assembly of the transcriptional machinery[74]. A number of genes containing ERE are involved in numerous cellular processes leading to cell growth and proliferation. For example the forkhead box (FOX) family member FOXM1 has previously reported to be elevated in breast cancer as well as in carcinomas of other origins[75]. Recently published data has confirmed that FOXM1 is a key mediator of the mitogenic functions of ERα and oestrogen in breast cancer cells and also suggests that the deregulation of FOXM1 may contribute to anti-oestrogen insensitivity[76].

The ovaries are the primary source of premenopausal oestrogen. Removal of the ovaries Oophorectomy (ovarinectomy) causes the levels of oestrogen to drop dramatically. A Dutch study showed that women who enter menopause before the age of 36 due to the side effects of chemotherapy for Hodgkin's Lymphoma, have a 90% decreased risk of subsequently developing breast cancer[77]. In the mid 1980's tamoxifen was identified as a suitable alternative to oophorectomy in premenopausal women with advanced breast cancer[78]. In postmenopausal

women the primary source of oestrogen is adipose tissue which may explain why increased BMI increases the risk of developing breast cancer in premenopausal women[67].

### 1.4ci SERMS

Now known as tamoxifen, the compound ICI 46,474 was synthetically synthesised in 1962 by Dora Richardson at ICI pharmaceuticals (AstraZeneca). It works by exerting an antagonistic effect on the estrogen receptor and causes a cytostatic effect of tumour cells causing them to become stuck in the G0/G1 phase of the cell cycle. It reduces recruitment of cells into the cell cycle often by reducing the production of growth factors.

In the UK tamoxifen is used to treat early and late stage breast cancer in both pre and post menopausal ER+ve women. Tamoxifen can have either estogenic or antiestrogenic effects depending on the target tissue; exerting a strongly antiestogenic effect on mammary epithelium andcan actually have an agonistic effect in bone and as a result prevents bone breakages by inhibiting the action of osteoclasts[79,80]. As a selective oestrogen receptor modulator (SERM) Tamoxifen also has an agonist effect on oestrogen receptors in the endometrium and patients treated with tamoxifen have an increased chance of developing endometrial cancer[81]. Tamoxifen has also been shown to exert an antiproliferative action by inducing the synthesis of TGF-β (a cytokine transforming growth factor) by acting as an autocrine regulatory molecule[82]. In breast cancer patients Tamoxifen has been shown to decrease circulating levels of insulin-like growth factor I (IGF-1) which is a potent mitogen[83,84].

Among premenopausal women with ER positive disease, the EBCTCG meta-analyses confirmed that five years of tamoxifen almost halved the annual recurrence rate and reduced the annual breast cancer mortality rate by a third[85].

Raloxifene is an alternative SERM to tamoxifen. In 2006 data collected from nearly 20,000 postmenopausal women recruited in the NSABP Study of Tamoxifen and Raloxifene (STAR) P-2 trial demonstrated that raloxifene was as effective as tamoxifen in reducing the risk of invasive breast cancer and had a lower risk of thromboembolic events and cataracts but a non-statistically significant higher risk of non-invasive breast cancer. The risk of other cancers, fractures, ischemic heart disease, and stroke was found to be similar for both drugs[86].

Fulvestrant (Faslodex ®) also known as ICI 182,780 is a selective oestrogen downregulator used to treat hormone receptor positive metastatic breast cancer in postmenopausal women whose tumours have progressed following treatment with other endocrine therapies such as Tamoxifen and Aromatase Inhibitors. Fulvestrant acts by down regulating and degrading ER so that oestrogen cannot attach to the receptor.

### 1.4cii Aromatase Inhibitors.

Five years of treatment with tamoxifen is no longer considered the optimal endocrine adjuvant therapy for postmenopausal women with ER positive breast cancer. A number of trials supported by the EBCTCG overview in 2005/2006 have shown a benefit from either substituting aromatase inhibitors for tamoxifen or using a sequential tamoxifen-AI regimen[85,87-90]. Aromatase inhibitors inhibit enzyme aromatase reducing oestrogen synthesis and fall into two classes. Class one aromatase inhibitors such as exemestane (Aromasin) are irreversible steroidal inhibitors, they form a covalent bond with the aromatase complex that is irreversible. Class two AIs such as anastrazole (Arimidex) and letrozole (Femara) are non steroidal competitive aromatase inhibitors. In premenopausal women the majority of oestrogen is produced in the ovaries, whereas in postmenopausal women oestrogen tends to be produced in the fat tissue from the conversion of androgens as a consequence AIs are used to treat postmenopausal women. Premenopausal women have an intact ovarian pituitary axis which means that inhibition of aromatase leads to increased LH and then increased oestrogen.

In the ATAC trial (Arimidex, Tamoxifen Alone or in Combination) the aromatase inhibitor anastrozole was compared with tamoxifen for 5 years in 9366 postmenopausal women with localised breast cancer. After a median follow-up of 68 months, anastrozole significantly prolonged disease-free survival (575 events with anastrozole *vs* 651 with tamoxifen, hazard ratio 0·87, 95% CI 0·78–0·97, p=0·01) and time-to-recurrence (402 *vs* 498, 0·79, 0·70–0·90, p=0·0005), and significantly reduced distant metastases (324 *vs* 375, 0·86, 0·74–0·99, p=0·04) and contralateral breast cancers (35 *vs.* 59, 42% reduction, 12–62, p=0·01)[91]. Researchers on the trial reported less withdrawal effects associated with anastrazole than tamoxifen. There were also fewer gynaecological and vascular events associated with anastrazole than tamoxifen. However two important side effects that were seen with the patients treated with anastrazole and not tamoxifen was arthralgia and bone fractures. In conclusion aromatase inhibitors have been shown to improve outcome in postmenopausal breast cancer in addition when treating early-stage, hormone-receptor-positive breast cancer, aromatase inhibitors have more benefits and fewer serious side effects than tamoxifen. However, the associated arthralgia and increased frequency of bone fractures can be considered as significant drawbacks in the usage. However drug combination therapies can be conducted that will reduce the incidence of bone fractures, this is discussed in the following section.

### 1.4ciii Bisphosphonates.

Bisphosphonates have been used in combination with aromatase inhibitors to combat the side effects that are detrimental to bone. However, they have been found to exert an additional serious side effect. In a small proportion of patients they have been shown to cause osteonecrosis of the jaw. Statins, which have bone strengthening properties, are now being

used as an alternative to Bisphophonates as they can protect against the detrimental effect that AIs have on the skeleton without causing osteonecrosis of the jaw[92-94].

### 1.4civ Pituitary Down Regulators.

Goserelin (Zoladex) is a pituitary down regulator and is an agonist of LHRH (lutenising hormone releasing hormone.) It is used to treat premenopausal women and acts by preventing the release of LH from the pituitary which prevents oestrogen from being released in the ovaries. LHRH agonists/surgery is used to prevent feedback upregulation of oestrogen production[95.]

### 1.4d Molecularly targeted biological therapies.

Whilst there are a multitude of candidate therapies targeted against specific molecular changes in breast cancer, to date the majority of clinically applied therapies either target the HER2 oncogene or the tumour vasculature. Molecularly targeted biological therapies for breast cancer treatment can be subdivided into two broad categories: those classed as anti-HER type and those that are classed as anti-vascular agents.

### 1.4di HER targeted therapies.

Her2 is a member of the type I RTKs including HER1, HER2 and HER4[96]. It plays a key role in proliferation, migration, preventing apoptosis and driving vascularisation[96,97,98]. The Her2 proto-oncogene, which is expressed on the surface of epithelial cells in many tissues including the breast[96] is amplified in around 15-25% of breast cancer and breast cancers that exhibit gene amplification are naturally more aggressive and cause early relapse and death in a significant proportion of patients. In addition to an antiprolifereative effect HER2 can promote metastasis. HER2 can be activated by EGF-like and heregulin ligands have been shown to increase invasiveness in an in vitro setting and cause an elevate levels of metastasis *in vivo*[99]. Activated HER members have been shown to enhance vascular invasion and angiogensis by upregulating angiogenic fators like VEGF and MMPs which potentiates the adhesion of tumour cells to endothelial cells[100].

#### 1.4.d.i.1 Trastuzumab (Herceptin.)

Trastuzumab is a recombinant, humanised monoclonal antibody directed against the extracellular domain of the HER2 protein. Original studies suggested that trastuzumab is beneficial to patients with advanced metastatic breast cancer. Trastuzumab can be used for both early and metastatic breast cancer settings and has been approved for early breast cancer following surgery, chemotherapy and sometimes radiotherapy. Trastuzumab has been shown to be more beneficial to patients in combination with chemotherapy than when used alone. Four major trials: HERA, NSABPB31, NCCTG and BCIRG looked at trastuzumab treatment in a total of more than 13,000 HER2 +ve patients with early breast cancer[101-104]. These four trials obtained

similar results, although trastuzumab was combined with different chemotherapies and had different sequencing of treatment and each trial included different patient populations. The trial showed a reduced the 3 year risk of recurrence by about 50%[101-104]. trastuzumab has also been shown to be effective in the metastatic setting in combination with chemotherapy[105-107].

One study looked at a total of 186 patients and found that trastuzumab was significantly superior to docetaxel alone in terms of ORR (61% vs. 34% $p$=0.0002), and OS (median 31.2 v 22.7 months $p$ = 0.0325), time to disease progression (median, 11.7 vs. 6.1; $p$=0.0001, time to treatment failure (median 9.8 vs. 5.3 month $p$ = 0.0001 and duration of response (median, 11.7 vs 5.7 months $p$ = 0.009[105].)

#### 1.4.d.i.2 Pertuzumab (Omnitarg.)

Pertuzumab is a monoclonal antibody that targets the extracellular domain of Her2 and prevents heterdimerisation of Her2 with other members of the EGFR/type I receptor tyrosine kinase family and thus prevents signal transduction. Pertuzumab also showed activity in phase 2 trials in trastuzumab-refractory metastatic breast cancer, and results suggested that the drug could reverse trastuzumab resistance[97,98].

#### 1.4.d.i.3 Lapatinib (Tyverb.)

Lapatinib gained a licence in Europe in 2008. It has been used in combination with the chemotherapy drug capecitibine to treat hormone and trastuzumab refractory Her2+ve breast cancer. Lapatinib inhibits receptor signal processes by binding to the ATP-binding pocket of the EGFR/HER2 protein kinase domain, preventing self-phosphorylation and subsequent activation of the signal mechanism[108].

### 1.4.d.ii Agents that target the tumour vasculature

#### 1.4.d.ii.1 Sunitinib (Sutent.)

Sunitinib is another small molecule tyrosine kinase inhibitor and has been used to treat renal and gastrointestinal cancer. It targets all receptors for platelet-derived growth factor receptors (PDGFRs) and vascular endothelial growth factor (VEGFs) receptor inhibiting tumour cell proliferation and angiogenesis[109]. It is currently being used in trials for other solid tumours including breast cancer in combination with a number of different chemotherapies including the taxane docetaxel and capecitabine.

#### 1.4.d.ii.2. Bevacizumab (Avastin.)

Bevacizimab is a humanised monoclonal antibody that blocks VEGF-A which stimulates angiogenesis. As a consequence it stops the growth of blood vessels supplying the breast tumour. It has been shown to slow the progression of metastatic breast cancer but does not

extend the survival period of patients[110]. Bevacizumab is being used in a number of trials in combination with paclitaxel and docetaxel.

#### 1.4.d.ii.3 PARP Inhibitor: Olaparib (AZD228.)

PARP inhibitors are a new group of biological therapies currently in phase I and II clinical trials. They act by inhibiting the enzyme Poly (ADP ribose polymerase (PARP) which has a role in DNA excision repair of single-strand DNA breaks. These DNA single-strand break accumulate causing double strand breaks and the replication fork to collapse. BRCA1 and BRCA2 are key regulators of homologous recombination repair pathway involved in the repair of DNA DSBs. Tumour models with compromised ability to repair double strand DNA breaks by the homologous recombination repair pathway such as those with BRCA1 and BRCA2 mutations, are highly sensitive to blockade of the repair of single strand DNA breaks via PARP inhibition, which provides the bases for a novel synthetic lethal approach to cancer therapy[111]. The PARP inhibitor olaparib (AZD2281) has been used in a proof of concept phase II study to investigate its efficacy against breast cancer. The results show that the olaparib at 400mg twice daily was active in women even with BRCA mutations and advanced breast cancer that was resistant to advanced chemotherapy[112]. Olaparib was even shown to be effective in treating triple negative breast cancers. It can be concluded that PARP inhibitors are promising novel biological therapies for dealing with breast cancers that have been previously difficult to treat including, BRCA1 and BRCA2 mutated cancers, triple negative tumours and advanced tumours that have previously failed to respond to many chemotherapies.

### 1.4e Chemotherapy.

Chemotherapy can be used in the neoadjuvant setting to shrink a tumour prior to surgery or radiation therapy. It can also as an adjuvant therapy to prevent recurrence following surgery or to treat metastatic or recurrent breast Cancer. Over the years chemotherapy has developed progressively in a number of incremental stages. The Cochrane overviews which collate data from multiple clinical trials provide an overview of the development of chemotherapy for breast cancer from single agents to current polychemotherapy treatments[113,114]. Poly-chemotherapy has been established as superior to mono-chemotherapy or no chemotherapy leading widespread adoption of combination therapy strategies such as E-CMF or FEC-T in the UK today.

Chemotherapeutic agents are often used in different combinations. CMF which was one of the earliest polychemotherapy treatments developed for adjuvant therapies is a combination of Cyclophophamide (DNA alkylating agent), Methotrexate (antimetabolite, antifolate) and Fluorouracil (antimetabolite pyrimidine analogue). Subsequently, the addition of anthracyclines to polychemotherapy schedules was shown to benefit patients when included in a number of different approaches eg, AC, FAC or E-CMF. AC is a combination of Adriamycin

(doxorubicin) and Cyclophophamide commonly used to treat node negative patients. The combination of FAC: Fluouracil, Adiramycin and cyclophosphamide can be used in the treatment of metastatic breast cancer. CMF can also be used in combination with the anthracycline epirubicin to give E-CMF[306].

The common anthracyclines: Adriamycin and Epirubucin act by intercalating into DNA and inhibit macromolecular biosynthesis, enhancing production of free radicals and disrupting membrane fluidity[115]. However, one important drawback of the anthracyclines is the cardiotoxic effects that they exert. One large meta-analysis including fifty-five randomly controlled trials found that a significantly greater risk of clinical cardiotoxicity was found with anthracycline compared with non-anthracycline regimens[116]. Cardiotoxicity is not experienced by patients treated with taxanes and as such makes them an attractive alternative to anthracycline based therapy[314].

The combination FEC of Fluorouracil, Epirubicin and Cyclophosphamide can be used also with the addition of the taxane Docetaxel, however the TACT trial which looked at the addition of Docetaxel to the standard anthracycline based chemotherapy regimen FEC showed no significant improvement for patients[117]: the outcome of the trial was disappointing. However, node negative and node positive patients that were ER negative and Her2 positive did benefit from the addition of docetaxel. However, further investigation of predictive biomarker defined subgroups may allow us to better understand and hence more effectively target certain subgroups of patients with taxane chemotherapy. Gemcitabine is a pyrimidine analogue that has been shown to be effective in combination with the taxane paclitaxel. For patients with Metastatic Breast Cancer, the addition of gemcitabine to paclitaxel extended time to progression and resulted in a better global rating of Quality of Life[118].

In summary, it can be established that poly-chemotherapy is superior to mono-chemotherapy for most patients[114], and that hormonal therapy can be used in conjunction with chemotherapy to treat early breast cancer[113]. In addition the addition of anthracylines to a standard regimen is superior to an anthracyline free treatment. Furthermore, it has been ascertained that the addition of a taxane is of superior benefit to some patient subgroups and that taxanes unlike the anthracyclines do not exert a cardiotoxic effect. Combined strategies involving chemotherapy and/or hormone and biological therapies, targeted to particular subgroups of patients is currently the central dogma of improving breast cancer patient outcome. Identifying these subgroups using novel and existing biomarkers will permit clinicians to adopt a tailored approach to cancer therapy, allowing a distinct shift from the “one size fits all paradigm.” This primary concern of my thesis is to investigate this concept in the context of taxane based therapy.

## 1.5 The Taxanes.

### 1.5a A Brief History of the Taxanes

The Taxanes are an incredibly powerful group of chemotherapeutic agents. They have been used successfully to treat breast, ovarian, Non Small Cell Lung Carcinoma (NSCLC), head and neck Cancer and Kaposi's Sarcoma (an AIDS related Cancer.) Currently, the two most clinically useful taxanes are paclitaxel (Taxol) and docetaxel (Taxotere.)

Paclitaxel was isolated from the bark of a species the Pacific yew tree; *Taxus brevifolia* by Munroe E Wall and Mansukh C Wani in 1967[119] at the research triangle institute in Northern California. The Pacific yew tree grows along the Pacific Northwest Coast of North America and this restricted development off this agent. To counteract this problem paclitaxel can be derived semi-synthetically from an inactive taxane precursor esterified 10 deacetyl baccatin III which is found in the needles of the European Yew *Taxus baccata*[120] or totally synthesised by a convergent strategy[121]. Docetaxel is semisynthetically derived by esterification of a side chain to 10 deacetyl baccatin III[320]. Very recently a team in Edinburgh managed to use cultured cambial meristematic cells to produce paclitaxel[122].

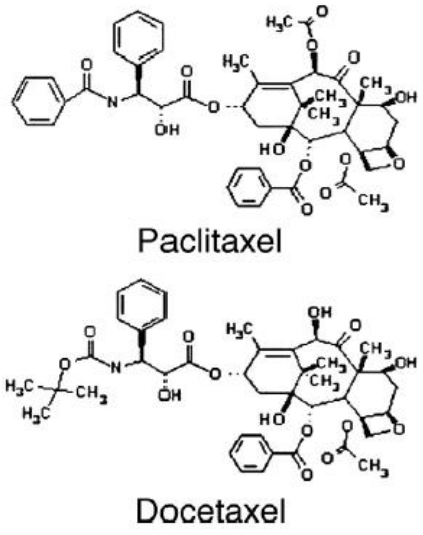


**Figure 1.2.** Chemical Structure of Paclitaxel and Docetaxel[123].

The Taxanes have been used in combination with anthracyclines and alkylating agents to great effect, improving both Overall Survival (OS) and Disease Free Survival (DFS)[124]. In recent times the taxanes have also been used to treat early breast cancer successfully in combination with Herceptin. The commercially available taxanes, paclitaxel (Taxol) and docetaxel (Taxotere), have become widely recognised as extremely active chemotherapeutic agents in the treatment of breast cancer[124], with a response rate of between 25 and 69% observed when used in first line treatment[125]. Clinically meaningful benefits were first shown in the metastatic setting, and

the large-scale exploration of their roles in the adjuvant therapy of early stage disease has lead to the widespread adoption of adjuvant chemotherapy schedules including taxanes[117]. Benefits have seen in the neoadjuvant setting as well, mainly with docetaxel[127]. Figure 1.3 shows a meta-analysis of disease free survival of trials for taxane vs. anthracycline based chemotherapy. Note that disappointingly the TACT trial did not show any overall benefit with the addition of docetaxel to a standard anthracycline based therapy[117].

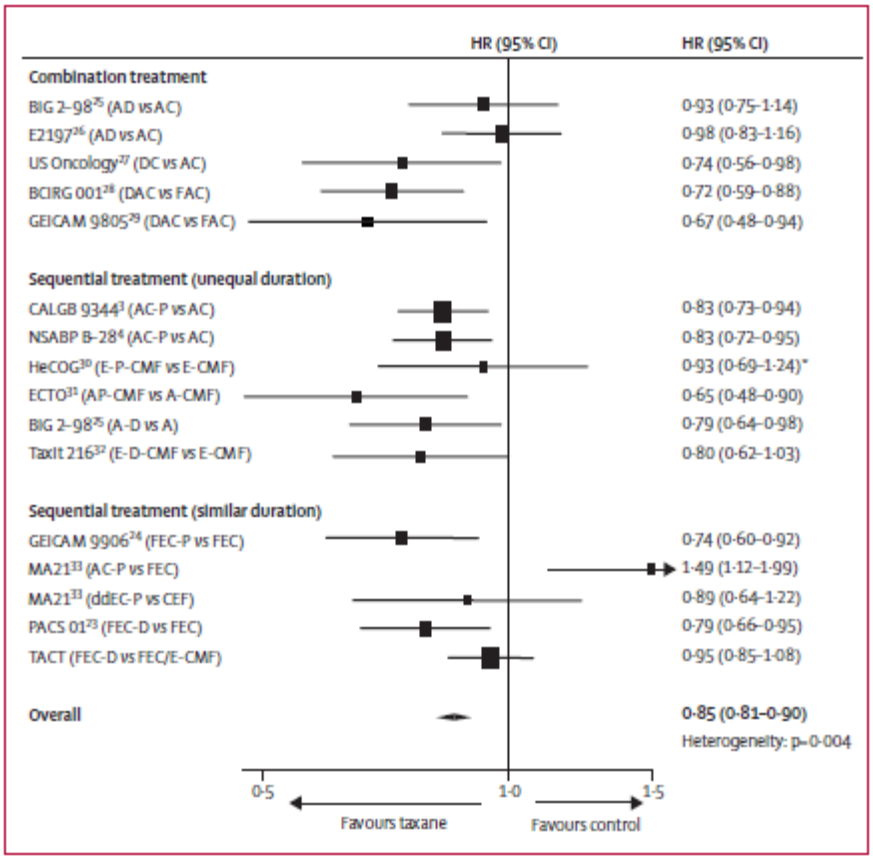


**Figure 1.3.** Meta-analysis of disease free survival for trials of taxane-based versus anthracycline based adjuvant chemotherapy. A=doxorubicin, C=cyclophosphamide, D=docetaxel, dd=dose dense, F= Fluouracil, P=Paclitaxel, E=Epirubicin, M=Methotrexate, Her=Hazard Ratio, HR from Cochrane Review. Adapted from Lancet TACT trial article[117].

This highlights the need to explore predictive biomarker-defined subgroups and identify groups of patients that will benefit from the addition of taxane based therapy. Figure 1.4 from the data from the TACT separated according to ER and HER status, and nodal status. This figure shows that the group of patients that benefit most from the addition of a taxane are ER -ve/HER2 +ve, and especially the node positive patients.

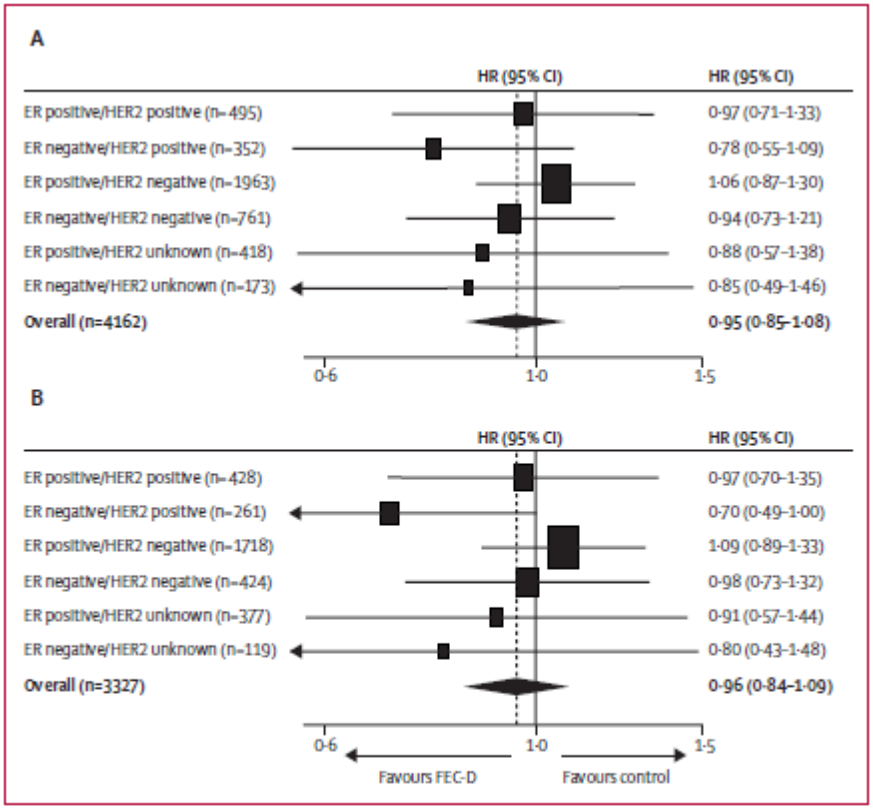


**Figure 1.4.** Hazard ratios for disease free survival by combined ER and HER2 status in A. all patients and B. node positive patients. ER = oestrogen receptor, FEC-D = fluouracil, epirubicin and cyclophosphamide followed by docetaxel. HER2 = human epidermal growth factor receptor 2, HR = Hazard Ratio Adapted from Lancet TACT trial article[117].

## 1.5b Mechanism of action of taxanes.

Taxanes are a potent and highly active group of drugs that interact with β-tubulin that has previously been incorporated into microtubules, stabilising the structure of the microtubule, thus impeding disassembly at the minus-end. Understanding how the taxanes interact with mechanisms of actions of the taxanes. Understanding how taxanes interact with microtubules is important to help comprehend the underlying mechanisms of actions of taxanes. Understanding these mechanisms will also help clinicians maximise the efficacy of the taxanes and allow them to identify patients that will most benefit from taxane therapy. This blocks cell signalling, arrests the cell cycle causing cells to apoptose leading to mitotic crisis.

Microtubules are long hollow cylindrical cores composed of α and β tubulin heterodimers. There is only around 40% homology between α and β tubulin; however, they share a very similar folding pattern. The N terminal region (residues 1-206) is involved in nucleotide binding, and has a Rossmann fold with alternating parallel β strands (S1-S6) and helices (H1-H6)[128]. The

central domain (residues 207-684) is involved in both longitudinal and lateral contacts between α and β tubulin monomers present in protofilaments, and is formed by an arrangement of mixed β sheets (S7-S10) and three helices (H8 – H10)[128].

Paclitaxel binds to a hydrophobic pocket within this central domain[128]. The tubulin subunit heterodimers are associated in a head to tail fashion to form protofilaments, which associate in a lateral manner to form hollow microtubules[128]. Since the lateral associations between protofilaments involve interactions between subunits of the same type, that is the so called B type lattice, the protofilaments are arranged in a parallel array, thereby imparting polarity to the structure. Consequently, the β-chains of the tubulin dimer are exposed at one end (plus) of the polymer, and the α-chains at the other end (minus.) In cells, microtubules are usually organised with their minus end associated with their microtubule organising centre (MTOC) near the nucleus, and radiate outward so that the plus ends are near the periphery of the cell[128].

Microtubules are filamentous protein fibre cylinders and are usually composed of 13 protofilaments with an overall diameter of 25nM, they have important roles in a wide variety of cellular activities including maintaining cell shape, cellular movement, intracellular trafficking of macromolecules and organelles, cell signalling, division and mitosis[123]- these important roles make microtubules a very attractive target for anticancer drugs, including the taxanes as well as the vinca alkaloids and the epothilones.

Microtubule targeting drugs function by suppressing microtubule dynamics, inhibiting the metaphase anaphase transition, blocking mitosis and inducing apoptosis[123]. Paclitaxel suppressed spindle microtubule dynamics by allowing microtubule attachment but alters the tension across the kinetochore during mitotsis[129,130]. With docetaxel, centrosome organisation is disrupted affect the late S phase, G2 and M phases which results in incomplete mitosis, accumulation of cells in the $G_2$M phase and cell death[131].

Paclitaxel attaches to the interior microtubule surface to inhibit its dynamics. It is thought to gain access to its binding sites by diffusing through small openings in the microtubule or fluctuations in the microtubule lattice[132] (see Figure 1.5.) Different downstream events have been implicated in taxane induced apoptosis, including the phosphorylation and concomitant inactivation of Bcl-2, activation of JNK, Raf1 and both caspase dependent and independent mechanisms[133].

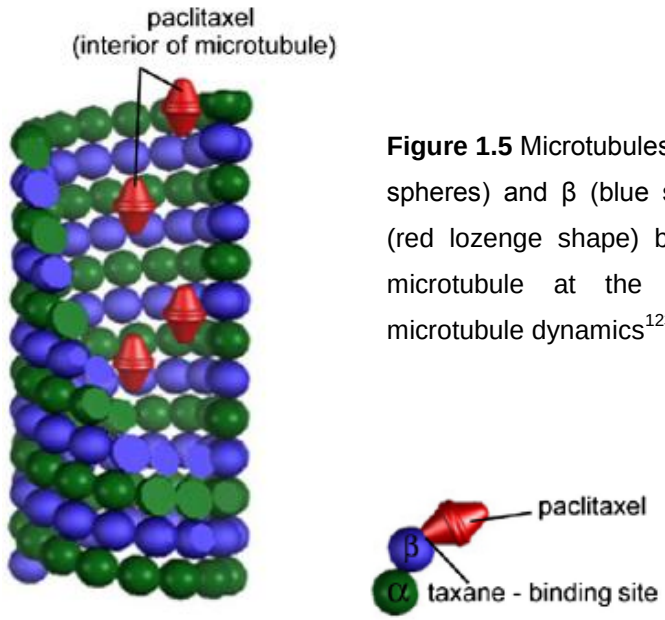


**Figure 1.5** Microtubules are made up of alternating α (green spheres) and β (blue spheres) tubulin subunits Paclitaxel (red lozenge shape) binds to the interior surface of the microtubule at the taxane-binding site, suppressing microtubule dynamics[123].

## 1.5c Taxanes chemoresistance

Response rates of paclitaxel are thought to be 27% in breast cancer and 42% ovarian cancer, and response rates of docetaxel around 39% breast cancer and 31% ovarian cancer[134-136]. Taxanes have been identified as highly effective chemotherapeutic agents that can lead to improvement and in the duration and quality of life of some patients. However, the majority eventually develop progressive disease after initial response. Taxane resistance represents a challenging obstacle to improving the overall response and survival rates of breast cancer patients. Although many potential mechanisms of taxane resistance in breast cancer have been identified, a clear picture of the means by which resistance occurs remains to be established. Identifying potential biomarkers of taxane resistance would allow clinicians to identify which patients will respond to treatment. There may be potential for developing combined therapies to target biomarkers, and revert taxane-resistant tumours to their sensitive state.

### 1.5.c.i Taxane resistance and microtubules.

The functional target of the taxanes is the microtubule. It is logical to conclude that alterations in microtubule dynamics and altered binding of paclitaxel to microtubules could be potential areas of interest for research into taxane resistance. It has been shown that higher expression of β-III tubulin expression predicted poorer outcomes in patients with NSCLC treated with taxanes[137]. One particular study has identified β-tubulin mutations in serum DNA isolated from 33% of patients with non small cell lung cancer[138]. To conclude, Microtubule dynamics and stability have been shown to be altered by β-tubulin mutations and this can alter binding of the taxanes to β tubulin subunits leading to resistance[139,140].

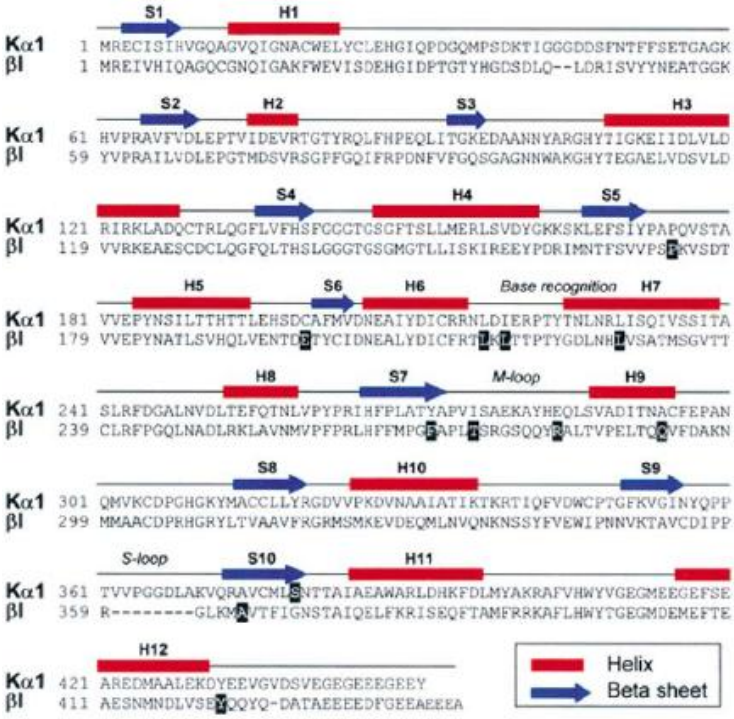


**Figure 1.6.** Primary sequences and secondary structure of the major human α and β tubulin isotypes. Helices (H1-H2) are represented as red rectangles and β sheets (S1-S10) are represented as blue arrows Mutations detected in paclitaxel resistant cell lines are highlighter in black[128].

Understanding how the taxanes interact with microtubules is incredibly important for comprehending the underlying mechanisms of actions of the taxanes. Understanding these mechanisms will also help clinicians maximise the efficacy of the taxanes and allow them to identify patients that will most benefit from taxane therapy. Alteration in tubulin isotype composition has been investigated in ovarian tumour samples. Taxol-resistant ovarian tumour samples displayed significant increases in class I (3.6 fold), class III (4.4 fold) and class IVa (7.6 fold) β-tubulin tubulin compared to primary untreated ovarian tumours[141]. However, one study attempted to induce β tubulin class I in Chinese hamster ovary (CHO) cells, this failed to confer resistance to paclitaxel[142]. This suggests that alteration in β-tubulin isotype expression may not be directly linked to the resistant phenotype, but represents a secondary effect that may require the participation of additional isotype specific regulatory proteins[128]. Figure 1.6 shows the mutations detected in paclitaxel resistant cell lines.

Microtubule associated proteins (MAPS) regulate microtubule dynamics by interacting with tubulin polmers and microtubules, play a role in cellular sensitivity to MI by modulating microtubule stability[128]. There are five subtypes of MAPs: MAP1A, MAP1B, MAP2, MAP4 and tau proteins. Tau functions primarily by enabling tubulin assembly and microtubule stabilisation[143]. Tau binds differentially binds to microtubules depending on the presence or absence of paclitaxel[144]. In the absence of paclitaxel, tau binds strongly to microtubules and dissociates slowly, whereas in the presence of paclitaxel tau binds moderately to microtubules, enhancing paclitaxel-induced polymerisation and dissociated rapidly[143]. There is increased paclitaxel

binding to the microtubule in the presence of low tau concentrations than in the presence of high tau concentration. This suggests that tau could be a potential biomarker for taxane resistance. One study found that tau expression was significantly lower in patients who achieved pathologic complete response to paclitaxel/FAC chemotherapy[145]. However the TACT trial found that although tau expression was associated with improved DFS there was no evidence of an interaction between tau and docetaxel benefit[146].

Oncoprotein 18, also known as Stathmin is a phosphoprotein that promotes destabilisation of microtubules and as a consequence alters microtubule dynamics, this occurs during interphase and mitosis. One study used RNA interference to target Stathmin which consequently induced microtubule polymerisation and promoted transition from $G_2$ to M phase[147]. This suggests that paclitaxel efficacy may be modulated by regulation of Stathmin function. *In vitro* MAP4 expression has been show to be correlated with increased paclitaxel resistance in p53 mutant cells[148]. MAPs are certainly interesting prospective biomarkers; however the way in which microtubule interacting proteins regulate microtubule dynamics is complex and potentially multi-factorial.

### 1.5.c.ii Multidrug resistance and the taxanes.

A great deal of research has been put into the role of multidrug resistance (MDR) in paclitaxel efficacy. MDR is where resistance to one drug results in cross resistance to another which is structurally unrelated. The ATP-binding cassette (ABC) transporter family are drug efflux pumps and key regulators of multidrug resistance. P-gyp is a member of the ABC family and is encoded by the mdr-1 gene on chromosome 7. When drugs bind to p-gyp, one of the ATP binding domains is activated and hydrolysis of ATP causing a conformational change in P-gyp causing drugs to be released into the extracellular space[149]. The National Cancer Institute used qPCR to look at expression levels of MDR-1 in the NCI-60 panel which is a 60 cell line drug screening panel. They concluded that the lower the expression-level of MDR-1, the higher the sensitivity of the cell line to paclitaxel[150].

### 1.5.c.iii HER2 and taxane resistance.

One study using MDA-MB-435 cells showed that the introduction of $p185^{HER2}$ conferred resistance to paclitaxel[304]. They proposed that paclitaxel induced inhibition of $p34^{cdc2}$ activation and apoptosis were inhibited in the G2/M phase in the HER2 overexpressing cell line by HER2 upregulating $p21^{WAF1/Cip1}$ (which associates with $p34^{cdc2}$)[304]. In another group of experiments, also using MDA-MB-435 cells, researchers showed that the HER2 kinase domain directly phosphorylated Cdc2 tyrosine 15 (Cdc-2Y15-p) and induced resistance to paclitaxel induced apoptosis which delayed M phase entry in the cell cycle[152]. One final set of in vitro experiments, using MCF-7 cells transfected with HER2 resulted in AKT phosphorylation and activation and

these cells showed increased resistance to paclitaxel doxorubicin and 5-fluouracil. Interestingly, they found that these cell lines could be reverted to their parent phenotype using dominant-negative expression vectors for PI3K/AKT[153]. It was recently shown that HER2 activation of PI3K-dependent signalling increased mammary epithelial cell invasive potential *in vitro*[154].

In the TACT trial, the patients that benefited most from the addition of docetaxel to an anthracycline based therapy were ER and HER2+ve which seemed to contradict some of the data shown *in vitro*[117]. However in other studies no association between HER2 expression and taxane response was seen in MBC. This observation was made in a retrospective study using the polyclonal Herceptest (Dako, Carpinteria, CA) and CB-11 (a monoclonal ab – Biogenex, San Ramon, CA)[155].

### 1.5.c.iv. Taxane resistance and the Spindle Assembly Checkpoint.

The spindle assembly checkpoint (SAC) or mitotic checkpoint plays an important role in accurate segregation of chromosomes, kintechore-chromatid tension and attachment[156] and loss of function of the spindle assembly checkpoint results in CIN[157]. Paclitaxel activates the SAC by causing mitotic arrest as a result of stabilising microtubules. The checkpoint genes Mad2 and BubR1 play a role in maintaining the SAC and it has been shown that suppression of these genes via paclitaxel treatment abolished the function of the checkpoint which resulted in paclitaxel resistance correlated with suppression of cyclin dependent kinase 1 activity[158]. In the same set of experiments overexpressing Mad2 in cells with a defective checkpoint which was attributed to low expression of Mad2 resulted in a restoration of the checkpoint, enhanced cyclin dependent kinase 1 activity and resulted in increased sensitivity to paclitaxel[158].

AURORA-A is a Serine-threonine kinase located in the centrosome and is frequently elevated in some epithelial cancers[159]. Amplification of AURORA-A has been shown to induce paclitaxel resistance as a result of overriding the SAC([159]. Despite the defective formation of spindles and the action of MAD-2 at the kinetechores, which indicated that the spindle assembly checkpoint was functioning, cells overexpressing AURORA-A entered anaphase inappropriately. This meant that cytokinesis failed to complete which resulted in a mitotic arrest and the appearance of multinucleated cells[159].

### 1.5.c.v Taxane resistance, cell-cycle related proteins and apoptotic mechanisms.

Regulation of the cell cycle plays a crucial role in the progression of cancer and the response to chemotherapeutic agents. Following inhibition of the mitotic spindle disassembly in G2/M, cytotoxicity requires activation if the spindle assembly checkpoint is to cause a mitotic arrest. Alternatively, aberrant mitosis (with improper exit from mitosis) in the absence of chromosome

segregation and cytokinesis producing tetraploid cells may occur, both of which result in apoptosis in the presence of an intact p53 checkpoint[318]. If all cell cycle checkpoints are incapacitated, taxane treatment may result in aneuploidism[160]. Interestingly the two taxanes exert differing effects on the cell cycle, with docetaxel targeting S, G2 and M phase, and paclitaxel targeting mainly G2 and M phases of the cell cycle[161,162]. Figure 1.7 shows that different doses of taxane can affect different stages of the cell cycle, leading to different outcomes[160].

Docetaxel inhibits centrosome formation during S phase and cells are particularly sensitive to docetaxel at this phase of the cell cycle. Figure 1.7 shows that low dose paclitaxel leads to mitotic slippage or an aberrant mitosis during late M phase which targets the tetraploid via the checkpoint leading to apoptosis. Moderate doses of paclitaxel inhibit mitotic spindle dynamics leading to arrest via the $G_2M$ checkpoint. High paclitaxel dose leads to the formation of microtubule bundles leading to necrosis during late $G_1$ phase.

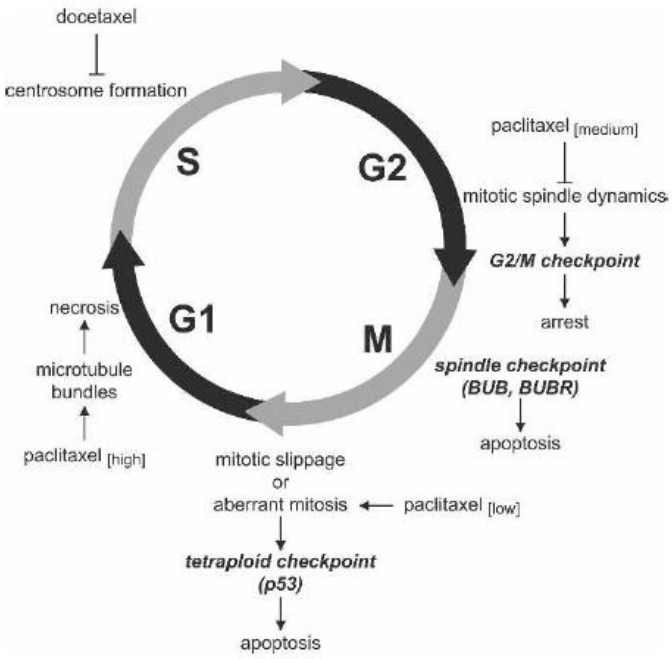


**Figure 1.7.** Effects of the Taxanes on the Cell cycle[160].

The cell cycle related tumour suppressor gene BRCA1 helps maintain genomic instability and is involved in the repair of DNA and transcriptional regulation. The disruption of the mitotic spindle by paclitaxel can activate the spindle and $G_2M$ checkpoints via the p38/MAPK pathway[163] and BRCA1 can sensitise breast cancer cells to paclitaxel induced apoptosis[164].

p53 was originally thought to be an oncogene but was subsequently identified as the first gene to be identified as a tumour suppressor gene. It plays an important role in the regulation of the cell cycle at the G1/S checkpoint. Although p53 is less frequently mutated in breast cancer than in many other solid mutations a broad meta-analysis of breast cancers found that around 20% of all cases expressed mutant p53[165].

A remarkable study found that 100% of medullary breast cancers were found to be p53 mutated[166]. Medullary cancers have found to have clinicopathologic similarities with BRCA1 associated cancers[167]. p53 can be a valuable biomarker for predicting response to chemotherapeutic agents, for example a study found that cancers with mutations in p53 were more likely to respond to paclitaxe[168]. However, the complete picture of p53 as a biomarker for taxane response is unclear. Research has been conducted to show that an increased $G_2$M arrest and apoptosis in the absence of p53 resulted in elevated paclitaxel chemosensitivity[169,170], whereas others have shown that apoptosis induced by taxanes is p53 independent[171,172]. The increase in p53 associated with taxane sensitivity may be explained by a concurrent increase in activity of the microtubule associated protein (MAP4) which induces the polymerisation of microtubule and so increases sensitivity[173,174]. Other studies showed that when paclitaxel exerts it effect on the cell cycle in mutant p53 cells, the presence of mutant p53 override control of the G1/S checkpoint which causes the cell cycle to progress towards $G_2$M[175].

Mutant p53 has also associated with an increase in taxane resistance. This may be explained by spindle checkpoint control which can be altered by mutations in p53 which increases resistance to the damage exerted by the drug[176]. There is also evidence to suggest that mutant p53 is unable to up regulate BAX the pro-apoptotic protein which reduces levels of apoptotic cells[177].

Cell death can be mediated by apoptotic mechanisms and perturbation of these mechanisms play an important role in drug response in cancer. Apoptosis can be exerted either by the mitochondrial or intrinsic pathway, or the death receptor or extrinsic pathway. The antiapoptotic PI3K/AKT pathway is frequently dysregulated in human cancer and in vitro in ovarian cancer the activation of AKT has been shown to confer resistance to paclitaxel[178] and inhibiting the PI3K/AKT pathway can sensitise cells to apoptosis induced by [182,183]. The Bcl-2 oncoprotein has been shown to bind paclitaxel, and *In vivo* the increased expression of phosphorylated Bcl-2 confers taxane chemosensitivity to both paclitaxel and docetaxel which is not seen in tumours with low levels of phosphorylated Bcl-2[238, 239(184,185)]. In addition, Felini *et al* generated two taxane resistant ovarian cell lines and established that these lines exhibited a consistent down regulation of Bcl-2[186]. They also looked at a small subset of paclitaxel resistant ovarian tumours using immunohistochemistry and observed that Bcl-2 was downregulated at the protein level when compared to paclitaxel sensitive lines[186].

There are numerous molecular and cellular mechanisms that have been implicated in breast cancer taxane resistance. These mechanisms can be associated with the target of the taxane microtubules including β-tubulin mutations and different β-tubulin, microtubule-associated proteins such as protein tau and Stathmin. Multidrug resistance is also an important marker of taxane resistance in some tumours. It is important to consider common breast cancer biomarkers such as HER and ER which may prove to be valuable tools in predicting response to taxane, as they have allowed researchers to identify subgroups of patients that are likely to benefit from the addition of a taxane to a standard chemotherapy. Another important target for potential taxane resistance biomarkers is the spindle assembly checkpoint which controls proper segregation of the chromosomes. Some candidate SAC potential biomarker genes are MAD2, BubR1, and the aurora Kinases. p53 and BRCA1 are two cell cycle mediating proteins that have been implicated in taxane resistance, but the definite mechanisms by how they do this remains unclear. Apoptotic mechanisms such as the Bcl-2 pathway have also proven to be intriguing areas of interest for future studies into taxane resistance.

In conclusion, taxane resistance is a considerable and multifactorial problem in the field breast cancer treatment and a number of promising potential biomarkers have been identified. Identifying useful markers of taxane resistance will allow clinicians to identify subgroups of patients that will benefit from an addition of a taxane to their therapy and also identify patients that will not benefit so that they will not be unnecessarily treated with toxic chemotherapy that will yield no therapeutic benefit. The use of a model of taxane resistance will prove an invaluable resource for identifying such patient subgroups and as such will help drive the move towards developing tailored therapies to the patient.

### 1.5d Side effects.

Cytotoxic effects of taxanes do not only depend on the specific drug, but also on the concentration used and on presence of cell cycle checkpoints in the cell that is being affected. Docetaxel has been shown to be between 2 and 4 times as potent as paclitaxel[131]. This may be because docetaxel has greater uptake, slower efflux and as a consequence a longer retention time than paclitaxel. Pharmacokinetics and pharmacodynamics of the taxanes show both agents to be extensively metabolised in the liver, and paclitaxel has a non linear pharmacodynamic behaviour while docetaxel has linear pharmacodynamic behaviour[131]. Docetaxel bind tubulin with greater affinity and has a wider cell cycle activity than paclitaxel[131].

The Taxanes are an extremely potent and effective group of chemotherapeutic drugs, however with this potency comes an array of side effects some of which can be significant. Both paclitaxel and docetaxel are generally fairly well tolerated. However, when used as single agents or in combination chemotherapy programs, the taxanes can cause toxicities that are distressing (e.g.,

alopecia, arthralgias/myalgias) and others that are potentially more serious (e.g., hypersensitivity[308] reactions, stomatitis/mucositis, peripheral neuropathy, bone marrow suppression [184,185].) These side effects and whether they are common with paclitaxel treatment, docetaxel treatment or with both are summarised in table 2. The most universally experienced side effect common to both taxanes is alopecia.

| REACTION | TAXANE |
|---|---|
| Hypersensitivity Reaction | *Common with both* |
| Bone Marrow Suppression (primarily Neutropenia) | *More common with docetaxel and extended paclitaxel infusions* |
| Peripheral Neuropathy | *More common with Paclitaxel* |
| Arthralgias/Myalgias | *More common with Paclitaxel* |
| Alopecia | *Universal with both taxanes* |
| Stomatitis/mucositis | *Both* |
| Fluid Retention | *Docetaxel only* |

**Table 1.3** Side effects associated with taxane treatment (adapted from[186].)

One of the most frequently described side-effects are hypersensitivity reactions which occur with both paclitaxel and docetaxel treatment. This hypersensitivity is often the result of reactions to Cremaphor, which is the solute in which the drug is delivered to patients. Unfortunately, in some circumstances these reactions can lead to fatalities. Patients need to be pretreated with steroids and antihistamine to reduce the chances of hypersensitivity reactions. This lead to the development of treatments like abraxane, an albumin bound injectable form of paclitaxel. Treatments like abraxane eliminate the need to pretreat with antihistamines and steroids and are also administered in a much shorter period of time than traditional solvent bound agents.

Neutropenia occurs with both taxanes but is more common with docetaxel. By shortening the duration of perfusion with paclitaxel the chance of neutropenia can be reduced. Thrombocytopenia can occasionally happen with both taxanes and also a drop in the level of platelets can occur with both drugs especially when they are administered in combination with carboplatin. Bone marrow colony stimulating factors such as G-CSF and GM-CSF can be used prophylactically to counteract these bone marrow toxicities.

Beginning approximately 24–48 h after the completion of paclitaxel treatment, patients may experience arthralgias/myalgias, often referred to as "flu-like symptoms"[184,185]. The most commonly prescribed treatment to combat this arthalgia and myalgia is via the use of NSAIDs. In

one study, approximately 80% of patients receiving an oral prednisone regimen, 10 mg twice a day for 5 days beginning 24 h after the completion of chemotherapy, noted a reduction in the severity of their previously experienced paclitaxel-associated arthralgias/myalgias.

Peripheral neuropathy can occur in patients treated with both taxanes but is more common with paclitaxel treatment. This neurotocixity is often worse when paclitaxel is used in combination with carboplatin and over shorter infusions. Although there is no treatment available to prevent or reverse this, after cessation of taxane the neuropathy gradually recedes[186].

During the early development of docetaxel, it was noted that a subset of patients developed serious problems with fluid retention, including peripheral oedema, ascites and pleural effusions[184,187,188]. This largely relies on the dose of docetaxel administered and can be avoided by administering dexamethasone prior to treatment.

Most drug interactions associated with the taxanes have been with paclitaxel. The most significant of these is between paclitaxel and doxorubicin which has been highly effective in treating breast cancer eliciting response rates ranging from 58-94%[189,190]. However these incredibly promising response rates are marred by the prevalence of cardiac toxicity associated with this combination. Dose schedule and sequence are important considerations to be investigated when optimising efficacy and minimising toxicities when using chemotherapy[191].

## 1.6 Breast cancer: no longer a single disease – impact of molecular profiling of breast tumours and cell lines.

Breast tumours exhibit a wide degree of heterogeneity and diversity on both a cellular and a molecular level and a large number of genes are involved in the complex processes of cellular proliferation, death and differentiation.

How the molecular biology of breast tumours correlates with phenotype, prognosis and clinical outcome is a complex issue. A number of key parameters have been successfully correlated to prognosis including; protooncogenes like HER2[192], mutations in the tumour suppressor gene TP53[193,194], the oestrogen inducible gene cathepsin D (an oestrogen inducible gene)[195], steroid and GF expression[196,197], histological[307] grade and metastasis to the lymph nodes. However, the power of the prognostic value is lost due to any internal correlations in large multivariate analyses[198,199].

In the last decade, gene expression profiling of breast tumours has emerged as a powerful tool that can be used to correlate tumour characteristics to clinical outcome in patients[200]. A number

of prolific studies using DNA microarrays have allowed a novel and distinct molecular portrait of breast cancer to begin to emerge[200,201,202].

One seminal study used cDNA from 78 cancers, 3 fibroadenomas and 4 normal breast tissue and cDNA was extracted and hybridised to microarrays[200]. Using the intrinsic gene set of 456 cDNA clones, selected to optimally identify the intrinsic characteristics of breast tumors, the 78 carcinomas and seven non malignant breast samples were analysed by hierarchical clustering[203] and the resulting data was used to correlate with clinical outcome. Figure 1.8 shows the cluster dendrogram of these 85 samples showing that they separate out into five/six distinct subtypes. These six subtypes were; basal, HER2/ERBB2 +ve, luminal A, Luminal B/C, and normal breast like[200].

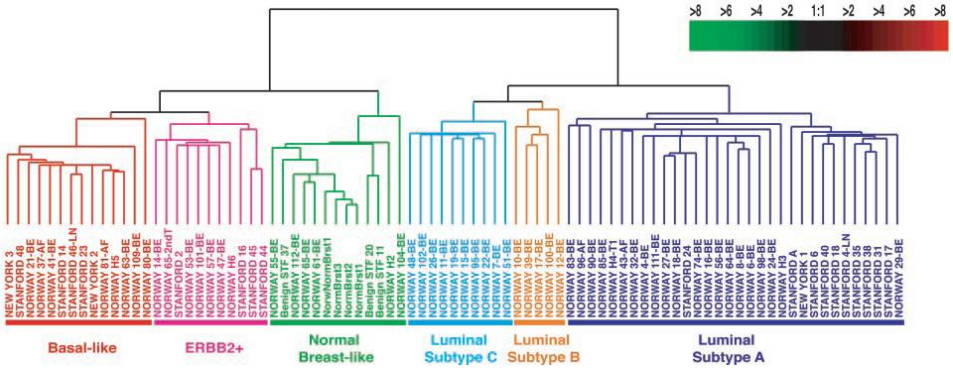


**Figure 1.8** Gene expression patterns of 85 experimental samples representing 78 carcinomas, 3 benign tumors, and 4 normal tissues, analyzed by hierarchical clustering using the 476 cDNA intrinsic clone set. The tumor specimens were divided into 5 (or 6) subtypes based on differences in gene expression. The cluster dendrogram showing the 5 (6) subtypes of tumours are coloured as: luminal subtype A, dark blue; luminal subtype B, yellow; luminal subtype C, light blue; normal breast-like, green; basal-like, red; and ERBB2+, pink[200].

Sørlie *et al* then went onto perform a survival analyses based on the gene expression signatures obtained from this set of microarray experiments, on a subcohort of patients with locally advanced breast cancer. Figure 1.9 shows the Overall Survival (OS) and Relapse Free Survival (RFS) obtained from this data set[200].

The data shows significantly different outcomes for patients belonging to each group. Patients designated to the basal like and HER2/ERBB2 positive subgroup had the worst prognosis.

Notably, the two estrogen receptor positive groups, luminal A (Dark blue) and luminal B and C (light blue) showed a very interesting disparity in outcome with the luminal A tumours having a significantly better prognosis than luminal B and C tumours.

Two years later Sørlie *et al* went on to publish further, more refined data on a larger set of 115 breast tumours. This data was based on a subset of 534 "intrinsic genes" and again showed the division into five distinct groups; luminal A, luminal B, ERBB2/HER2+ve, Basal and Normal Breast like. This study found that basal tumours had the worst prognosis, luminal B tumours had a moderate prognosis and luminal A tumours had the best prognosis26/240[208].

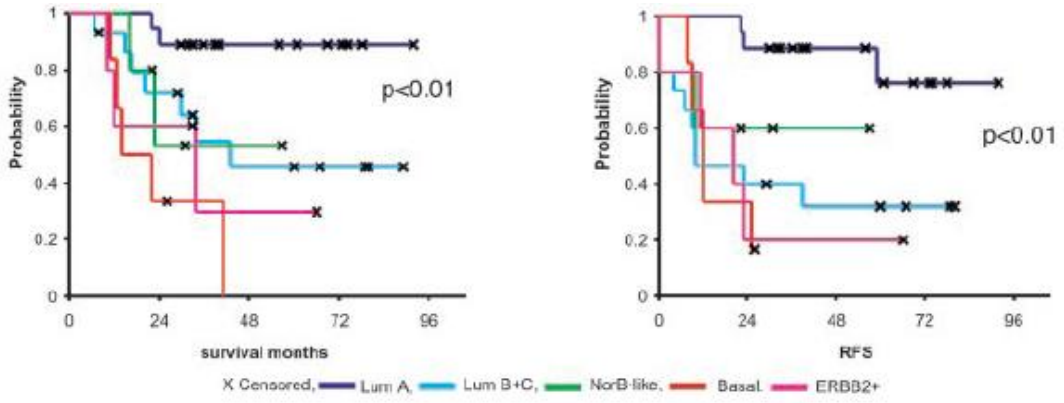


**Figure 1.9.** Kaplan Meier curves showing Overall Survival (OS) on the left hand panel. and Relapse Free (RFS) on the right hand panel patients divided into one of five groups based on gene expression signatures obtained from microarray data Luminal A tumours are represented by the purple line, Luminal B and C are represented by the bright blue line, normal breast tissue samples are represented by the green line, basal tumours are represented by the red line, and HER2/ERBB2 positive tumours are represented by the pink line[200].

In addition, they ascertained that BRCA1 tumours were associated with a basal profile[204]. These series of experiments also identified tumours that could not be classified into one of the five original groups (shown in gray re. figure 1.10). These "unclassifiable" tumours prove intriguing as they emphasise the need to elucidate further indicators in gene expression signatures that will reflect the true complexity of the heterogeneity of the breast tumour population. More complex gene signatures that correlate with clinical outcome should in theory give rise to more distinct subgroups of tumours and as such allow clinician to customise the patient to a individual treatment regimen.

These gene expression profiling experiments illustrated the potential for developing more complex gene signatures which could improve and refine breast cancer taxonomy and allow patients to be allocated into a group of individuals with a similar predicted clinical outcomes[200,198].

Using similar technology, there is potential for identifying smaller and more distinct subgroups of patients combined with detailed clinical information. With this, the opportunity arises for clinicians to tailor a "bespoke" treatment to each individual patient.

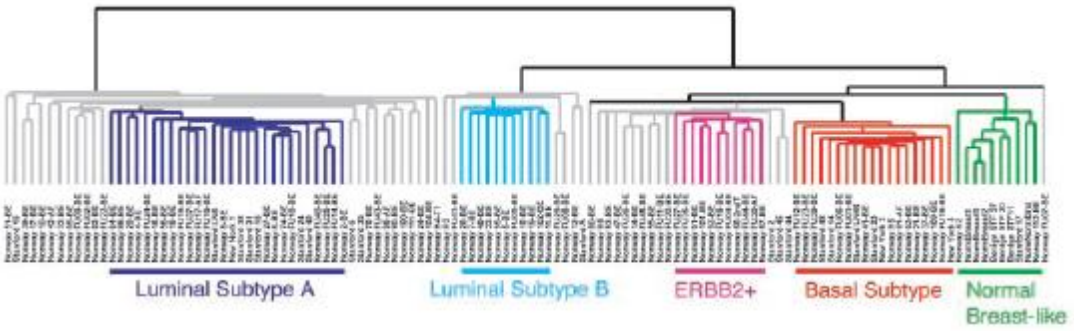


**Figure 1.10** Cluster Dendrograms: Heirarchical clustering of 115 tumour tissue and 7 non-malignant tissues using the "intrinsic gene set." Experimental dendrogram showing the clustering of the tumours into five subgroups. Branches corresponding to tumours with low correlation to any subtype are shown in gray[201].

This could extend the potential of gene expression profiling from deriving a prognostic to a predictive value for the patient and would allow clinicians to potentially predict whether patients in certain subgroups would have a better or worse prognosis to a particular therapy. In recent years the potential for gene signatures to be used to guide the use of chemotherapeutics has grown however, arguably this in part has been harmed by the disappointing withdrawal of the controversial paper by Potti *et a*[205].

It is also possible to use similar technology to classify breast cancer cell lines into distinct breast tumour subgroups[199]. This group looked at recurring genomic and transcriptional characteristics of 51 breast cancer cell lines and 145 primary breast tumors and showed that, although some significant differences were identified the tumours and cell lines to an extent mirrored each other[199]. The cell lines that comprise the system also exhibit the substantial genomic, transcriptional, and biological heterogeneity found in primary tumors.

This study was valuable as it suggested that cell lines could be used as a model for particular subsets of breast tumours. Gaining a clearer understanding of how patterns of gene expression in particular subsets of tumours/cell lines function within a biological, heterogenous setting will allow researchers to improve the management of breast cancer by modulating the response to therapy[199]. Genome expression profiling may prove to be a powerful tool in model *in vitro* systems to allow identification of different subgroups of cell lines that may or may not respond to therapy, such as the taxanes. Obtaining a molecular portrait or signature of taxane resistant cell lines could be extremely valuable in helping discover potential molecular pathways that are implicated in resistance mechanisms.

# Chapter 2

## Materials and Methods

## 2.1 Cell Culture.

### 2.1.a.i Maintenance of cell lines

In the original plan for this project a panel of five cell lines were selected to generate taxane resistant cell lines:

- BT20 – Basal A, (triple –ve)
- BT474 – Luminal, ( ER+ve),
- **MDA-MB-231 , Basal B (ER-ve, Her2 –ve)**
- MDA-MB-453, Luminal (ER +ve,)
- **ZR75-1 – Luminal B – (ER+ve, Her2 -ve.)**

All five cell lines were maintained in 25cm$^2$ flasks in 6mls of Dulbecco's Modified Eagle Medium (D-MEM) 1X liquid (High Glucose) (Gibco 21969-035.) Each bottle of D-MEM was supplemented with 10% heat inactivated Hi-Foetal Calf Serum (FCS) (Gibco 10108-165), 5ml penicillin-streptomycin combined antibiotic (Gibco 15070063) and 5ml L-glutamine (Gibco – 25030024.) All cell lines were maintained at 37°C in a 5% $CO_2$ atmosphere.

### 2.1.b.i Passaging of cell lines

When cell lines reached 70-80% confluency the media was discarded and then they were washed twice in PBS and aspirated. 2mls (3mls for a 75cm$^2$ flask and 6mls for a 175cm$^2$ flask) of trypsin 0.25% EDTA (Gibco-25200072) were added to each flask. Flasks were placed in the incubator for 3 minutes to allow cells to detach. Flasks were then removed from the incubator and the trypsin was neutralised using 3mls (4mls for a 75cm$^2$ flask and 7mls for a 175cm$^2$ flask) of DMEM as above. Cells were then pipetted into a fresh 15 ml tube and centrifuged at 1000 x G. The supernatant was discarded and the cell pellet was resuspended in the appropriate volume of DMEM in preparation for splitting into new flasks.

### 2.1.c.i Cell preservation in and recovering cells from liquid nitrogen.

Cells from 4 x 25cm$^2$ flasks were trypsinised as shown in section 2.1.b.ii but after centrifugation each flask was resuspended in 1ml of recovery cell culture freezing media (Gibco - 70% basal medium, 20% FBS, 10% DMSO - 12648010) and placed in individual cryovials on ice. Each cryovial was labelled with the type of cell line, the taxane resistance dose, passage number, date of freeze down and the initials of the person freezing them down. Each vial was placed in a cell freezing device (Nalgene® Mr. Frosty C1562) which was placed in the -80°C freezer for two days. The cells were then taken from the -80°C freezer and placed in the liquid nitrogen storage facility and the location of each vial was recorded in the liquid nitrogen database.

To recover cells from liquid nitrogen the position of each was located on the liquid nitrogen database and was removed from the tank and placed on ice to take up to the cell culture facility. The vial was then washed in 1.5ml of warm DMEM and resuspended in 1ml of DMEM and placed in a further 5mls of DMEM and added to a 25cm$^2$ flask.

### 2.1.d.i Preparation of cells for treatment with taxanes

Cells were routinely passage until ready for treatment with one of the taxanes: paclitaxel or docetaxel, media was replenished twice weekly or as required.

### 2.1.d.ii Preparation of taxanes

A 300μM stock of each drug was made up as follows. 1mg paclitaxel (Sigma 417017, Chemical formula $C_{47}H_{51}NO_{14}$, MW – 853.906) was dissolved in, 3905μl DMSO and stored in 350μl aliquots. 5mg docetaxel – (01885 – 5mg Sigma.) Docetaxel Chemical Formula $C_{43}H_{53}NO_{14}$, MW – 807.879) was dissolved in 20.6 ml DMSO and stored in aliquots of 350μl. Aliquots of both drugs were stored at -20°C in a black box to protect them from light degradation. A 100μM substock of both drugs was then prepared by adding 330μl of 300μM drug to 670μl DMSO and then stored in freezer and wrapped in foil and then stored at -20°C wrapped in foil until used to prepare additional dilutions as required. 100nM or 1μM working stock was prepared in DMSO and stored at 4°C for ~1 week wrapped in foil. Table 2.1 illustrates the appropriate doses for treatment in a 25cm$^2$ flask.

| CONC | DILN | CONC | DILN | CONC | DILN | CONC | DILN |
|---|---|---|---|---|---|---|---|
| **0.5nM** | 30µl | **8nM** | 480µl | **28nM** | 168µl* | **80nM** | 480µl* |
| **1nM** | 60µl | **10nM** | 600µl | **30nM** | 180µl* | **90nM** | 540µl* |
| **2nM** | 120µl | **12nM** | 720µl | **35nM** | 210µl* | **100nM** | 600µl* |
| **3nM** | 180µl | **15nM** | 900µl | **40nM** | 240µl* | **120nM** | 720µl* |
| **4nM** | 240µl | **18nM** | 108µl* | **50nM** | 300µl* | **150nM** | 900µl* |
| **5nM** | 300µl | **20nM** | 120µl* | **60nM** | 360µl* | **180nM** | 1080µl* |
| **6nM** | 360µl | **25nM** | 150µl* | **70nM** | 420µl* | **200nM** | 1200µl * |

**Table 2.1** Doses and concentrations for taxane treatment in a 25cm$^2$ flask containing a total of 6ml media, including taxane. Doses marked with an * require being made up using the stronger 1µM working solution**.**

**2.1.d.iii Generation of taxane resistance through dose escalation and maintenance of cells during taxane exposure.**

Each cell line was exposed to a dose of 1nM taxane supplemented in their culture media. Surviving cells maintained in drug for several weeks whilst quiescent. If no cells survived the initial treatment with 1nM a lower dose of 0.5nM was explored. For 3 cell lines: MDA-MB-453, BT474 and BT20, no dose at which a proportion of cells survived could be identified and these cells were rejected as unable to adapt to taxane exposure. However, for three cell lines even after reducing the dose of taxanes to 0.5nM, cells were consistently killed and no resistant cells were derived despite several attempts. These cell lines were therefore rejected.

For cell lines exposed to taxanes, cells were maintained in taxane containing media at the original dose until evidence of cell growth was observed. Even when cells were not growing, the media containing the same drug dose of taxane was replaced biweekly to refeed the cells. Refeeding the cells involved aspirating off the old media, washing the cells twice in PBS and

replacing the media containing the taxane. Once cells were growing successfully in taxanes, they were passages, multiple aliquots of "resistant" cells were frozen and the dose of taxane increased. This process was repeated using the experimental schedule shown in the diagram in figure 2.1 until cells reached levels of taxane "resistance" sufficient for experimentation to commence.

Only two of the five cell lines successfully adapted to sequentially increased doses of taxane treatment and went onto develop resistance to taxanes; MDA-MB-231s and ZR75-1s. Paclitaxel resistant MDA-MB-231, paclitaxel resistant ZR75-1 and docetaxel resistant ZR75-1 were successfully generated. The MDA-MB-231 cell line has been designated mesenchymal like and the ZR75-1 cell line was derived from ductal carcrinoma[206]. These cell lines were generated by treating the native parental cell lines with incrementally increasing doses of taxane in the experimental schedule shown in the diagram in figure 2.1.

At each point along this dose regimen cells were frozen down and stored in liquid nitrogen so that the entire spectrum of taxane resistant cells was available for future experimentation. The MDA-MB-231 PACR cell line achieved a highest paclitaxel resistance dose of 100nM (indicated by the turquoise ring in figure 2.1), the ZR75-1 PACR and DOCR cell lines achieved a highest resistance dose of 50nM. These experiments focused primarily on the 25nM resistant cells which were determined to be the most clinically relevant dose of taxane. A suboptimal dose of 5nM, a "superoptimal" dose of 50nM and the native, taxane sensitive cells were included, these selected doses are illustrated in figure 2.1 indicated by the pink rings.

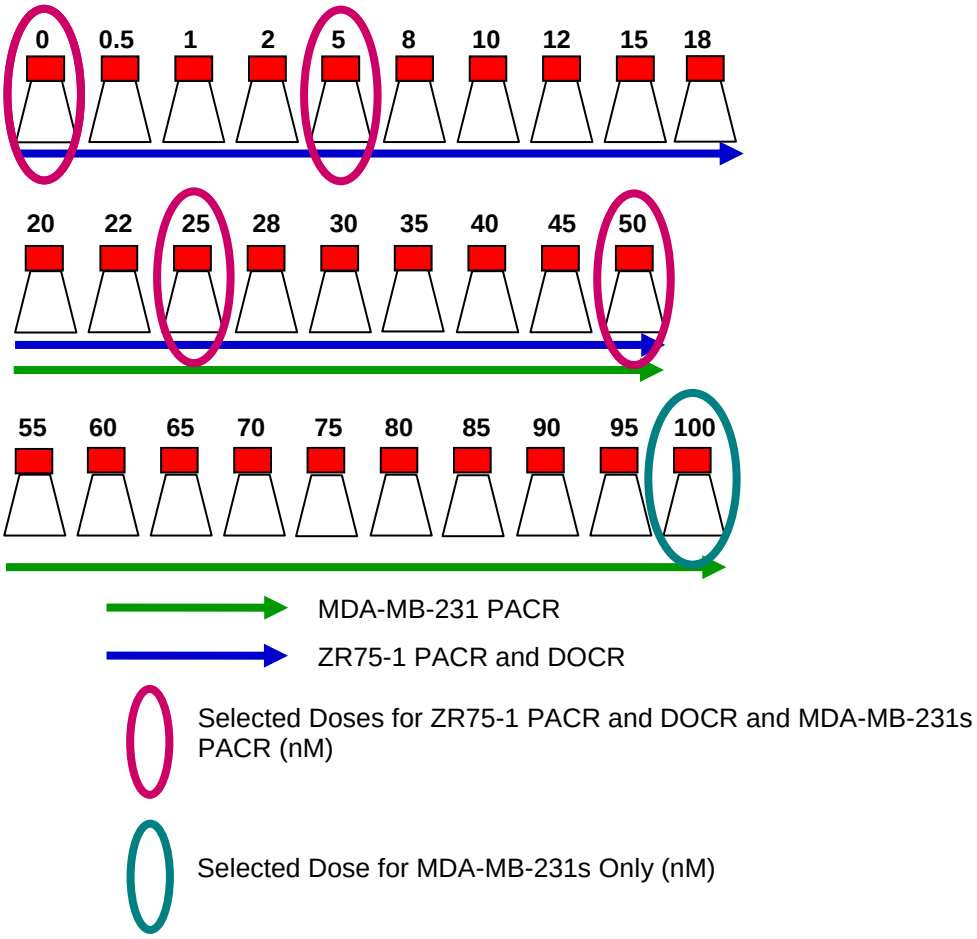


**Figure 2.1** Incremental dose escalation of taxane to generate isogenic taxane resistant cell lines. Green line indicates the extent of paclitaxel resistance achieved in the MDA-MB-231 PACR cell line. The blue lone indicates the extent of paclitaxel and docetaxel resistance achieved in the ZR75-1 PACR and DOCR cell lines. The pink rings indicate the selected doses of interest for the MDA-MB-231 PACR, ZR75-1 PACR and DOCR cells. The turquoise ring indicates the additional 100nM Paclitaxel dose selected for further research in the MDA-MB-231 paclitaxel resistant cells alone.

### 2.1.e.i Counting cells using a Coulter counter

When setting up large scale cell culture experiments a Beckman Coulter, counter was used to count cells. Cells were trypsinised as described in section 2.1.b.i and resuspended in DMEM and made up to 10ml. The cell suspension was then passed three times through a 10ml syringe with a green 21 gauge needle. 200µl of the cell suspension was then placed in a coulter pot containing 9.8mls of 0.9% NaCl and counted in triplicate on the Beckman Coulter Z2 series coulter counter. The mean cell count was recorded. The cell size on the counter was set between 9 and 21µM. The multiplication factor of the coulter counter is 100 x to give the cell concentration per ml. For smaller experiments the same method of preparation was used but the cells were counted on a haemocytometer.

### 2.1.e.ii Setting up MDA-MB-231 cells for cell count experiments

Preliminary cell count experiments suggested that the optimal duration of taxane treatment, that exerted the most cytotoxic effect was 96 hours after first cells plating down for 24 hours in the media in which the cell line is normally grown.

All cell count experiments were set up in the same way. Cells from each cell line used in the experiment were harvested by trypsinisation and seeded at a concentration of 10,000 cells per $25cm^2$ flask in the appropriate media (in which they are usually grown) for 24 hours. Each flask was then washed twice in PBS and incubated in DMEM containing the appropriate dose of drug. For each cell line and each dose of drug there were quadruplicate flasks.

The first exploratory cell count experiment looked at a short term exposure of paclitaxel to the MDA-MB-231 native, 5, 25 and 100nM PACR cell lines. The cells were exposed to drug for 24 hours using four doses of paclitaxel, 0, 5, 25 and 100nM paclitaxel.

This experiment was dissected further by looking at the native and 25nM PACR MDA-MB-231 cells for the extended drug treatment of 96 hours. Each group of quadruplicate flasks was treated with one of six doses of taxane; 0, 3, 5, 10, 25 or 50nM of paclitaxel. Each flask of cells was harvested and used in cell cycle analysis experiments using flow cytometry, details of which are noted in section 2.1.g.

The native and 100nM PACR cells were then investigated. After plating down 10,000 cells per $25cm^2$ flasks for 24 hours in the medium in which they are normally grown and then washing twice in PBS and re-plating in one of six doses of taxane for 96 hours namely 0, 1, 3, 5, 10, 15 or 30nM paclitaxel. Each flask of cells was harvested and used in cell cycle analysis experiments using flow cytometry, details of which are noted in section 2.1.g.i-2.1.i. A different panel of taxane doses were used in this experiment to respond to the previous results obtained from the flow cytometry, cell cycle analysis part of the previous experiment, using the native and 25nM PACR cells. A narrower range of paclitaxel dose was used in this experiment, as in the previous experiment the greatest amount of cell cycle activity occurred between the 5 and 30nM paclitaxel.

### 2.1.e.iii.Conformation of stable transformation of taxane resistant cells

Once resistant cells had been grown in the presence of taxane for several months they had to be tested to ascertain whether the taxane resistant phenotype was stable when these cells were grown long term in the absence of taxanes. This was tested in the MDA-MB-231 PACR cell lines alone as this was the main cell line of interest in the early stages of our research. To do this the MDA-MB-231 25nM PACR cells were split by trypsinisation and dividing the cell pellet in two.

The first half of the cell pellet was reseeded in a flask containing 25nM paclitaxel as normal and was passaged as normal in culture for 6 months. The second half of the pellet was reseeded in a flask containing blank media and no paclitaxel, this culture was then passaged as normal and maintained in the absence of drug for 6 months in tandem with the cells maintained in the presence of drug.

An experiment was set up to rechallenge these 25nM PACR cell lines with paclitaxel to confirm whether the acquisition of taxane resistance resulted in a stable change in phenotype. The 25nM PACR MDA-MB-231 cells that were maintained in the drug free media were designated "MDA-MB-231 25nM PACR DF" to distinguish them from the other paclitaxel resistant cells. The 25nM MDA-MB-231 PACR cells that were maintained in the presence of paclitaxel were included as a positive control and paclitaxel sensitive parental MDA-MB-231 cells were included as a negative control.

Each of the three cell lines were grown in duplicate 75cm$^2$ flasks and harvested by trypsinisation according to section 2.1.b.i. The cells were pooled and counted using a coulter counter (described in section 2.1.e.i) and split into 24 x 25cm$^2$ flasks at a concentration of 10,000 cells per flask. They were grown for 24hrs in the media to which they are grown in normally, namely blank media for the sensitive native and the MDA-MB-231 25nM PACR DF cells and media supplemented with 25nM paclitaxel for the 25nM PACR MDA-MB-231 cells.

After the 24 hours plating down the cells were washed twice in PBS and each group of cells was then plated down in quadruplicate in one of six different concentrations of paclitaxel: 0, 3, 5, 10, 25 or 50nM. The flasks were then incubated for a further 96hrs. Each flask was then trypsinised and counted using a coulter counter as described in 2.1ei. This experiment was repeated twice.

### 2.1.e.iv Setting up ZR75-1 native and 25nM PACR cells for cell count experiments

The cell count experiment for the ZR75-1 native and 25nM PACR was set up in an identical way to the MDA-MB-231 native and 25nM PACR cells as detailed in section 2.1.e.ii. The same duration of drug treatment and concentration of paclitaxel concentration were used. Results are detailed in section 3.2.a.i.

### 2.1.e.v Setting up ZR75-1 native and 25nM DOCR cells for cell count experiments

The cell count experiment for the ZR75-1 native and 25nM DOCR was set up in an identical way to the MDA-MB-231 native and 25nM DOCR cells as detailed in section 2.1.e.iii. The same duration of drug treatment and concentration of paclitaxel concentration were used.

**2.1.f.i Setting up MDA-MB-231 native and PACR and ZR75-1 native, PACR, DOCR cells for illumina experiments**

In the initial exploratory experiment the MDA-MB-231 native, 5nM, 25nM and 100nM were used in duplicate 25 $cm^2$ flasks. In the subsequent, expanded, illumina experiment the following panel of cell lines was grown up in 25$cm^2$ flasks: MDA-MB-231, native, 5nM, 25nM and 50nM PACR; ZR75-1, native, 5nM, 25nM and 50nM PACR and DOCR. The 100nM PACR MDA-MB-231 cells were replaced with the 50nM PACR dose level as the 100nM PACRs had shown anomalous behaviour in terms of their enhanced cell growth in the presence of paclitaxel (re figure 3.3) In addition, using the 50nM dose level allowed the illumina data to be compared with that obtained from the taxane resistant ZR75-1 cells.

The panel of eleven cell lines was grown to 70-80% confluence and trypsinised and collected as a cell pellet according to section 2.1.b.i, extracted according to section 2.3.a.i and amplified according to section 2.3.a.ii. The process of growing up the cells was repeated a further three times to give four biological replicates. It is important to note that cells grown in flasks should always be trypsinised prior to RNA extraction using a RNeasy Qiagen mini kit and the pellet should be washed in PBS and spun down again to remove all the remaining trypsin.

**2.1.f.ii Setting up MDA-MB-231 native and PACR and ZR75-1 native, PACR, DOCR cells for aCGH experiments.**

The cell lines were grown up in the same way as for the illumina experiments (re 2.1.f.ii) and harvested via scraping prior to extraction of the DNA using the Qiagen Blood and cell culture DNA maxi kit (13362.) Samples were maintained in TE buffer pH 8.0.

**2.1.f.iii Setting up MDA-MB-231 native, PACR and DOCR cells for qPCR**

The same panel of cell lines was grown up and extracted as detailed in 2.1.f.i in quadruplicate and pooled. QPCR was then performed as detailed in section 2.3.d.i.

**2.1.f.iv Setting up MDA-MB-231 native, PACR, and DOCR cells for Western Blotting.**

The same panel of cell lines was grown up according to section 2.1.f.i, harvested and lysed according to section 2.3.f.i and run on Western blots according to section 2.3.f.ii-2.3.f.viii.

**2.1.g.i Cell Preparation for Cell Cycle Analysis**

Cells were prepared, and harvested in tandem with cell count as detailed in section 2.1.e.ii, 2.1.e.iv and 2.1.e.v experiments according to section 2.1.e.ii, Cells were counted with a Coulter counter (according to section 2.1.e.ii, 2.1.e.iv and 2.1.e.v) and between 0.5 and 1 million cells were retained from each sample. They were spun down in FACS tubes at 1,000 x g and suspended in 200µl citrate buffer covered in parafilm and stored at -20°C prior to analysis.

### 2.1.g.ii The Vindelov's method of cell preparation for flow cytometry.

Two common methods of preparing cells for cell cycle analysis using a FACS machine are ethanol fixation and Vindelov protocol[207]. From my previous experience working with both methods, I concluded that the Vindelov method was preferable for a number of reasons. Generally speaking, the Vindelov method achieved more consistent reproducible results with appreciably lower %CV than ethanol fixation. Cells also tended to clump much more with the ethanol fixation method which is problematic when analysing the cells.

The Vindelov's methods uses three different treatment solutions; A, B, and C. Solution A trypsinises the cells and separates the sample into a single cell suspension, solution B neutralises the trypsin, and solution C stains the cells with Propidium Iodide. Propidium Iodide is a stain which interchelates into the DNA of cells. When excited by blue laser light (488nM) the PI dye fluoresces in FL2. The intensity is proportional to the DNA content of the cells. The detectors in the electronic system convert detected light into proportional electronic signals. Information on the % coefficient of variation (%CV) and linearity (relationship between the channel number of a particular population and the intensity of the measured parameter are required for the quality control of the data. Each of the solutions A, B and C was defrosted, keeping solution C on ice after thawing. The samples (in citrate buffer) were defrosted at RT.

**Citrate Buffer:** 85.5g sucrose (S9378, Sigma Aldrich, Poole, Dorset, UK) and 11.76g trisodium citrate (301287F, BDH Laboratory Supplies) were dissolved in 800mL distilled water and pH was adjusted to 7.6 using [HCl]. This solution was then made up to 1000mL with $dH_2O$.

**Stock solution:** 2000mg of trisodium citrate (301287F, BDH Laboratory Supplies), 121mg Trizma ® base (T1378, Sigma Aldrich), 1044mg spermine tetrachloride (S2876, Sigma Aldrich), and 2mL Nonidet NP40 (N3516, Sigma Aldrich) were dissolved in 1800mL distilled water. The pH was adjusted to 7.6 and made up to 2000mL with distilled water.

**Solution A:** Prepared by dissolving 15mg of trypsin (T0303, Sigma Aldrich) in 500mL of Stock solution pH 7.6 and was dispensed into 20mL aliquots and frozen at -20°C.

**Solution B:** Prepared 250mg trypsin inhibitor (93621 Fluka Chemicals, Poole Dorset, UK) and 50mg RNAse A (R4875, Sigma Aldrich) in 500mL stock solution pH 7.6 and was dispensed into 20mL aliquots and frozen at -20°C.

**Solution C:** Prepared by dissolving 208mg propidium iodide (81845, Fluka Chemicals) and 500mg spermine tetrahydrochloride (S2876, Sigma Aldrich) in 500mL Stock Solution pH 7.6, and was dispensed into 20mL aliquots and frozen at -20°C.

In the initial experiment CRBC, TRBC or human lymphocytes were added as internal DNA ploidy standards. A "prep" test was also conducted to ascertain the most appropriate time for trypsinisation in the first step of the protocol. In this case, three untreated native ZR75-1 samples, in triplicate, were treated with 450µl of solution A, briefly vortexed and incubated for between 1, 2 or 6 minutes. The most appropriate time for trypsinisation was determined to be 2 minutes and this was then used for all further experiments.

375µl of solution B was then added to each sample, vortexed and then incubated for a further 10 minutes. 250µl of solution C was then added to each sample, briefly vortexed and was then incubated on ice in the dark for a further ten minutes. They were kept on ice prior to analysis.

#### 2.1.g.iii. Analysing cells prepared with the Vindelov's protocol using flow cytometry

MDA-MB-231 cell samples, which were analysed early on in my PhD were immediately analysed in FACScalibur (Becton Dickinson) and the data was obtained with the cellQuest 1.2.2 programme. Results were analysed using ModFit LT1.01. The ZR75-1 cell samples, which were obtained later on in my PhD, were analysed by Elisabeth Freyer at the MRC using the FACAria machine (also from Becton Dickinson) and data was obtained using the FlowJo programme. This was because the cellQuest programme was no longer available as the computer that was used with it had become obsolete.

#### 2.1.h.i. Statistical analysis of cell count and cell cycle analysis data.

On each of the cell count and cell cycle experiments (detailed in 2.1) a 2 way Anova (F test) with replication was performed using Excel 2007[313]. The two parameters for the ANOVA tests with the cell count experiments were cell line and taxane dose and the two parameters for the cell cycle analysis were stage of the cell cycle and taxane dose. There were four replicates for each sample and the value was set at 0.05%. 2 way Anovas using Excel, using dose and cell lines as the two dimensions.

### 2.2 Generating taxane resistant xenografts.

#### 2.2.a.i Establishing MDA-MB-231 native and 25nM PACR cells as xenografts in mice

Having established that MDA-MB-231 25nM PACR DF cells could be grown long-term in the absence of paclitaxel and still retained their paclitaxel resistant phenotype (section 2.1.e.iii.) Establishing this fact allowed me to design experiments to take our isogenic paclitaxel resistant cell lines in to an *in vivo* setting by growing the cell lines as xenografts in mice.

For the first experiment to establish the cell lines as xenografts the MDA-MB-231 native and MDA-MB-231 25nM PACR cells were grown to 70-80% confluence in 14 x 175 $cm^2$ flasks to produce an excess of cells for implantation. Each flask for the two cell lines were trypsinised

(details in section 2.1.b.i) and pooled separately. The cell suspension was then passed three times through a 50ml syringe with a green 21 gauge needle and counted using a haemocytometer to determine the cell concentration. The appropriate volume of cells was then centrifuged for 5mins at 8,000 x G and washed in PBS, this was then repeated twice and the cell pellet was resuspended in 2,500 µl of DMEM (including an excess to compensate for dead volume in the injecting syringe.)

5 x CD-1 Nude female mice were assigned to each group, one to be injected with MDA-MB-231 native cells and the other to be injected with MDA-MB-231 25nM PACR cells. Recommendation from colleagues who had previously generated xenograft tumours from breast cell lines suggested that between 5 and 10 million cells per flank should be injected into the mice.

10 million cells in 200µl DMEM were injected subcutaneously in each flank of the five mice in each group to generate a maximum of 10 tumours for each cell line. The tumour size was then measured biweekly until a maximum end diameter of 1.44$cm^3$ was achieved. At this point the tumour was then removed and split in two: one half to be retained in liquid nitrogen and then other to be formalin fixed and paraffin embedded to be prepared and cut for microarrays. Unfortunately, the xenografts in the MDA-MB-231 25nM PACR group failed to grow even after an extended period of growth of 67 days. At this point all the remaining mice were culled and the tumours were retained as detailed above. The implantations of mouse xenografts and drug treatment (detailed in subsequent sections) were carried out by Morwenna Muir at the Biomedical Research Facility. The author is very grateful for all her hard work and dedication in carrying out this work and caring for the animals.

### 2.2.a.ii Establishing MDA-MB-231 native and 25nM PACR cells as xenografts in mice using matrigel

As the 25nM PACR MDA-MB-231 cells failed to grow in mouse xenografts I designed another experiment incorporating the extracellular matrix matrigel as a growth medium to increase the likelihood of establishing taxane resistant cell lines in mice. Cells were grown up, harvested and counted as detailed in section 2.2ai. For both cell lines 2 x 10 million cells each diluted in 100µl DMEM were injected subcutaneously into the left flank of 5 x CD-1 Nude mice. This process was then repeated for another 5 mice for each of the two cell lines, this time mixing the 100µl of cells in DMEM with an equal volume of matrigel, maintained on ice throughout and injected them into the right flank of the mice (BD Biosciences – 304234.) The tumours were then measured biweekly as in shown in section 2.2.a.i.

The MDA-MB-231 25nM PACR tumours still failed to grow even in the presence of matrigel as a growth medium and after 31 days all four groups of mice were culled and their tumours were retained as detailed in section 2.2.a.i.

In one final attempt to establish the PACR MDA-MB-231 cells as xenografts this experiment was repeated, as detailed in this section with a reduced number of cells, this time only injecting 5 million cells per flank. Cells for each injection were suspended in 100µl DMEM and an equal volume of matrigel and this time only 4 animals were included for each cell line (MDA-MB-231 native and 25nM PACR) giving a total of 8 tumours per cell line group.

### 2.2.b.i Establishing ZR75-1 native and taxane resistant cells as xenografts in mice using matrigel

As the 25nM PACR MDA-MB-231 cells failed to grow as xenografts in mice the ZR75-1 cells were used as an alternative. This was problematic in one respect as these cells had not previously grown in the absence of taxane long term to establish whether they would retain their taxane resistant phenotype when transplanted into animals. These experiments were carried out toward the end of the PhD and there was not sufficient time to repeat the same experiment for the taxane resistant ZR75-1 cell lines and maintain them long term in the absence of drug before implanting them in the animals. However, the experiments progressed and xenograft experiments using the ZR75-1 cell lines were designed and carried out.

Once the cell lines became established as xenografts after implantation they could be tested to establish whether the taxane resistant phenotype had been retained by treating the animals with taxane and seeing if there was a perceived difference in response to taxane treatment in the taxane resistant and native xenograft animals. The additional benefit of working with the ZR75-1 cells was that both paclitaxel resistant and docetaxel resistant cells cold be included in this series of experiments.

### 2.2.b.ii Initial investigative growth curve for ZR75-1 native, 25nM PACR and DOCR resistant cells as xenografts in mice using matrigel.

2 batches of native cells (a control for each taxane resistant cell line) and one batch each of 25nM PACR and DOCR cells were bulked up in 175cm$^2$ flasks. They were then trypsinised and harvested according to section 2.2.a.ii. We assigned four mice to each of the four groups of cell lines. Each mouse was injected in both flanks with one of the four cell lines with 5 million cells in 100µl DMEM mixed with an equal volume of matrigel.

As the ZR75-1 cell line is oestrogen dependent, the mice were administered with a 17-β oestradiol 60 day slow release pellet (0.72mg/pellet SE-121 Innovative research of America) at

the time of implantation. The size of each xenograft tumour was measured biweekly. The xenografts were maintained until they reached maximum size 1.44$cm^3$ and were culled at day 32 post-implantation, the tumours were retained as detailed in 2.2.a.i. Each of the four cell lines grew in a very similar way to one another. These xenografts grew very rapidly which caused us to consider lowering the number of cells at implantation.

**2.2.b.iii Establishing optimal cell numbers at implantation for ZR75-1 native, 25nM PACR and DOCR resistant cells as xenografts in mice using matrigel.**

Although it was a positive result to establish ZR75-1 25nM PACR and DOCR cell lines and their native counterparts as xenograft models in mice, when they were implanted with 5 million cells per injection the resulting xenografts grew very rapidly. As a result we sought to obtain the optimal number of cells for implantation that would allow reasonable tumours to develop and grow at a rate that would allow a window of opportunity to treat the mice with taxanes before the tumours grew too large and began to ulcerate. To do this only the native ZR75-1 cell lines were looked at, as in the initial growth experiment detailed in section 2.2b.iii showed that the native, PACR and DOCR ZR75-1 cell in xenograft grew in a very similar way to one another.

Three groups of animals were established and two animals were assigned to each group. ZR75-1 native cells were bulked up in 6 x 175 $cm^2$ flasks trypsinised and harvested as detailed in section 2.2.a.i. The first group of mice were implanted with 0.5 million cells, the second group of animals were implanted with 1 million cells and the final group was implanted with 2 million cells in each flank. The xenografts were grown for 49 days, this allowed it to be established which was the appropriate number of cells to implant in future experiments. Tumours were not retained as the material was not of any real interest for further experimentation.

**2.2.b.iv Taxane cross resistance experiment in taxane resistant ZR75-1 mouse xenografts.**

From our previous experiment detailed in section 2.2b.iii it was determined that the appropriate number of ZR75-1 cells to be implanted was 1 million per flank. 3 identical experiments were set up; one using the native ZR75-1 cells, one using the 25nM PACR cells and one using the 25nM DOCR cells. In each of the three experiments three groups of mice were established: group A to be treated with a drug free vehicle, group B to be treated with paclitaxel and group B to be treated with Docetaxel. Four animals were assigned to each of the three groups. Details of how the drug free vehicle, paclitaxel and docetaxel are made up are detailed in section 2.2.b.v. The mice treated with paclitaxel were treated with a dose of 20mg/kg whereas the mice treated with docetaxel were treated with a dose of 10mg/kg, this is to account for the fact that docetaxel is between two and four times as potent as paclitaxel.

Native, 25nM PACR and DOCR cells were bulked up in 6 x 175cm$^2$ flasks and trypsinised and counted according to section 2.2.a.i. 2 injections were given to each animal, one in each flank. 1 million cells were administered per injection in 100 µl DMEM mixed with an equal volume of matrigel. At the time of implantation the mice were administered a 17-β oestradiol 60 day slow release pellet. The tumours were then left to grow for 11 days to establish prior to treatment with one of the three drugs, or drug free vehicle treatments.

### 2.2.b.v Preparation of taxanes for cross resistance experiment in taxane resistant ZR75-1 mouse xenografts

After the 11 days of tumour growth each of the mice were then treated by subcutaneous injection with either: drug free vehicle, 20mg/kg paclitaxel or 10 mg/kg docetaxel. Mice were treated over the course of one week (directly after the 11 days tumour growth post implantation) on days 0, 2, and 4. The drug free vehicle was a 1:1:8 mixture of absolute ethanol for molecular biology (Sigma-Aldrich E7023):cremophor (Sigma-Aldrich 95921): sterile PBS. To make up the paclitaxel, 20mg of dried drug (Sigma Aldrich - Paclitaxel T74025MG) was diluted in 1ml of absolute ethanol. To make up the docetaxel, 10mg of dried drug (Sigma Aldrich – 018555MG Docetaxel) was diluted in 1ml of absolute ethanol. The drugs took some time to dissolve and were then kept as a stock solution at -20°C in a 1.5ml eppendorf wrapped in foil to protect it from light degradation. The drugs were made up fresh immediately prior to injection, they were mixed up with the same 1:1:8 ratio as the drug vehicle with the taxane dissolved in ethanol replacing the drug free absolute ethanol. It is important to note that the PBS should be maintained at RT to ensure that the drug dissolved successfully in the vehicle. On the first day of drug treatment each animal was weighed to determine the correct volume of to make up. The drug was made immediately prior to injection up as detailed previously in this section. To illustrate, a 20g mouse would be given a subcutaneous injection 200µl of vehicle, paclitaxel or docetaxel, and a 30g mouse would be given a subcutaneous injection of 300µl.

The animals were monitored after injection to observe if any harmful reactions to drug or vehicle occurred. The injections were then repeated on day 3 and five of the experiment and then the tumour were measure three times a week until the tumours reached maximum size.

## 2.3. A transcriptomic and genomic analysis of taxane resistant cell lines.

### 2.3.a.i Extracting RNA from Taxane Resistant cell lines for illumina experiments and qPCR.

Cells were grown up according to section 2.1.f.i. The cell pellets were then loosened by flicking the tube (Incomplete loosening of the cell pellet may lead to inefficient lysis and reduced RNA yields) and the appropriate volume of buffer RLT (Qiagen - RNeasy mini kit – 74104) was added to each sample (350µl for < 5 x $10^6$, 600µl 5 x $10^6$.) The sample was then vortexed briefly or

pipetted to mix. Each sample was homogenised by pipetting the lysate directly onto a Qiashredder spin column placed in a 2 ml collection tube (Qiagen – Qiashredder – 79654) and was centrifuged for 2 minutes at full speed on a bench top centrifuge. Note, incomplete homogenization leads to significantly reduced RNA yields and can cause clogging of the RNeasy spin column. Homogenization with a rotor stator or QIAshredder homogenizer generally results in higher RNA yields than with a syringe and needle. 1 volume of 70% ethanol was added to each homogenised lysate and was mixed well by pipetting. Up to 700µl of the sample including any precipitate that may have formed, was transferred to an RNeasy spin column placed in a 2 ml collection tube. The lids were closed gently and the samples were centrifuged for 15secs at 8000 x g (10,000 rpm). The flow through was discarded and the collection tube was reused. 700µl buffer RW1 was added to the spin column and was centrifuged for 15secs at 8000 x g (10,000rpm) to wash the spin column membrane. The flow through was discarded and the collection tube was reused.

500µl buffer RPE was added to the RNeasy spin column and centrifuged at 15secs at 8,000 x g (10,000 rpm) to wash the spin column membrane. The flow through was discarded and the collection tube was reused. 500µl RPE buffer was added to the RNeasy spin column and was centrifuges for 2mins at 8,000 x g (10,000 rpm) to wash the spin column membrane. The spin column was then placed in a new 2ml collection tube (discarding the old collection tube with the flow through. The sample was then centrifuged at full speed for 1 min. The spin column was then placed in a new 1.5ml collection tube and 30-50µl RNAse-free water was added directly to the spin column membrane. The sample was then centrifuged for 1 min at 8000 x g (10,000 rpm) to elute the RNA. If the expected RNA yield was low this step could be repeated. Samples were then placed on ice and a 2µl was retained for analysis using the agilent bioanalyser. The remaining sample was stored at -80°C. The quality of each sample was then analysed using the Agilent bioanalyser to obtain an RIN (RNA Integrity) number.

### 2.3.a.ii Assessing RNA quality and Concentration using the Agilent Bioanalyser.

In preparation for analysis Agilent Reagents were brought to RT for 30 minutes (Agilent – RNA 6000 complete kit – PN 5067-1511.) 550µl of gel (red topped tube) was pipetted directly onto a filtering column and was spun at 3000 x G for 10 min on a benchtop centrifuge and aliquot into 8 equal aliquots and label with the date of filtration. All reagents were applied to the chip using reverse pipetting to reduce eliminate air bubbles from the gel and minimise pipetting loses. RNA samples and the RNA ladder from the agilent kit were taken out of the kit and kept on ice. The gel-dye mix was then prepared by adding 1µl blue dye per 65µl gel per chip. The sample was then vortexed well and spun down at 13,000 rpm (maximum speed on a bench top centrifuge.) The gel-dye mix can be used for 2 chips.

The RNA and the ladder were then denatured by placing them on the heat block at 70°C for 2mins. After 2 minutes they were then placed on ice immediately. Prior to running each chip and after each chip was run the electrodes of the agilent bioanlyser (2100 bioanylser – Agilent) were cleaned by adding 350µl of RNAse Zap solution (Ambion – RNAse Zap 250mls - AM9780) to the cleaning chip for 10secs followed by RNAse free water for 10 seconds. The machine was then left open for 10secs to dry the electrodes. After the gel-dye mix was spun, 9µl of it was applied by reverse piptetting to the well in the chip marker "**G.**" The chip was then pressurised for exactly 30 seconds on the chip priming station. 9µl of the remaining gel dye mix was then applied to the two remaining wells marked with a "G." 5µl of marker was applied to all the remaining wells including the ladder well, and a further 6µl was added to each well that left empty (with no sample.) 1µl of ladder was then applied to the well marked with a picture of a ladder. 1µl of each sample was applied to the appropriate well. The chip was then vortexed for 1 min at 2400 rpm using the vortex supplied by Agilent. The chip was then placed into the machine and the electrophoresis was run, selecting the Eukaryote total RNA Nano II series for total RNA and eukaryote mRNA Nano series for labelled cRNA.

The resulting data was then saved as a PDF to the LabData file. This data allows the RIN (RNA Integrity Number) to be obtained, which is software tool designed to help scientists estimate the integrity of total RNA samples. RIN is measured on a scale of 0-10 with 10 being the highest integrity and 0 the lowest. Determining the RIN means that sample integrity is no longer determined by the ratio of the ribosomal bands, but by the entire electrophoretic trace of the RNA sample, includes the presence or absence of degradation products.

### 2.3.b.i Amplification of RNA extracted from cell lines for illumina analysis using the Ambion TotalPrep RNA amplification Kit

RNA extracted from cell lines was amplified using the Illumina Total Prep RNA amplification kit (Ambion – IL1791.)

### 2.3.b.ii Reverse transcription to synthesis first strand cDNA

A maximum volume of 11µl of total RNA (50-500ng recommended) was pipetted into a non-stick sterile RNAse free, 0.5ml microcentrifuge tube. Nuclease free water was added as necessary to bring all the samples up to 11µl. At RT the Reverse transcription master mix was prepared in a nuclease free tube in the order shown in table 2.2. For each master mix, enough was assembled to account for all samples and a 5% excess was included.

| Reverse Transcription Master mix (for a single 20µl reaction) | |
|---|---|
| Amount | Component |
| 1µl | T7 Oligo (dT) Primer |
| 2µl | 10 x First Strand Buffer |
| 4µl | dNTP mix |
| 1µl | RNase Inihibitor |
| 1µl | Array Script |

**Table 2.2** Reverse Transcription Master mix for a single 20µl reaction using the total Prep RNA amplification kit.

Samples were then mixed well by vortexing and then centrifuged briefly (~5sec) using a microcentrifuge to collect the reverse transcription mastermix at the bottom of the tube and placed on ice. 9µl of reverse transcription master mix was transferred to each RNA sample was mixed thoroughly by pipetting up and down 2 or 3 times, then flicking the tube for 3 or 4 times and centrifuging briefly in a microcentrifuge to collect the reaction in the bottom of the tube. Samples were then placed in a hybridisation oven or air incubator at 42°C and incubated for 2hrs.

### 2.3.b.iii Second Strand cDNA Synthesis

A second strand master mix was prepared in a nuclease-free tube in the order listed in table 2.3.

| Second Strand Master Mix (For a single 100µl reaction) | |
|---|---|
| Amount | Component |
| 63µl | Nuclease Free Water |
| 10µl | 10 x Second Strand Buffer |
| 4µl | dNTP Mix |
| 2µl | DNA Polymerase |
| 1µl | RNase H |

**Table 2.3** Second strand master mix for total prep RNA amplification kit.

The mastermix was then gently mixed by vortexing and centrifuged briefly using a microcentrifuge to collect the sample the bottom of the tube and was then placed on ice. 80µl of the second strand master mix was added to each sample and was mixed thoroughly by pipetting up and down 2 or 3 times, then flicking the tube for 3 or 4 times and centrifuging briefly in a microcentrifuge to collect the reaction in the bottom of the tube. Tubes were then placed in a

thermal cycler. It is important to cool the thermal cycler block for 16°C before adding the reaction tubes as subjecting the reactions to temperatures greater than 16°C will compromise cRNA. Samples were incubated at 16°C in the thermal cycler for two hours, covered with the heated lid turned off.

### 2.3.b.iv cDNA Purification

After the 2 hour incubation at 16°C the reactions were placed on ice. 250µl of cDNA binding buffer to each sample and mix thoroughly by pipetting up and down 2 or 3 times, then flicking the tube for 3 or 4 times. Tubes were then quickly spun down using a microcentrifuge. The cDNA sample/cDNA binding buffer was pipetted onto the centre of a cDNA filter cartridge (in a wash tube.) Samples were then centrifuged for 1 minute at 10,000 x g, or until the mixture in through the filter. The flow through was discarded and the cDNA filter cartridge was re placed in the wash tube.

500µl of wash buffer was then applied to each cDNA filter cartridge and the sample was centrifuged for 1 min at 10,000 x g, or until the wash buffer is through the filter. The flow through was then discarded and the cDNA filter cartridge was centrifuged again to remove trace amounts of wash buffer. The cDNA filter cartridge was then transferred to a cDNA elution tube.

10 µl of nuclease free water (preheated to 50-55°C) to the centre of the filter in the cDNA filter cartridge. Samples left at RT for 2 minutes and then centrifuged for 1.5mins at 10,000 x g or until all the nuclease free water was through the filter. A second aliquot of 9µl of preheated nuclease free water was added to the filter and was centrifuged for a further 2mins. Roughly 17.5µl of eluate containing cDNA was collected in the tube.

### 2.3.b.v *In Vitro* transcription to synthesise cRNA

An IVT master mix was prepared at RT by adding the reagents detailed in table 2.4 into a nuclease free microcentrifuge tube in the following order.

| IVT Mastermix for a single 25µl reaction | |
|---|---|
| Amount | Component |
| 2.5µl | T7 10X Reaction Buffer |
| 2.5µl | T7 Enzyme Mix |
| 2.5µl | Biotin NTP Mix |

**Table 2.4** IVT Master Mix for a single 25µl reaction using the total prep RNA amplification kit.

The Mastermix was then mixed by gentle vortexing and centrifuged briefly (~5 sec) to collect the IVT master mix at the bottom of the tube and then placed on ice. 7.5µl of the IVT master mix was then transferred to each cDNA sample (volume 17.5µl.) Tubes were mixed thoroughly by pipetting up and down 2 or 3 times, then flicking the tube for 3 or 4 times and were centrifuged briefly to collect the reaction mixture at the bottom of the tube. Once the reaction mixture was assembled the samples were placed at 37°C. The duration of the IVT reaction was determined by the amount of input RNA used in the amplification reaction (re table 2.5.) A hybridisation oven was used for this step to maintain a constant temperature and prevent condensation from forming on the walls of the tube.

| Input RNA | Recommended IVT incubation |
|---|---|
| 100-500ng | 4-14hr |
| <100ng | 14hr |

**Table 2.5** Recommended IVT incubation for Input RNA

This reaction was then stopped by 75µl nuclease free water to each sample to bring the final volume to 100µl.

### 2.3.b.vii cRNA purification

350µl of cRNA binding buffer was added to each cRNA sample. 250µl of ACS reagent grade 100% ethanol was then added to each sample and was mixed by pipette the mixture up and down three times. Each sample was then pipetted immediately onto the centre of the filter in the cRNA filter cartridge. Samples were then centrifuged for 1 min at 10,000 x g or until all the mixture was through the filter. The flow through was then discarded and the cRNA filter cartridge was placed back in the cRNA collection tube.

650µl wash buffer was then applied to each cRNA filter cartridge. Samples were then centrifuged for 1 min at 10,000 x g, or until the wash buffer was through the filter. The flow through was then discarded and the cRNA filter cartridge was the centrifuged for a further 1 min at 10,000 x g, or until all the wash buffer was through the filter. The flow through was discarded and the cRNA filter cartridge was spun for a further 1 min to remove trace amounts of the buffer. The cRNA collection tube was then transferred to a fresh cRNA collection tube.

100µl of nuclease free $H_2O$ preheated to 50-60°C was added to the centre of the filter, left at RT for 2mins and then centrifuged for 1.5mins at 10,000 x g, or until the nuclease-free water is through the filter. At this final stage the tube contained 100µl of cRNA in nuclease free water.

The quality of the labelled cRNA was assessed using the agilent bioanalyser using the eukaryote mRNA Nano series according to section 2.2.a.i.

### 2.3.c Whole-Genome Gene Expression Direct Hybridization Assay

The labelled cRNA samples was provided to Louise Evenden at the WTCRF and she performed the whole-genome gene expression direct hybridisation assay to the human ref 8 vs. 2 illumina chips (Illumina – kit with 2 bead chips #25-213.) Each HumanRef-8 v2 BeadChip simultaneously assays eight samples with > 22,000 probes per sample targeting genes and known alternative splice variants from the RefSeq database release[208]. The kit includes, two BeadChips, hybridization and wash buffers, and wash trays.

### 2.3.c.i Hybridisation to bead chip

750ng of cRNA was brought up to a total volume of 5µl using RNase free water and mixed. Samples were then left at RT for 10mins to resuspend cRNA. The hybridisation buffer (HYB) and humidity control buffer (HCB) were placed in a 58°C oven (Illumina part # 198361 (115V) or 198379 (230V)) for 10mins to dissolve any salts that may have precipitated in the storage. If any salts remained undissolved, the buffers were incubated for a further 10mins. The buffers were then cooled to RT and mix thoroughly. For each sample 10µl of the HYB was added.

The illumina hybridisation chamber gasket (illumina part #210930) was placed into the BeadChip hybridisation chamber (illumina part #210948). 200µl of HCB was then dispensed into the humidifying buffer reservoirs (222682), only adding buffer to reservoirs next to loaded Bead Chips. The hybridisation chamber was sealed with a lid and kept on the bench at RT until all the bead chips were loaded into the Hybridisation chamber. All the BeadChips were removed from their packages (BD-25-213.)

The BeadChip is sealed by the coverseal tab with tweezers and the chips were slid into the hybridisation chamber insert so that the barcode lines up with the barcode symbol on the insert. The assay sample was heated at 65°C for 5 minutes and then briefly vortexed, the briefly centrifuged to collect the liquid in the bottom of the tube. The sample was then allowed to cool to RT before using. The sample was pipetted immediately after cooling to room temperature. The Hybridisation chamber inserts containing BeadChips were loaded into the hybridisation chamber. 15µl of the assay sample was dispensed onto the large sample port of each array. The lid was sealed onto the hybridisation chamber carefully to avoid dislodging the hybridisation chamber inserts. The samples were then incubated for 16-20 hrs at 58°C with a rocker speed set at five. (Note: the LAPATAX samples were labelled using the Nugen protocol – 2.3.d these samples were hybridised at a lower temperature of 48°C at this stage in the illumina protocol.)

### 2.3.c.ii Wash and Staining the Bead Chip

1 x high-wash buffer was made up by adding 50ml of 10 x high wash buffer stock solution to 450ml RNAse-free water. The water bath insert was placed into a heat block and 500ml of prepared 1X high temp watch buffer was added (Hybex Microarray Incubation System Heating Base, SciGene - 1057-30-0 (115V) or 1057-30-2 (220V) Waterbath insert for Hybex Heating Base, SciGene - 1057-35-0.) The heat block temperature was set to 55°C to pre-warm the high temperature wash buffer to the correct temperature. The heat block lid was closed and left overnight.

The following day wash buffer E1BC was made up by adding 6ml of E1BC buffer to 2L RNAse-free water. Block E1 buffer (4ml/chip) was then warmed to RT. 2ml per chip of block E1 was prepared with streptavadin-Cy3 (2µl of 1mg/ml stock per chip.) A single conical tube was used for all BeadChips and was stored in the dark until the detection. 1 litre of diluted E1BC buffer was then placed in a Pyrex No. 3140 beaker.

The hybridisation chamber was removed from the oven and disassembled. Using powder free gloved hands, all BeadChips were removed from the hybridisation chamber and they were submerged them, face up at the bottom of the beaker. The coverseal was then removed from the first BeadChip, ensuring that the entire BeadChip remains submerged during removal. Using tweezers, the peeled BeadChip was transferred into a slide rack submerged in the staining dish containing 250ml wash E1BC solution (this solution was used in subsequent steps.)

After this was repeated for all chips the slide rack handle was used to transfer the rack into the Hybex Waterbath insert containing High-Temp wash buffer. The chips were then incubated static for 10mins (55°C) with the Hybex lid closed. The slide rack was then immediately transferred back into the staining dish containing wash buffer E1BC. The rack was briefly agitated, then shaken on an orbital shaker for 5mins at maximum speed without allowing solution to splash out of the disk. The rack was then transferred to a clean staining dish containing 250ml 100% Ethanol (fresh.) The ethanol was then agitate using the rack handle and was then shaken for 10mins. The rack was then transferred to a clean staining dish containing fresh 250ml wash E1BC buffer. The solution was then briefly agitated using a rack handle and then shaken on an orbital shaker for 2mins. 4ml of E1 blocking buffer was then pipette into the wash trays. The BeadChip was then transferred face up into BeadChip wash trays on rocker and rocked at medium speed for 10mins.

2mls of Block E1 buffer was pipetted + streptavidin-cy3 into fresh well trays. The BeadChip was then transferred face up into wash trays on rocker. The cover was then placed on the tray and was rocked at medium speed for 10mins. 250ml of wash E1BC solution was added to a clean

staining dish. The BeadChip was then transferred to the slide rack submerged in the staining dish. The solution was then briefly agitated and then shaken at RT on an orbital shaker for 5mins. A rack of BeadChips was then spun at 275 x g for 4mins. The dry chips were then stored in a slide box until scanned.

### 2.3.c.iii Scanning the Bead Chip

The BeadChip was then scanned on the Illumina BeadArray Reader. During the scan process, the BeadChip barcode was scanned, ensuring effective data management, resulting images were then available for registration, extraction, and analysis using Illumina's BeadStudio software.

### 2.3.c.iv System Controls for the Illumina Whole-Genome Gene Expression Direct Hybridization Assay system.

Seven control categories are built into the Whole-Genome Gene Expression Direct Hybridization Assay system: covering every aspect of an array experiment, from the biological specimen to sample labelling, hybridization, and signal generation. The BeadStudio is an application that was used to automatically track the control performance generating a report for each array in the matrix. Full details of the controls present on the array are detailed in appendix 8 of the whole-genome gene expression direct hybridization assay protocol which can be found at www.illumina.com/products/mouseref-8_expression_beadchip_kits_v2.ilmn.

### 2.3.d.i Gene expression analysis of taxane resistant cell lines using qPCR

Cells were grown up and harvested according to section 2.1.f.iii and RNA was extracted and quantified according to 2.3.a.i-2.3.a.ii. Gene expression assays from Applied Biosystems were chosen to be able to detect all isoforms of the chosen genes and were also chosen to cross exon boundaries so as not to detect genomic DNA. qPCR runs were performed with the help of Alison Munro to whom I am very grateful.

5-fold standard curves (500ng, 100ng, 20ng, 4ng, 0.8ng) were run for each gene expression assay using RNA extracted from our eleven taxane resistant breast cancer cell lines. This was performed to check the efficiency of the assay to ensure a linear relationship. An acceptable range for efficiency is 90-110% which equates to a slope of between -3.10 and -3.60; the optimal slope being -3.32 (100% efficiency). It is also important that the R2 value for the curve is over 0.985 as this indicates the points of the standard curve fit closely to the "best fit" line. Any genes that were out with these ranges were discarded and not included in the analysis.

Plates were set up as Relative Quantification plates using SDS 2.4 where RPL37A (a housekeeping gene) was used as a control to normalise data. All genes and controls were run in quadruplicate. The PCR was set up using the Superscript III Platinum One-Step Quantification

RT-PCR system with ROX (Applied biosystems through Invitrogen - 11732-020) with conditions (50°C 15mins, 95°C 2mins, then forty cycles of 95°C 15secs and 60°C 30secs.) Once all the plates were run all the files were opened into a new study using RQ Manager 1.2.1 allowing all plates to be analysed with the same conditions. All baseline and threshold levels were set manually – baseline from 3 to a point ~2 CTs before amplification and threshold to approx the middle of the log phase of amplification.

Once all levels were set and the data was analysed (by pressing "analyse all" button) the results data was exported to a text file to allow importing into DataAssistv2.0 which allows better manipulation of the data and allow you to look at individual samples from plates i.e. each cell line. Once in Data Assist each cell line was selected individually and data was normalised to RPL37A and then the Native was set as the calibrator to assess how much each gene differed from the original cell line (with increasing resistance). CTs of 40 were not used in calculations as this would give false data for genes that have not amplified. CT values, delta CTs, 2^-delta CTs and fold changes were exported into excel files.

### 2.3.e.i Array Comparative Genomic Hybridisation

Microarray based comparative genomic hybridisation (aCGH) was developed in the late 1990s. It can be used to screen entire genomes rapidly at high resolution with minimal cytogenetic expertise for analysis[209]. aCGH uses labelled test and reference DNA which is hybridised to probes on a microarray, that are then scanned to produces and image of differential signal intensities (i.e. dual channel/colour microarray[209].) Areas of deletion gain and amplification on the genome can be detected using aCGH, however polyploidy and balanced chromosomal translocations cannot be detected using aCGH. aCGH can be used to detect changes in copy number down to a single copy. Arrays can be fully tiled, encompassing the entirety of the genome or partially tiled, as in the case of the array we used for our experiments. The partially tiled array we used was composed of Bacterial Artificial Chromosomes which are large insert genomic clones which vary in length from 100-200 kb in length.

### 2.3.e.ii Array Comparative Genomic Hybridisation: Protocol

Our cell lines were grown up, harvested and the DNA was extracted according to section 2.1.f.ii. Our aCGH experiments were performed in conjunction with Maryou Lambros in the Molecular Pathology laboratory run by Jorge Reis-Filho at Breakthrough Breast Cancer research in the institute of Cancer Research. 29K BAC partially tiled microarray platform was used (a fully tiled array was composed of 32K BACS.)

Two different types of experiment were carried out; the first used pooled female DNA from blood as a reference sample and each of the members of our panel of taxane resistant and

sensitive cells as a test sample. Test samples were: MDA-MB-231 Native, 5nM, 25nM and 50nM PACR, ZR75-1 native, 5, 25, or 50nM PACR and 5, 25, and 50nM DOCR. This mapped the changes in each of the cell-lines in comparison to normal human DNA to track the accumulation in alterations with increasing taxane resistance. The 2nd set of aCGH experiments used the parental cell line as a reference and each of their respective taxane resistant samples as test samples to track specific alterations between cell lines with different degrees of taxane resistance. This 2nd method of experimentation is particularly valuable as it allowed the genomic data to be mapped to the transcriptomic data obtained from the illumina microarrays.

### 2.3.e.ii DNA labelling using the Bioprime aCGH labelling Kit

For the aCGH protocol the Bioprime labelling kit was used (Invitrogen - 108-944-011.) This labelling using the Bioprime labelling kit is illustrated in figure 2.2 (figure adapted from the bioprome labelling kit protocol.)

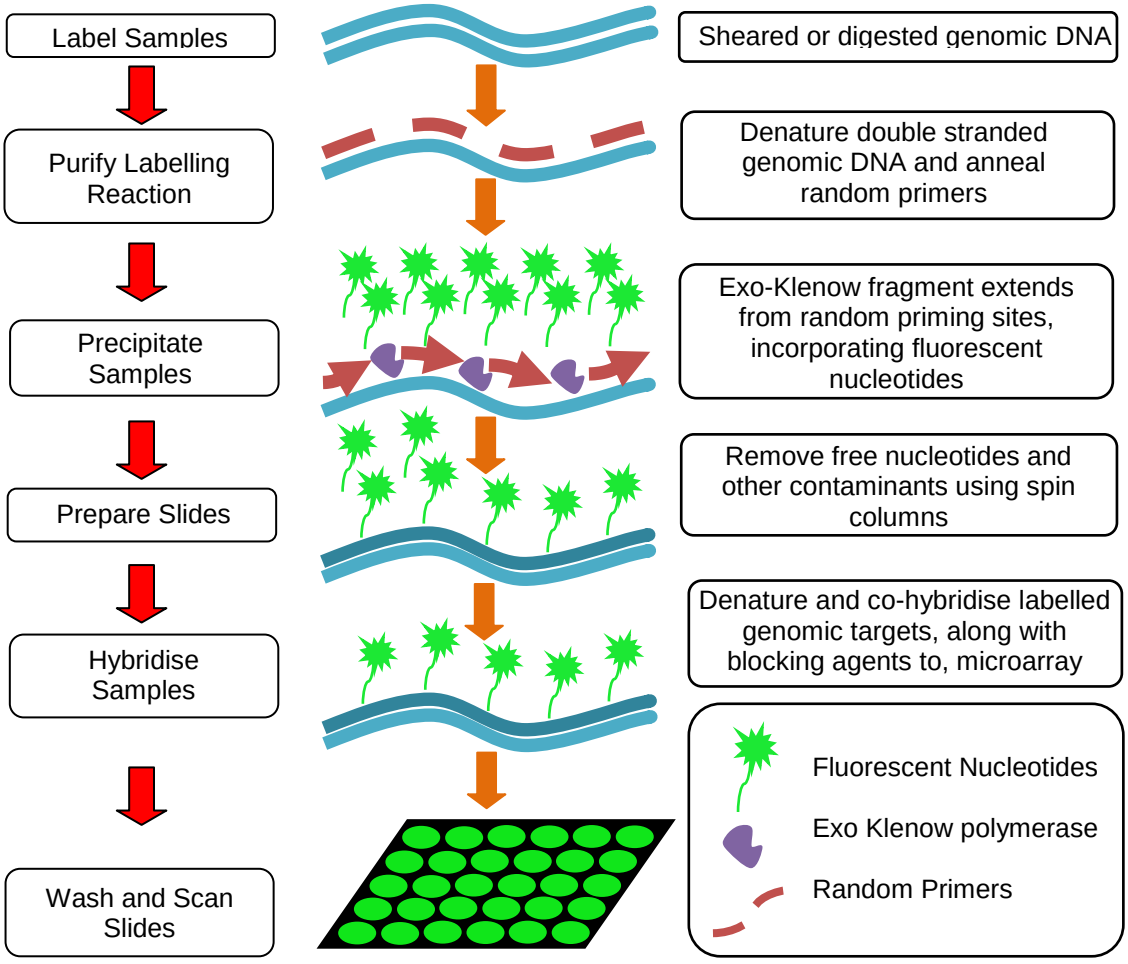


**Figure 2.2** Labelling, Purifying and precipitating samples for aCGH using the Invitrogen Bioprime Labelling kit (figure adapted from kit protocol.)

Approximately 350-400ng tumour or reference DNA was added to 0.5ml thin walled tubes. UF water was added to samples to a total of 21µl. 20µl random primers were added to each sample and they were denatured for 5mins at 95°C (PCR block.) After denaturation, samples were left on ice for 10mins to ensure minimal re-annealing. To each tube 5µl dNTP stock, 3µl Cy3 or Cy5 and 1µl Exo Klenow fragment were added, then samples were incubated at 37°C O/N (PCR block.) Exo-Klenow polymerase incorporates fluorescently modified nucleotides more effectively providing higher yields than standard Klenow, for greater reproducibility of results. Cy3 probe was added to test samples and Cy5 probe was added reference samples (25nM -Cy3-dCTP and Cy5-dCTP - PA53021 - PA55021 - GE.) dNTP stock consisted of 12dATP, dGTP, dTTP and 6µl CTP: 100mM stocks in 1ml of TE buffer stored at -20°C. Cy3 and Cy5 dye: 1.0 mM Cy dye, 0.6 mM dCTP, and 1.2 mM dATP, dGTP, and dTTP.

### 2.3.e.iii Purification of Labelled DNA.

The second day of the aCGH protocol involved purifying the labelling reaction using the Qiagen miniElute kit (28400.) 270µl of buffer PB from the kit was added to each sample. Buffer PB contains guanidine hydrochloride and isopropanol to denature proteins in the sample. Each sample was vortexed, spun down briefly on a microcentrifuge and supernatant was transferred to the mini elute column. The columns were then spun down at 11K x g for 1 min. The flow through was discarded and the column was placed back into the same collection tube. 700µl of buffer PE was then added to each column and was spun down at 11K x g for 1 min. The columns were then placed in appropriately labelled eppendorf tubes. 12µl of buffer EB was then added to the spin columns and the tubes were allowed to stand for 1 min. The tubes were then spun down for 1 min at 11K x g.

### 2.3.e.iv Precipitating Labelled DNA

The precipitation stage of the protocol was carried out by combining tumour and reference DNA for each comparison (~ 22µl) in a thick 0.5ml tube. 100µl of cot-1 DNA (1µg/µl) was then added to each tube. Human Cot-1 DNA® (15279-011 - Invitrogen) is placental DNA that is predominantly 50-300bp in size and enriched for repetitive DNA sequences[210,211].

The Cot-DNA dramatically enhances aCGH results by blocking non-specific hybridisation. 12µl 3M NaOAc pH 7.0 was then added to each tube with 300µl ice cold 100% etOH. Samples were then precipitated -80°C for 1-2 hours. After precipitation, samples were centrifuged at 11K x g for 30mins. Supernatant was removed leaving a purple pellet. Pellet was then washed with 500µl 70% etOH. Supernatant was removed and the pellet was dried in the dark for 15mins. Samples can be stored at -20°C.

## 2.3.e.v Slide Preparation Protocol

After samples were prepared according to section 2.3.e.i-iv, they were hybridised to slides and scanned to calculate the fluorescence ratios between the Cy3 labelled test sample and the Cy5 labelled reference sample (re figure 2.3. adapted from bioprime labelling kit protocol.)

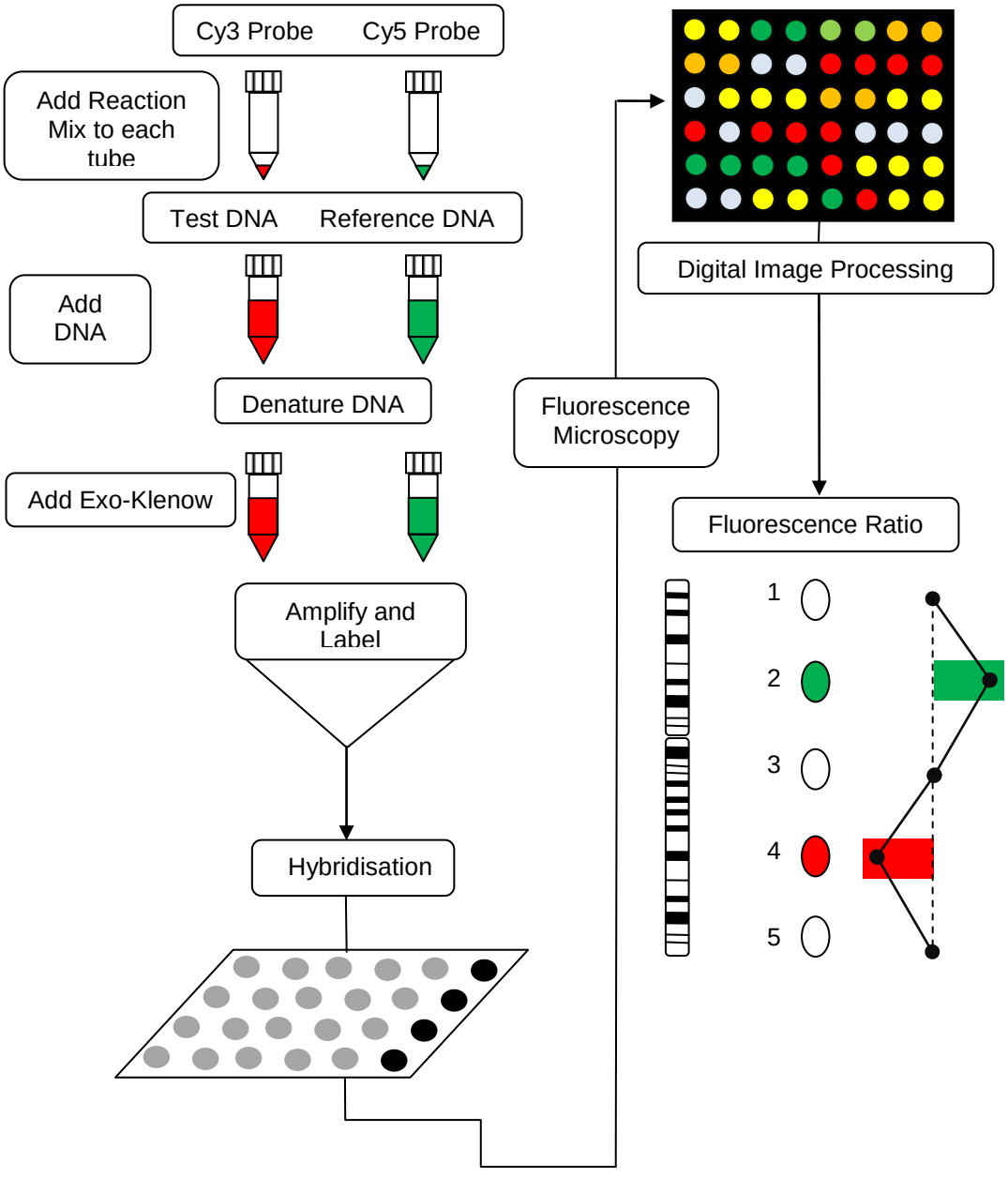


**Figure 2.3** Hybrisidisation and scanning slides for aCGH.

The prehybridisation wash buffer was prepared as follows.

| **Slide Prehybridisation Buffer:** | **100ml** | **200ml** |
|---|---|---|
| Deionised Formamide | 25ml | 50ml |
| 20 x SSC | 0.5ml | 1ml |
| BSA | 0.5g | 1g |
| UF water | 49.5ml | 99ml |

BSA (Sigma – A-9418-10g) was prepared by dissolving 1g BSA in 49.5ml dd$H_20$, filter sterile (0.2µm) followed by formamide, SSC and SDS. Deionised formamide (Q-Biogene – FORMD003), 20 x SSC (GE Healthcare – US19629), 20 x SDS (GE healthcare – US75832.) The pre-hybridisation buffer for the slides was pre-warmed to 42°C. The slides (Corning GAPSII coated glass slides - Corning, NY, USA – 40005) were placed in the pre-hyb buffer in a 50ml falcon tube and then incubated for a minimum of 45mins at 42°C. Prior to hybridisation the slides were rinsed in d$H_2O$ by tipping slides in 4 x 50 ml falcon tubes, full of UF $H_2O$. Slides were then spun dry at 270 x g for 2mins.

### 2.3.e.vi. Hybridisation Protocol

Hybridisation buffer was prepared as follows:

| **Hybridisation Buffer:** | **500µl** | **5ml** |
|---|---|---|
| Deionised Formamide | 250µl | 2.5ml |
| Dextran Sulphate | 50mg | 500mg |
| 20 x SSC | 50µl | 500µl |
| 20% SDS | 50µl | 500µl |
| 100µg/µl yeast tRNA | 20µl | 200µl |
| UF $H_2O$ | 130µl | 1.3ml |

Dextran Sulphate (Sigma – D-8906-10g), Yeast tRNA (Invitrogen - 15401-011).

45µl of hybridisation buffer was added to the purple pellet and then left at RT in the dark for 30-45mins. Tubes were then vortexed and briefly on a benchtop microcentrifuge making sure the pellet was completely reconstituted in the hybridisation buffer.

Samples were denatured for 15mins at 70°C and re-annealed for 30mins at 37°C using a PCR block. The sample was then applied to a coverslip. The prepared slide was then lowered onto the coverslip and then the slides were placed into a hybridisation chamber. The slides were incubated at 42°C overnight.

### 2.3.e.vii. Washing the Slides in preparation for scanning

Wash buffers were prepared as follows:

| **Wash 1:** | **100ml** | **200ml** | **500ml** |
|---|---|---|---|
| 20 x SSC | 10ml | 20ml | 50ml |
| 20% SDS | 0.5ml | 1ml | 5ml |
| UF $H_20$ | 89.5ml | 179ml | 477.5ml |
| **Wash 2:** | **100ml** | **200ml** | **500ml** |
| 20 x SSC | 10ml | 20ml | 50ml |
| Formamide | 50ml | 100ml | 250ml |
| UF $H_2O$ | 40ml | 80ml | 200ml |
| | | | |
| **Wash 3:** | **100ml** | **200ml** | **500ml** |
| 20 x SSC | 1ml | 2ml | 5ml |
| UF | 99ml | 198ml | 495ml |

The slides were washed for 15mins at 45°C with wash buffer 1 (2 x SSC, 0.1% SDS.) The coverslip was then carefully removed by allowing it to slowly slip of the slide and the slides were then washed in wash buffer 2 (2 x SSC, 50% formamide pH7.0) for 15mins at 45°C. Slides were then washed again in wash buffer 1 for 30mins at 45°C. The two final washes were in wash buffer 3 (0.2 x SSC) for 15mins at RT. The slides were then centrifuged at 270 x g.

### 2.3.e.viii Scanning the Slides and Analysing the Data.

Following hybridization and washes, slides were scanned using an Axon 4000B scanner (Axon Instruments, Burlingame, CA, USA) and images were processed using Genepix Pro 5.1 image analysis software (Axon Instruments). The statistical analysis for these experiments was performed by Alan McKay using R 2.01 and bioconductor 1.5 at Breakthrough Breast Cancer Research at ICR.

For each BAC clone, the median localised background signal was subtracted and the Cy3:Cy5 signal intensity ratio was calculated and then subjected to print loess normalisation. Print loess normalisation is a well tested general purpose normalisation method of normalisation that is used specifically to adjust data from microarrays that arise from the microarray technology[151].

Replicate spots of the BAC clones were averages and those with poor reproducibility between replicates (Standard Deviation>0.2) were excluded from the dataset. Also clones with no mapping information or poor or missing values in >70% of samples were excluded[212].

For each BAC on the array genome plots of log 2 ratios were plotted on the y axis and the chromosomes were plotted in chromosome order, short (p) arm then long (q) arm. The data was smoothed using local polynomial adaptive weights smoothing (aws), and smoothed log2 ratio ≤ −0.12 were categorized as losses; those ≥ 0.12 as gains were categorised as gains and those in between these two figures were categorised as unchanged. Amplifications were defined as smoothed log2 ratio values ≥ 0.45[213].

### 2.3.f. Western Blotting

#### 2.3.f.i Preparation of Cell Lysates

10 µl of PMSF was added to 500µl of 10 x cell lysis buffer (Cell Signalling Technology - 9803) and 4490µl of dd$H_20$ at RT. Flasks were then washed twice in ice cold PBS, aspirated then 600µl of 1 x CLB was added to each flask and cells were scraped on ice. Lysates were placed in labelled 1.5ml tubes and spun down at 1200 rpm for 5 minutes at 4°C. The supernatant was retained and placed in a fresh labelled 1.5ml tube. To quantify each lysate the Bicinchoninic Acid Kit for Protein Determination from Sigma (Sigma - BCA1-1KT) was used.

#### 2.3.f.ii Preparation of Buffers and Gels for Western Blotting

**1X Cell Lysis Buffer:** 20 mM Tris-HCl (pH 7.5)
150 mM NaCl
1 mM $Na_2$EDTA
1 mM EGTA
1% Triton
2.5 mM sodium pyrophosphate
1 mM beta-glycerophosphate
1 mM $Na_3VO_4$
1 µg/ml leupeptin
1mM PMSF is added immediately before use (PMSF – Sigma P7626 – MW - 174.19.)

**Tris Buffers**: 1M Tris pH 8.85 (60.5g) (Tris)
0.375 M pH Tris pH 6.8 (22.7g)
Dissolved in d$H_20$ and make up to 500ml. Adjust conc. with HCl and store at 4˚C for 4 weeks. (Tris Base – Sigma – T4661)

**10% SDS w/v:** 50g Sodium Dodecyl Sulphate. (SDS – Sigma – L3771)
Dissolved in d$H_20$ and made up to 500 ml. Filtered through a Whatman No.1 if necessary and stored at RT**.**

**AMPS 10% w/v:** 100mg ammonium persulphate (AMPS – Sigma – A3678)
Dissolved in $dH_20$ (1ml) and stored at 4°C for 4 weeks or at RT for 1 week.

| **Resolving Gel:** | 7.5% gel | 10% gel | 12% gel |
|---|---|---|---|
| 30% Acrylamide* | 6 .00 ml | 8.10 ml | 9.60 ml |
| IM Tris pH 8.85 | 9.00 ml | 9.00 ml | 9.00 ml |
| 10% SDS | 0.24 ml | 0.24 ml | 0.24 ml |
| $dH_2O$ | 8.76 ml | 6.66 ml | 5.16 ml |
| 10 % AMPS | 0.06 ml | 0.06 ml | 0.06 ml |

| **Stacking Gel:** | **3.6%** |
|---|---|
| 30% Acrylamide (*Sigma - A3449) | 1.08 ml |
| 0.375M Tris pH 6.8 | 3.00 ml |
| 10% SDS | 0.09 ml |
| $dH_20$ | 4.80 ml |
| 10% AMPS | 0.03 ml |
| TEMED | 0.03 ml |

Enough to make 2 stacking gels for a Biorad mini Protean tank. AMPS and TEMED (Biorad - 1610801) were added to the gel mix last.

**3 x Sample Buffer:**

| | |
|---|---|
| Tris Base | 75.00 mg |
| SDS | 0.75g or (7.5 mls of 10% SDS) |
| β – Mercaptoethanol | 3.75 ml |
| Glycerol | 7.50 ml (pipette slowly) |
| Bromophenol Blue Sat Solution | 250 µl |

Dissolved in $dH_20$, to 25ml, aliquoted, stored at -20°C. β–Mercaptoethanol (Sigma - M7154), Glycerol (Sigma - G8773), Bromophenol blue (Sigma - B8026)

**Electrode buffer:**

| | |
|---|---|
| Tris Base | 2.27g |
| Glycine | 10.82g |
| 10 % SDS | 7.5ml |

Made up to 0.75L with $dH_20$

**Ladders/ Markers:** Kept at –20°C in aliquots

Prestained protein marker, broad range, 5ul for a mini gel (NEB- P7708S).

Biotinylated protein marker, 5ul for a mini gel. (CST - 7727)

Full range rainbow molecular weight marker, 5µl for a mini gel (GE – RPN800E.)

**1 x Towbin Transfer Buffer:**

25mM Tris Base 3.03g

192mM Glycine 14.4g

Methanol pH8.3 200ml

The addition of methanol is for use with PVDF membranes (Polyvinylidine fluoride) Volume is adjusted to IL with $dH_20$. PVDF membranes were soaked successively in 100% methanol, $dH_20$ and then transfer buffer to remove excess salts (Millipore - Immobilon-P Membrane - PVDF, 0.45 µm pore size - IPVH 304.)

**Blocking Agents:** **Roche blocking agent (Roche - 11500694001)**

1% - 1 ml of 10% Blocking solution + 9ml TBST

0.5% - 0.5 ml of 10% Blocking solution + 9.5ml TBST

**Milk 5% w/v**

5g Marvel dried Skimmed Milk in 100ml TBST

**1 X TBS:**

| | |
|---|---|
| Tris Base | 18.15 g |
| NaCl | 26.28 g |

Dissolved in $dH_20$ and adjusted to pH 7.5 with conc HCl, then made up to the total volume of 3L with $dH_20$. NaCl (Sigma - 7653) To make TBS-T 0.1% 1 ml of Tween was added to IL TBS (Sigma - P5927).

### 2.3.f.iii Running a western polyacrylamide gel

Western blots were run using the Biorad Mini Protean 3 system. Lysates were prepared and quantified according to section 2.3.f.i and buffers and reagents were prepared according to section 2.3.f. Equal concentrations of protein (usually between 10 and 25µg) were diluted in 3 x loading buffer and the diluted to equal volume. Samples were then denatured for 5mins at 95°C, then spun down briefly and placed on ice. A mini protein gel tank was half filled with electrode buffer and then the internal gel apparatus was inserted into the tank. The internal cavity of the gel apparatus was filled with electrode buffer (2.3.f.ii for 0.75L), and then the rest of the tank filled with the remaining buffer. Samples were then loaded on to a polyacrylamide gel, details of how to make the gel are in section 2.3.f..ii. A 7.5-15% gel was selected according to the band size or separation required for proteins of interest. 5µl of marker was then loaded onto the gel:

either the full range rainbow marker from GE or the broad range marker from NEB and the biotinylated marker from CST (re section 2.3.f.ii). The gel was then run at 80V for 15mins and then for 200V for 1 hour or until the gel front is nearing the bottom of the gel.

**2.3.f.iv. Running the gel transfer.**

Proteins were then transferred to a permeabilised immobilon P membrane (roughly 8.5-9cm x 6-6.5cm) via wet transfer using Towbin transfer buffer (section 2.3.f.ii) either at 100V for 1hour at RT (with of frozen insert in the gel tank) or overnight at 30V in a cold room at 4°C.

**2.3.f.v Blocking the Transferred Membrane**

The membrane was blocked in 15mls of blocking agent for 1 hour on a rocker at RT (either 0.5% Roche blocking solution or 5% Marvel in TBS-T detailed in 2.3.f.iii.)

**2.3.f.vi Incubating the transferred membrane in primary and then secondary antibodies**

The membrane was then blocked overnight with primary antibody in either 0.5% Roche blocking agent or 5% Marvel in TBS-T at 4°C on a rocker. The primary antibody was then poured off and the membrane was rinsed twice in TBS-T and then was washed for 5mins in TBS-T three times at RT. The membrane was then washed for 5mins at RT in 0.5% Roche blocking agent or 5% Marvel in TBS-T twice at RT. The membrane was then incubated with secondary antibody in either 0.5% blocking agent or 5% Marvel in TBS-T at RT on a rocker for 1 hour. The membrane was then rinsed twice in TBS-T and washed 3 times for 5mins in TBS-T on a rocker at RT. The final two washes were done using TBS for 5mins at RT.

**2.3.f.vii Exposing the membrane to Luminol**

Luminol substrate was made up 30mins in advance to exposing the membrane (Roche - 11500694001.) 150µl of activator was added to 15mls substrate and was incubated at RT for 30mins. The membrane was incubated with the luminol mix for 1 minute on a rocker at RT in the dark. The membrane was then sandwiched between two transparency films and placed in an x-ray cassette a sheet of hyperfilm (GE healthcare - RPN3103K) was exposed to the luminal activated membrane. The exposure was repeated several times (new film each time) for different periods until optimal exposure is reached: 5secs, 15secs, 30secs, 1min.

**2.3.f.viii. Stripping the membrane and re-probing with actin**

Re-probing with a housekeeping gene allows normalisation to test the primary antibody and controls for protein loading. To this the membrane was washed in TBS for 15mins at RT (or it could be stored, sealed in a plastic bag or kept in a plastic box (wet) and stored in the cold room.) The membrane was then stripped and the membrane was re-probed with actin (42kDa).

The membrane was transferred to a box containing Western stripping buffer (100mM glycine pH 2.5 - 3.76g of glycine in 500ml distilled water, final volume at pH 2.5) The membrane was then incubated for 1 hours at RT on a rocking platform. The stripping buffer was poured off and the membrane was rinsed twice in TBS and then washed twice in TBS for (as per western protocol – 5min at RT on a rocker.)

The blot was now ready to probe. To re-probe with actin the membrane was then blocked in 0.5% blocking medium (or 5% Marvel) in TBS-T according to the Western protocol, (re. 2.3.f.v and 2.3.f.vi) then the actin primary antibody was added to the blocking buffer. The actin primary was diluted at 1:200,000 or alternatively 1:500,000 (Anti-Actin (Ab-1) Mouse mAb (JLA20) - CP01 – Calbiochem – which is kept stored in small aliquots at -20°C) and incubated overnight at 4°C. in blocking reagent and the membrane was incubated for 1 hour. The membrane was again washed according to the Western protocol.

The Actin secondary antibody was diluted at 1;120,000 of 1mg/ml (Calbiochem - goat anti-mouse IgM H&L chain specific peroxidase conjugate – 401225 – kept at 4°C in small aliquots) in 0.5% blocking reagent or 5% Marvel in TBS-T. The final part of this process was performed as per the Western protocol (re. section 2.3.f.vii.)

## 2.4 Transcriptomic analysis of material from the LAPATAX trial.

### 2.4.a.i The LAPATAX trial; storing and collection of material.

Lapatax (EORTC 10054) is a phase I-II study of lapatanib and docetaxel as neoadjuvant treatment for HER-2 positive locally advanced/inflammatory or large operable breast cancer[214]. The design of the phase I dose escalation phase is detailed in figure 2.4. In this phase of the trial the objective was to recommend a dose of lapatinib and docetaxel to be given prior to surgery for 3 cycles to patients that are Her2+ve locally advanced, inflammatory, or large resectable breast cancer patients after 3 cycles of FEC (fluorouracil, Epirubicin hydrochloride, cyclophosphamide.) The study was designed to determine the Maximum Tolerated Dose (MTD) based of the documentation of the acute dose limiting toxicity (DLT). The safety of this dose was then confirmed after 3 cycles of FEC in a bridging phase. Dose escalation was done in a step wise manner. The doses used in the Phase I dose escalation are detailed in Table 2.6.

| Dose Level | Lapatinib mg/day | Docetaxel mg/$m^2$ |
|---|---|---|
| -1* | 750 | 75 |
| 1 | 1000 | 75 |
| 2 | 1250 | 75 |
| 3 | 1000 | 85 |
| 4 | 1250 | 85 |
| 5 | 1000 | 100 |
| 6** | 1250 | 100 |

**Table 2.6** Dose levels of Lapatinib and Docetaxel used in the LAPATAX dose escalation
*A dose level of -1 was planned in case of severe toxicity at
**Prophylactic GCSF is given.

In phase II patients were randomised into one of two treatment arms (detailed in figure 2.5.) In arm 1 patients received FEC chemotherapy, docetaxel and lapatinib ditosylate at the MRD as determined by the bridge step of phase I. The doses established in the Phase I dose escalation phase and recommended for phase II were lapatinib 1250mg/day and 100mg/$m^2$ of Docetaxel with Prophylactic GCSF.

In arm 2: Patients received FEC chemotherapy as in the bridge step of phase I. Patients then receive docetaxel IV over 60 minutes and trastuzumab IV over 30-90 minutes on days 1, 8 and 15 respectively. Treatment with docetaxel and trastuzumab repeats every 3 weeks for 3 courses in the absence of disease progression or unacceptable toxicity. All patients undergo surgery to remove the tumour and then receive trastuzumab 1 or 3 times weekly for a year. Patients in the phase I portion (or bridge step) could also receive at least 3 courses of and anthracycline based regimen.

Patients undergo tumour biopsies periodically during study for laboratory studies. Transcriptomic studies of the material from the LAPATAX trial were carried by extracting RNA from the tissue and carrying out an analysis by illumina profiling and qPCR.

One of the secondary objectives of the phase II part of the study was designed to identify genes that may predict response in patients treated with docetaxel and lapatinib ditosylate.

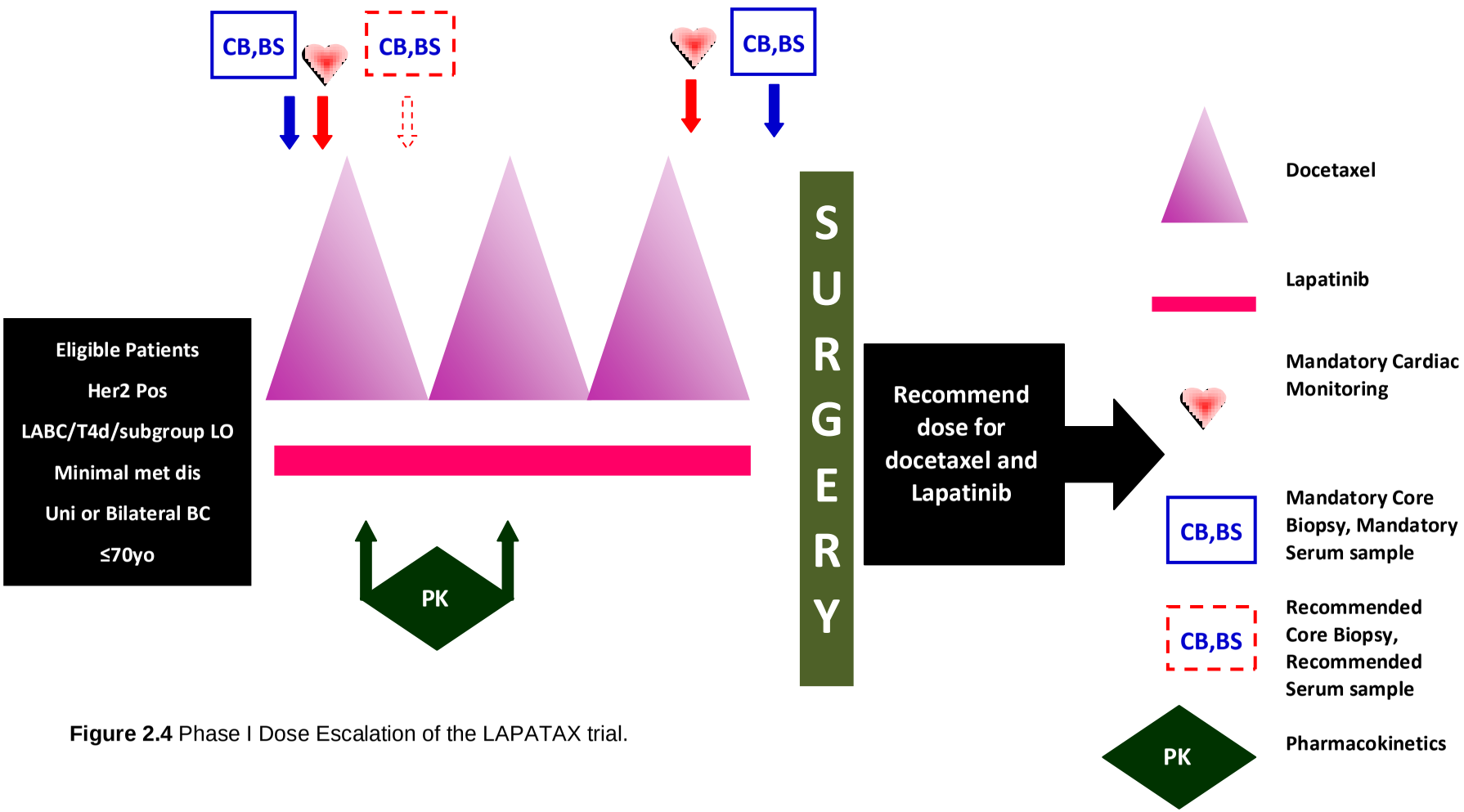


**Figure 2.4** Phase I Dose Escalation of the LAPATAX trial.

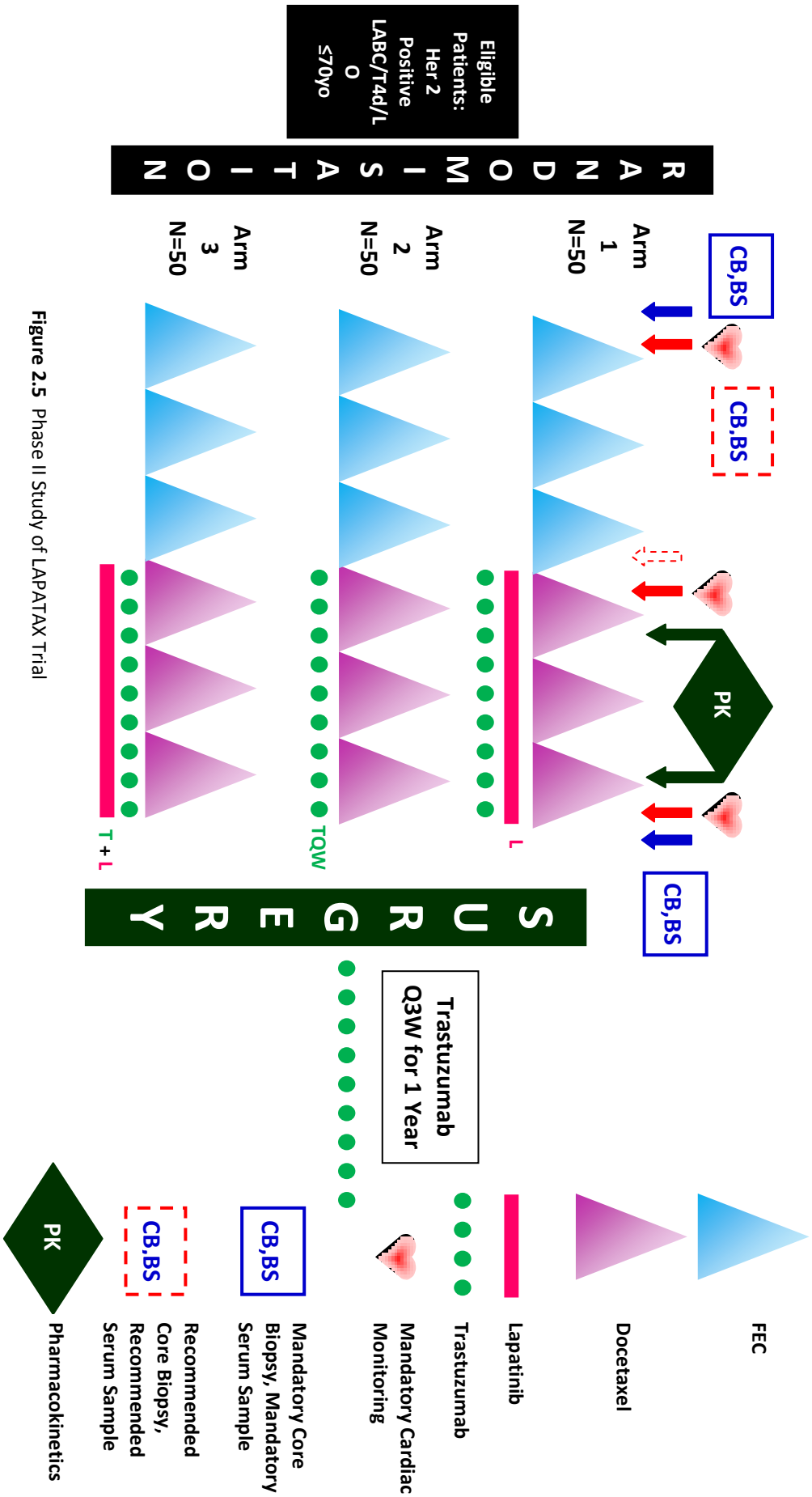


**Figure 2.5** Phase II Study of LAPATAX Trial

### 2.4.a.ii.Stabilising Frozen tumour samples from the LAPATAX trial in RNA later ICE.

A total of 32 tumour samples were received embedded in OCT from the LAPATAX trial. 22 of these samples were matched pairs of pre and post treatment samples from the dose escalation phase. There were 10 pre-treatment samples. Twenty eight of samples arrived already embedded in OCT. Four of the samples arrived simply as frozen tumours and were embedded in OCT by Bob Morris in the Pathology department at the Western General Hospital. In addition a section of each of the 32 tumours that were received was taken and assessed for quality and percentage tumour material present.

RNA*later*-ICE (available from Ambion – 10 x 25ml bottles -4427575) is a reagent for transitioning frozen tissue to a state that is easily processed for extraction of high quality RNA. Upon receipt of the LAPATAX samples (kept on dry ice) each tumour was submerged in an excess (roughly 2ml) of pre-chilled (-70°C at least overnight) RNA later ICE, and invert the tube three times, the sample could be stored at -20°C at least overnight. Once RNA was stabilized overnight, the specimens can be stored at –20°C indefinitely. During the extraction and amplification stages of the LAPATAX samples I was helped by Dr. Vicky Sabine to whom I am very grateful.

### 2.4.a.iii Tissue Homogenisation of LAPATAX tumour samples

Before and after the homogenisation step the work area was cleaned with RNAse Zap wipes (Ambion – AM9786.) Each OCT embedded sample was taken from dry ice to RT and the sample including the RNA later ICE was poured from the tube into a weigh boat. The tumour easily separated from the OCT and the OCT was disposed of. The sample was weighed and a 100mg portion, to be extracted was cut off using a scalpel. The remaining tumour was placed back in the original tube in RNA later ICE and returned to -20°C. From this point on the tumour was extracted at RT.

Sample was then cut up into 1mm pieces using a fresh scalpel blade each time. If the sample has a high fat content it is important to try and remove this. Using forceps the tissue was then transferred into a tube containing 2ml of buffer RLT + 20μl 2βME/ sample (2ml RLT is recommended in RNeasy Midi Maxi Handbook for 20-130mg tissue, Buffer RLT - RNeasy mini kit from Qiagen – 74104, 2βME – Sigma Aldrich - M3148-25ML.) The sample was then homogenised for one minute at maximum speed using the tissueruptor homogeniser and repeat if necessary (Qiagen – 9001273, disposable probes for tissueruptor homogeniser – 990890.) The homogenate is kept at RT whilst homogenising further specimens. A new homogeniser head and weigh boat is used for each sample. At this point samples could be left for up to 4 hours at RT.

**2.4.a.iv RNA Extraction from tissue with RNeasy-Mini Columns**

The homogenate was transferred by 1ml into two 1.5ml tubes to clear by centrifugation. The homogenate were spun for 3 min at max speed (8000 x G) in a bench top centrifuge at RT. The supernatant was carefully decanted into pre-labelled 15ml tubes, avoiding transferring the pellet and any residue on the top of the supernatant, twisting the tube as it was poured so it stuck to the side of the tube. The transferred volume is 1+1~2ml. 2ml (1 volume) of 70% ethanol (made up using molecular grade ethanol – Sigma Aldrich E7023 and dd$H_20$) to the cleaned lysates and was vortexed for 10-15secs. It is important not to centrifuge these samples at this stage.

The samples were applied by 700µl into the pre-labelled RNeasy mini-columns (Qiagen – 74104) and spun down for 15secs in a micro-centrifuge at max speed. The flow through was discharged. The applying and spinning was repeated until all the sample has been applied onto the column. The collection tubes were reused in the next step. 350µl of buffer RW1 was added to the RNeasy-mini columns and the lid was closed gently. The tubes were then spun down for 15secs in a microcentrifuge at max speed. The flow through was discharged.

10µl DNAse I stock solution was added to 70µl buffer RDD from Qiagen RNeasy Mini kit - 74104.) The sample was mixed by gently inverting the tube and centrifuged briefly to collect residual liquid from the sides of the tube (DNase I is very sensitive to physical denaturation; therefore the tube should not be vortexed and only inverted.) DNAse I incubation mix (80µl/sample) was added directly to the RNeasy spin column membrane and place on the bench-top (20-30°C) for 15mins. It is important that the DNase I incubation mix was added directly to the RNeasy spin column membrane otherwise DNase I digestion will otherwise be incomplete if it sticks to the walls or O-ring of spin column. 350µl of buffer RW1 was then applied to the RNeasy-mini columns and the lid was closed gently. The samples were then spun down for 15secs in a micro-centrifuge at maximum speed. The flow through was discharged and the collection tubes were used in the next step.

500µl of buffer RPE was then added to the RNeasy mini columns. The lid was closed gently and then the tubes were spun down for 15secs in a micro-centrifuge at max speed and the flow through was discharged. Again the collection tubes were in the next tubes in the next step. Another 500µl of RPE was added into the RNeasy-mini columns and their lids were closed gently. The samples were spun down at maximum speed in a micro-centrifuge, the flow through was discharged.

The RNeasy mini-columns were placed in new collection tubes their lids were then closed gently and they were spun down for 1 min in a micro-centrifuge at maximum speed. To elute the RNA

the RNeasy-mini columns were transferred into pre-labelled 1.5ml collection tubes. 30µl of RNAse free water was pipetted on to the membrane and the lid was closed gently. Samples were then centrifuged in a micro-centrifuged at full speed for 1 minute at RT. Each RNA sample was then placed on ice and 2µl aliquots for Agilent assessment into pre-labelled 0.5ml tubes. Samples were then stored at -80°C.

### 2.4.b. Amplification of RNA extracted from Tissue using the Nugen WT-Ovation™ FFPE System V2

Although the Ambion TotalPrep RNA amplification worked well for RNA extracted from cell lines we had difficulty getting this kit to work for the RNA extracted from tissue from the LAPATAX trial. As an alternative we used the Nugen WT-Ovation FFPE system V2 (Nugen - #3400) which worked well for the RNA extracted from tissue.

#### 2.4.b.i First Strand cDNA synthesis

Nuclease free water was taken from -20°C and equilibrated to RT. The first strand reagents were thawed and placed in ice. For each RNA sample, 2µl of first strand primer mix A1 was placed into a 0.2ml PCR thin walled tube and the tube was placed on ice. 5µl of total RNA (50 – 100ng) was added to the primer, the tubes were flicked and spun down using a micro-centrifuge. Tubes were then placed in a thermal cycler (65°C – 2 min, hold at 4°C.) When the cycler reached 4°C the tubes were spun down and then placed on ice. The first strand master mix was prepared by adding 2.5µl of Buffer Mix A2 ver 3 to 0.5µl of Enzyme mix A3 ver1 per sample and was mixed well. 3µl of the first strand master mix was then added to each tube, which were then placed in a thermal cycler (4°C – 2 min, 25°C – 30 min, 42°C – 15 min, 70°C – 15 min, hold at 4°C). Once the thermal cycler reached 4C the tubes were removed, spun down and placed on ice.

#### 2.4.b.ii Second Strand cDNA Synthesis

Agencourt RNAClean beads that are provided with the WT Ovation kit were re-suspended and left at RT. The second strand reagents were thawed, each reagent was spun down and placed on ice. The second strand master mix was assembled by combining 9.75µl buffer mix B1ver3 and 0.25µl Enzyme mix B2ver2. 10µl of second strand master mix was then added to each first strand reaction tube, tubes were mixed and spun down. All tubes were placed in a thermal cycler and programmed for 4°C – 1 min, 25°C – 10 min, 50°C – 30 min, 70°C – 5 min and then hold at 4°C. Once the thermal cycler reached 4°C the tubes were spun down and placed on ice.

#### 2.4.b.iii Purification of Double-stranded cDNA

The RNAClean magnetic bead suspension was mixed by inverting several times, At RT 32µl of the bead suspension was added to each tube, was mixed and incubated at RT for 10mins. The

samples were then transferred to a magnetic plate and allowed to stand for 5mins, 45µl of binding buffer was then removed. 200µl of freshly prepared 70% ethanol was then added to each tube and was allowed to stand for 30secs. Then the ethanol was removed with a pipette. The ethanol wash was then repeated twice and all excess ethanol was removed and then the beads were allowed to air dry for 15-20mins.

### 2.4.b.iv SPIA amplification

The Single Primer Isothermal Amplification (SPIA) reagents were thawed. Reagents C1, C2, C5 were vortexed and Reagent C3 was inverted 3 times. All reagents, including reagent C6 were spun down and placed on ice. To prepare the SPIA master mix, per sample the following reagents were combined, 50µl V2ver5 + 20µl Primer mix1 C1ver5 + 0.7µL Enhancer C6ver1 + 10µL Enzyme Mix C3ver5. 80µl of SPIA master mix was then added to each second strand reaction on ice. Samples were mixed and spun down and the tubes were ten placed in the thermal cycler and programmed at 4°C – 1 min, 47°C – 30 min, hold at 4°C. When the temperature reached 4°C the tubes were removed from the cycler, spun down and the tubes were placed on ice. The second SPIA master mix was then prepared by combining 30 µL Buffer Mix C2 ver 5 + 20µL Primer Mix 2 C5 ver 1 + 2.3µL Enhancer C6 ver 1 + 30µL Enzyme Mix C3 ver 5 and mixing well. On ice 80µl of SPIA master mix 2 was added to each reaction tube and mixed, then 80µl was added to a second reaction tube. Tubes were then placed in the thermal cycler and programmed for 4°C – 1 min, 47°C – 60 min, 95°C – 5 min, hold at 4°C. Once the thermal cycler reached 4℃ samples were spun down, place on ice and then purified with the Zymo DNA clean up kit.

### 2.4.b.iv Purification of Amplified SPIA cDNA using the Zymo DNA Clean & Concentrator-25™ kit

The amplified SPIA cDNA was purified by adding 2 volumes of DNA binding buffer (Zymo - D4005) to volume each volume of DNA sample in a 1.5ml micro-centrifuge tube, samples were then mixed briefly by vortexing. The mixture was transferred to Zymo spin columns in a collection tube. Tubes were then centrifuged for 30secs at <10,000 x g. The flow through was discarded and 200µl wash buffer was added to the columns which were centrifuged for 30secs at >10,000 x g. The wash step was then repeated. 30-50µl water (provided with the Nugen kit) was added directly to the column matrix. The columns were transferred to a new 1.5ml micro-centrifuge tune and then centrifuged for 30secs at 10,000 x g to elute the DNA.

### 2.4.b.v Purification of Labelled cDNA Product using Qiagen Mini Elute Spin Columns

The Purification of labelled cDNA was carried out using the Qiagen miniElute kit (Qiagen 28004.) 300µl of buffer ERC was added to a labelled 1.5ml tube and the full reaction (45µl) was added. It was then vortexed and spun down briefly. The entire reaction buffer mix (345µl) was

then added to labelled mini elute spin columns. Columns were then centrifuged for 1 min at >10,000 x g. The flow through was discarded and the filter was replaced in the collection tube. Samples were then washed by adding 500µl of buffer PE, centrifuging for 1 min at <10,000 x g, discarding the flow through and repeating this step. Columns were then placed back in their collection tube and spun for an additional 2mins at <10,000 x g. The column tips were blotted onto a clean filter paper to remove residual wash buffer. The columns were then placed in a new 1.5ml collection tube and 10-15µl of RT nuclease free water from the kit was added to the centre of each column. Columns were allowed to stand at RT for 1 min. The tubes were then centrifuged for 1 min at >10,000 x g leaving 10.15µl of purified labelled cDNA.

#### 2.4.b.vi Encore BiotinIL Module

cDNA biotin labelling in preparation for hybridisation to the illumina whole genome expression BeadChips was carried out using the Encore BiotinIL module (Nugen - 4210-48.) The first stage involved uracil-DNA glycosylase (UNG) is added to remove the Uracil base incorporated during the amplification process, creating and abasic site in the cDNA strand. Samples are then labelled via chemical attachment of a biotin moiety to the abasic site. Samples are then purified to prepare them for array hybridisation

#### 2.4.b.vii UNG Treatment Protocol

UNG buffer (L1) was thawed at RT and mixed by vortexing for 2 seconds and then spun down in a micro-centrifuge for 2 seconds and then placed on ice. UNG enzyme (L2) was inverted several times and the tube was spun down for 2secs and the placed on ice. For each reaction 25µl (2-4µg) of purified amplified cDNA was pipette into a 0.2ml PCR tube on ice (adding water if necessary to bring the samples up to 25µl.) 5µl of the UNG buffer was added to each sample and they were then pipette up and down to mix well. 5µl of UNG enzyme was then added to each sample and then mixed. Tubes were capped and spun down for 2secs to mix thoroughly. Tubes were then placed in a pre-warmed thermal cycler and run for 30mins at 50C and then held at 4°C. Tubes were removed from the thermal cycler and spun for 2secs to collect condensation and the placed on ice.

#### 2.4.b.viii Labelling Protocol

Labelling buffer (L3) and labelling reagent (L4) were thawed at RT and then mixed by vortexing, spinning briefly and placing on ice. 5µl of labelling buffer was added to each cDNA sample tube and the sample was mixed well. Tubes were capped and spun down for 2 seconds to mix thoroughly. 5µl of labelling reagent (L4) was added to each cDNA sample tube and mixed. Tubes were capped and spun down for 2secs to mix thoroughly. Tubes were placed in a thermal cycler for 60mins at 50°C and then held at 4°C. After completion tubes were spun down to collect condensation. The purification step detailed in section 2.4.b.v.iii was then repeated.

# Chapter 3

## Results:

### Characterisation of Taxane Resistant Breast Cancer Cell lines.

## 3.1. Establishing and characterising isogenic taxane resistant cell lines.

### 3.1.a.i Generating isogenic taxane resistant cell lines.

Taxane resistant cells were generated according to the procedure outlined in section 2.1diii. For the three cell lines we generated we retained sub-clones of the cell lines as they became increasingly resistant to drug exposure and stored cell pellets in liquid nitrogen at the following dose levels.

**MDA-MB-231 PACR:** 0.5, 1, 2, 5, 8, 10, 12, 15, 18, 20, 22, 25, 28, 30, 35, 40, 45, 50, 55, 60, 65, 70, 75, 80, 85, 90, 95 and 100nM

**ZR75-1 PACR and DOCR:** 0.5, 1, 2, 5, 8, 10, 12, 15, 18, 20, 22, 25, 28, 30, 35, 40, 45 and 50nM.

### 3.1.a.ii Selecting appropriate taxane resistant cell lines for further experimentation.

A review of current literature suggested a wide range of circulating levels of taxanes in women undergoing treatment with taxane containing chemotherapy, perhaps indicative of genetic/individual differences in metabolising these agents[191, 127.] Both Paclitaxel and Docetaxel binds highly to plasma protein (paclitaxel 95% bound, docetaxel 90%)[215, 216]. The metabolism of taxanes is primarily hepatic and renal clearance is minimal (<5% excreation in urine)[217] and both taxanes are metabolised by enzyme systems of cytochrome p450 and are eliminated in the bile[216]. Doses have to be adjusted for patients with hepatic dysfunction and taxanes can be used safely in patients with renal problems. After consulting with my clinical supervisor (Dr. Charlie Gourley) I concluded that the 25nM PACR cells represented a dose level most likely to reflect clinically relevant levels of taxanes. In addition, I included cells resistant to a lower concentration (5nM) and higher concentrations (100nM or 50nM) as comparators. The parental, non resistant cell lines were also included as controls (positive or negative dependent on the individual experiment.) However, samples from all points in the dose escalation schedule were retained, as in the future it may be pertinent to conduct a more detailed analysis of the sequential development of genetic or transcriptomic aberrations (see chapter 5.)

### 3.1bi Effect of exposure of native and PACR MDA-MB-231 cells to increasing doses of taxane over 24 hours.

The effect of exposure of the parental and isogenic taxane resistant cells on cell survival, to increasing doses of taxane was determined as follows: parental (sensitive) and paclitaxel resistant cell lines were seeded into 25cm$^2$ tissue culture plates (as described in 2.1.e.ii) and exposed to increasing doses of paclitaxel (prepared as described in 2.1.d.ii) for 24 hours before harvesting and performing direct cell counts using a Coulter counter (as detailed in 2.1.e.i) MDA-MB-231 Native, 5nM, 25nM and 100nM PACR cells were treated with either: blank media, 5nM, 25nM or 100nM Paclitaxel for 24 hours.

As paclitaxel concentration increases from zero, to 5, 25 and 100nM, as predicted, the number of native surviving cells falls sharply (figure 3.1 blue bar) to 89, 50 and 46% respectively.

When 5nM PACR cells (figure 3.1 red bar) are treated with each of the four paclitaxel doses paclitaxel they tolerate the 5nM paclitaxel well (100% surviving cells remain) but reduce in number when treated with 25 or 100nM paclitaxel (in both cases 74% survive.)

The 25nM PACR cells (3.1 figure green bar) also tolerate the lower doses of paclitaxel (99% of cells remain) well but begin to reduce in number when treated with 25 or 100nM paclitaxel (86 and 79% cell remain.) The Native, 5nM and 25nM PACR cells all behaved as predicted by having an increased tolerance for paclitaxel treatment.

The 100nM PACR cells (re. figure 3.1 purple bar) did not behave as predicted. As the concentration of paclitaxel increased, the 100nM PACR survived better in the presence of higher concentrations of paclitaxel (figure 3.1 blue bar.) As the paclitaxel concentration increased from 5, to 25 and 100nM the percentage of remaining cells unexpectedly increased from 100 to 133 and 125% respectively. This suggests a change must have occurred in the 100nM cells to cause this taxane dependent phenotype. However, this anomaly does not occur in tumours in a clinical setting. This initial experiment sought to set the stage for further cell count experiments.

Anova analyses were performed on the resulting data, comparing each cell line in a pairwise fashion to obtain a *p* value. *p* values are listed in table 3.1 and show that there are significant differences in cell count between each of the four cell lines when compared to one another.

| Comparison | *p*-Value |
|---|---|
| Native vs. 5nM PACR | $7.66^{-08}$ |
| Native vs. 25nM PACR | $3.29^{-12}$ |
| Native vs. 100nM PACR | $3.29^{-12}$ |
| 5nM PACR vs. 25nM PACR | 0.000226 |
| 5nM PACR vs. 100nM PACR | $6.5^{-10}$ |
| 25nM PACR vs. 100nM PACR | $7.16^{-08}$ |

**Table 3.1** *P* values of Anova tests from pairwise comparisons of MDA-MB-231 native, 5nM, 25nM and 100nM PACR cell lines.

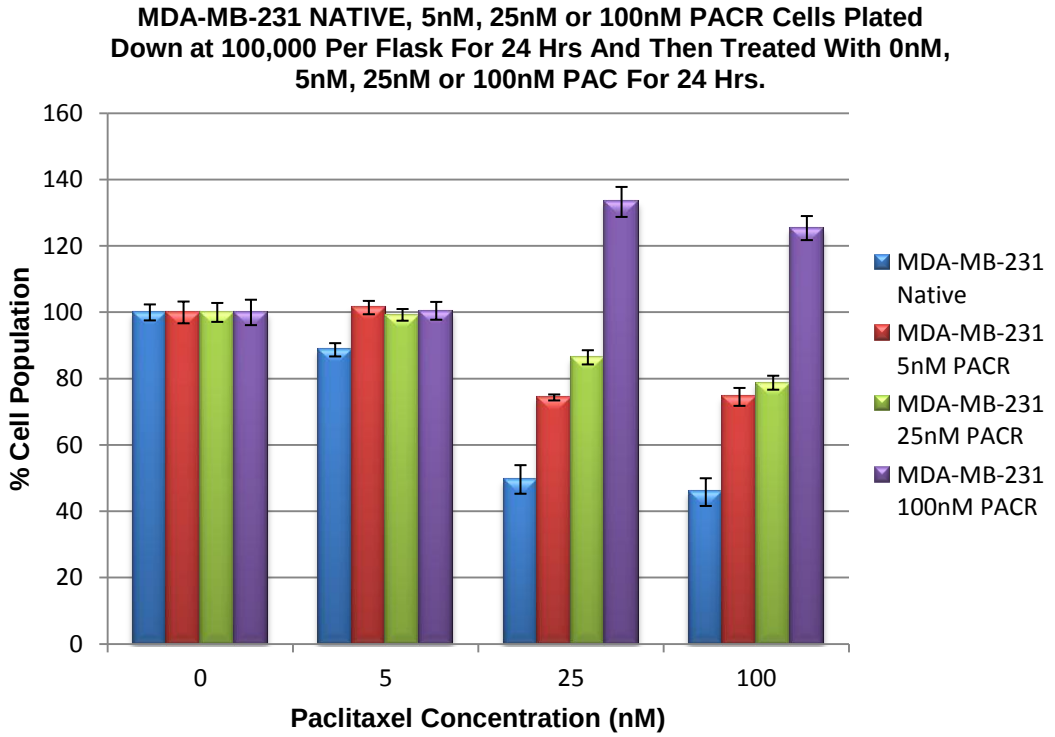


**Figure 3.1.** MDA-MB-231 Native, 5nM, 25nM and 100nM PACR cells treated with either blank media, 5nM, 25nM or 100nM Paclitaxel for 24 hours. The X axis shows increasing paclitaxel dose measured in nM. The Y axis represents the percentage cells with untreated cells being taken as a baseline of 100%. Native cells are represented by the blue bar, 5nM PACR cells are represented by the red bar, 25nM PACR cells are represented by the green bar and 100nM PACR cells are represented by the purple bar.

### 3.1.b.ii Cell Counts of MDA-MB-231 Native and 25nM PACR cells treated with paclitaxel for 96 hours.

This experiment sought to evaluate the impact of extending the period of drug treatment on the native and the 25nM Paclitaxel resistant MDA-MB-231 cells after treatment with increasing doses of paclitaxel. As the concentration of paclitaxel increased from 0 to the suboptimal doses of 3 and 5nM (re figure 3.2 represented by the dark green bar) the proportion of native cells fell sharply to 29% and 22% respectively. At mid range to high doses; 10, 25 and 50nM drug, the native proportion of cells continued to fall to 16, 13 and 9% respectively.

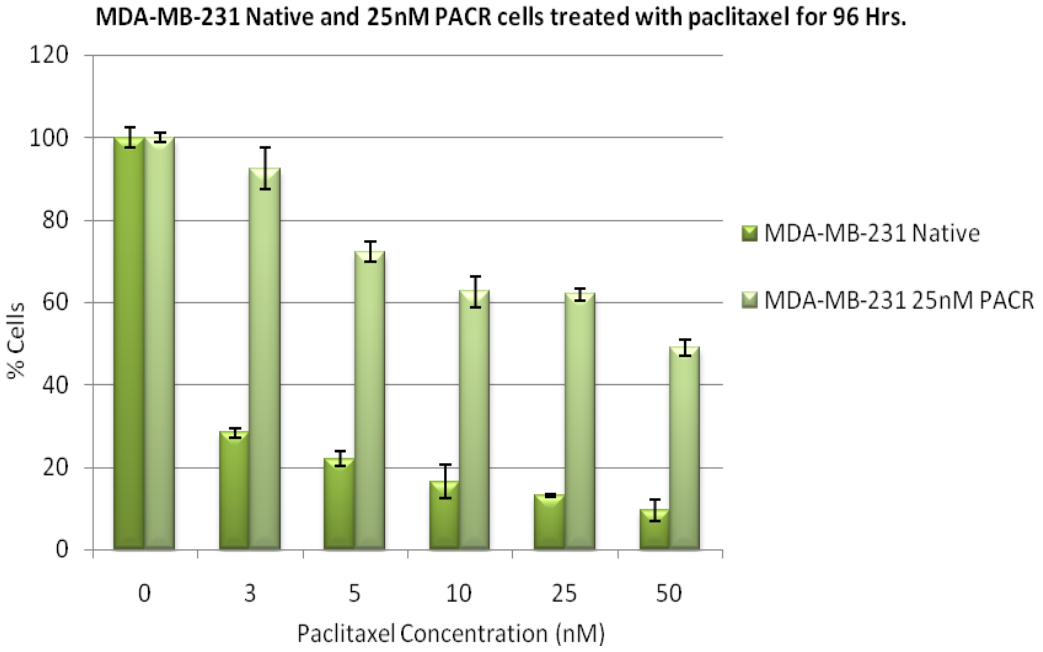


**Figure 3.2.** MDA-MB-231 Native and 25nM PACR cells treated with either blank media, or 3, 5,10,25 or 50nM Paclitaxel for 96 hours. The X axis shows increasing paclitaxel dose measured in nM. The Y axis represents the percentage cells, with untreated cells being taken as a baseline of 100%. Native cells are represented by the red bar, and 25nM PACR cells are represented by the green bar.

The 25nM PACR cells (figure 3.2 represented by the light green bar) tolerated the lowest dose of 3nM Paclitaxel well, with 93% cells surviving. 25nM PACR cells also tolerate the mid to high range doses of 5, 10 and 25nM paclitaxel well, with 72, 63 and 62% of their respective cells surviving. At the highest dose of 50nM the 25nM PACR cells still tolerate the drug with 49% of cells remaining. There was a highly significant difference when comparing the cell counts of the native to the 25nM PACR cell lines when treated with increasing doses of paclitaxel ($p$ value = $3.08^{-16}$ determined using ANOVA)

This experiment proves that isogenic paclitaxel resistant MDA-MB-231 cells were successfully generated and able to tolerate a dose level of 25nM paclitaxel. The $IC_{50}$ of the native cells was determined to be 2.2nM. At the chosen dose levels established in this experiment it was impossible to determine the $IC_{50}$ using the linear equation of the trendline of the data however, treatment with 50nM paclitaxel does exert a reduction in cell number to 49% of the untreated total suggesting an $IC_{50}$ of ~ 50nM. The $IC_{75}$ of the 25nM PACR cells is 3.3nM.

### 3.1.b.iii Cell Counts of MDA-MB-231 Native and 100nM PACR cells treated with Paclitaxel for an extended period.

This Experiment was designed to explore further the unexpected finding with the 100nM PACR cells in the first exploratory cell count (re figure 3.3.)

When native MDA-MB-231 Cells (3.3 figure dark purple) are treated with increasing doses of paclitaxel: 0, 1, 3, 5, 15, and 30nM the percentage of remaining cells reduces from 100, to 55, 18, 20 ,19 and 13% respectively.

When the 100nM PACR cells are treated with these same doses of drug, the same unexpected pattern as seen with the 24 hour treatment is seen, the percentage of surviving cells (relative to untreated cells) actually rose from 100% with the untreated cells to 119, 201, 206, 259, and 287% respectively with increasing drug dose.

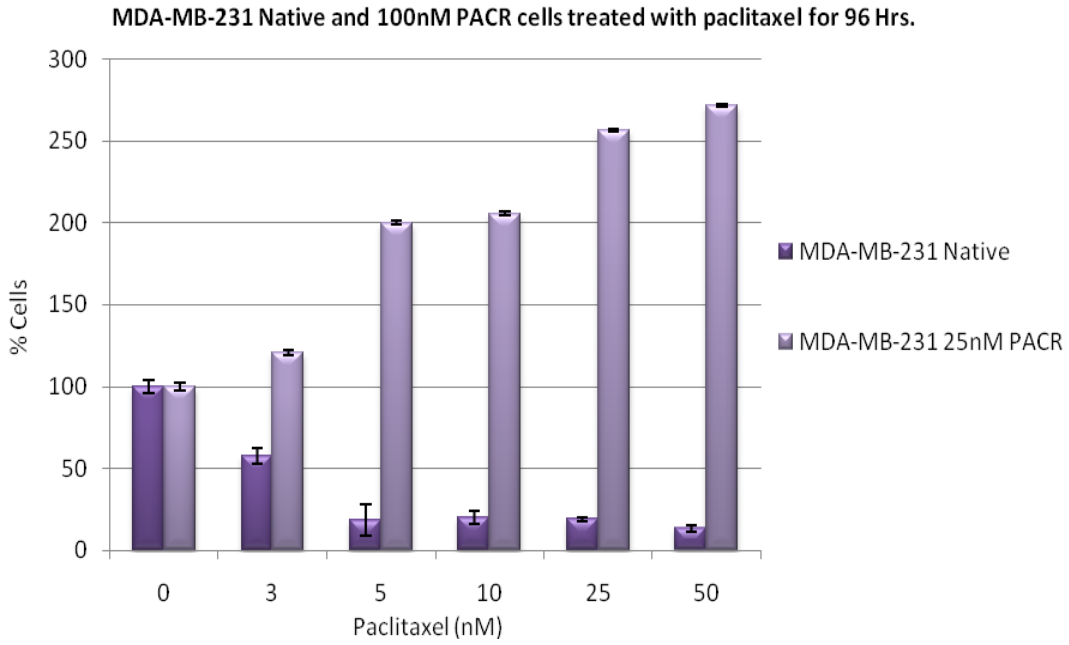


**Figure 3.3.** MDA-MB-231 Native and 100nM PACR Cells treated with either, blank-media or 1, 3, 5, 10 15 or 30nM Paclitaxel for 96 hours. The X axis shows increasing paclitaxel dose measured in nM. The Y axis represents the percentage cells, with untreated cells being taken as a baseline of 100%. Native cells are represented by the dark purple bar, and 100nM PACR cells are represented by light purple.

A highly significant difference was found when comparing the cell counts of the native to the 100nM PACR cell lines when treated with increasing doses of paclitaxel ($p$ value = $1.0^{-33}$.) This experiment proves that the unexpected behaviour of the 100nM PACR MDA-MB-231 can be

repeated over extended dose schedules. Although this result is very interesting and unusual it is important to consider that this behaviour is unlikely to be borne out in real tumours in the clinic. The 100nM dose is also beyond the standard doses that would be used in the clinic. This unusual behaviour exhibited by the 100nM PACR cells suggested that the cells have become resistant to higher levels of PACR that are seen in the clinical setting. As a consequence of this I chose not to further investigate the 100nM PACR cells, although I am willing to revisit this interesting anomalous result in the future. In this experiment the $IC_{50}$ for the native cells was determined to be 2.7nM which is encouraging as it was 2.2nM in previous experiments. It was impossible to generate an $IC_{50}$ for the 100nM PACR cells.

### 3.1.b.iv Cell Counts of MDA-MB-231 Native, 25nM PACR Cells Maintained Out of Drug and 25nM PACR Cells Maintained in Drug: Are 25nM PACR Clones Stable or do they Revert to the Parent Phenotype?

To complete this series of cell count experiments for the MDA-MB-231s I tested whether PACR cells retained their resistant phenotype when maintained in the absence of drug. When the Native cells (figure 3.4 represented by the red bar) are treated with paclitaxel increasing in concentration from 3, 5, 10, 25 and 50nM the percentage of cell relative to the untreated native cells drops to 19, 18, 12, 9 and 8% respectively.

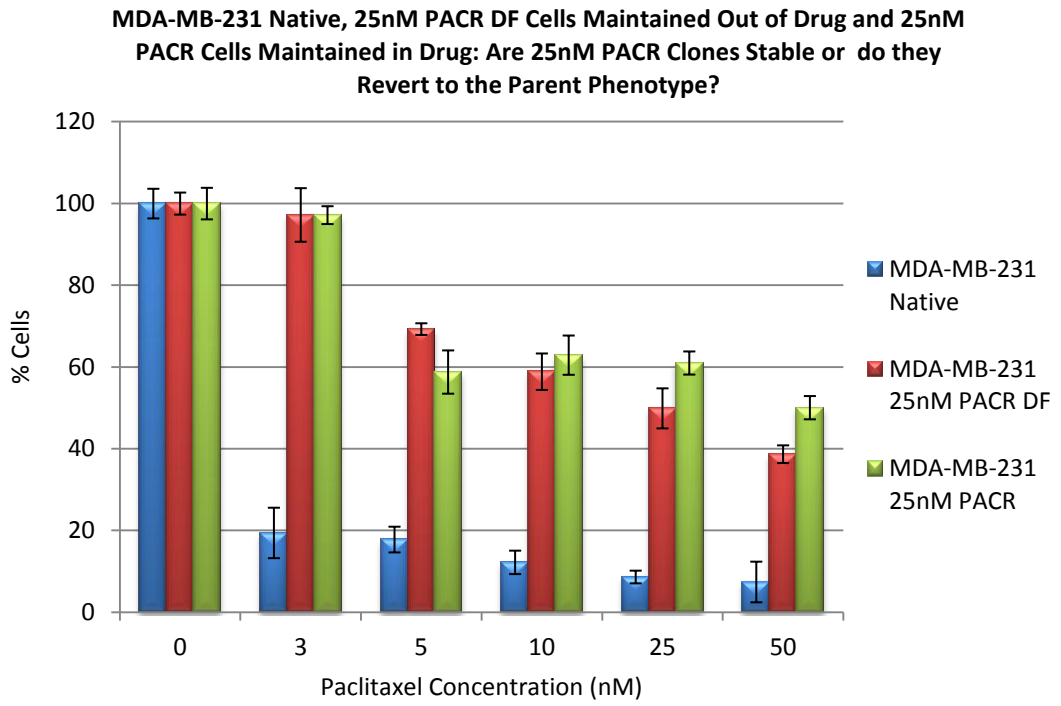


**Figure 3.4** Prior to this experiment, 25nM paclitaxel resistant cells were separated into two groups; one group was maintained and passaged, as normal in the presence of paclitaxel, the second group of cells was maintained in the absence of drug paclitaxel. Both groups were maintained and passaged for a period of six months I designated the cells maintained in the presence of drugs the PACR cells and the cells maintained in the absence of drug the PACR-DF. Each of the three groups of Cells; Native, PACR and PACR-DF cells were treated with either blank media or 3, 5, 10, 25 or 50 nM paclitaxel for 96 hours The Native cells are represented by the blue bar, the PACR-DF cells are represented by the red bar and the PACR cells are represented by the green bar. The X axis shows increasing paclitaxel dose measured in nM. The Y axis represents the percentage cells, with untreated cells being taken as a baseline of 100%.

The MDA-MB-231 cells that had previously been maintained out of paclitaxel reduced in cell number relative to the untreated baseline of 100% to 97, 69, 59, 50 and 39% in the groups treated with increasing paclitaxel concentration.

The PACR cells that had been previously been maintained in long term culture in the presence of drug showed a similar if not identical pattern of response to the cells that had been maintained in a drug free environment prior to the experiment. As paclitaxel concentration increased from 3 to, 5, 20 25 and 50nM the percentage of cells remaining after treatment relative to the cells given no drug fell to 97, 61, 63, 61 and 50%. The IC50 for the native cells 1.9nM, 5.0nM for the MDA-MB-231 25nM maintained in the absence of drug and 5.7nM for the MDA-MB-231 Native

cells maintained in the presence of paclitaxel. 2 way Anovas were condcted on the cell count data between each of the three cell lines in a pairwise fashion and the resulting *p* values are shown in table 3.2.

The Anovas showed that the there was a significant difference in cell counts between each of the 25nM PACR-DF and the 25nM PACR cell line and the native line with respective *p* values of $p = 3.94^{-20}$, $p=9.87^{-22}$. When comparing the cell counts of the 25nM PACR-DF and 25nM PACR a *p* value = 0.09728 was obtained showing that there was no significant difference between the two lines (note $\alpha = 0.05$), indicating that they have a very similar paclitaxel resistant phenotype.

| Comparison | *p*-Value |
|---|---|
| **Native vs. 25nM 25nM PACR-DF** | $3.94^{-20}$ |
| **Native vs. 25nM PACR** | $9.87^{-22}$ |
| **25nM PACR-DF vs. 25nM PACR** | 0.09728 |

**Table 3.2** *p* values of Anova tests from pairwise comparisons of Native MDA-MB-231, 25nM PACR-DF (maintained long term out of drug), and MDA-MB-231 25nM PACR (maintained in drug) cell line, cell count data detailed in section 3.1.b.iv.

This Experiment confirms that isogenic paclitaxel resistant MDA-MB-231 cell lines that retain their resistant properties in the absence of drug and did not revert to their parental phenotype have been generated. This is a key experiment in the investigation as it meant that experiments could be designed, transferring the *in vitro* model into an *in vivo* xenograft model. This transition would considerably widen the scope of my work, allowing me to construct more clinically relevant experiments and ideas.

## 3.2 Generation of Taxane Resistant ZR75-1 Cells.

### 3.2a Cell Counts of ZR75-1 Native and 25nM PACR cells treated with paclitaxel for an extended period.

ZR75-1 cells that are resistant to paclitaxel were also generate. An experiment was set up using the same conditions as for the MDA-MB-231 25nM PACR cells.

As the concentration of paclitaxel increases from zero to the lower doses of 3 or 5nM paclitaxel, the percentage of remaining native cells (represented by the dark turquoise bar in figure 3.5) drops from 100 to 98 and 56% respectively. When the native cells are treated with 10 and 25nM of paclitaxel the percentage of remaining cells drops to 26%. At the highest dose of 50nM paclitaxel the percentage of remaining cells drops again to 17%.

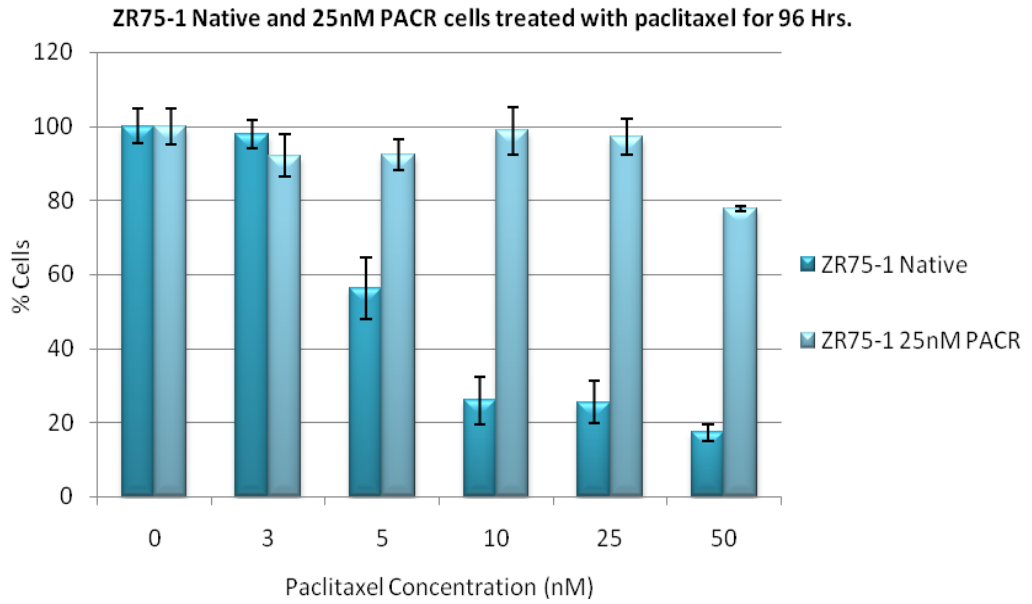


**Figure 3.5** ZR75-1 Native and 25nM PACR cells treated with either blank media, or 3, 5,10,25 or 50nM Paclitaxel for 96 hours. The X axis shows increasing paclitaxel dose measured in nM. The Y axis represents the percentage cells, with untreated cells being taken as a baseline of 100%. Native cells are represented by the dark turquoise bar, and 25nM PACR cells are represented by the pale turquoise bar.

The 25nM PACR cells were treated with up to 25nM of paclitaxel without reducing in number to 92% of the untreated cells. On treatment with the higher dose of 50nM the percentage of remaining cells drops to 78%. An Anova test on the data was conducted and it was found that there was a significant difference in the cell counts of the ZR75-1 native and PACR cell lines when treated with increasing doses of paclitaxel ($p$ value = $6.1^{-5}$.)

The $IC_{50}$ of the ZR75-1 native cells when treated with paclitaxel is 3.7nM. The $IC_{50}$ of the PACR ZR75-1 cells cannot be determined as the proportion of remaining cells does not drop below 75% even at the highest dose of 50nM. A number of conclusions can be drawn from this experiment. Firstly, it can be concluded that the 25nM PACR ZR75-1 cells are indeed resistant to paclitaxel. Secondly the ZR75-1 Native cells tolerate paclitaxel better than MDA-MB-231 cells, this poses the question do ZR75-1 native cells have a low level of inherent resistance to paclitaxel, and why might they have this low level of reistance? ZR75-1 cells are ER+ve and HER2 –ve, The TACT trial showed that tumours that were ER+ve and HER2-ve did not benefit from the addition of a taxane to a standard anthracycline regimen[117]. Finally, the 25nM PACR ZR75-1 cells seem to be more resistant to paclitaxel than the 25nM PACR MDA-MB-231.

**3.2b Cell Counts of ZR75-1 Native and 25nM DOCR cells treated with Docetaxel for 96 hours.**

In addition to our paclitaxel resistant MDA-MB-231 and ZR75-1 cells, docetaxel resistant ZR75-1 cells were generated. To confirm that the ZR75-1 cells are indeed resistant to docetaxel I set up the same experiment for the ZR75-1 DOCR cells as I did for the MDA-MB-231. When native ZR75-1 cells (re dark orange bar bar, figure 3.6 next page) are treated with 3nM docetaxel, the remaining cells relative to the untreated cells drop to 18% of the untreated. As the concentration of docetaxel used for treatment increases, there is not much variation in the percentage of remaining cells.

On treating 25nM docetaxel resistant cells (represented by the pale orange bar figure 3.6) with 3, 5, 10 25 and 50nM docetaxel the cells are reduced to 88, 89, 92, 80 and 60% of the untreated cells respectively.

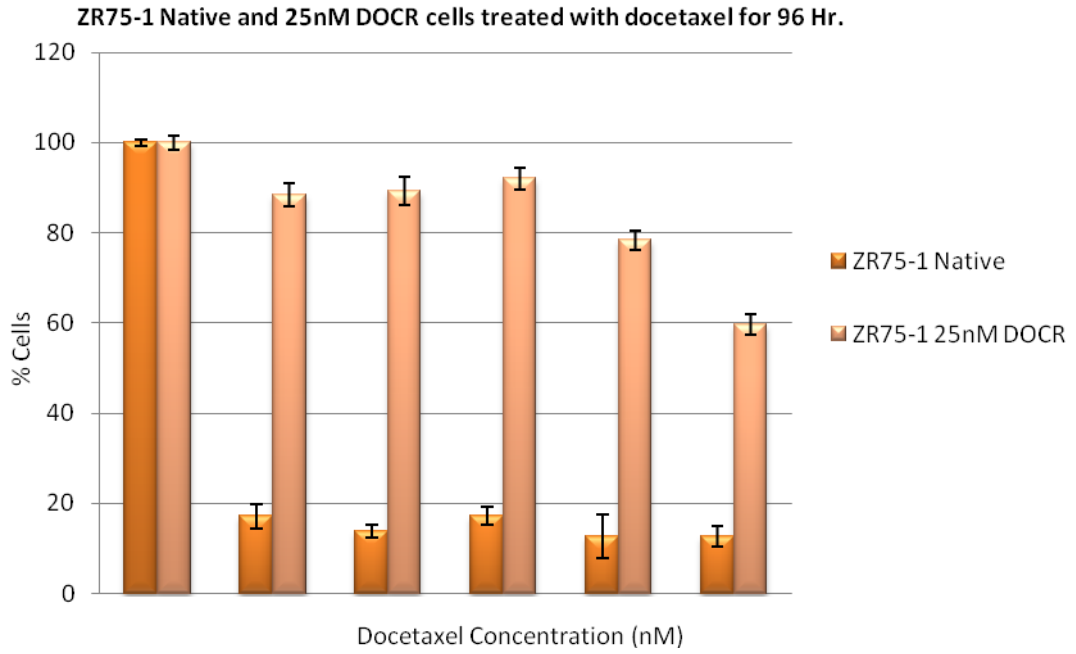


**Figure 3.6** ZR75-1 Native and 25nM DOCR cells treated with either blank media, or 3, 5,10,25 or 50nM Paclitaxel for 96 hours. The X axis shows increasing paclitaxel dose measured in nM. The Y axis represents the percentage cells, with untreated cells being taken as a baseline of 100%. Native cells are represented by the dark orange bar, and 25nM DOCR cells are represented by the pale orange bar.

The $IC_{50}$ of the native ZR75-1 cells when treated with docetaxel is 4.9nM. The $IC_{50}$ of the ZR75-1 DOCR cells when treated with docetaxel cannot be determined as the proportion of cell remaining after docetaxel even at the highest dose is 60%. An Anova test was conducted on the

data and found that the there was a significant difference in the cell counts of the ZR75-1 native and DOCR cell lines when treated with increasing doses of paclitaxel (*p* value = $1.63^{-36}$.)

Again, a number of important conclusions and observations can be drawn from this experiment. Firstly it can be concluded that ZR75-1 cell line that is resistant to docetaxel has been sucessflly created. Secondly, it was observed that the native cells seem to tolerate paclitaxel better than docetaxel (paclitaxel $IC_{50}$=3.7, docetaxel $IC_{50}$= 4.9. This confirms previous in vitro studies which suggest that docetaxel is a more potent drug than paclitaxel; docetaxel is approximately twice as potent as paclitaxel on a mg-per-mg basis[31]. Finally, it can be concluded that the pattern of resistance when DOCR cells are treated with docetaxel is similar to that seen when PACR cells are treated with paclitaxel.

## 3.3 Cell Cycle analysis of Taxane Resistant Breast Cancer Cell lines.

### 3.3a Initial Prep test for Trypsinisation Step in Vindelov's Protocol.

Before embarking on large scale cell cycle analysis experiments using Flow cytometry, the duration of the trypsinisation step in the Vindelov's protocol has to be established[245(218)]. Figure 3.7 shows the data obtained from the 2 minute (top left panel) 4 minute (top right panel) and 6 minute prep test (bottom left panel) using the MDA-MB-231 native cells. The data from these prep tests were analysed using the Modfit programme.

The red peak on the left hand side of each of the three panels in figure 3.7 represents the cells occupying the G0/G1 phase of the cell cycle. The very broad yellow humps in the centre of each plot are the S phase cell population, and the broad green humps to the right of each plot represent the G2/M population. Each of these three plots looks very similar to one another and broadly reflects what a "normal" cell cycle unperturbed any treatment should look like. So, to establish what the most appropriate trypsinisation time was, the analysed data needed to further dissected.

Table 3.3 shows the number of events modelled in each experiment, the % of cells in each phase of the cell cycle, the percentage of debris in each sample, the % of cells that are diploid and the % Coefficient of Variation.

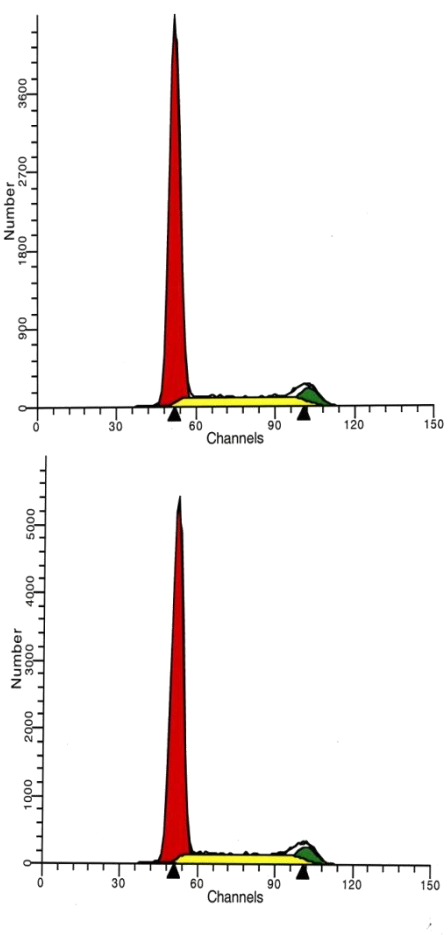


**Figure 3.7.** Vindelov's Protocol Initial Prep Test. Top left panel is the 2 minute prep test, top right is the four minute test and the bottom right is the 6 minute prep. In each panel the red peak represents the G0/G1 population, the very broad yellow hump represents the S phase population and the moderately broad green hump represents the G2/M cell population.

For each sample, between thirty and forty thousand cells were modelled, and all of them were diploid. The percentage of cells in each phase of the cell cycle is not affected by the duration of trypsinisation and only a very small amount of debris was formed. Ultimately the % CV can be used to ascertain which of the three prep tests had the least amount of variation in the sample. The % CV is a normalized measure of dispersion of a probability distribution. It is calculated by taking the ratio of the standard deviation to the mean. So, the lower the %CV the lower amount of variation there is across a sample.

The sample with the lowest % CV was the 2 minute prep test and as such could be determined as the most appropriate duration for the trypsinisation step in the Vindelov's protocol for future experiments. However, there is very difference in %CV between the three prep times so it is reasonable to conclude that trypsinisation time had very little effect on the variation at these time periods.

| Duration of Prep Test | Events | Dip G0:G1 | Dip S | Dip G2/M | G2/G1 | Debris | % Dip | % CV |
|---|---|---|---|---|---|---|---|---|
| **2 mins** | $3 \times 10^4$ | 74 | 19 | 7 | 2 | 1 | 100 | 3.7 |
| **4 mins** | $3.8 \times 10^4$ | 73 | 20 | 7 | 2 | 1 | 100 | 3.9 |
| **6 mins** | $3.2 \times 10^4$ | 73 | 20 | 7 | 2 | 0.5 | 100 | 4.0 |

**Table 3.3** Shows data from 2, 4 and 6 minute preparation tests analysed using the modfit data analysis software. The first column of data shows the number of events modelled during the cell cycle analysis. The second column shows the percentage of diploid cells in the G0 and G1 phase of the cell cycle. The third column shows the percentage of cells in S phase and the fourth shows the percentage of cells in G2/M phase. Column Five shows the ratio between the G2 and G1 phase cells, which is 2 in a completely diploid population. Column six shows how many cells are diploid expressed as a percentage. The final column shows the % coefficient of Variation across the population in each prep test.

**3.3bi Flow Cytometry Based Cell cycle analysis of Native MDA-MB-231 cells treated with paclitaxel.**

The cells generated during the initial cell count experiments were then used in subsequent cell cycle analysis experiments (re section 3.1.b.ii.) On treatment with increasing doses of paclitaxel the proportion of cells in the G0/G1 phase of the cell cycle falls dramatically from 70% with the untreated cells to roughly 18% at the highest two doses (re 3.8 figure blue bar.)

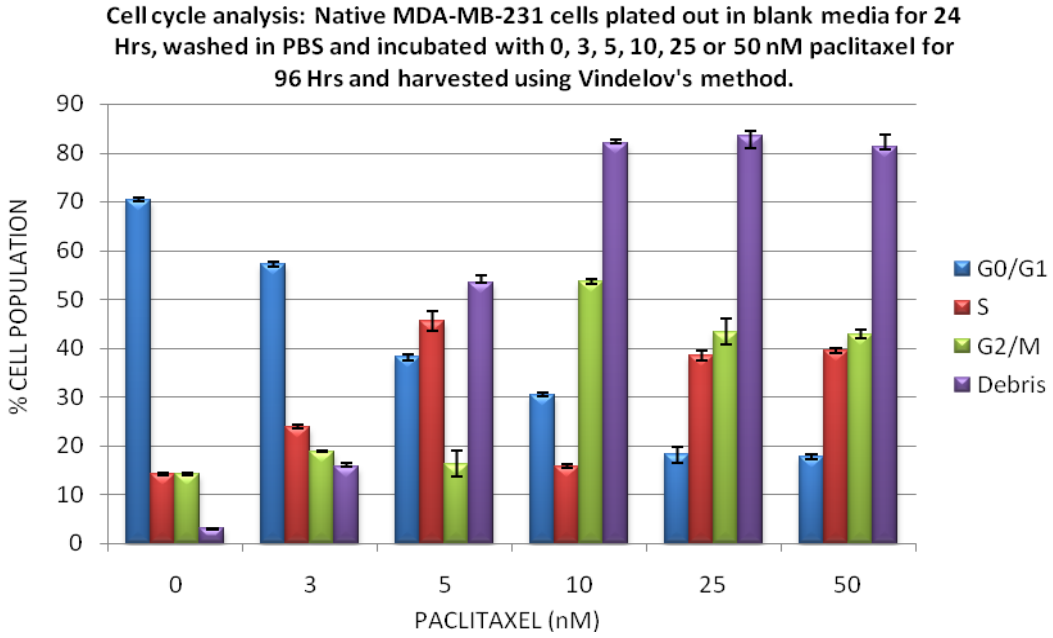


**Figure 3.8.** MDA-MB-231 Native cells are treated with, either blank media, or 3, 5, 10, 25 or 50nM Paclitaxel for 96 hours. The X axis shows increasing paclitaxel dose measured in nM. The Y axis represents the percentage of the cell population inhabiting each stage of the cell cycle. The blue bar represents the cells in G and G1 phase of the cell cycle. The red bar represents the cells in S phase on the cell cycle. The green bar represents those cells in the G2 and M phase of the cell cycle. The purple bar represents the percentage of debris in each sample.

The untreated MDA-MB-231 sample has roughly 14% of the cell population in the S phase of the cell cycle (re figure 3.8 red bar.) When native cells were treated with 3nM of paclitaxel, the fraction of cells in S phase increased to 24% and then rises again to 46% in the 5nM paclitaxel treated cells. When the 10nM dose is administered to the cells the proportion of cells in S phase falls again to 16%. However, at the two highest doses of paclitaxel; 25 and 50nM the proportion of cells inhabiting the S phase of the cell cycle climbs again to 39 and 40% respectively. This shows that low dose paclitaxel can cause an increase in the number of cells that stuck in S phase

by blocking their exit. This increase is alleviated at the mid range doses and then again perpetuated at the highest doses.

Roughly 14% of cells inhabit the G2/M phase of the cell cycle in the untreated sample (re figure 3.8 green bars.) On treatment with 3nM Paclitaxel the proportion of G2/M cells rises slightly to 19%. When the dose is increased to 5nM the G2/M population falls again, only slightly to 16%. These low doses of paclitaxel seem to have no significant effect on the G2/M phase of the cell cycle. When the paclitaxel dose is increased to 10nM, there is a marked increase and 54% of cells are in the G2/M phase. This suggests that paclitaxel is exerting a G2/M block upon the cell cycle. At the highest doses roughly 43 or 44% of cells are in G2/M phase suggesting that the G2/M block is still perpetuated at the highest dose of the drug.

When the concentration of paclitaxel increases the proportion of debris increases rapidly as cells are beginning to die (Re figure 3.8 purple bar.) In untreated cells the amount of debris is only around three percent whereas in the cells treated with the highest two doses of paclitaxel the debris reaches over 80%. It is important to note that the although these experiments measure the level of debris in each sample the cell cycle measurements are made on the viable cells in the population.

When making a pairwise comparison of each of the three cell cycle stages (G0/G1, S and G2/M) using a t test, there is a statistically significant difference between the percentage of cells in each cell cycle stage between the untreated cells and the cells treated with the highest dose of paclitaxel ($p = 4.4^{-10}$, $p = 1.2^{-8}$, $p = 1.88^{-5}$, respectively.)

In conclusion, treatment with paclitaxel exerts a G2/M block upon MDA-MB-231 Native cells causing cells to build up in the G2/M phase and fail to return to G0/G1 phase. The initiation of the G2/M block also causes the cells to fail to move in S phase when treated with moderate doses of paclitaxel. This is slightly alleviated as a small proportion of cells seem to escape the G2/M block and allow a slight build up in S phase.

### 3.3cii Flow Cytometry Based Cell cycle analysis of 25nM PACR MDA-MB-231 cells treated with paclitaxel.

When conducting an identical experiment using the 25nM PACR MDA-MB-231 cells, a very different pattern of distribution of cells across the cell cycle is seen.

When the paclitaxel resistant cell line is treated with increasing doses of paclitaxel the proportion of cells in the G0/G1 phase of the cell cycle gradually increases from to 59% in the

untreated cells to a peak of 75% in the 25nM treated cells (figure 3.9 blue bar.) At the highest dose of 50nM, the proportion of cells in G0/G1 phase falls again to 65%.

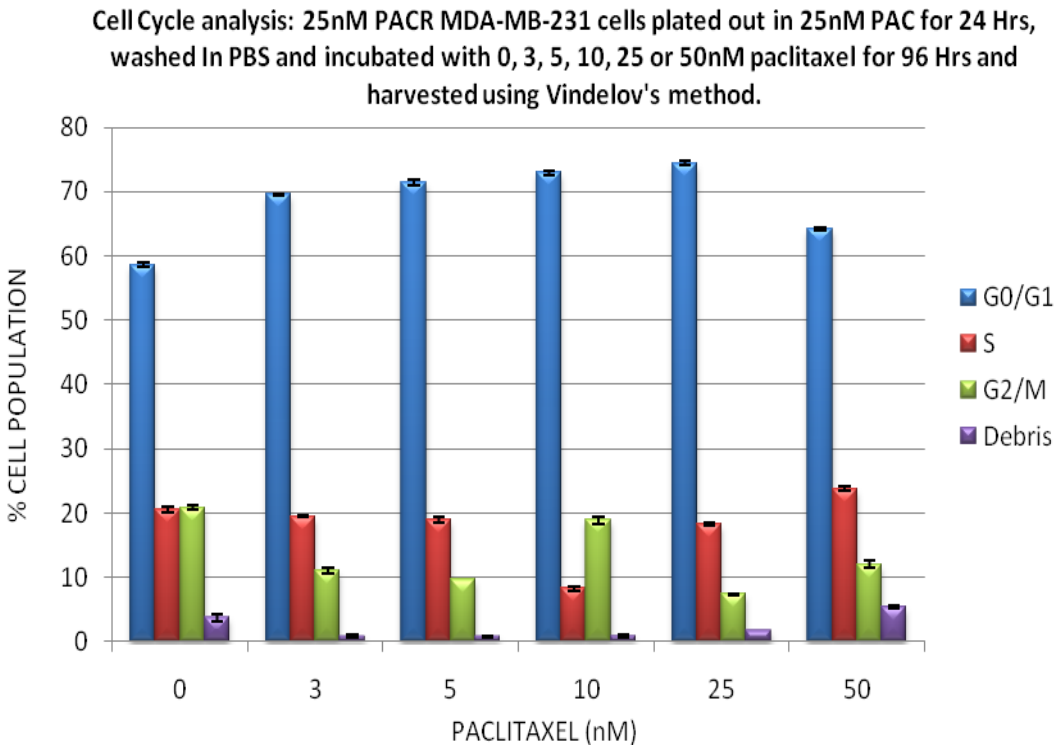


**Figure 3.9.** MDA-MB-231 25nM PACR cells were treated with either blank media, or 3, 5,10, 25 or 50nM Paclitaxel for 96 hours. The X axis shows increasing paclitaxel dose measured in nM. The Y axis represents the percentage of the cell population inhabiting each stage of the cell cycle. The blue bar represents the cells in G and G1 phase of the cell cycle. The red bar represents the cells in S phase on the cell cycle. The green bar represents those cells in the G2 and M phase of the cell cycle. The purple bar represents the percentage of debris is each sample.

The proportion of cells in S phase stays relatively unchanged from the untreated cells when samples are treated with low dose paclitaxel at around 19 or 20% (figure red bar 3.9.) At the moderate dose of 10nM the S phase content falls to about 8%. However, when cell are treated with the two highest doses of paclitaxel the S phase content grows again to 18 and 24% respectively.

The G2/M content of the untreated PACR cells is roughly 21%. Low dose paclitaxel treatment causes the G2/M content to drop to around 10 or 11% (figure green bar 3.9.) The moderate, 10nM paclitaxel dose elicits an increase in G2/M content to 19%. However, at the two highest doses of paclitaxel G2/M content drops to 7% then rises again to 12%. This shows no real

consistent pattern of increase or decrease in G2/M content in the MDA-MB-231 PACR cells when paclitaxel concentration increases.

As the paclitaxel concentration increases the debris content remains low and only varies between 1 and 5% (re figure 3.9 purple bar.)

When making a pairwise comparison of each of the three cell cycle stages (G0/G1, S and G2/M) using a t test, there is a statistically significant difference between the percentage of cells in that cell cycle stage in the untreated cells and the cells treated with the highest dose of paclitaxel ($p$ = 0.00046, $p$ = 0.00016, p = $8.89^{-7}$ respectively.)

In conclusion the paclitaxel resistant MDA-MB-231 cells seem to tolerate treatment with paclitaxel well and seem to completely escape the G2/M block that is elicited in the native cells when treated with the drug.

### 3.3.c.iii Flow Cytometry Based Cell cycle analysis of Native MDA-MB-231 cells treated with paclitaxel.

Additional cell cycle experiments were performed upon the native and 100nM PACR MDA-MB-231 cells. They were plated out, harvested and according to section 2.1.e.ii and 2.1.g.i. Figure 3.10 shows the resulting data from this experiment on the following page. As the concentration of paclitaxel increases, the percentage of MDA-MB-231 native cells inhabiting the G0/G1 phase of the cell cycle decreases (re blue bar figure 3.10) and the cells in the S phase and then the G2/M phase of the cell cycle increase. The percentage of debris increased with increasing paclitaxel concentration (re purple bar figure 3.10.)

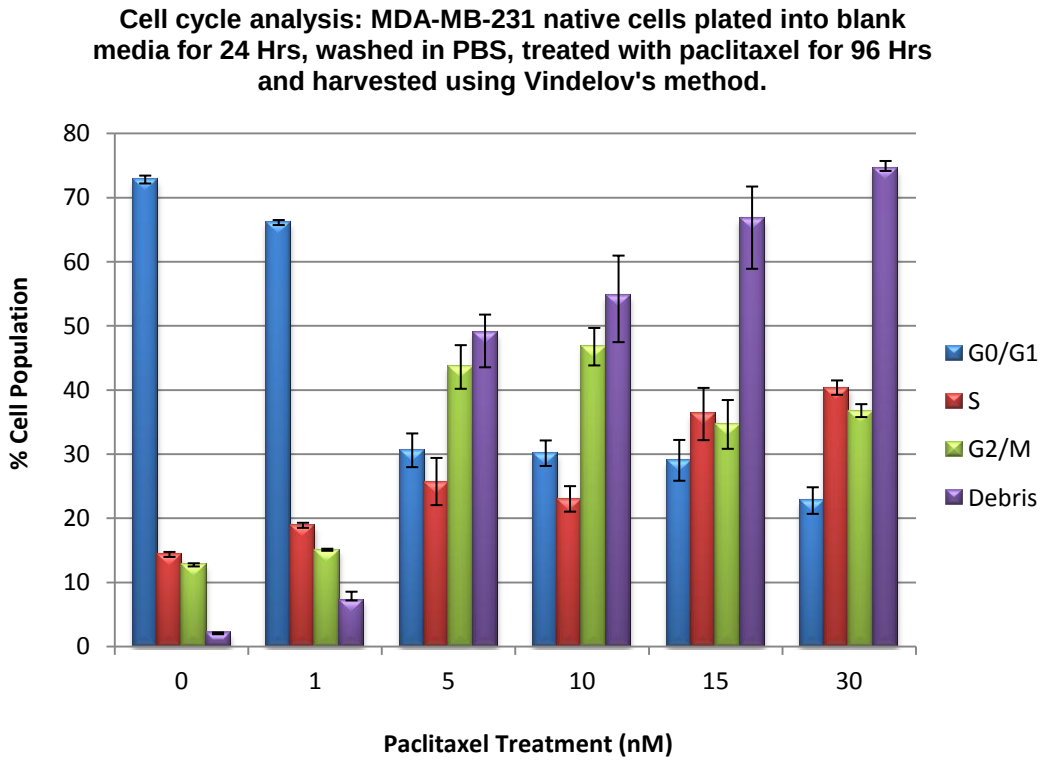


**Figure 3.10.** MDA-MB-231 native cells were treated with either blank media, or 1, 5,10, 15 or 30nM Paclitaxel for 96 hours. The X axis shows increasing paclitaxel dose measured in nM. The Y axis represents the percentage of the cell population inhabiting each stage of the cell cycle. The blue bar represents the cells in G and G1 phase of the cell cycle. The red bar represents the cells in S phase on the cell cycle. The green bar represents those cells in the G2 and M phase of the cell cycle. The purple bar represent the percentage of debris is each sample.

When making a pairwise comparison of each of the three cell cycle stages (G0/G1, S and G2/M) using a t test, there is a statistically significant difference between the percentage of cells in that cell cycle stage in the untreated cells and the cells treated with the highest dose of paclitaxel ($p$ = $7.02^{-5}$, $p$ = $1.05^{-5}$ $p$ = $6.32^{-5}$ respectively.)

These findings are reflective of the pattern of changing cell cycle dynamics shown in figure 3.10. This experiment is broadly similar to what was determined in section 3..3.b.i for the paclitaxel treated MDA-MB-231 native cells that were generated in conjunction with the 25nM PACR cells and showed that treatment with paclitaxel exerts a G2/M block in native MDA-MB-231 cells.

**3.3.c.iv Flow Cytometry Based Cell cycle analysis of 100nM PACR MDA-MB-231 cells treated with paclitaxel.**

In conjunction with the previous experiment (section 3.3.c.iii) flow cytometry based cell cycle analysis was performed upon the MDA-MB-231 100nM PACR cells. Cells were plated out harvested and prepared according to section 2.1.e.ii and 2.1.g.i. As the concentration of paclitaxel increases MDA-MB-231 100nM PACR cells build up in G0/G1 phase (re figure 3.11 blue bar.) The proportion of S phase cells remains relatively unchanged on increasing paclitaxel concentration (re figure 3.11 red bar.) The proportion of MDA-MB-231 100nM PACR cells in the G2/M phase of the cell cycle reduces as the concentration of paclitaxel increases (re figure 3.11 green bar.) There is no increase in the proportion of debris as the concentration of paclitaxel increases (re figure 3.11 purple bar.)

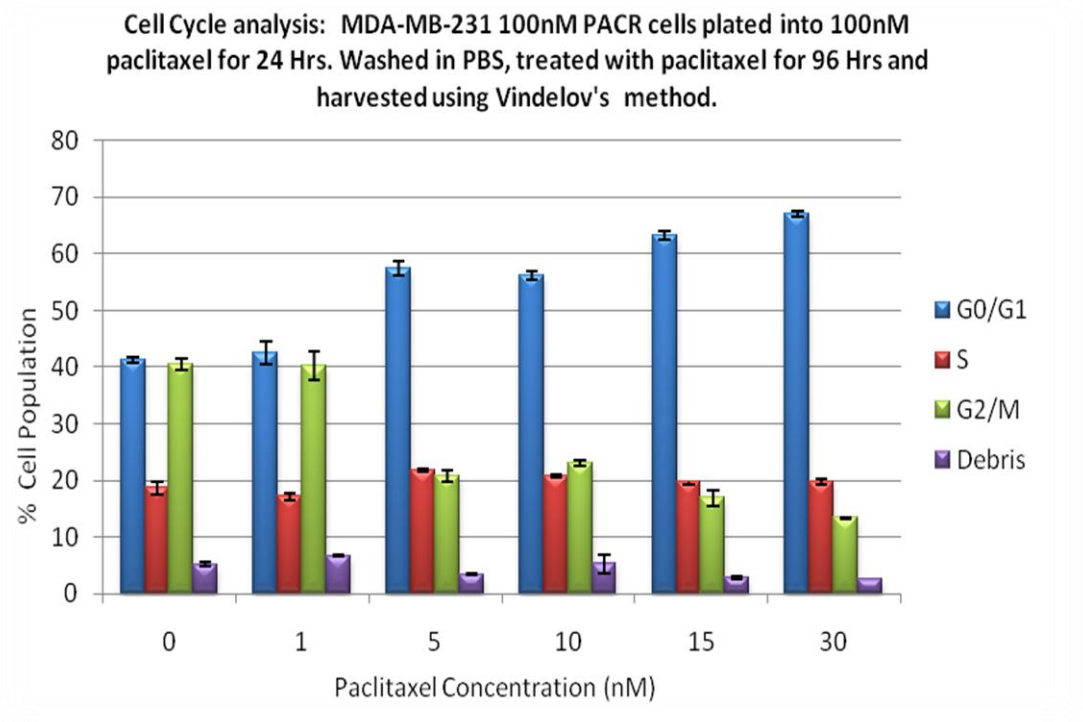


**Figure 3.11.** MDA-MB-231 100nM PACR cells were treated with either blank media, or 1, 5,10, 15 or 30nM Paclitaxel for 96 hours. The X axis shows increasing paclitaxel dose measured in nM. The Y axis represents the percentage of the cell population inhabiting each stage of the cell cycle. The blue bar represents the cells in G and G1 phase of the cell cycle. The red bar represents the cells in S phase on the cell cycle. The green bar represents those cells in the G2 and M phase of the cell cycle. The purple bars represent the percentage of debris is each sample.

When making a pairwise comparison of each of the three cell cycle stages (G0/G1, S and G2/M) using a t test, there is a statistically significant difference between the cell cycle stage in the untreated cells and the cells treated with the highest dose of paclitaxel in the G0/G1 and G2/M

phase but not in the S phase portion of the cell population ($p$ = $8.67^{-9}$, $p$ = $2.89^{-6}$, $p$ = 0.466 respectively.)

In conclusion, the paclitaxel resistant MDA-MB-231 cells seem to tolerate treatment with paclitaxel well and seem to completely escape the G2/M block that is elicited in the native cell when treated with the drug. The MDA-MB-231 100nM PACR cells seemed to have a high proportion of S phase cells when treated with no paclitaxel or low dose paclitaxel.

### 3.3di. Flow cytometry based cell cycle analysis of Native ZR75-1 cells treated with paclitaxel.

The same set of experiments were them performed using the ZR75-1 Native and PACR cells treated with paclitaxel and the ZR75-1 Native and DOCR cells treated with docetaxel (detailed in section 2.1.e.iv and 2.1.e.v.) The computer used for analysing the FACS data using the MDA-MB-231 cells was decommissioned, so in this set of experiments the same Vindelov's protocol (re 2.1.g.i – 2.1.g.iii) was used but the samples were analysed using the FAC Aria scanner and the resulting data was analysed using the FlowJo programme. Samples were run on the FACS Aria by Elisabeth Freyer at the MRC to whom the author is very grateful.

Unfortunately, the only set of cells that were successfully analysed was the ZR75-1 native cells from the first experiment; those treated with paclitaxel. The paclitaxel treated ZR75-1 Native and the docetaxel treated ZR75-1 Native and ZR75-1 DOCR cells could not be analysed.

We consulted with Elisabeth Freyer and she suspected that in these three groups of cells the samples failed to be sufficiently separated in to a single cell suspension for analysis. This may have been because the trypsin in solution A of the Vindelov's protocol was not working properly or because the cell samples were not sufficiently vortexed during the protocol. In the future, for the purpose of publication this experiment will be repeated using the ZR75-1 PACR cells treated with paclitaxel, and the ZR75-1 native and DOCR cells treated with docetaxel, this time using new Vindelov's solutions.

However, the ZR75-1 native cells treated with paclitaxel were successfully analysed and the resulting data, analysed using FlowJo is shown in figures 3.12 – 3.15. Each of these figures represents the best example of each of the four replicates at each dose. The data is then summarised in table 3.4.

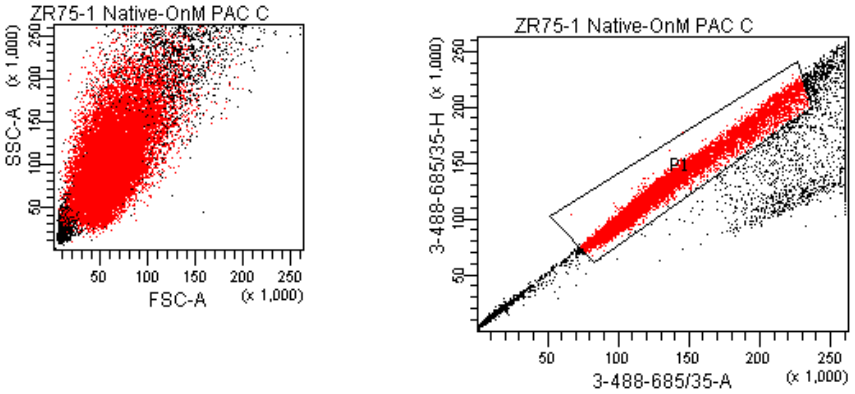


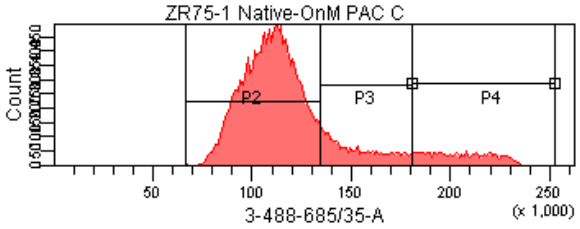


| | | | | |
|---|---|---|---|---|
| Experiment Name: | JK PI 19052010 | | | |
| Specimen Name: | ZR75-1 Native | | | |
| Tube Name: | OnM PAC C | | | |
| Record Date: | May 19, 2010 1:11:46 PM | | | |
| Population | #Events | %Parent | 3-488-685/... Mean | 3-488-685/... %CV |
| All Events | 27,544 | #### | 132,726 | 51.4 |
| P1 | 20,444 | 74.2 | 122,782 | 26.5 |
| P2 | 15,984 | 78.2 | 108,413 | 11.8 |
| P3 | 2,586 | 12.6 | 152,049 | 9.0 |
| P4 | 1,874 | 9.2 | 204,954 | 7.4 |

**Figure 3.12.** Cell cycle analysis of ZR75-1 native cells treated with 0nM paclitaxel. Top left panel shows the FSC-A vs. SSC-A. The top right panel shows the same data shows the height of the PI signal vs. the area of the PI signal (allowed single cells to be gated and excluded any 2N cells stuck together that would incorrectly appear as 4N as the single cells are those that appear on the diagonal axis. The central panel shows the area of the PI signal vs. the Count of cell signal. P2 represents the cells in G0/G1, P3 represents the cells in S phase and P4 represents the cells in G2/M phase. The bottom panel shows summary of the data detailing the percentage of cells in each stage of the cells cycle and the %CV of the experiment.

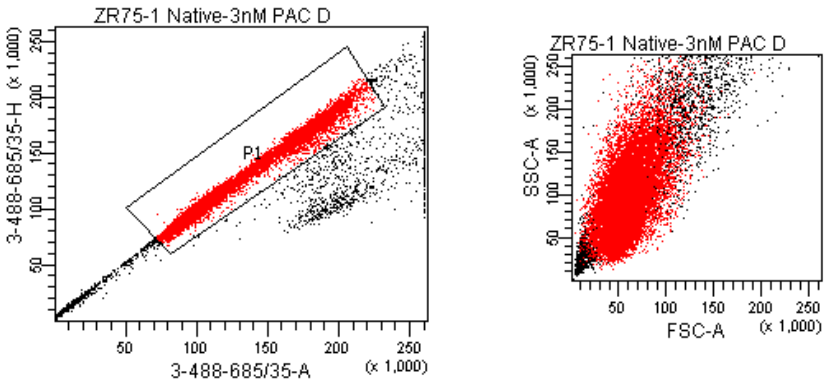


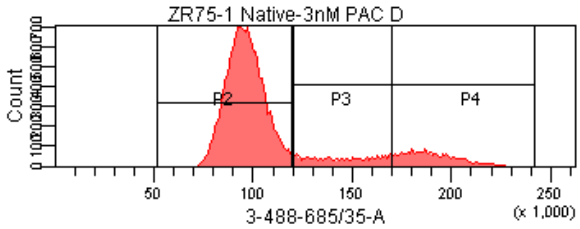


Experiment Name: JK PI 19052010
Specimen Name: ZR75-1 Native
Tube Name: 3nM PAC D
Record Date: May 19, 2010 1:20:50 PM

| Population | #Events | %Parent | 3-488-685/... Mean | 3-488-685/... %CV |
|---|---|---|---|---|
| All Events | 24,094 | #### | 118,450 | 48.7 |
| P1 | 20,134 | 83.6 | 112,021 | 30.1 |
| P2 | 15,732 | 78.1 | 95,987 | 9.3 |
| P3 | 1,927 | 9.6 | 144,860 | 10.5 |
| P4 | 2,428 | 12.1 | 189,703 | 6.7 |

**Figure 3.13.** Cell cycle analysis of ZR75-1 native cells treated with 3nM paclitaxel. Top left panel shows the FSC-A vs. SSC-A. The top right panel shows the same data shows the height of the PI signal vs. the area of the PI signal (allowed the single cells to be gated and excluded any 2N cells stuck together that would incorrectly appear as 4N as the single cells are those that appear on the diagonal axis. The central panel shows the area of the PI signal vs. the Count of cell signal. P2 represents the cells in G0/G1, P3 represents the cells in S phase and P4 represents the cells in G2/M phase. The bottom panel shows summary of the data detailing the percentage of cells in each stage of the cell cycle and the %CV the experiment.

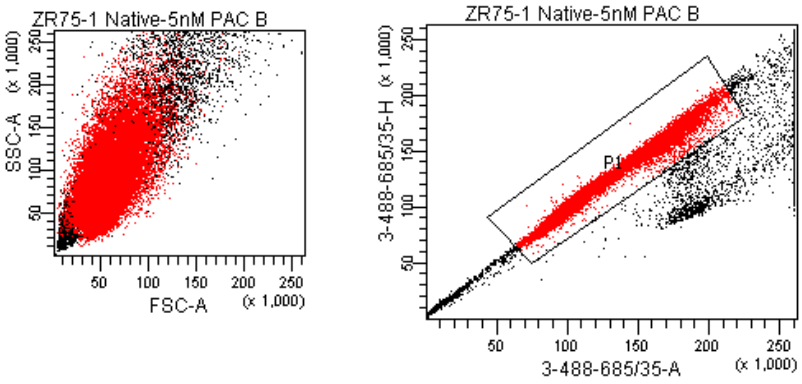


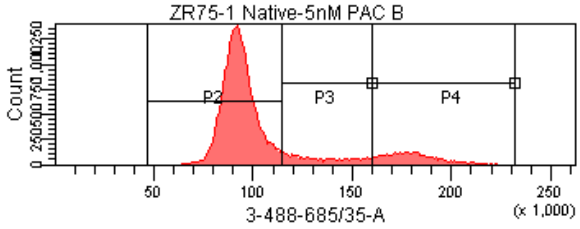


| | |
|---|---|
| Experiment Name: | JK PI 19052010 |
| Specimen Name: | ZR75-1 Native |
| Tube Name: | 5nM PAC B |
| Record Date: | May 19, 2010 1:27:24 PM |

| Population | #Events | %Parent | 3-488-685/... Mean | 3-488-685/... %CV |
|---|---|---|---|---|
| All Events | 37,468 | #### | 117,099 | 52.1 |
| P1 | 30,274 | 80.8 | 107,523 | 29.1 |
| P2 | 23,695 | 78.3 | 92,826 | 8.4 |
| P3 | 2,837 | 9.4 | 133,904 | 10.5 |
| P4 | 3,742 | 12.4 | 180,585 | 7.0 |

**Figure 3.14.** Cell cycle analysis of ZR75-1 native cells treated with 5nM paclitaxel. Top left panel shows the FSC-A vs. SSC-A. The top right panel shows the same data shows the height of the PI signal Vs the area of the PI signal (allowed the single cells to be gated and and excluded any 2N cells stuck together that would incorrectly appear as 4N as the single cells are those that appear on the diagonal axis. The central panel shows the area of the PI signal vs. the Count of cell signal. P2 represents the cells in G0/G1, P3 represents the cells in S phase and P4 represents the cells in G2/M phase. The bottom panel shows summary of the data detailing the percentage of cells in each stage of the cells cycle and the %CV the experiment.

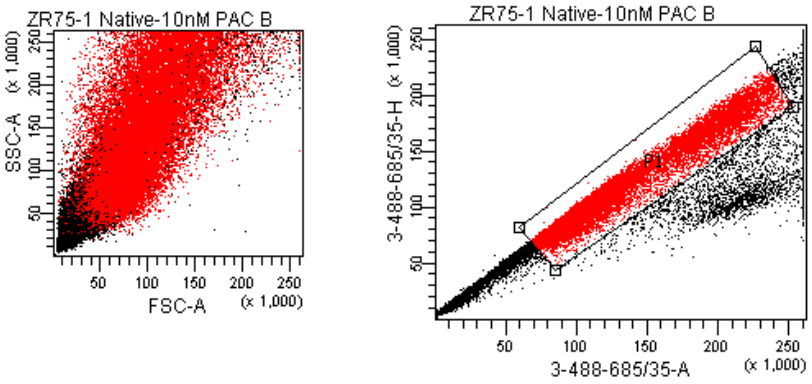


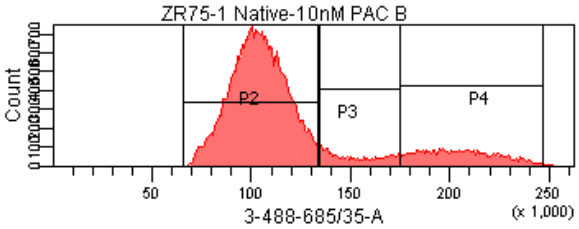


| | | | | |
|---|---|---|---|---|
| Experiment Name: | JK PI 19052010 | | | |
| Specimen Name: | ZR75-1 Native | | | |
| Tube Name: | 10nM PAC B | | | |
| Record Date: | May 19, 2010 1:42:24 PM | | | |
| Population | #Events | %Parent | 3-488-685/... Mean | 3-488-685/... %CV |
| All Events | 76,748 | #### | 81,098 | 103.0 |
| P1 | 30,621 | 39.9 | 120,810 | 31.9 |
| P2 | 24,302 | 79.4 | 103,444 | 12.8 |
| P3 | 1,970 | 6.4 | 151,961 | 8.5 |
| P4 | 4,238 | 13.8 | 204,929 | 8.7 |

**Figure 3.15.** Cell cycle analysis of ZR75-1 native cells treated with 10nM paclitaxel. Top left panel shows the FSC-A vs. SSC-A. The top right panel shows the same data shows the height of the PI signal Vs the area of the PI signal (allowed the single cells to be gated and excluded any 2N cells stuck together that would incorrectly appear as 4N as the single cells are those that appear on the diagonal axis. The central panel shows the area of the PI signal vs.the Count of cell signal. P2 represents the cells in G0/G1, P3 represents the cells in S phase and P4 represents the cells in G2/M phase. The bottom panel shows summary of the data detailing the percentage of cells in each stage of the cells cycle and the %CV the experiment.

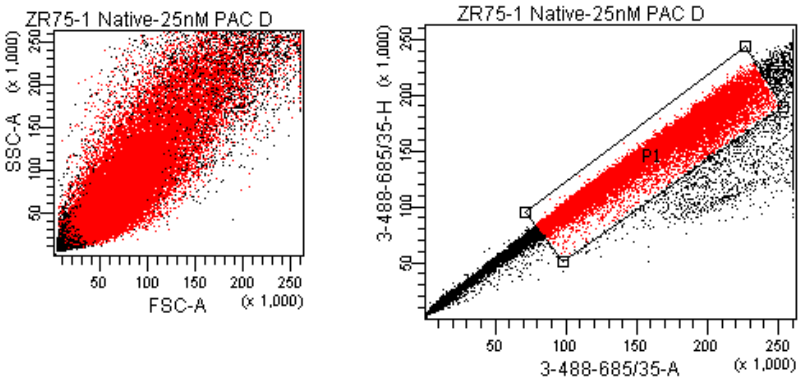


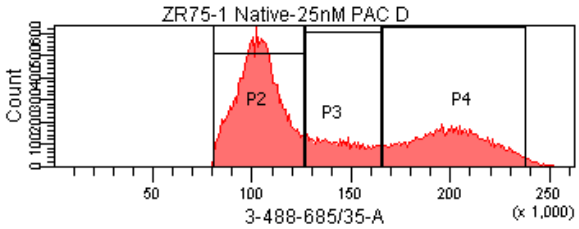


| | |
|---|---|
| Experiment Name: | JK PI 19052010 |
| Specimen Name: | ZR75-1 Native |
| Tube Name: | 25nM PAC D |
| Record Date: | May 19, 2010 2:02:22 PM |

| Population | #Events | %Parent | 3-488-685/... Mean | 3-488-685/... %CV |
|---|---|---|---|---|
| All Events | 57,817 | #### | 116,920 | 75.2 |
| P1 | 27,263 | 47.2 | 139,852 | 32.7 |
| P2 | 14,664 | 53.8 | 103,019 | 9.9 |
| P3 | 3,854 | 14.1 | 144,293 | 7.6 |
| P4 | 8,324 | 30.5 | 199,890 | 9.1 |

**Figure 3.16.** Cell cycle analysis of ZR75-1 native cells treated with 25nM paclitaxel. Top left panel shows the FSC-A vs. SSC-A. The top right panel shows the same data shows the height of the PI signal vs. the area of the PI signal (allowed the single cells to be gated and excluded any 2N cells stuck together that would incorrectly appear as 4N as the single cells are those that appear on the diagonal axis. The central panel shows the area of the PI signal vs. the Count of cell signal. P2 represents the cells in G0/G1, P3 represents the cells in S phase and P4 represents the cells in G2/M phase. The bottom panel shows summary of the data detailing the percentage of cells in each stage of the cells cycle and the %CV the experiment.

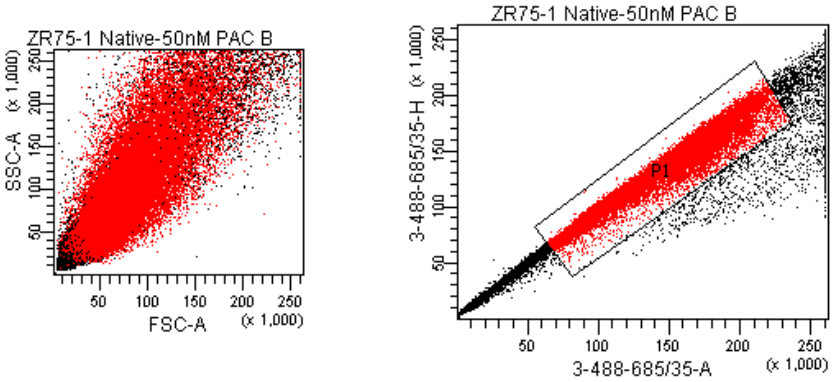


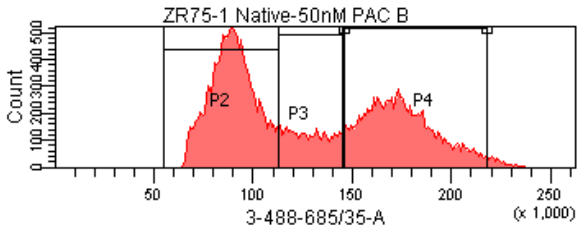


Experiment Name: JK PI 19052010
Specimen Name: ZR75-1 Native
Tube Name: 50nM PAC B
Record Date: May 19, 2010 2:06:39 PM

| Population | #Events | %Parent | 3-488-685/... Mean | 3-488-685/... %CV |
|---|---|---|---|---|
| All Events | 60,009 | #### | 102,717 | 83.5 |
| P1 | 28,762 | 47.9 | 128,849 | 33.1 |
| P2 | 13,439 | 46.7 | 89,179 | 12.1 |
| P3 | 3,911 | 13.6 | 128,088 | 7.4 |
| P4 | 10,961 | 38.1 | 174,605 | 9.8 |

**Figure 3.17.** Cell cycle analysis of ZR75-1 native cells treated with 50nM paclitaxel. Top left panel shows the FSC-A vs. SSC-A. The top right panel shows the same data shows the height of the PI signal Vs the area of the PI signal (allowed the single cells to be gated and excluded any 2N cells stuck together that would incorrectly appear as 4N as the single cells are those that appear on the diagonal axis. The central panel shows the area of the PI signal vs. the Count of cell signal. P2 represents the cells in G0/G1, P3 represents the cells in S phase and P4 represents the cells in G2/M phase. The bottom panel shows summary of the data detailing the percentage of cells in each stage of the cells cycle and the %CV the experiment.

Figure 3.18 shows the collated data for the cell cycle experiments using ZR75-1 native cells treated with increasing doses of paclitaxel. The data shows that with increasing concentration of paclitaxel the proportion of cells in the G0/G1 phase of the cell cycle reduces. With increasing paclitaxel dose the proportion of cells in S phase reduces from 0 – 10nM and then increases again from 10 – 50nM paclitaxel. The cells in the G2/M phase of the cell cycle increases from 0-50nM. This suggests that with increasing paclitaxel concentration a G2/M block is exerted upon the ZR75-1 cells. This also suggests that paclitaxel exerts a G2/M block upon both the MDA-MB-231 and ZR75-1 native cell lines.

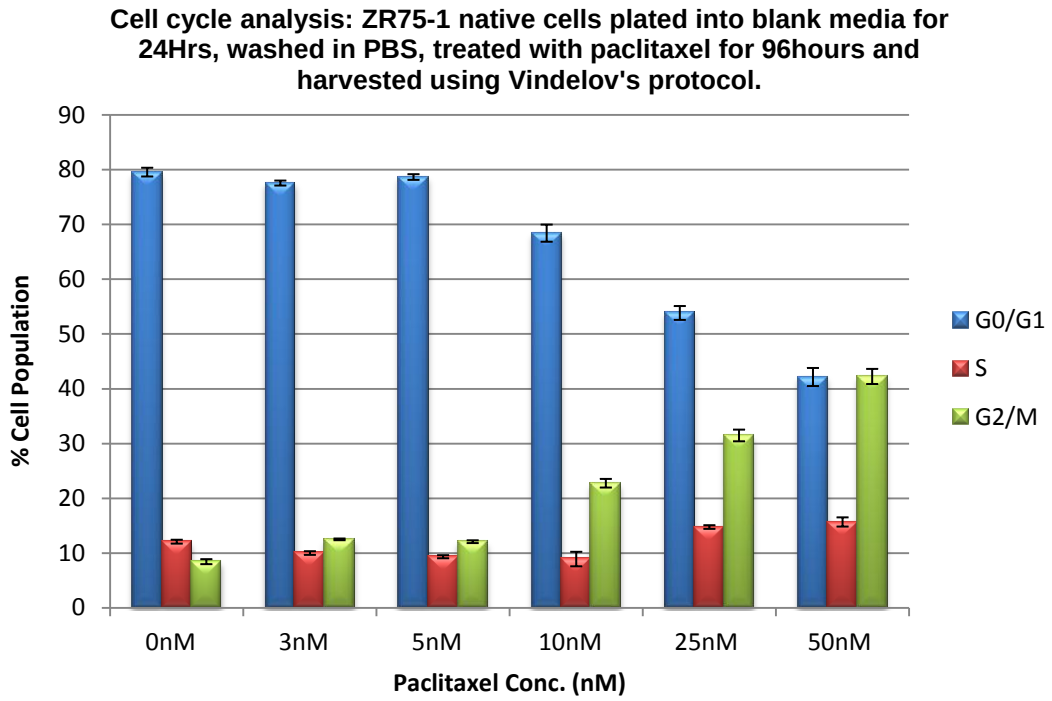


**Figure 3.18**. ZR75-1 Native cells showing changes in stages in the cell cycle with increasing paclitaxel concentration.

# Chapter 4

## Results:

### Taxane Resistant Breast Cancer Cell Lines Grown As Mouse Xenografts

## 4.1. Developing taxane resistant xenografts in mice.

A series of experiments were developed to establish the cell lines as xenografts in mice. The details of how these experiments were carried out are described in section 2.2.a.i – 2.2.b.v.

Establishing the taxane resistant cell lines as xenografts in mice aimed to bring this work into an *in vivo* environment and observe whether the taxane resistant phenotype would be perpetuated in this environment. Growing xenografts of cell line and tumour material is an useful discovery tool as they can be used to evaluate and predict pre-clinical response[219-221]. On this basis a platform on which a variety of complex drug treatment experiments could be performed was established. All xenograft experiment were performed using CD-1 Nude female mice in collaboration with Valerie Brunton/Morwenna Muir. CD-1 nude mice are animals which lack a thymus, are unable to produce T-cells and are therefore immunodeficient. They were developed by the transfer of the Crl:NU-Foxn1nu gene to a CD-1 mouse through a series of crosses and backcrosses at Charles River laboratories (see www.criver.com.)

Initially the author sought to establish the MDA-MB-231 native and 25nM PACR cell lines as a xenograft model. It had already been determined that the 25nM PACR MDA-MB-231 cell line retained a paclitaxel resistant phenotype after in vitro passing in a drug free environment (see. 2.1.e.iii and results figure 3.4.)

### 4.1a MDA-MB-231 Native and 25nM PACR Mouse Xenografts

Figure 4.1 shows the tumour growth of the initial experiment establishing MDA-MB-231 native and 25nM PACR mouse xenografts. The red line with squares indicates the native cell line and the green line with the triangles indicates the 25nM PACR cell line. The error bars are taken from the standard error of tumour measurements estimated by calliper measurements of individual tumours across all animals. Additional data for this experiment is summarised in table 4.1.

The native cells grew rapidly over the course of the experiments and as the experiment progressed the standard errors increased indicating increased variability. However, some 3 of the native mice became ulcerated towards the end of the experiment which may have lead to the increased variability at this stage. Although the 25nM PACR cells appeared to grow in tandem with the native cells for the first three or four days after this point they shrank again. This suggests that the initial “growth” was merely an injection site artefact.

| | MDA-MB-231 Native | MDA-MB-231 25nM PACR |
|---|---|---|
| **# Mice injected** | 5 | 5 |
| **# Sites Injected** | 10 | 10 |
| **Successful Tumours** | 6 | 0 |
| **Failed Tumours** | 4 | 10 |
| **Mice culled – ill health** | 0 | 0 |

**Table 4.1.** Summary of xenograft experiment using MDA-MB-231 Native and 25nM PACR cell lines.

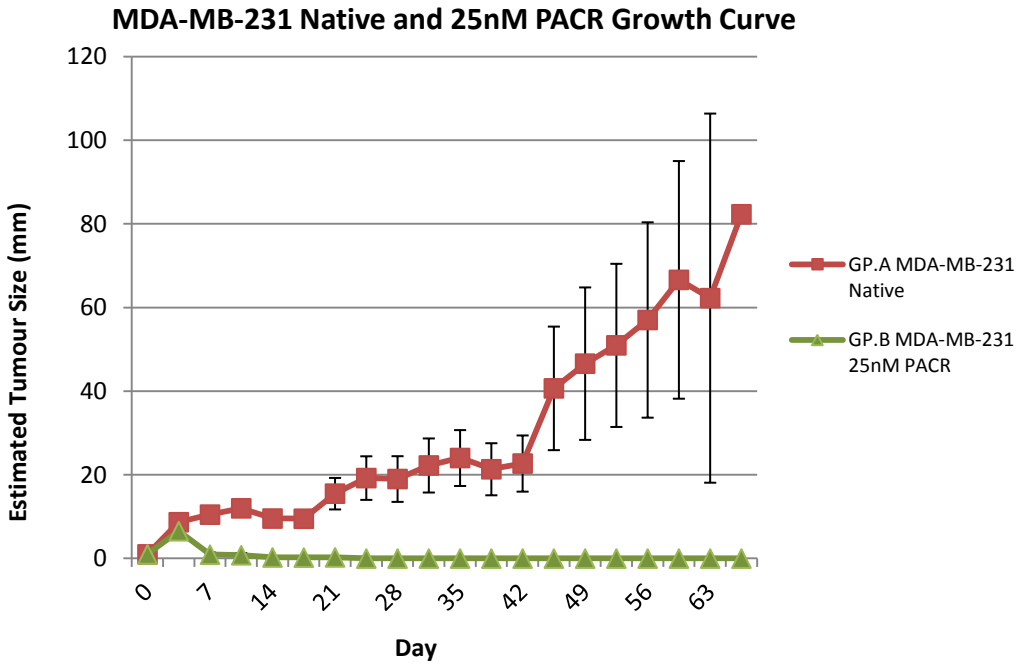


**Figure 4.1** Tumour growth of MDA-MB-231 native and 25nM PACR cells (maximum duration.) Estimated tumour size is shown up the Y axis and time in days is shown along the x axis. The MDA-MB-231 native cells are shown by the red line with squares and the MDA-MB-231 25nM PACR cells are shown by the green line with triangles. The error bars shown are the standard errors.

**4.1.ai Using matrigel to establish MDA-MB-231 native and MDA-MB-231 25nM PACR cell lines as xenografts in mice.**

The co-injection of cells was then tested with the basement membrane mix "matrigel" from BD biosciences to attempt to improve the outcome of establishing the 25nM PACR xenografts[222].

The basement membrane matrix BD matrigel is a solubilised basement membrane preparation extracted from the Engelbreth-Holm-Swarm (EHS) mouse sarcoma. EHS is a tumour rich in extracellular matrix proteins: laminin, collagen IV, heparin sulphate proteoglycans and entactin/nidogen, TGF-β, EGF, ILGF, FGF, tissue plasminogen activator (re. www.bdbiosciences.com.) Additional data for this experiment is summarised in table 4.2.

| | MDA-MB-231 Native Non Matrigel | MDA-MB-231 Native Matrigel | MDA-MB-231 25nM PACR Non Matrigel | MDA-MB-231 25nM PACR Matrigel |
|---|---|---|---|---|
| **# Mice injected** | 4 | 4 | 4 | 4 |
| **# Sites Injected** | 4 | 4 | 4 | 4 |
| **Successful Tumours** | 4 | 4 | 0 | 0 |
| **Failed Tumours** | 0 | 0 | 4 | 4 |
| **Mice culled – ill health** | 0 | 0 | 0 | 0 |

**Table 4.2.** Summary of xenograft experiment using MDA-MB-231 Native and 25nM PACR cell lines, -/+ matrigel. Each mouse was injected in one flank with cells containing matrigel and the other with cells containing no matrigel.

This first experiment detailing the use of matrigel to establish native and 25nM PACR MDA-MB-231 xenografts in mice is described in section 2.2.a.ii. The results of this experiment are shown in figure 4.2. The dark red line with squares indicates the MDA-MB-231 native cells injected normally in no matrigel, the pale red line with the triangles indicates the MDA-MB-231 MDA-MB-231 native cells implanted in 50% matrigel, the pale green line with crosses indicates the MDA-MB-231 25nM PACR cells implanted normally in no matrigel and the dark green line with crosses with a vertical strike indicates the MDA-MB-231 25nM PACR cells implanted in 50% matrigel. Estimated tumour size is measured up the Y axis and time is measured in days along the X axis.

The MDA-MB-231 native cells implanted in no matrigel (dark red line figure 4.2) produced tumours which increased in tumour growth rapidly over the first three days of the experiment then took a very slight dip around day seven. From day seven until day twenty four the cells grew rapidly and then again had a slight dip in tumour growth at day twenty eight after which the cells recover and begin to grow at a steady rate.

The MDA-MB-231 native cells injected in the presence of 50% matrigel (pale red line figure 4.2) grew rapidly over the first three days and then, like the same cells implanted in no matrigel took a slight dip at day seven, after this they recover gradually over the next three days and then the tumour growth increases rapidly from day ten to fourteen. Comparing the native cell implanted in the absence of matrigel to those implanted in the presence of 50% matrigel it was established that the native cells grow at an increased rate in the presence of matrigel than cells grown in their absence (2 way ANOVA $p$=0035.)

Over the first three days of the experiment the MDA-MB-231 25nM PACR cell implanted in no matrigel (pale green line fig 4.2) appeared to grow at a similarly rapid rate to the native cells grown in the absence of matrigel. After day three, until the completion of the experiment these tumours regressed suggesting again that the initial "growth" was simply an artefact of the injection site and the cells did not form established tumours.

Over the first three days of the experiment, the MDA-MB-231 25nM PACR cells grown in the presence of 50% matrigel (dark green line figure 4.2) appeared to grow at a similarly rapid rate as the MDA-MB-231 native cells grown in the presence of matrigel (dark red line fig 4.2) At this early stage of the experiment the MDA-MB-231 25nM PACR cells co-injected with matrigel appear to grow at a faster rate than the same cells grown in the absence of matrigel. However, this may be because immediately following injection, matrigel can remain at the injection site before being absorbed which would make early tumours appear larger than they really are. After day three, until the completion of the experiment the size of the 25nM PACR cells grown in the presence of matrigel like their counterparts grown in the absence of matrigel gradually and steadily reduced to zero. Again, it can be inferred from this that the initial "growth" seen over the first few days of the experiment were an artefact of the injection site.

The pattern of tumour growth over the experiment in the 25nM PACR cells grown in the presence of matrigel is very similar to the pattern of tumour growth exhibited by the cells grown in the absence of matrigel, however, the growth rate is always higher in the 25nM PACR cells injected in the presence of matrigel than those grown in the absence of matrigel.

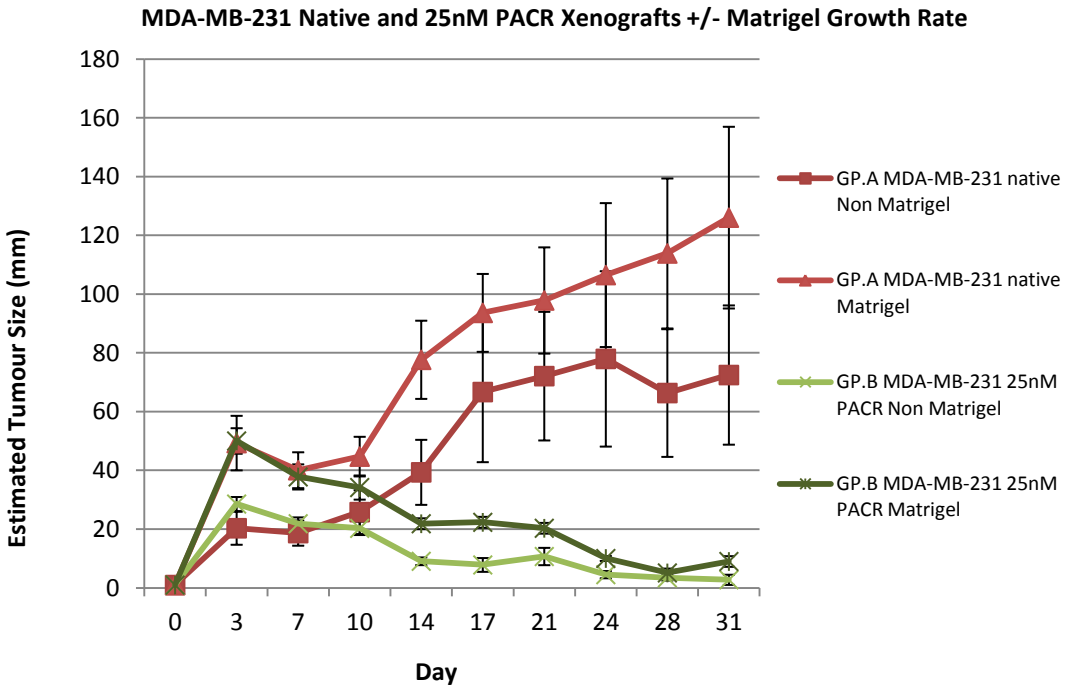


**Figure 4.2** MDA-MB-231 native and 25nM PACR xenografts grown +/- 50% matrigel (moderate duration.) Estimated tumour size is measured up the Y axis and time in days is measured along the X axis. The dark line indicates the MDA-MB-231 native cells implanted normally in the absence of matrigel, the pale red line indicates the MDA-MB-231 native cells implanted in the presence of 50% matrigel, the pale green line indicates the MDA-MB-231 25nM PACR cell implanted normally in the absence of matrigel and finally the dark green indicates the MDA-MB-231 25nM PACR cells implanted in the presence of 50% matrigel. Each data point has an error bar which represents the standard errors for each group of replicates.

From this experiment three conclusions could be drawn: firstly that only the native cell lines grow successfully as xenografts, secondly, that the native cells grow better in the presence of matrlgel (p value = 0.035), and finally it can be concluded that the 25nM PACR cells do not successfully establish xenografts either in the presence or the absence of matrigel.

### 4.1.b. Combining growth rates of MDA-MB-231 and 25nM PACR in the absence and presence of matrigel.

We then combined the growth rate of the native xenografts +/- matrigel (pale red line with squares figure 4.3), and combined the growth rate of MDA-MB-231 25nM PACR xenografts +/- matrigel (pale green line with triangles figure 4.3) and plotted the resulting graph (figure 4.3.) Additional data for this experiment is summarised in table 4.1.

Figure 4.3 confirms that the experiment failed to establish satisfactory mouse xenografts using MDA-MB-231 25nM PACR cells.

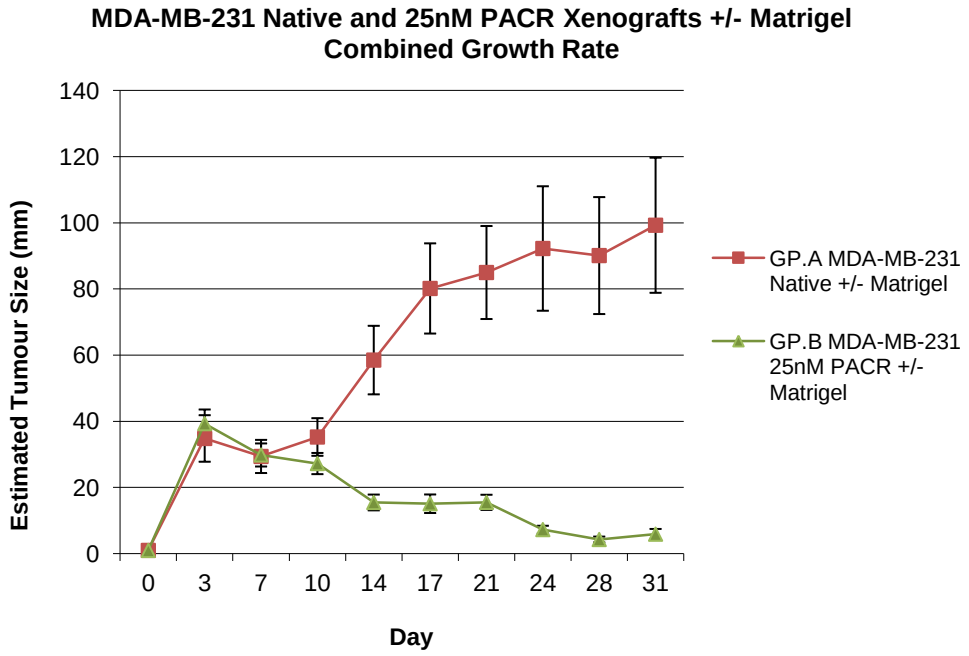


**Figure 4.3** Combined Tumour growth of MDA-MB-231 native and 25nM PACR xenografts +/- matrigel (moderate duration.) Tumour growth is recorded up the Y axis and time in days is recorded along the X axis. The pale red line indicates the combined growth rate of the MDA-MB-231 native cells +/- matrigel and the pale green cell line indicates the combined growth rate of the MDA-MB-231 25nM PACR cells +/- matrigel. Each data point has an error bar which represents the standard errors for each group of replicates combining the +/- matrigel data.

**4.1.c.i A final attempt to establish MDA-MB-231 native and 25nM PACR cell lines in mouse xenografts.**

As previous attempts to establish the MDA-MB-231 25nM PACR cell lines as xenografts had failed one last experiment was carried out to see if this would be achieved before moving on to trying the same experiments with another of the taxane resistant cell lines. Additional data for this experiment is summarised in table 4.3.

In this experiment, both the native (re figure 4.4 pale red line with squares) and the 25nM PACR (re figure 4.4 pale green line with triangle) cells were implanted in 50% matrigel. Once again, this led to the successful establishment of MDA-MB-231 native cells as xenografts but no observed growth in the 25nM PACR injected mice.

| | MDA-MB-231 Native + Matrigel | MDA-MB-231 25nM PACR + Matrigel |
|---|---|---|
| **# Mice injected** | 4 | 4 |
| **# Sites Injected** | 8 | 8 |
| **Successful Tumours** | 8 | 0 |
| **Failed Tumours** | 0 | 8 |
| **Mice culled – ill health** | 3* | 0 |

**Table 4.3.** Summary of data in MDA-MB-231 Native and 25nM PACR cell line xenografts implanted in 50% matrigel. * 3 mice culled due to ulceration on day 35 of expt.

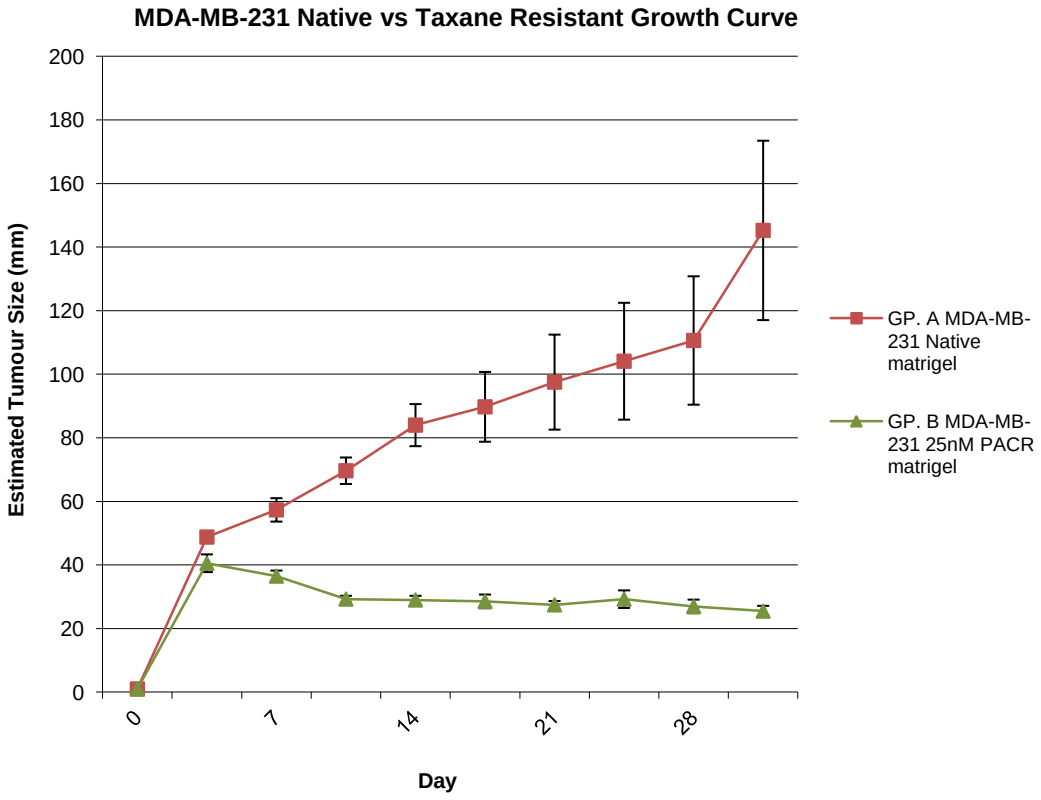


**Figure 4.4** MDA-MB-231 native and 25nM PACR xenografts grown in 50% matrigel (moderate duration.) Growth rate is measured up the Y axis and time in days is measured along the X axis. The pale red line with the squares along the plot indicates the MDA-MB-231 native cells implanted in the presence of 50% matrigel, the pale green line indicates the MDA-MB-231 25nM PACR cell implanted in the presence of 50% matrigel. Each data point has an error bar which represents the standard errors for each group of replicates.

It is impotant to consider why the MDA-MB-231 25nM PACR cell line failed to grow as xenografts in mice. The existing data was therefore examined to identify changes in gene expression which might explain these observations.

The expression data in section 5.1.a.i shows a progressive and consistent increase in the expression of the gene TSPAN13 with increasing paclitaxel resistance in the MDA-MB-231 cell lines (figure 5.4 bottom row, right hand side.) This data is further validated by the qPCR data shown in section 4.3 (figure 5.43.) This pattern of increasing expression of TSPAN13 with increasing paclitaxel resistance is only seen with the MDA-MB-231 lines and not with either the ZR75-1 PACR or DOCR cell lines. TPSANS are cell surface proteins which play roles in cell development, growth and motility, all of which would influence whether xenografts are successfully established or not. TSPAN13 is also known as NET-6 and has been transfected via a GFP construct into MDA-MB-231 cells which are known to normally express this gene at a particularly low level[223]. T-SPAN13 has been identified as a potential tumour suppressor gene and when it was transfected into MDA-MB-231 they exhibited phenotypic changes including elevated antiproliferative activity *in vitro* and *in vivo*, reduced anchorage, independent growth and invasion[223]. It is possible that the increase in expression of this gene may have conferred this change in phenotype.

This hypothesis is supported by additional transcriptomic data shown in the cell line KEGG pathway analysis in chapter 5 which identified members of the focal adhesion pathway that had increased expression in the MDA-MB-231 50nM PACR cell lines. This Kegg hsa04510 focal adhesion pathway showed significant dysregulation of the following genes in the MDA-MB-231 PACR cell line: ACTB ITGA2 ACTN1 ITGB5 ITGA3 BIRC3 COL5A1 CTNNB LAMB3 PAK2 CCND2 COL6A3 VEGFA SHC1 (*p* value = 0.01, FDR =1.) These pathway members are not increased in the ZR75-1 PACR and DOCR cell lines. Finally, the MDA-MB-231 cell line showed increasing expression of ER with increasing paclitaxel resistance (see section 5 qPCR data.) Perhaps the resistant cell lines required a level of oestrogen to grow in mouse xenografts. This could be provided by 17-β oestradiol 60 day slow release pellet (0.72mg/pellet SE-121 Innovative research of America.

These observations are interesting and perhaps in this context it would be appropriate to investigate some of these properties using the MDA-MB-231 native and 25nM PACR *in vitro* in future experiments. Anchorage could be investigated using matrigel in vitro. The invasive and migration potential of the native relative to the PACR MDA-MB-231 cell lines could be investigated by conducting invasion and scratch wound assays. Knocking down TSPAN13 in the paclitaxel resistant cell lines and observing whether this affects the anchorage, invasion and migration *in vitro* should be considered as a possibility for future studies.

## 4.2. Establishing ZR75-1 Native, 25nM PACR and DOCR cells as xenografts in mice.

As previous experiments failed to successfully establish the MDA-MB-231 25nM PACR cell as xenografts in mice, future experiments switched to attempting to establish xenografts using the ZR75-1 native, 25nM PACR and DOCR cells as an alternative.

The first experiments using the ZR75-1 cell lines are detailed in section 2.2.b.i and 2.2.b.ii. ZR75-1 cells are oestrogen dependent so mice were implanted subcutaneously with a 17-β oestradiol 60 day slow release pellet (0.72mg/pellet SE-121 Innovative research of America) at the time of injection with tumour cells. In this initial experiment native ZR75-1 cells were injected into two groups of mice (group A and B), PACR cells into one group of mice (Group C) and implanted DOCR cells into one group of mice (group D.) The secondary objective of this initial experiment was, if the xenografts grew at a satisfactory rate, to allow future treatment with taxane and conduct a cross resistance experiment with the two taxanes, which is why two groups of native cells were included as controls, so that one group could be treated with paclitaxel or a control and the other group could be treated with either docetaxel or a control.

Additional data for this experiment is summarised in table 4.4.

| | ZR75-1 Nat | ZR75-1 Nat | ZR75-1 PACR | ZR75-1 DOCR |
|---|---|---|---|---|
| **# Mice injected** | 4 | 4 | 4 | 4 |
| **# Sites Injected** | 8 | 8 | 8 | 8 |
| **Successful Tumours** | 8 | 8 | 8 | 8 |
| **Failed Tumours** | 0 | 0 | 0 | 0 |
| **Mice culled – ill health** | 1* | 1** | 1*** | 0 |

**Table 4.4.** Summary of experiment using ZR75-1 native, PACR and DOCR cell line xenografts. Mouse culled due to ulceration on *D19 **D28 ***D25.

Figure 4.5 illustrates the initial xenograft experiment using the ZR75-1 cell lines. Tumour growth is recorded up the y axis and the time in days is recorded along the x axis. The pale red line with the squares indicates the first group of native ZR75-1 xenografts, the dark purple line with the triangles indicates the second group of native ZR75-1 xenografts, the pale green line with the rhombuses indicates the ZR75-1 PACR xenografts and the pale blue line with the cross with a vertical strikethrough indicates the 25nM DOCR xenografts. As the experiments show all

four group of cell lines grow at a very similar rate to one another showing no significant differences.

The ZR75-1 native and taxane resistant cell lines grew very rapidly and unfortunately this meant that some animals went on to ulcerate very quickly. Therefore, it was decided to experiment with injecting lower cell numbers to determine the appropriate number of cells to implant so that the xenografts would grow more slowly and allow time to treat the xenografts with taxane and hence conduct a cross resistance experiment.

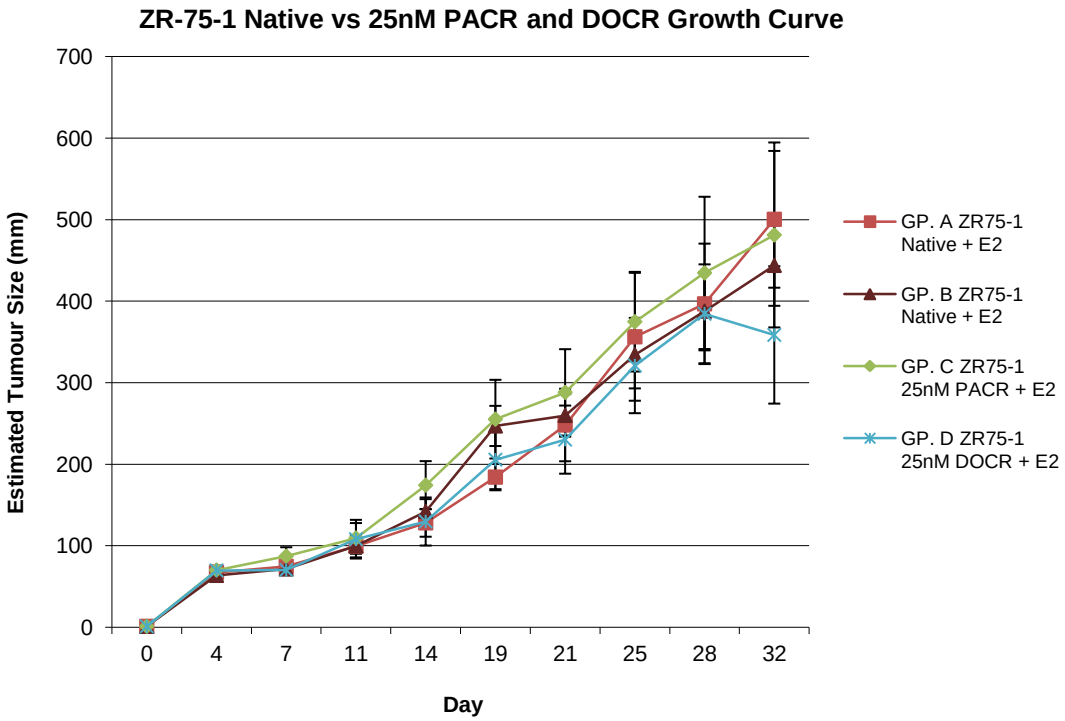


**Figure 4.5** Initial xenograft establishing experiment using ZR75-1 cell lines. (moderate duration) Estimated tumour size is recorded up the y axis and the time in days is recorded along the x axis. Pale red line with the squares indicates the first group of native ZR75-1 xenografts, dark purple line with the triangles indicates the second group of native ZR75-1 xenografts, pale green line with the rhombuses indicates the ZR75-1 PACR xenografts and pale blue line with the cross with a vertical strikethrough indicates the 25nM DOCR xenografts. Error bars indicate the standard errors of the each of the tumours in that particular group of individuals at that time point.

**4.2.a.ii Establishing the appropriate number of cells for implantation into mice and establishing xenografts for taxane cross resistance experiments.**

The details of how this experiment to determine the appropriate implantation density was carried out are described in section 2.2.b.iii. In this experiment three different levels of cells were looked at to implant into the animals: 0.5, 1.0 and 2 million cells. Only the ZR75-1 native cells were used in this experiment as it had already been established that the ZR75-1 native, PACR and DOCR cells all grew at very similar rates to one another. Additional data for this experiment is summarised in table 4.5.

| | 0.5 million cells/inj | 1 million cells/inj | 2 million cells/inj |
|---|---|---|---|
| **# Mice injected** | 2 | 2 | 2 |
| **# Sites Injected** | 3 | 3 | 3 |
| **Successful Tumours** | 3 | 3 | 3 |
| **Failed Tumours** | 0 | 0 | 0 |
| **Mice culled – ill health** | 0 | 0 | 0 |

**Table 4.5**. Summary of experiment using ZR75-1 native cell lines to establish the appropriate volume of cells to inject for future experiments.

In figure 4.6 the dark red line with the squares indicates the growth rate of tumours in animals injected with 0.5 million cells per flank, the mid red line with the triangles indicates the animals injected with 1.0 million cells per flank and the pale pink line with the crosses indicates animals implanted with 2.0 million cells per flank.

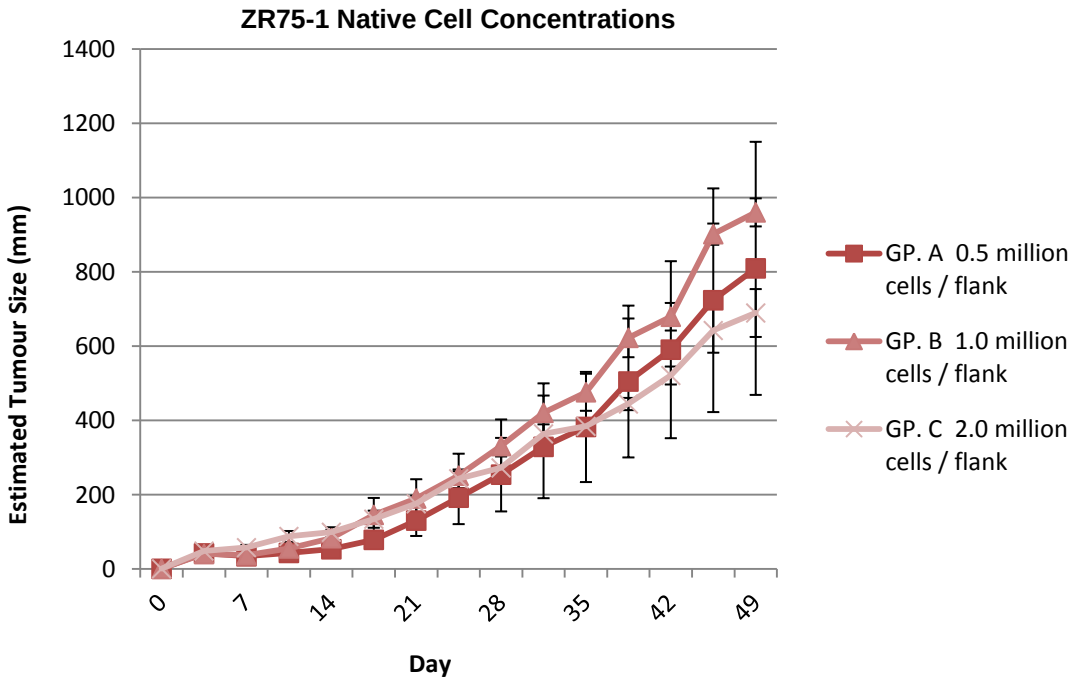


**Figure 4.6 ZR75-1 native cell line** Dark red line with the squares: animals injected with 0.5 million cells per flank, the mid red line with the triangles: animals injected with 1.0 million cells per flank and pale pink line with crosses: animals implanted with 2.0 million cells per flank. (maximum duration) Estimated tumour size is detailed up the y axis and time in days is measure along the x axis. Error bars are standard errors of tumour growth in each group at each time point.

The xenografts injected at a cell density of 0.5, 1.0 and 2.0 million per flank grew at similar rates to one another over the course of the experiment and although the standard errors were not very large there was some overlap between the three groups of tumours. From this it could ascertained that 0.5 million cells per flank was the most appropriate amount of cells to implant as there was very little difference in tumour growth to the other cell implantation densities, 0.5 million cells per flank could be quickly and economically generated for future experiments and the slower growing tumours would allow time to perform the cross resistance experiments before tumours grew too large.

### 4.2.b. Testing cross resistance for docetaxel and paclitaxel in native and taxane resistant ZR75-1 mouse xenografts.

Three ZR75-1 xenograft cross resistance experiments were carried out according to section 2.2.b.iv – 2.2.b.v, implanting 0.5 million cells per flank (with matrigel and oestrogen pellets.) The animals were treated with either: blank drug-free vehicle, paclitaxel in vehicle or docetaxel in vehicle.

Animals treated with paclitaxel were given a dose of 20mg/kg and those treated with docetaxel were given a dose of 10mg/kg. This is because docetaxel is considered approximately twice as potent as paclitaxel to avoid confounding the experiment by using doses considered equipotent. Animals were injected with tumour cells on day -11 and grown until 0 on which they were treated with drug by subcutaneous tail vein injection. The drug treatment was repeated again on day 2 and day 4.

#### 4.2.b.i. Cross resistance experiment using native ZR75-1 xenografts.

The first of the experiments tested the cross resistance of the native ZR75-1 cells. The native ZR75-1 cross resistance experiment is shown in figure 4.7. Additional data for this experiment is summarised in table 4.6.

| | Cremophor/etOH | Paclitaxel 20mg/kg | Docetaxel 10mg/kg |
|---|---|---|---|
| **# Mice injected** | 4 | 4 | 4 |
| **# Sites Injected** | 8 | 8 | 8 |
| **Successful Tumours** | 8 | 8 | 8 |
| **Failed Tumours** | 0 | 0 | 0 |
| **Mice culled – ill health** | 2 | 0 | 3** |

**Table 4.6**. Summary of experiment using ZR75-1 native cell line xenografts treated with blank drug vehicle (cremophor/etOH), paclitaxel (20mg/kg) or docetaxel (10mg/kg.) *Two mice culled on day 18 and 28 due to ulceration. **One mouse killed due to drug on day 4 and two mice killed due to ulceration on day 28 and 35.)

The tumour growth of animals treated with blank drug free vehicle (cremophor) is shown by the red line with the rhombuses. The tumour growth of tumours belonging to animals treated with 20mg/kg paclitaxel is indicated by the pale green line with triangles and that of animals treated with 10mg/kg is indicated by the blue line with rhombuses. The tumour growth is indicated up the y axis and time in days is indicated along the x axis. The day of implantation is indicated by X on the x axis and treatment began on day zero.

For the first 18 days of the experiment the native xenografts treated with either blank drug vehicle, paclitaxel or docetaxel all grow at a similar rate. When the native xenografts are treated with blank drug vehicle (figure 4.7 red line) between day 18 and 25 day of the experiment they grow faster than the native xenografts treated with paclitaxel (green line) and docetaxel (blue

line) over the same time period. At day 28 the tumour growth of the native xenografts treated with blank drug vehicle appears to reduce, however this change in tumour growth is biased, as two mice within this group with the largest tumours had to be culled prior to this point due to ulceration. These ulcerated mice that were culled had large tumours so their removal from the experiment may greatly impact the mean estimation of tumour growth.

The native xenografts treated with 20mgs/kg paclitaxel (green line) had reduced tumour growth when compared to the xenografts treated with blank drug vehicle or docetaxel between day 18 and 25 of the experiment. At day 28 the native xenografts treated with paclitaxel begin to grow at an increased rate compared to the xenografts treated with blank drug vehicle and at a decreased rate compared to the xenografts treated with docetaxel.

It can be inferred that the pattern of growth of the paclitaxel treated native xenografts was less perturbed than the xenografts treated with blank drug vehicle and docetaxel, as only one individual in this group was accidentally given a partially subcutaneous IV tail vein injections and no animals were culled due to ulceration or bloating.

Between day 18 and 25 of the experiment the native xenografts treated with docetaxel (blue line) grow at an increased rate compared to the xenografts treated with paclitaxel and a reduced rate compared to the xenografts treated with blank drug vehicle alone. From day 28 onwards the xenografts treated with docetaxel grew at an increased rate compared to the xenografts treated with either paclitaxel or blank drug vehicle alone. It is possible that the growth of the docetaxel treated native xenografts may be perturbed by the accidental subcutaneous IV tail vein injection or it may have been altered due by the removal of two animals due to culling as a result of ulceration on day 28 and on day 35.

Although over the first portion of the experiment from day zero to day 25, the pattern of growth of the native xenografts treated with no drug seems to be as might be expected as they grow at a faster rate than the xenografts treated with taxane, after day 25 the data becomes difficult to interpret. The increased tumour growth of the native xenografts treated with docetaxel may suggest that docetaxel does not exert an inhibitory effect on the growth of native xenografts.

The accidental partially subcutaneous IV tail vein injections, removal of animals from the experiment due to culling as a result of severe ulceration and the fact that two different technicians measured the tumours over the course of the experiment may all potentially have had a deleterious effect on the experimental conditions. It is also important to consider that there are large standard errors on the paclitaxel and drug free vehicle treated xenografts. Between day seven and day eighteen the measurements were made by a different animal

technician than the rest of the experiment; it is possible that there may be variation in measurements from one individual to another. Methods of quality of assurance, like making multiple measuments and consistently taking the measurement from the largest part of the tumour should help eliminate variation from one technician's measurements to another.

One day two of the experiment one individual from group A (blank drug vehicle), one individual from group B (paclitaxel) and two individuals from group C (docetaxel) were accidentally give IV tail vein injections that were half subcutaneous. Again on day four of the experiment one of the individuals in group C received a tail vein injection that was subcutaneous, this was one of the mice that had already received a tail vein injection that was not correctly administered on day two. On day 18 and day 28 of the experiment one mouse each from the group administered with blank drug vehicle was found to be badly ulcerated and was culled (see table 4.6.) On day four of the experiment one mouse in group C (docetaxel) died upon injection with the drug. Again on day 28 and day 35 of the experiment one mouse each from the group administered with docetaxel was found to be excessively bloated and so was culled.

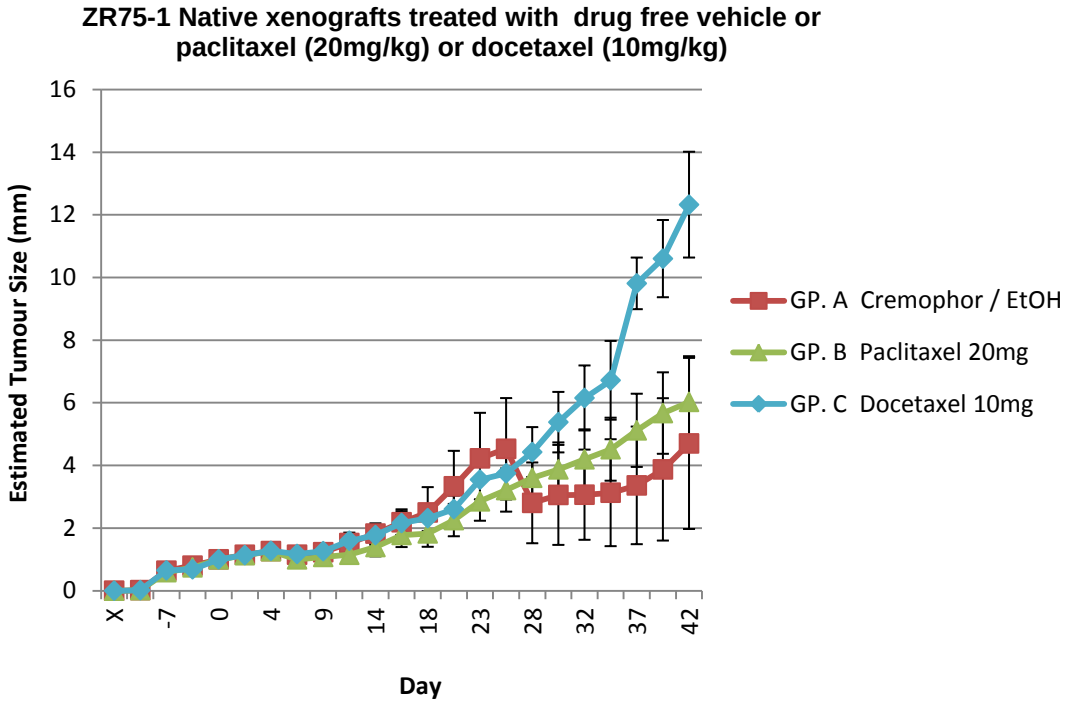


**Figure 4.7** Taxane cross resistance of native xenografts (moderate duration) Treatment with blank drug free vehicle (cremophor) is shown by the red line with the rhombuses. Treatment with 20mg/kg paclitaxel is indicated by the pale green line with triangles and treatment with 10mg/kg docetaxel is indicated by the blue line with rhombuses. Tumour growth is indicated up the y axis and time in days is indicated along the x axis. Day of implantation is indicated by X on the x axis. Treatment began on day zero. Drug was administered on day zero, day two and day four.

We replotted this data, looking at the early stages of the experiment before the majority of ulcerated mice had to be culled (re figure 4.8.) The cremophor treated mice had larger tumours that those treated with paclitaxel or docetaxel during the early stages of the experiment, although this effect was not statistically significant it is an encouraging observation to bear in mind for future experiments.

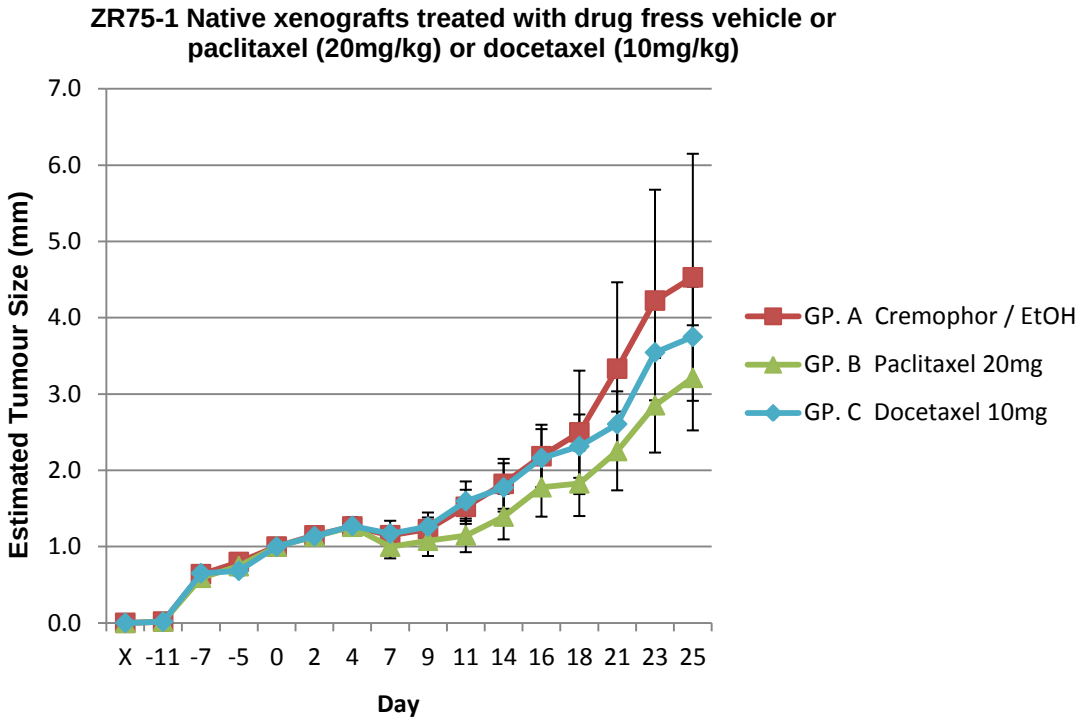


**Figure 4.8** Initial phase of taxane cross resistance experiment using native xenografts (minimum duration.) Treatment with blank drug free vehicle (cremophor) is shown by the red line with the rhombuses. Treatment with 20mg/kg paclitaxel is indicated by the pale green line with triangles and treatment with 10mg/kg docetaxel is indicated by the blue line with rhombuses. Tumour growth is indicated up the y axis and time in days is indicated along the x axis. Day of implantation is indicated by X on the x axis. Treatment began on day zero. Drug was administered on day zero, day two and day four.

Unfortunately, this experiment is affected by bias as two of the native mice with large tumours were culled due to their tumours ulcerating and three of the four docetaxel treated mice were culled due to ulceration and a reaction prior to drug treatment. This suggests that we have not yet optimised the model and that some of the tumours are still growing too fast. Perhaps fewer cells need to be injected so that they would grow more slowly and the experiment cold be conducted over a longer schedule. This would also allow us to also increase the drug dose schedule. The tail vein injections were not conducted consistently and a number of the injections were partially or fully subcutaneous, this may limit the interpretation of the data.

Although there were a number of problems to overcome in this experiment a number of factors have been identified that will allow future experiments to be improved and made more robust. In addition an encouraging pattern of growth has be observed with native xenograft tumours treated with either taxane growing more slowly than the tumours of animals receiving no drug treatment.

#### 4.2.b.ii. Cross resistance experiment using 25nM PACR xenografts.

The second experiment looked at taxane cross resistance in 25nM PACR xenografts. The data is shown in figure 4.9 and is displayed in the same way as figure 4.7. Additional data for this experiment is summarised in table 4.7.

| | Cremophor/etOH | Paclitaxel 20mg/kg | Docetaxel 10mg/kg |
|---|---|---|---|
| **# Mice injected** | 4 | 4 | 4 |
| **# Sites Injected** | 8 | 8 | 8 |
| **Successful Tumours** | 6 | 8 | 8 |
| **Failed Tumours** | 2 | 0 | 0 |
| **Mice culled – ill health** | 0 | 0 | 2 |

**Table 4.7**. Summary of experiment using ZR75-1 PACR cell line xenografts treated with blank drug vehicle (cremophor/etOH), paclitaxel (20mg/kg) or docetaxel (10mg/kg.)*

On day zero of the experiment one individual from group A (drug free vehicle treated) and two individuals from group C (docetaxel treated) were accidentally given IV tail vein injections partially subcutaneously. This happened again on day two to two individuals in group B (paclitaxel treated.) On day four one individual from group C could not be injected as the mouse tail was crusted and scabby so could not be intravenously injected and another individual from the same group was given a tail vein injection that was entirely subcutaneous. Again, from day 21 to day 31 the measurements were made by a different member of technical staff. Finally on day 35, 2 mice in group C had to be culled due to ulceration (re. table 4.7.)

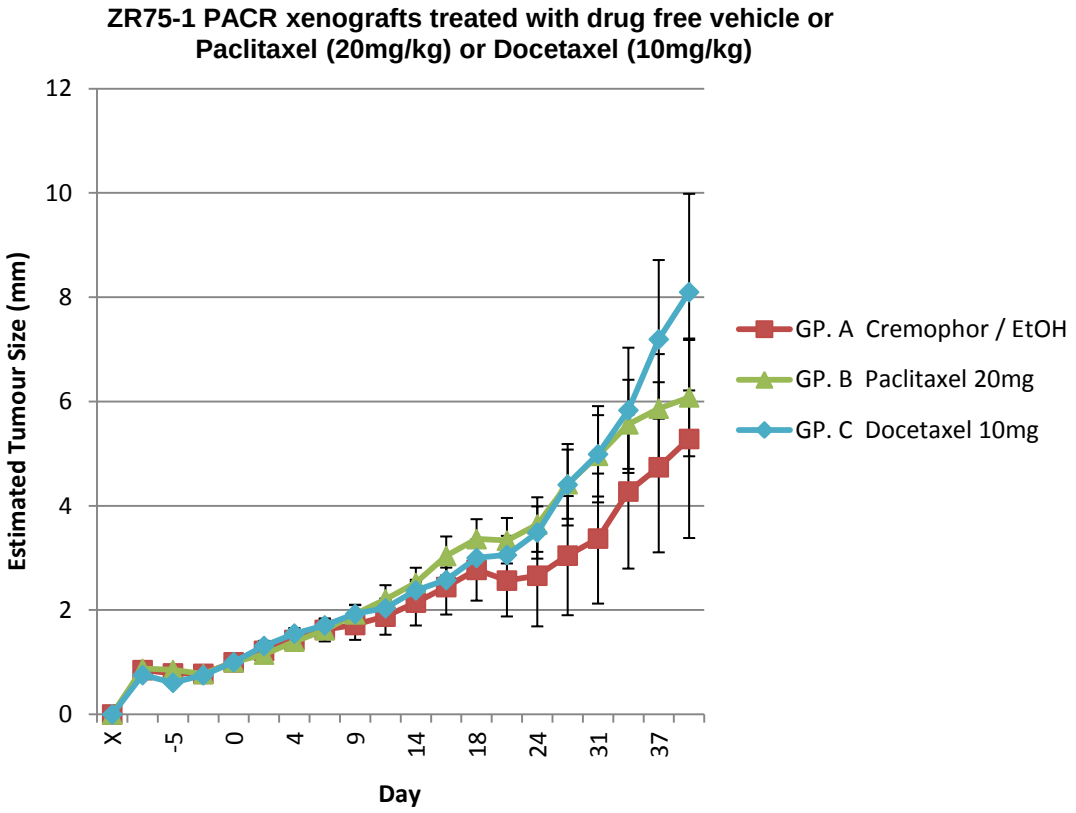


**Figure 4.9** Taxane cross resistance of 25nM PACR xenografts (moderate duration.) Treatment with blank drug free vehicle (cremophor) is shown by the red line with the rhombuses. Treatment with 20mg/kg paclitaxel is indicated by the pale green line with triangles and treatment with 10mg/kg docetaxel is indicated by the blue line with rhombuses. Tumour growth is indicated up the y axis and time in days is indicated along the x axis. Day of implantation is indicated by X on the x axis. Treatment began on day zero. Treatment began on day zero and was repeated on day 2 and day 4.

Over the course of the experiment the PACR xenografts treated with drug free vehicle (red line), paclitaxel (green line) and docetaxel (red line) show similar growth to one another. There is more separation of the tumour growth towards the end of the experiment, however there are also larger error bars at the later stages of the experiment.

Because one of the animals in the docetaxel group had to be culled (on day 35), we replotted this data looking at the first 33 days of the experiment following initial drug treatment (figure. 4.10.)

Figure 4.10 shows that the paclitaxel resistant xenografts grew larger tumours when treated with paclitaxel and docetaxel than when treated with blank drug vehicle alone and although this effect is not statistically significant, this observation suggests that the paclitaxel resistant

phenotype may be perpetuated in xenografts and that there may be cross resistance to docetaxel in the paclitaxel resistant xenografts.

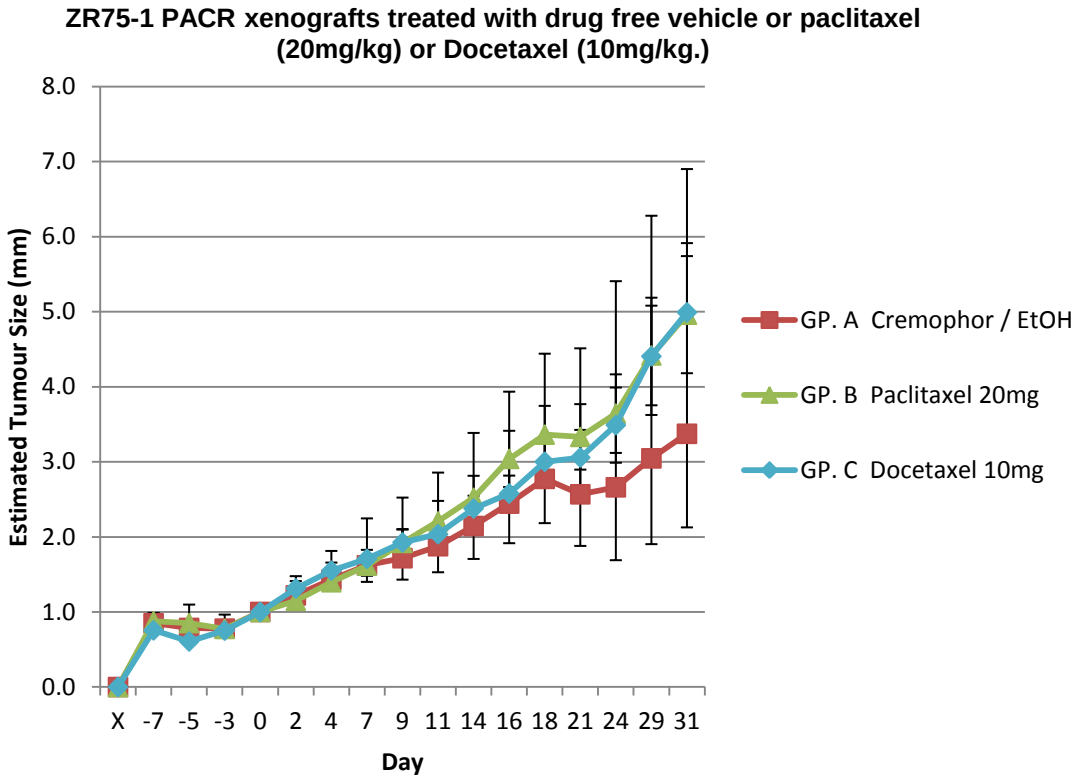


**Figure 4.10.** Initial phase of taxane cross resistance experiment using 25nM PACR xenografts (minimum duration.) Treatment with blank drug free vehicle (cremophor) is shown by the red line with the rhombuses. Treatment with 20mg/kg paclitaxel is indicated by the pale green line with triangles and treatment with 10mg/kg docetaxel is indicated by the blue line with rhombuses. Tumour growth is indicated up the y axis and time in days is indicated along the x axis. Day of implantation is indicated by X on the x axis. Treatment began on day zero. Treatment began on day zero and was repeated on day 2 and day 4.

### 4.2.b.iii. Cross resistance experiment using 25nM DOCR xenografts.

The third and final experiment looked at taxane cross resistance in 25nM PACR xenografts. The data is shown in figure 4.11 and is displayed in the same way as in figure 4.7 and 4.9. Additional data for this experiment is summarised in table 4.8.

| | Cremophor/etOH | Paclitaxel 20mg/kg | Docetaxel 10mg/kg |
|---|---|---|---|
| **# Mice injected** | 4 | 4 | 4 |
| **# Sites Injected** | 8 | 8 | 8 |
| **Successful Tumours** | 6 | 8 | 8 |
| **Failed Tumours** | 2 | 0 | 0 |
| **Mice culled – ill health** | 1* | 1** | 3*** |

**Table 4.8**. Summary of experiment using ZR75-1 DOCR cell line xenografts treated with blank drug vehicle (cremophor/etOH), paclitaxel (20mg/kg) or docetaxel (10mg/kg.) *Culled due to ulceration on day 37, ** culled due to ulceration on day 35, *** 1 died on injection, prior to receiving drug on day 2, 2 culled due to ulceration on day 30 and 35.

On day zero, three individuals from group A (drug free vehicle treated) one individual from group B (paclitaxel treated) and three individuals from group C (docetaxel treated) were accidentally injected partially subcutaneously. This happened again on day two for two individuals from group B and one individual from group C. On day four one individual from group A and two individuals from group B were IV injected partially subcutaneously. From day 14 to day 24 of the experiment the tumours were measured by a different member of technical staff than the rest of the experiment. In the cremophor treated group one animal failed to establish sufficient tumours.

On day 37 of the experiment one individual from group A became ulcerated and had to be culled. Another individual from group B became ulcerated and had to be culled on day 35. In addition on day two, one individual from group C fitted and died on injection, prior to receiving drug. On day 30 and 35 of the experiment two individuals from group C became ulcerated and were culled.

The DOCR xenografts grew at a similar rate when treated with drug free vehicle and paclitaxel and grow more rapidly when treated with docetaxel (figure 4.11.) This suggests that the DOCR phenotype may be perpetuated in the xenografts and that there is unlikely to be paclitaxel/docetaxel cross resistance in the DOCR xenografts.

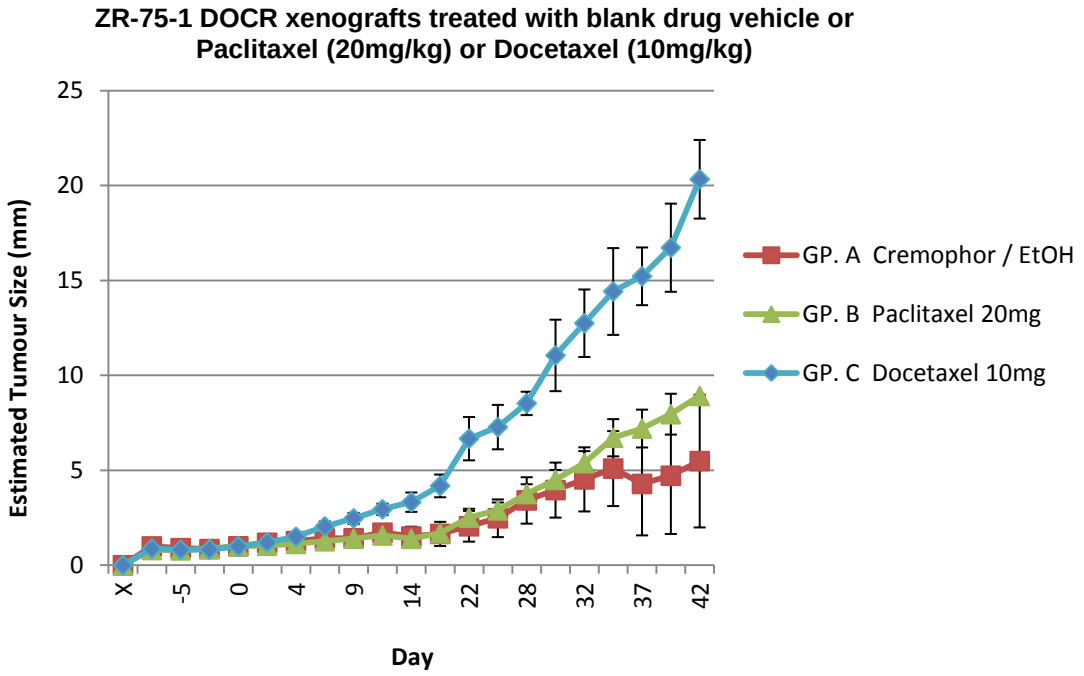


**Figure 4.11.**. Taxane cross resistance of 25nM DOCR xenografts (maximum duration.) Treatment with blank drug free vehicle (cremophor) is shown by the red line with the rhombuses. Treatment with 20mg/kg paclitaxel is indicated by the pale green line with triangles and treatment with 10mg/kg docetaxel is indicated by the blue line with rhombuses. Tumour growth is indicated up the y axis and time in days is indicated along the x axis. Day of implantation is indicated by X on the x axis. Treatment began on day zero and was repeated on day 2 and day 4.

The data was then replotted looking at the initial phase of the DOCR xenograft experiment before animals were culled due to ulceration (although one animal died prior to injection with drug) which is shown in figure 4.12. Figure 4.12 shows clearly that the DOCR tumours grow much larger when they are treated with docetaxel than when treated with blank drug vehicle. This suggests that the DOCR cells have maintained their docetaxel resistant phenotype and that the DOCR xenografts are not cross resistant to paclitaxel. Using an ANOVA test the author ascertained that there was no significant difference between the cremophor and paclitaxel treated DOCR lines (p value = 0.897.) However, there were statistically significant differences when comparing the Cremaphor and the docetaxel treated line ($p$ value = 0.013) and also when comparing the paclitaxel and the docetaxel treated DOCR xenografts ($p$ value = 0.0025.)

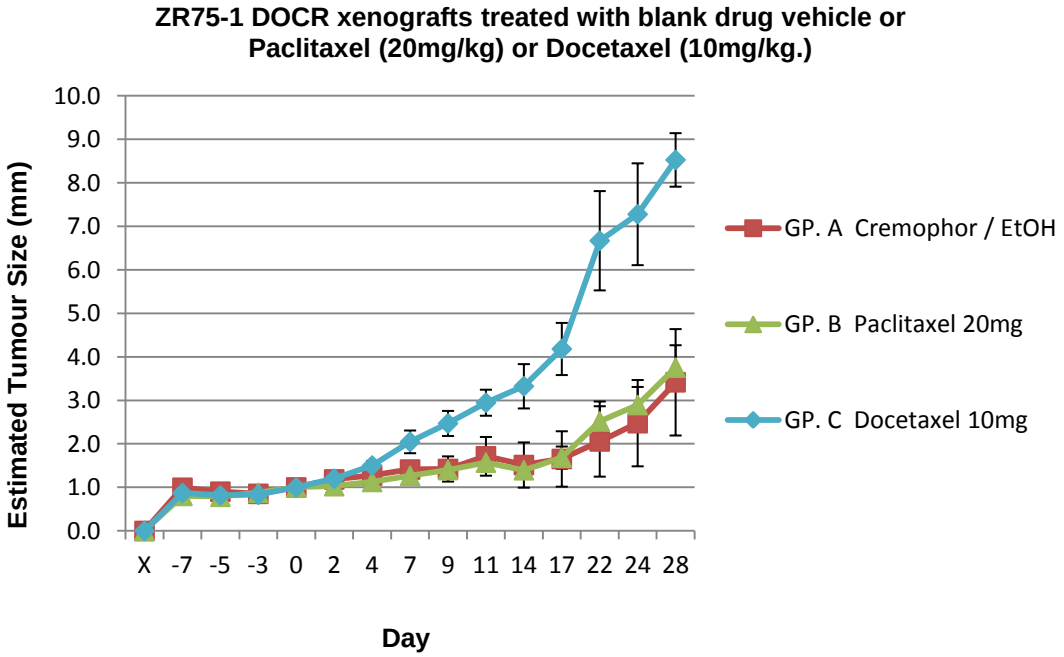


**Figure 4.12.**. Initial phase of taxane cross resistance experiment using 25nM DOCR xenografts (moderate duration.) Treatment with blank drug free vehicle (cremophor) is shown by the red line with the rhombuses. Treatment with 20mg/kg paclitaxel is indicated by the pale green line with triangles and treatment with 10mg/kg docetaxel is indicated by the blue line with rhombuses. Tumour growth is indicated up the y axis and time in days is indicated along the x axis. Day of implantation is indicated by X on the x axis. Treatment began on day zero and was repeated on day 2 and day 4.

The cross resistance experiments are complicated by a number of factors. Firstly, a number of animals died during the course of the experiment due to ulceration or fitting prior to injection with drug, secondly a number of animals were partially or completely injected subcutaneously and finally the measurements were not made by the same member of staff each time. The other factor to consider is that there are varying reports of how much more potent docetaxel is than paclitaxel[123, 184, 185, 191, 215, 217]. In addition there was a time pressure on the experiment which meant that we could not test the PACR and DOCR ZR75-1 cell lines long term in the absence of taxane to see if they reverted to the native phenotype *in vitro*. This experiment would be pertinent to carry out before proceeding with future xenograft experiments. It would also be appropriate to perform an *in vitro* cross resistance experiment that reflects the *in vivo* xenografts to see if the same behaviour is observed.

The xenograft experiments were conducted over a variety of different time periods; minimum, maximum or average duration and it is important to bear this in mind when interpreting the data.

This last series of three xenograft experiment poses a number of questions. Are the xenografts still growing too fast? Would reducing the cell number further allow the number of animals dying due to ulceration to be reduced? If the number of cells was lowered perhaps the experiment could be conducted over a longer period of time and perhaps extend the dose schedule, and frequency of dosing to maximise the effect of the drugs.

However, taxane resistant xenografts from isogenic native and resistant cell lines have been successfully generated to use as a model. The results of these experiments are provocative, they suggest that the native xenografts are sensitive to the taxanes. However, the later stages of this experiment are compromised by the death of two native animals with large tumours. The PACR seem to maintain their phenotype in xenografts and may also be resistant to docetaxel. It has been confirmed that the DOCR xenografts have maintained their phenotype *in vivo* and are resistant to docetaxel but not paclitaxel.

These results are intriguing and encouraging, future experiments to optimise cell number, and dose schedule will be valuable to further elucidate the pattern of resistance maintained by the native and taxane resistant cell lines in the *in vivo* model. It would also be pertinent to investigate the anchorage, metastatic and invasive potential of these cell lines *in vitro*.

As far as the author is aware, this is the first time that isogenic taxane resistant breast cancer cell lines have been generated and used to grow as xenograft tumours.

# Chapter 5

## Results:

### A Genomic and Transcriptomic Whole Genome Investigation into Taxane Resistant Breast Cancer Cell lines.

## 5.1. Array Comparative Genomic Hybridisation Analysis of Taxane resistant cell lines.

### 5.1.a. MDA-MB-231 cell lines.

Array comparative genomic hybridisation was performed on DNA samples harvested and extracted according to section 2.3.f.ii and 2.3.e.i-2.3.e.viii. The initial aCGH experiments were performed using the MDA-MB-231 PACR cell lines. Two different types of experiments were conducted, the first used DNA from pooled female blood as a reference sample and MDA-MB-231 native, 5nM, 25nM and 100nM PACR as reference samples. Figure 5.1-5.4 shows aCGH profiles of pooled female blood versus native, 5nM, 25nM and 100nM PACR cell lines respectively. The second set of experiments used DNA from the native cells as a reference sample and DNA from the taxane resistant cells as test samples. These sedon sets of experiments are detailed futher on in chapter 5.

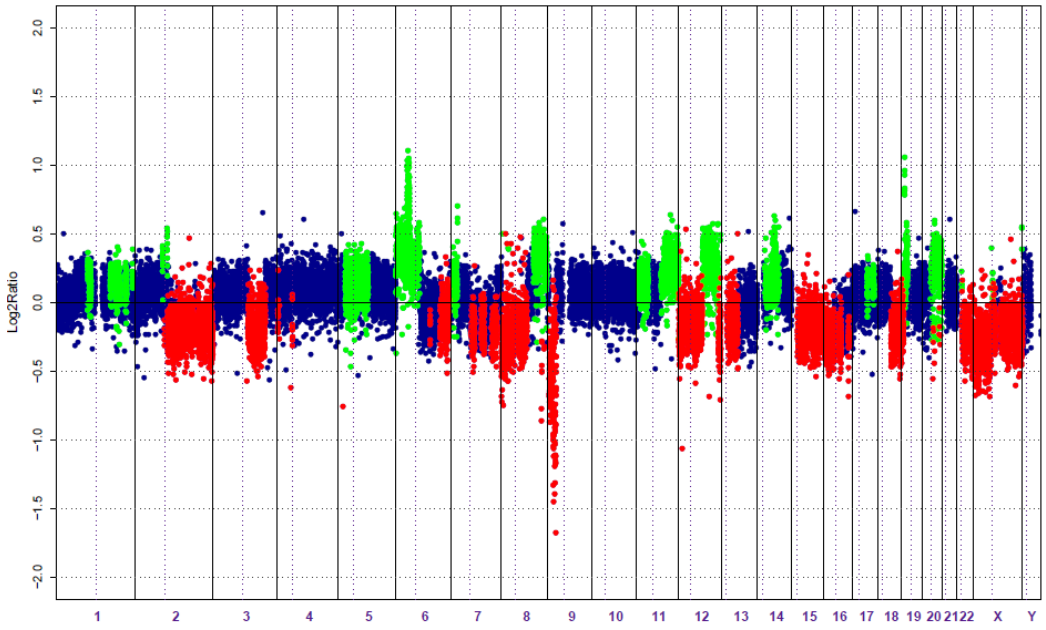


**Figure 5.1 Female DNA vs. Native MDA-MB-231** This plot charts cbs Log2Ratios of test to reference signal intensity from BAC clones in an aCGH experiment using DNA from pooled female blood as a reference sample and DNA from Native MDA-MB-231 cells as a test sample. Navy dots represent BAC clones which remain unchanged, the green dots represent the BAC clones in which there is an area of gain on the genome, and the red dots represent the BAC clones in which there is an area of loss of the genome. The Log2ratio is measured on the Y axis and on the X axis the genome runs in chromosome order from 1 to the sex chromosomes. The dotted lines represent the position of the centromere. The p or short arm on each chromosome is followed by the q or long arm. The cbs algorithim recursively split chromosomes into segments based on the maximum t statistic estimated by each permutation (re Mathworks.com.)

By considering these four figures together, a more general picture of how the breast cancer cell lines differ from normal human tissue could be observed. This has allowed a demonstration of how radically breast cancer cell lines differ from normal healthy tissue. There are extensive regions of loss and gain in all four MDA-MB-231 cell lines when compared to pooled female blood. On each of the aCGH plots each clone on the array is represented by a dot, areas of loss of copy number in the genome are shown in red, areas of gain are shown in green and areas in which there is no change is shown in blue. Chromosome 16 and the X chromosome show considerable areas of loss when compared to normal tissue. There is also a very large area of gain in chromosome 5.

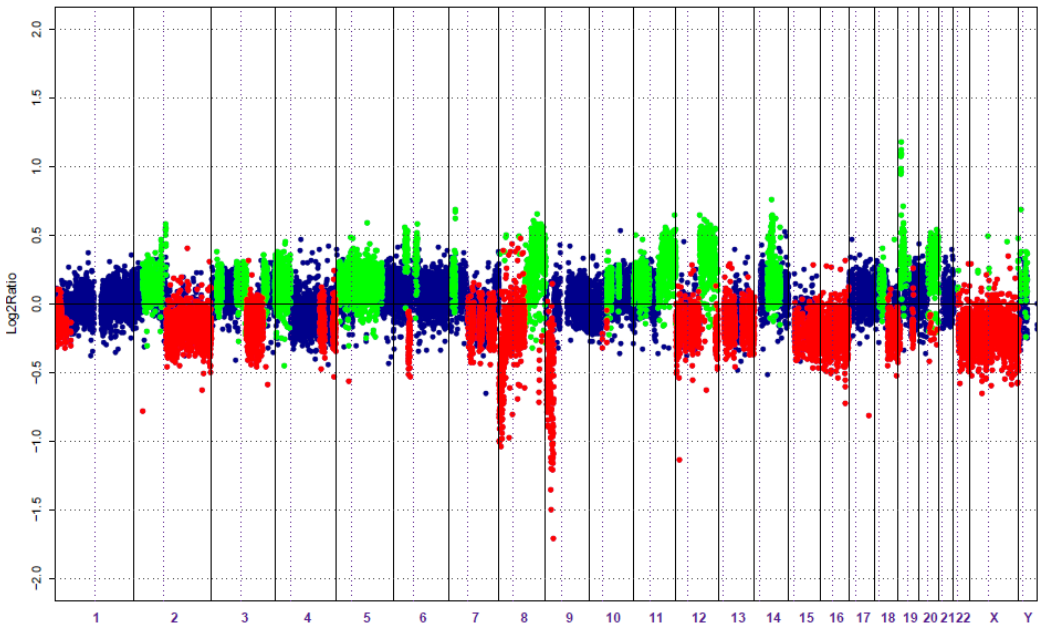


**Figure 5.2 Pooled Female DNA vs. 5nM PACR** This plot charts cbs Log2Ratios of test to reference signal intensity from BAC clones in an aCGH experiment using DNA from pooled female blood as a reference sample and DNA from 5nM PACR MDA-MB-231 cells as a test sample. Navy dots represent BAC clones which remain unchanged, the green dots represent the BAC clones in which there is an area of gain on the genome, and the red dots represent the BAC clones in which there is an area of loss of the genome. The Log2ratio is measured on the Y axis and on the X axis the genome runs in chromosome order from 1 to the sex chromosomes. The p or short arm on each chromosome is followed by the q or long arm. The dotted lines represent the position of the centromere. The cbs algorithim recursively split chromosomes into segments based on the maximum t statistic estimated by each permutation (re Mathworks.com.)

A study by Forzan *et al* published in Cancer Research used aCGH to identify any recurring genetic alterations in 38 breast cancer cell lines and compared them to uncultured breast tumour tissue[112(230)]. The most commonly identified chromosomal gains were in chromosome 1p, 1q, 3q, 5p, 7p, 7q, 8q, 17q, 20p and 20q, and the most commonly observed losses in 1p, 4p, 8p, 10q, 11q, 18p, 18q, 19p, Xp and Xq[224]. Roughly 2.5 times as many genetic changes were observed in cells lines than in tumours with an average of 19 genetic changes were detected (nine losses and 10 gains) per cell lines[225]. This suggests that cell lines are more susceptible to change than tumours and that this may be a result of long term culture potentially inducing more fragile sites within the genome.

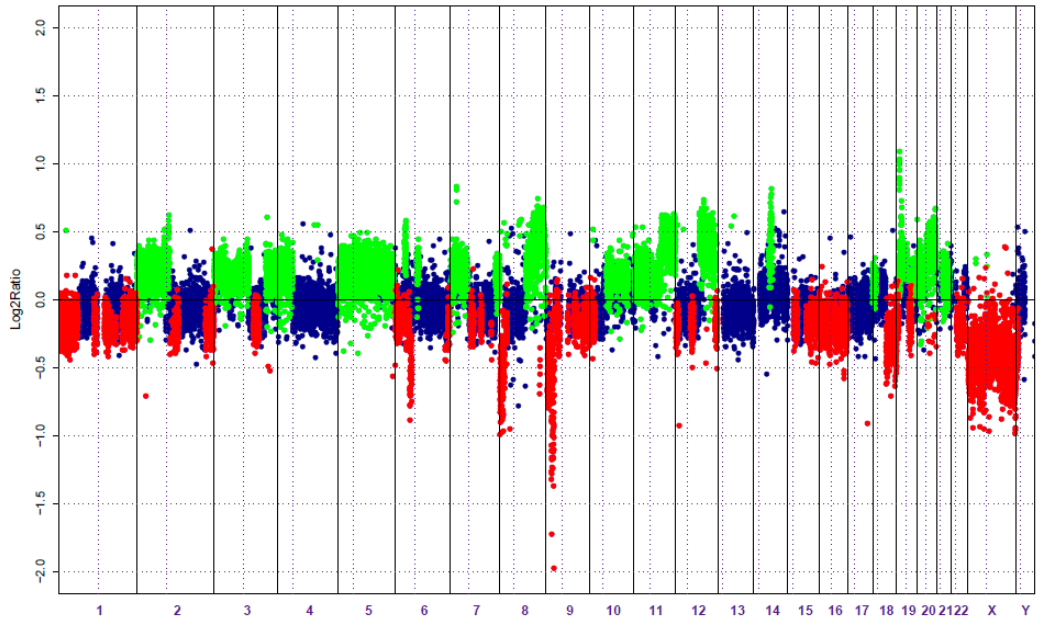


**Figure 5.3 Pooled Female DNA vs. 25nM PACR MDA-MB-231** This plot charts cbs Log2Ratios of test to reference signal intensity from BAC clones in an aCGH experiment using DNA from pooled female blood as a reference sample and DNA from 25nM PACR MDA-MB-231 cells as a test sample. Navy dots represent BAC clones which remain unchanged, the green dots represent the BAC clones in which there is an area of gain on the genome, and the red dots represent the BAC clones in which there is an area of loss of the genome. The Log2ratio is measured on the Y axis and on the X axis the genome runs in chromosome order from 1 to the sex chromosomes. The p or short arm on each chromosome is followed by the q or long arm. The dotted lines represent the position of the centromere. The cbs algorithim recursively split chromosomes into segments based on the maximum t statistic estimated by each permutation (re Mathworks.com.)

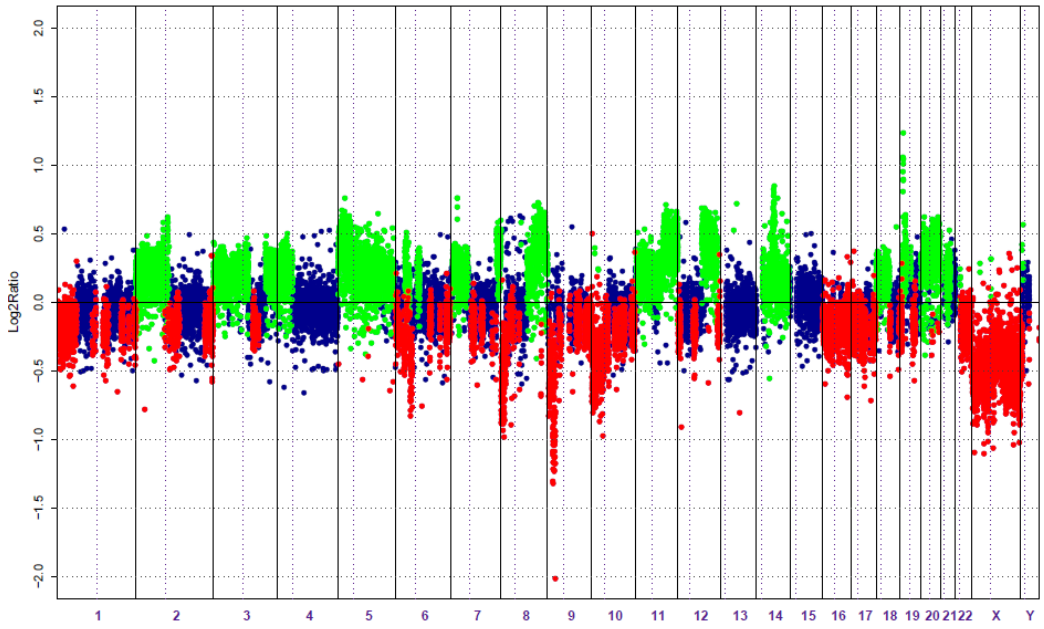


**Figure 5.4 pooled Female DNA vs. 100nM PACR MDA-MB-231** This plot charts cbs Log2Ratios of test to reference signal intensity from BAC clones in an aCGH experiment using DNA from pooled female blood as a reference sample and DNA from 100nM PACR MDA-MB-231 cells as a test sample. Navy dots represent BAC clones which remain unchanged, the green dots represent the BAC clones in which there is an area of gain on the genome, and the red dots represent the BAC clones in which there is an area of loss of the genome. The Log2ratio is measured on the Y axis and on the X axis the genome runs in chromosome order from 1 to the sex chromosomes. The dotted lines represent the position of the centromere. The p or short arm on each chromosome is followed by the q or long arm. The cbs algorithim recursively split chromosomes into segments based on the maximum t statistic estimated by each permutation (re Mathworks.com.)

However, it is important to point out that the most prominent alterations identified in this investigation were the same in cell lines as in tumours[230]. In the native and MDA-MB-231 native and PACR cell lines the identified areas of loss and gain extend as the level of paclitaxel resistance increases. To dissect and identify exactly how areas of loss and gain extend with increasing resistance, a second set of experiment which used DNA from the native MDA-MB-231 cell line as a reference sample and DNA from each of the PACR MDA-MB-231 cell lines as test samples was conducted. The aCGH plots obtained from these experiments are recorded in figure 5.5-5.7.

By looking at the plots in figure 5.5-7 the progressive changes in the MDA-MB-231 cell genome with increasing paclitaxel resistance were mapped. The following areas of gain extended at

paclitaxel resistance increased 2p25.3-23.3, 2q21.2-q24.33, 3p24.3-q13.3, 4p16.1-q12, 5q14.3-q31.1, 8q21.13-24.3, 11q15.1-q25 and the centromeric region of 14 (re figure 5.5-5.7 areas encircled with green rings) and the following area of loss extend as resistance increases 1p36.13-q44, 6p25.3-q12 8p, 19q and the x chromosome.

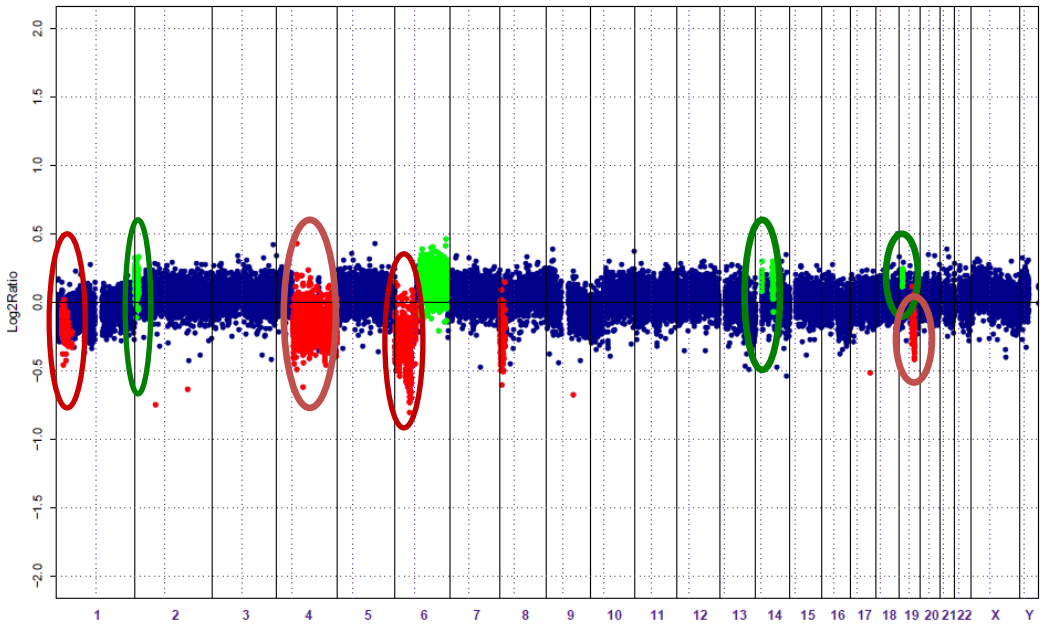


**Figure 5.5 MDA-MB-231 Native vs. 5nM PACR** This plot charts cbs Log2Ratios of test to reference signal intensity from BAC clones in an aCGH experiment using DNA from Native MDA-MB-231 cells as a reference sample and DNA from 5nM PACR MDA-MB-231 cells as a test sample. Navy dots represent BAC clones which remain unchanged, the green dots represent the BAC clones in which there is an area of gain on the genome, and the red dots represent the BAC clones in which there is an area of loss of the genome. The Log2ratio is measured on the Y axis and on the X axis the genome runs in chromosome order from 1 to the sex chromosomes. The p or short arm on each chromosome is followed by the q or long arm. The dotted lines represent the position of the centromere. The cbs algorithim recursively split chromosomes into segments based on the maximum t statistic estimated by each permutation (re Mathworks.com.)

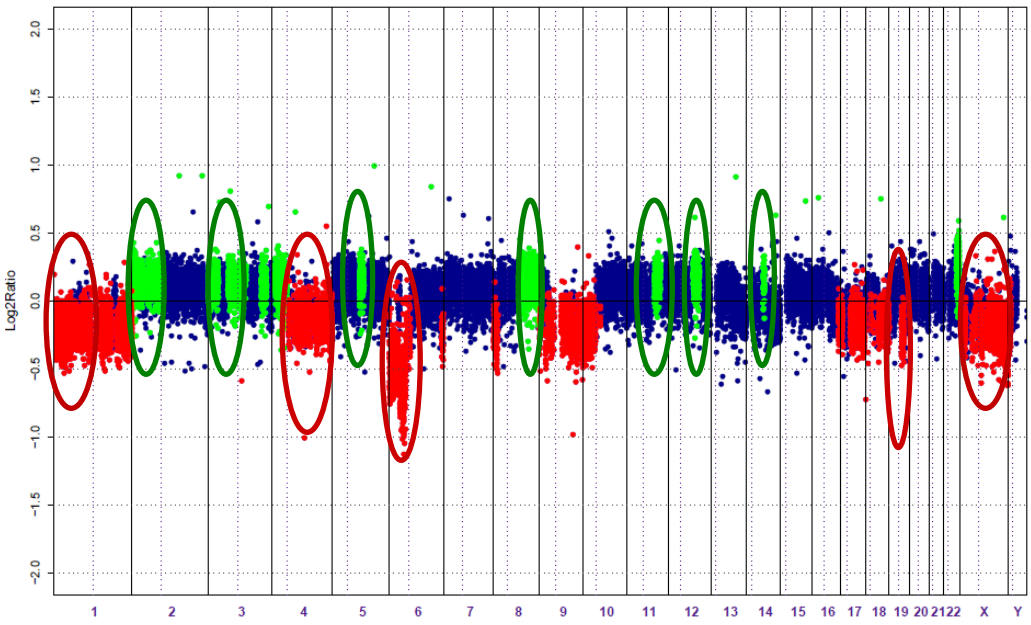


**Figure 5.6 MDA-MB-231 Native vs. 25nM PACR** This plot charts cbs Log2Ratios of test to reference signal intensity from BAC clones in an aCGH experiment using DNA from Native MDA-MB-231 cells as a reference sample and DNA from 25nM PACR MDA-MB-231 cells as a test sample. Navy dots represent BAC clones which remain unchanged, the green dots represent the BAC clones in which there is an area of gain on the genome, and the red dots represent the BAC clones in which there is an area of loss of the genome. The Log2ratio is measured on the Y axis and on the X axis the genome runs in chromosome order from 1 to the sex chromosomes. The p or short arm on each chromosome is followed by the q or long arm. The dotted lines represent the position of the centromere. The cbs algorithim recursively split chromosomes into segments based on the maximum t statistic estimated by each permutation (re Mathworks.com.)

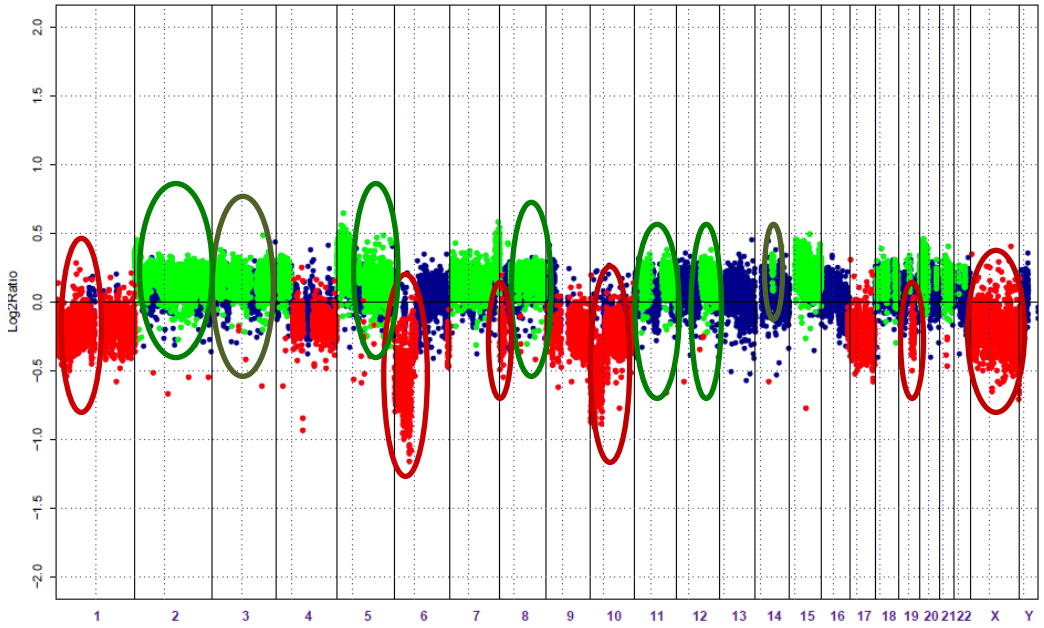


**Figure 5.7 MDA-MB-231 Native vs. 100nM PACR** This plot charts cbs Log2Ratios of test to reference signal intensity from BAC clones in an aCGH experiment using DNA from Native MDA-MB-231 cells as a reference sample and DNA from 100nM PACR MDA-MB-231 cells as a test sample. Navy dots represent BAC clones which remain unchanged, the green dots represent the BAC clones in which there is an area of gain on the genome, and the red dots represent the BAC clones in which there is an area of loss of the genome. The Log2ratio is measured on the Y axis and on the X axis the genome runs in chromosome order from 1 to the sex chromosomes. The p or short arm on each chromosome is followed by the q or long arm. The dotted lines represent the position of the centromere. The cbs algorithim recursively split chromosomes into segments based on the maximum t statistic estimated by each permutation (re Mathworks.com.)

These two sets of experiments were repeated for all of the taxane resistant cell lines. The first set of these experiments used DNA from pooled female blood as a reference sample and DNA from each of the MDA-MB-231 native, 5nM, 25nM and 50nM PACR samples as test samples. Figure 5.8-5.11 are repeats of the experiments shown in figure 5.1-5.4. Comparing these two sets of four plots it was shown that the technique has been effectively replicated across the two runs. In this second set of experiments the 50nM PACR cell line was included instead of the 100nM PACR. The 50nM PACR cells (fig 5.11) were used instead of the 100nM PACR cells (fig. 5.4) as the 100nM PACR cells had shown anomalous behaviour in our cell count experiments re figure 3.3.

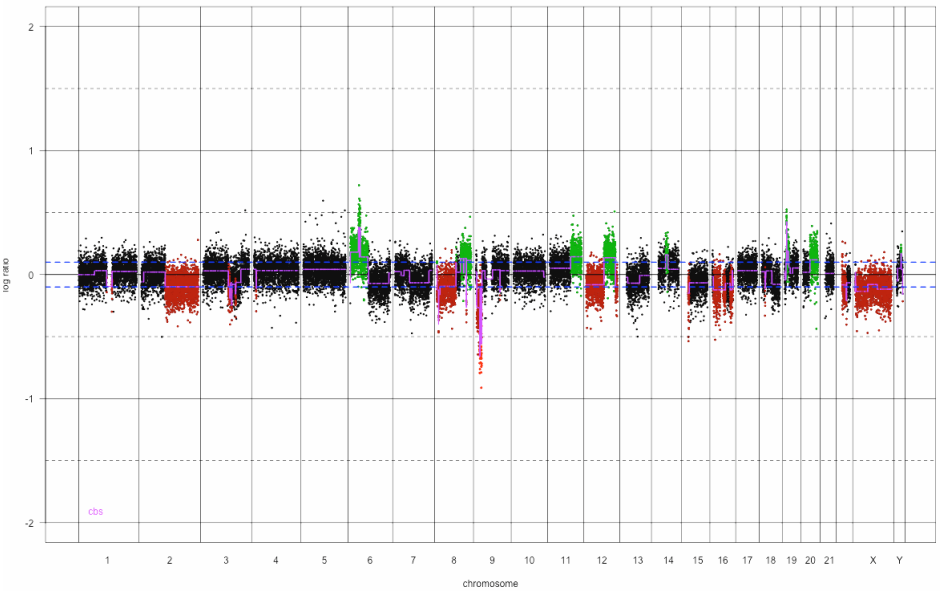


**Figure 5.8 and 5.9 Pooled Female vs. Native MDA-MB-231 Native (top) and Pooled female blood vs. 5nM PACR (bottom)** This plot charts cbs Log2Ratios of test to reference signal intensity from BAC clones in an aCGH experiment using DNA from pooled female DNA as a reference sample and DNA from Native or 5nM PACR MDA-MB-231 cells as a test sample. Navy dots represent BAC clones which remain unchanged, the green dots represent the BAC clones in which there is an area of gain on the genome, and the red dots represent the BAC clones in which there is an area of loss of the genome. The Log2ratio is measured on the Y axis and on the X axis the genome runs in chromosome order from 1 to the sex chromosomes. The p or short arm on each chromosome is followed by the q or long arm. The cbs algorithim recursively split chromosomes into segments based on the maximum t statistic estimated by each permutation (re Mathworks.com.)

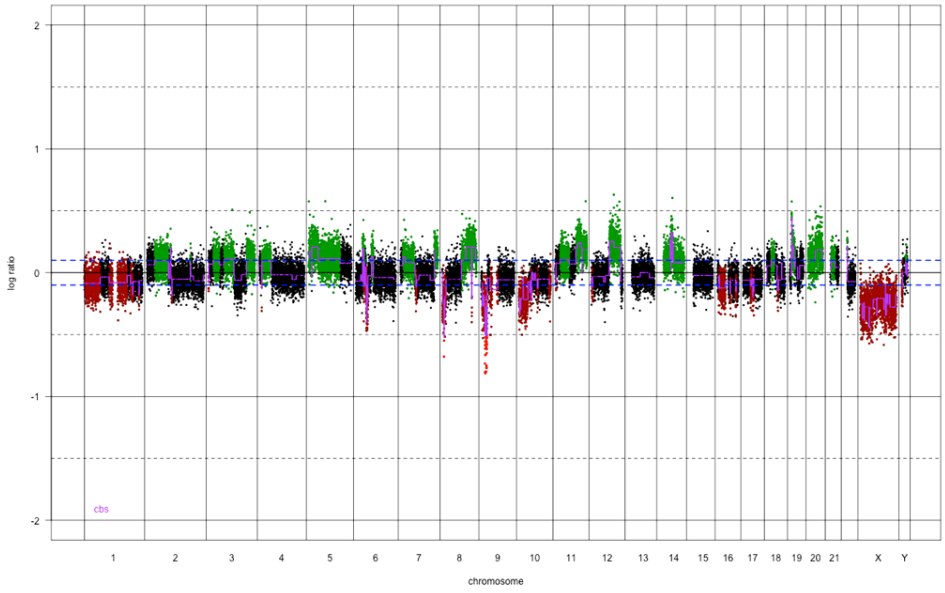

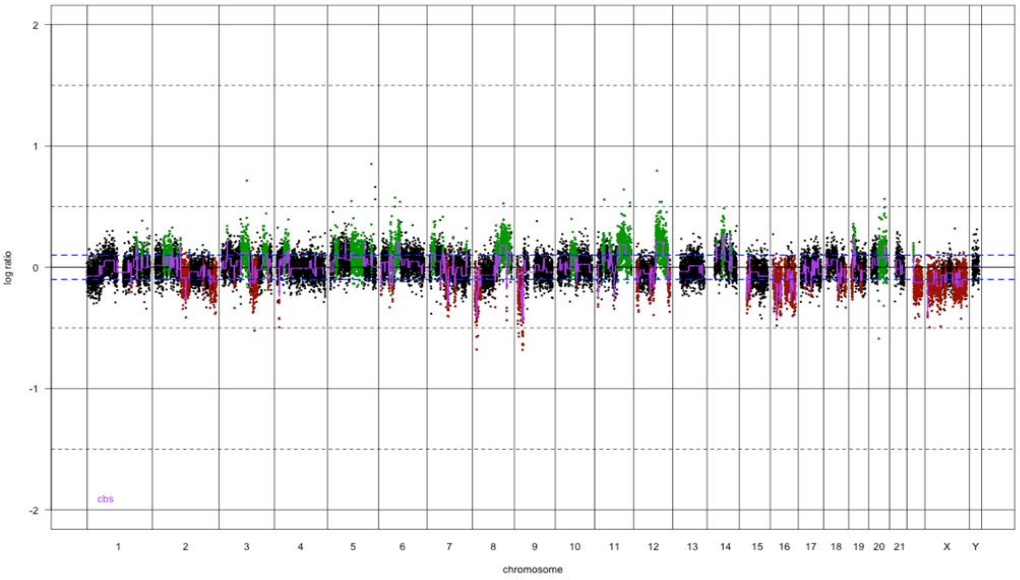


**Figure 5.10 and 5.11 Pooled Female DNA vs. 25nM PACR MDA-MB-231 (top) and 50nM PACR (bottom)** This plot charts cbs Log2Ratios of test to reference signal intensity from BAC clones in an aCGH experiment using DNA from pooled female blood as a reference sample and DNA from 25nM or 50nM PACR MDA-MB-231 cells as a test sample. Navy dots represent BAC clones which remain unchanged, the green dots represent the BAC clones in which there is an area of gain on the genome, and the red dots represent the BAC clones in which there is an area of loss of the genome. The Log2ratio is measured on the Y axis and on the X axis the genome runs in chromosome order from 1 to the sex chromosomes. The p or short arm on each chromosome is followed by the q or long arm. The cbs algorithim recursively split chromosomes into segments based on the maximum t statistic estimated by each permutation (re Mathworks.com.)

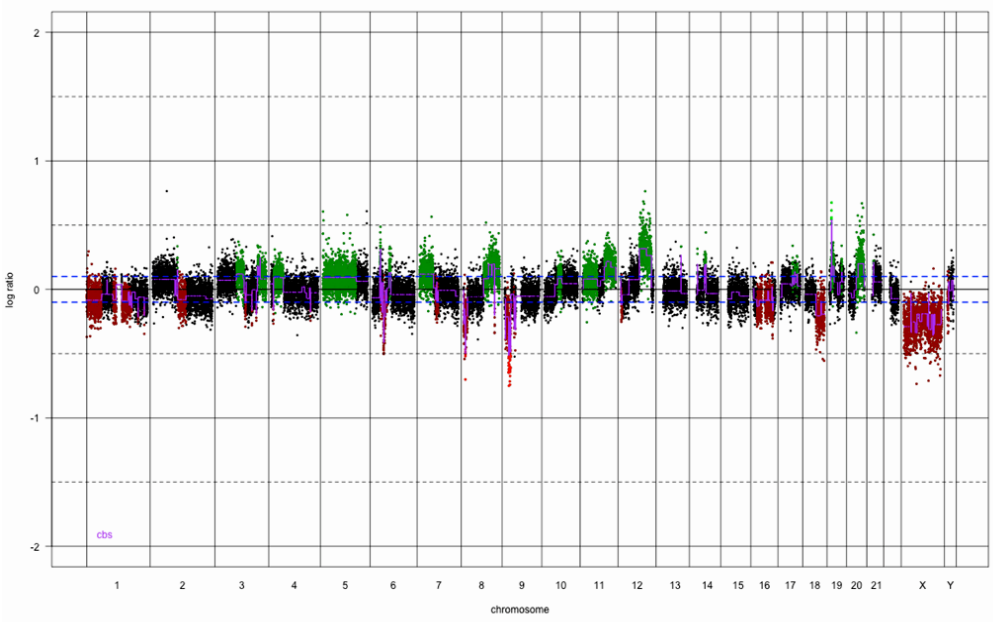

Figure 5.12-5.14 show the second set of experiments using the MDA-MB-231 natives as a reference sample and the 5nM 25nM and 50nM PACR MDA-MB-231 cell lines as test samples. By comparing these plots to the plots in the first set of -replicates shown in figures 5.5-7 it can be established which regions of gain and loss that extend with paclitaxel resistance are common across both experiments.

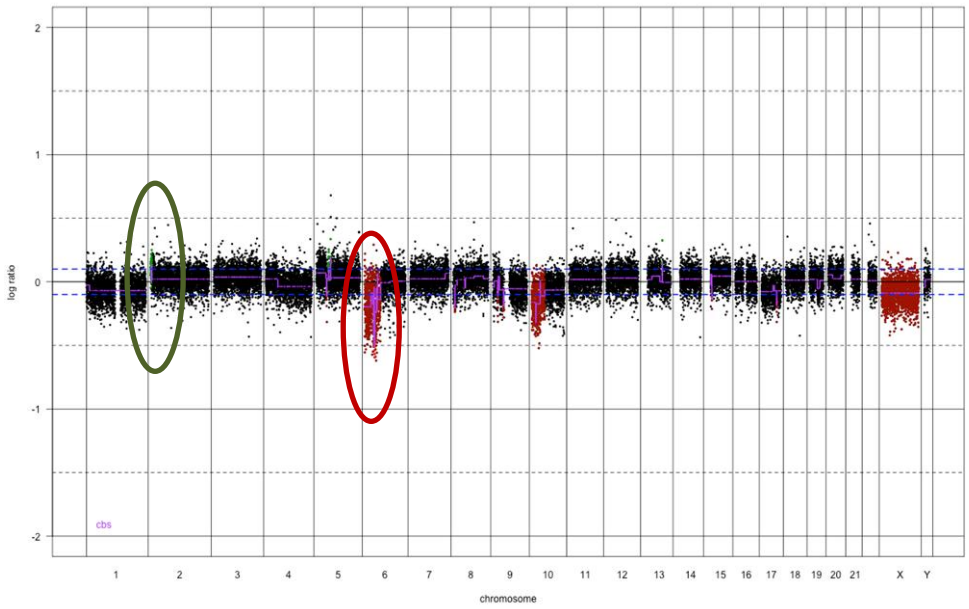


**Figure 5.12 MDA-MB-231 Native vs. 5nM PACR** This plot charts cbs Log2Ratios of test to reference signal intensity from BAC clones in an aCGH experiment using DNA from Native MDA-MB-231 cells as a reference sample and DNA from 5nM PACR MDA-MB-231 cells as a test sample. Navy dots represent BAC clones which remain unchanged, the green dots represent the BAC clones in which there is an area of gain on the genome, and the red dots represent the BAC clones in which there is an area of loss of the genome. The Log2ratio is measured on the Y axis and on the X axis the genome runs in chromosome order from 1 to the sex chromosomes. The p or short arm on each chromosome is followed by the q or long arm. The cbs algorithim recursively split chromosomes into segments based on the maximum t statistic estimated by each permutation (re Mathworks.com.)

The areas of loss in chromosome 1p and 6p are common to both sets of experiments and so are the areas of gain in chromosome 12. It is important to note that there will be some variation as the highest doses of paclitaxel resistance differ in the two experiments. (re figure 5.7)

Areas of amplification and deletion were also identified in the second set of experiments. There are also regions of deletion in 6p21.1 of 5nM and 25nM PACR MDA-MB-231 and 6p21.2 of the 25nM PACR cells and deletion in 2q13, 15q11,2 and 16 q11.2 regions of the 50nM PACR cells. There is a region of amplification in 6p21.1 of the MDA-MB-231 25nM PACR cells. There are regions of amplification in 1q32.3, 4q21.21-21.22, 8p12, 8p11.21, 11q13.2, 12q14.1, 12q14.2, 12q15, 15q11.2 and 15q22.2-q22.3 of MDA-MB-231 50nM PACR cells.

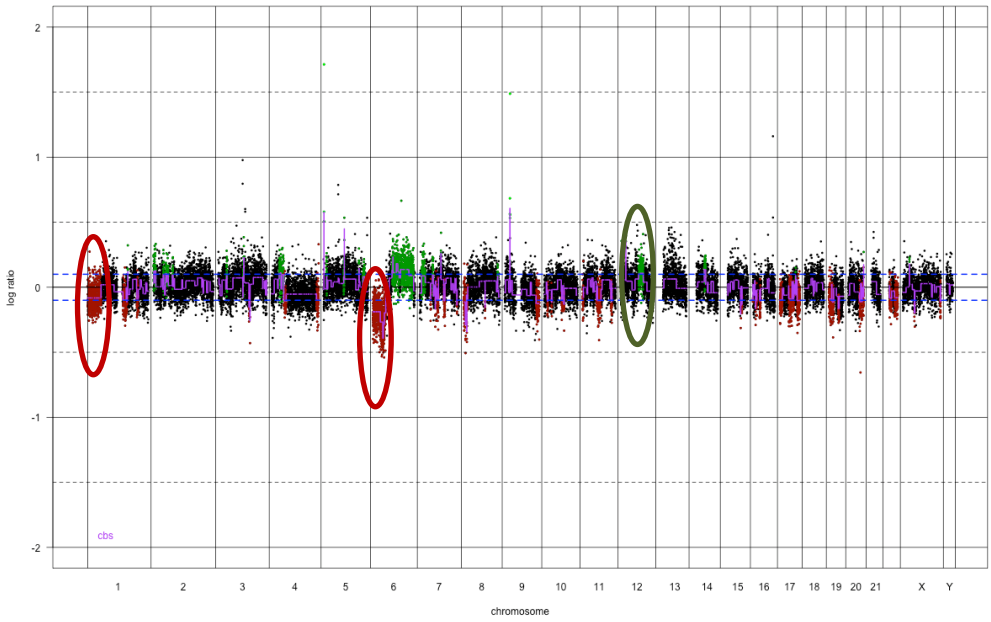


**Figure 5.13 MDA-MB-231 Native vs. 25nM PACR** This plot charts cbs Log2Ratios of test to reference signal intensity from BAC clones in an aCGH experiment using DNA from Native MDA-MB-231 cells as a reference sample and DNA from 25nM PACR MDA-MB-231 cells as a test sample. Navy dots represent BAC clones which remain unchanged, the green dots represent the BAC clones in which there is an area of gain on the genome, and the red dots represent the BAC clones in which there is an area of loss of the genome. The Log2ratio is measured on the Y axis and on the X axis the genome runs in chromosome order from 1 to the sex chromosomes. The p or short arm on each chromosome is followed by the q or long arm. The cbs algorithim recursively split chromosomes into segments based on the maximum t statistic estimated by each permutation (re Mathworks.com.)

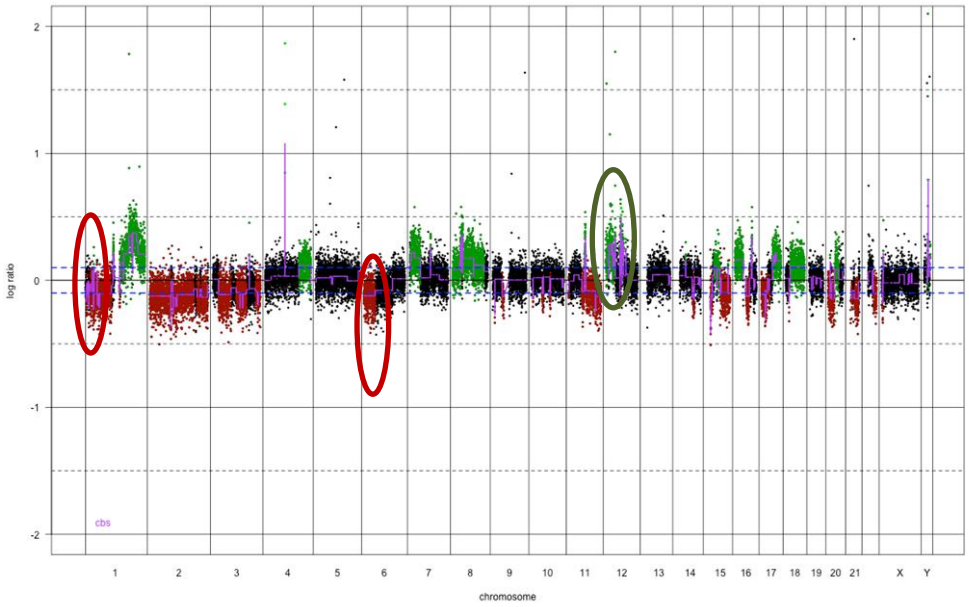


**Figure 5.14 MDA-MB-231 Native vs. 50nM PACR** This plot charts cbs Log2Ratios of test to reference signal intensity from BAC clones in an aCGH experiment using DNA from Native MDA-MB-231 cells as a reference sample and DNA from 50nM PACR MDA-MB-231 cells as a test sample. Navy dots represent BAC clones which remain unchanged, the green dots represent the BAC clones in which there is an area of gain on the genome, and the red dots represent the BAC clones in which there is an area of loss of the genome. The Log2ratio is measured on the Y axis and on the X axis the genome runs in chromosome order from 1 to the sex chromosomes. The p or short arm on each chromosome is followed by the q or long arm. The cbs algorithim recursively split chromosomes into segments based on the maximum t statistic estimated by each permutation (re Mathworks.com.)

**5.1.b ZR75-1 Cell Lines.**

The same set of experiments were then performed in the ZR75-1 cell lines. Figure 5.15-18 shows the plots of the experiments using DNA pooled female blood as a reference samples and DNA from each of the native, 5nM, 25nM and 50nM PACR ZR75-1 cell lines as test samples. Again it can seen that each of the breast cancer cell lines radically differ from normal healthy tissue with extensive regions of loss and gain. It is also apparent that some areas are gained in ZR75-1s that are lost in the MDA-MB-231 and vice versa.

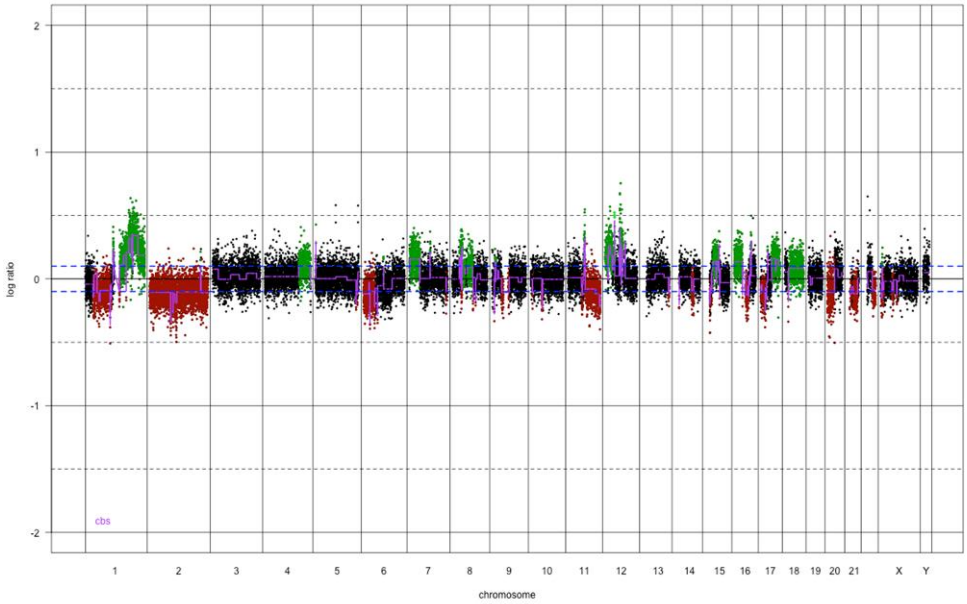


**Figure 5.15 Pooled Female blood vs. ZR75-1 Native** This plot charts cbs Log2Ratios of test to reference signal intensity from BAC clones in an aCGH experiment using DNA from pooled female blood as a reference sample and DNA from Native ZR75-1 cells as a test sample. Navy dots represent BAC clones which remain unchanged, the green dots represent the BAC clones in which there is an area of gain on the genome, and the red dots represent the BAC clones in which there is an area of loss of the genome. The Log2ratio is measured on the Y axis and on the X axis the genome runs in chromosome order from 1 to the sex chromosomes. The p or short arm on each chromosome is followed by the q or long arm. The cbs algorithim recursively split chromosomes into segments based on the maximum t statistic estimated by each permutation (re Mathworks.com.)

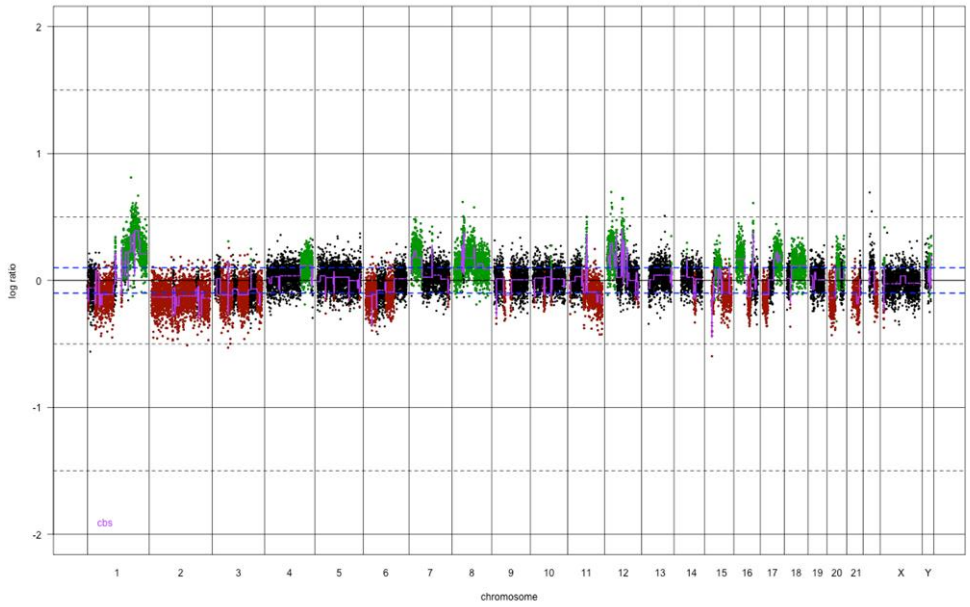


**Figure 5.16 and 5.17 Pooled Female DNA vs. ZR75-1 5nM and 25nM PACR** This plot charts cbs Log2 Ratios of test to reference signal intensity from BAC clones in an aCGH experiment using DNA from pooled female blood as a reference sample and DNA from ZR75-1 5nM or 25nM PACR cells as a test sample. Navy dots represent BAC clones which remain unchanged, the green dots represent the BAC clones in which there is an area of gain on the genome, and the red dots represent the BAC clones in which there is an area of loss of the genome. The Log2ratio is measured on the Y axis and on the X axis the genome runs in chromosome order from 1 to the sex chromosomes. The p or short arm on each chromosome is followed by the q or long arm. The cbs algorithim recursively split chromosomes into segments based on the maximum t statistic estimated by each permutation (re Mathworks.com.)

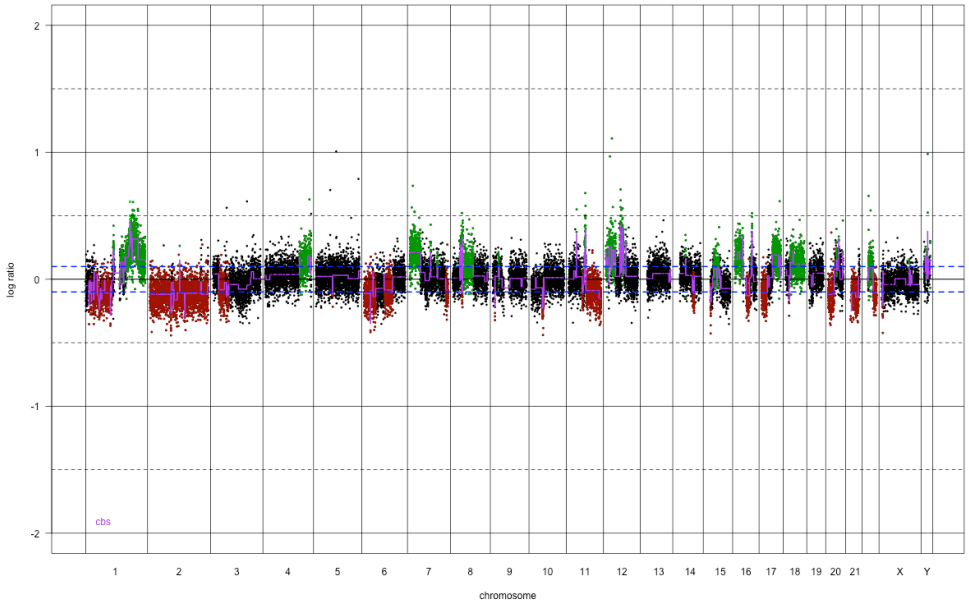

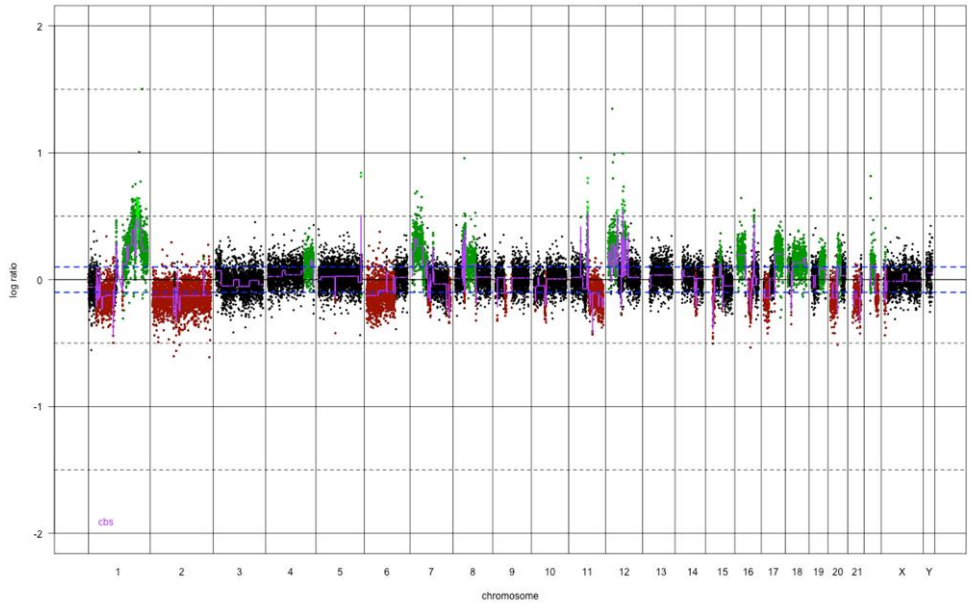


**Figure 5.18 Pooled Female DNA vs. ZR75-1 50nM PACR** This plot charts cbs Log2Ratios of test to reference signal intensity from BAC clones in an aCGH experiment using DNA from pooled female blood as a reference sample and DNA from 50nM PACR ZR75-1 cells as a test sample. Navy dots represent BAC clones which remain unchanged, the green dots represent the BAC clones in which there is an area of gain on the genome, and the red dots represent the BAC clones in which there is an area of loss of the genome. The Log2ratio is measured on the Y axis and on the X axis the genome runs in chromosome order from 1 to the sex chromosomes. The p or short arm on each chromosome is followed by the q or long arm. The cbs algorithim recursively split chromosomes into segments based on the maximum t statistic estimated by each permutation (re Mathworks.com.)

Figure 5.19-21 shows the plots of experiments using DNA from the ZR75-1 native cell line as a reference sample and DNA from each of the ZR75-1 PACR cell lines as test samples. There is an extensive area of loss over the whole of chromosome 3 when the 5nM PACR ZR75-1 cells are used as test sample against the native background and there are also small regions of loss in 12p, 16q and 18p. There is an extensive area of gain over the whole of chromosome 8.

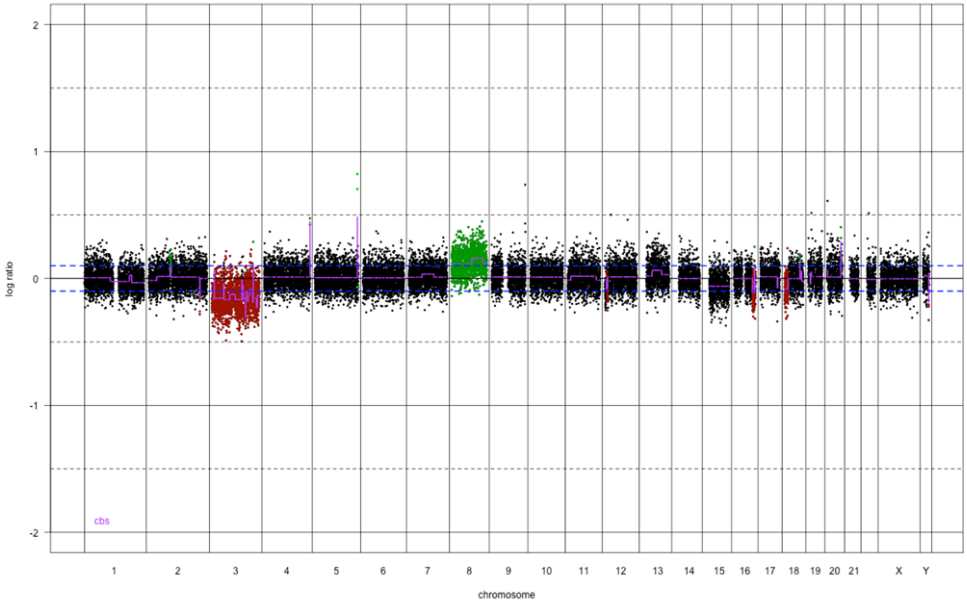


**Figure 5.19 ZR75-1 Native vs. 5nM PACR** This plot charts cbs Log2Ratios of test to reference signal intensity from BAC clones in an aCGH experiment using DNA from Native ZR75-1 as a reference sample and DNA from 5nM PACR ZR75-1 cells as a test sample. Navy dots represent BAC clones which remain unchanged, the green dots represent the BAC clones in which there is an area of gain on the genome, and the red dots represent the BAC clones in which there is an area of loss of the genome. The Log2ratio is measured on the Y axis and on the X axis the genome runs in chromosome order from 1 to the sex chromosomes. The p or short arm on each chromosome is followed by the q or long arm. The cbs algorithim recursively split chromosomes into segments based on the maximum t statistic estimated by each permutation (re Mathworks.com.)

In the experiment comparing the ZR75-1 25nM PACR to the native cells there are regions of loss in 1q, 3p, 7q, 10p, 12p, 15p and 16q. There are small regions of gain in 4q the centromeric region of chromosome 10, and 11p.

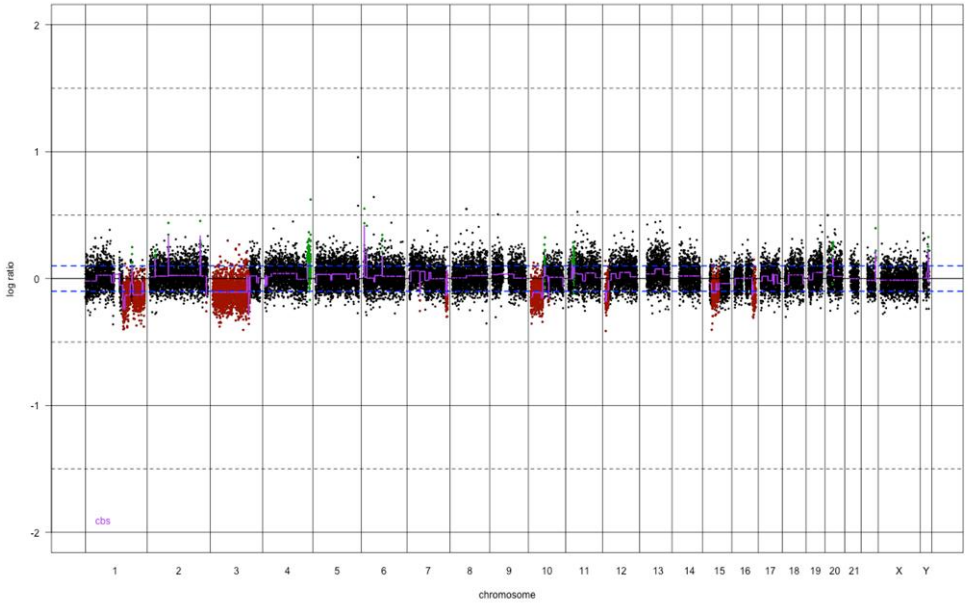


**Figure 5.20 ZR75-1 native vs. 25nM PACR** This plot charts cbs Log2Ratios of test to reference signal intensity from BAC clones in an aCGH experiment using DNA from ZR75-1 Native cells as a sample and DNA from 25nM PACR ZR75-1 cells as a test sample. Navy dots represent BAC clones which remain unchanged, the green dots represent the BAC clones in which there is an area of gain on the genome, and the red dots represent the BAC clones in which there is an area of loss of the genome. The Log2ratio is measured on the Y axis and on the X axis the genome runs in chromosome order from 1 to the sex chromosomes. The p or short arm on each chromosome is followed by the q or long arm. The cbs algorithim recursively split chromosomes into segments based on the maximum t statistic estimated by each permutation (re Mathworks.com.)

When the 50nM PACR cells are compared to the Native cells there are regions of loss in the 1q, 7q, 10p, 12p, 15p, and 16q. There are regions of gain in 7p, 9p, the centromeric region of chromosome 15 and 19q (re figure 5.21). When comparing each of the three cell lines with the native cells there are no common areas of gain but there are two common areas of loss at 12p and 16q. When just observing the top two resistance levels there are no common areas of gain but there are 5 common areas of loss: 1q, 7q,10p 12p, and 16q.

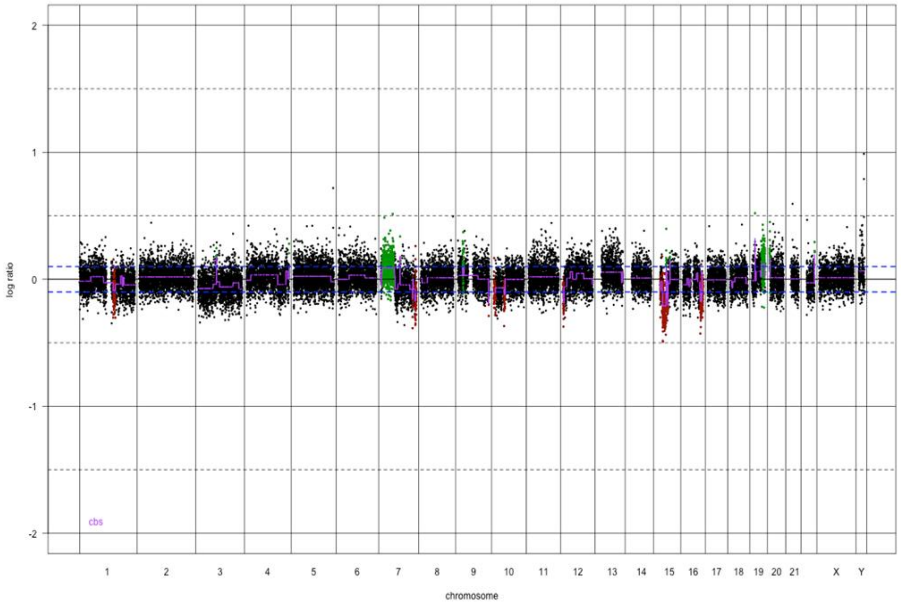


**Figure 5.21 ZR75-1 native vs. 50nM PACR** This plot charts cbs Log2Ratios of test to reference signal intensity from BAC clones in an aCGH experiment using DNA from ZR75-1 reference sample and DNA from 50nM PACR ZR75-1 cells as a test sample. Navy dots represent BAC clones which remain unchanged, the green dots represent the BAC clones in which there is an area of gain on the genome, and the red dots represent the BAC clones in which there is an area of loss of the genome. The Log2ratio is measured on the Y axis and on the X axis the genome runs in chromosome order from 1 to the sex chromosomes. The p or short arm on each chromosome is followed by the q or long arm. The cbs algorithim recursively split chromosomes into segments based on the maximum t statistic estimated by each permutation (re Mathworks.com.)

Figure 5.22 – 5.24 are the plots of aCGH data from the experiments using pooled female DNA as a reference sample and the native, 25 and 50nM DOCR samples as test samples. Note the 5nM DOCR samples failed both the runs comparing it with pooled female blood and with the native samples. This first plot replicates the plot shown in 5.15.

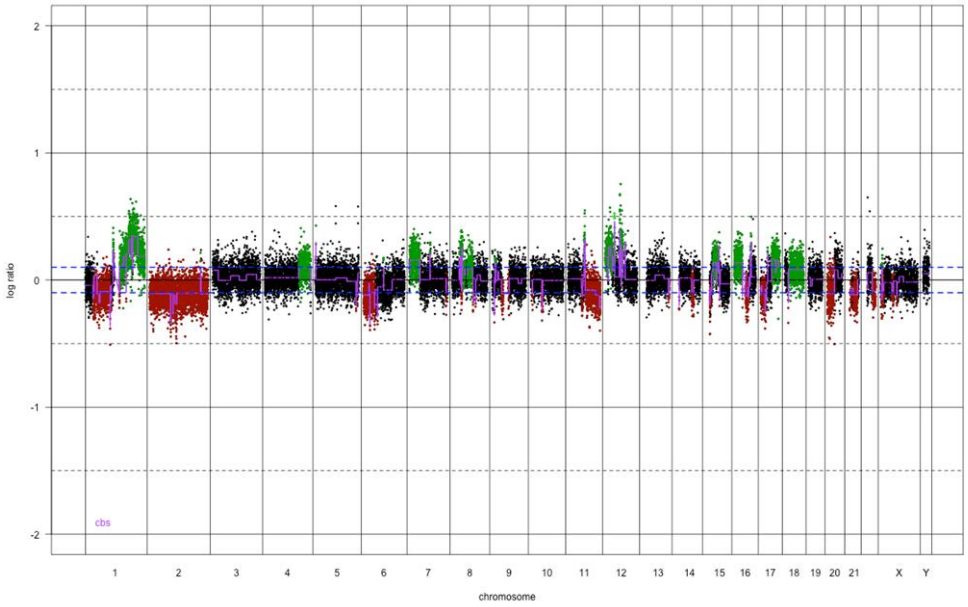


**Figure 5.22 Pooled female DNA vs. ZR75-1 native** This plot charts cbs Log2Ratios of test to reference signal intensity from BAC clones in an aCGH experiment using DNA from pooled female blood as a reference sample and DNA from Native ZR75-1 cells as a test sample. Navy dots represent BAC clones which remain unchanged, the green dots represent the BAC clones in which there is an area of gain on the genome, and the red dots represent the BAC clones in which there is an area of loss of the genome. The Log2ratio is measured on the Y axis and on the X axis the genome runs in chromosome order from 1 to the sex chromosomes. The p or short arm on each chromosome is followed by the q or long arm. The cbs algorithim recursively split chromosomes into segments based on the maximum t statistic estimated by each permutation (re Mathworks.com.)

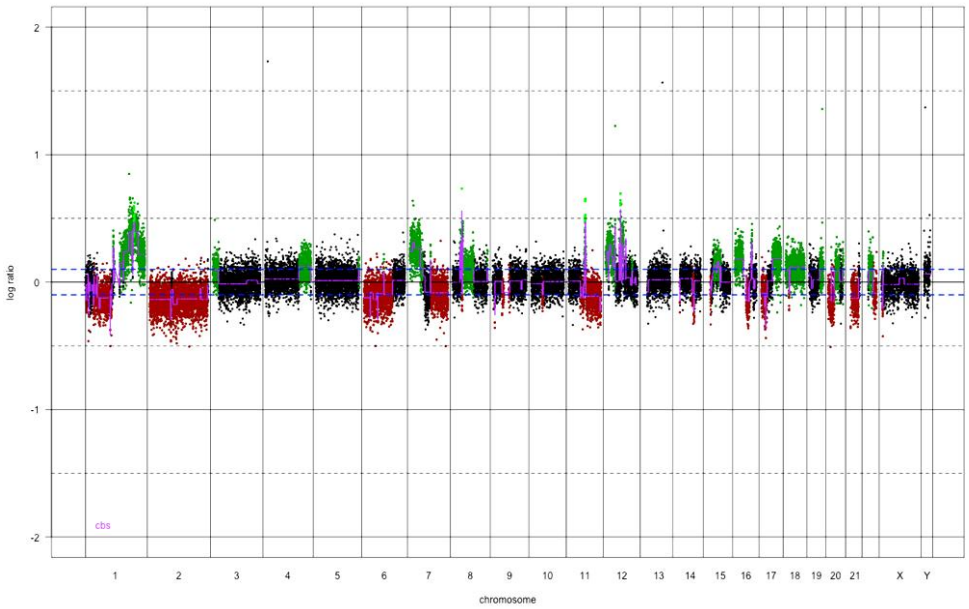


**Figure 5.23 and 5.24 Pooled female DNA ZR75-1 25nM DOCR (top) and 50nM (bottom)** This plot charts cbs Log2Ratios of test to reference signal intensity from BAC clones in an aCGH experiment using DNA from pooled female blood as a reference sample and DNA from 25nM or 50nM DOCR ZR75-1 cells as a test sample. Navy dots represent BAC clones which remain unchanged, the green dots represent the BAC clones in which there is an area of gain on the genome, and the red dots represent the BAC clones in which there is an area of loss of the genome. The Log2ratio is measured on the Y axis and on the X axis the genome runs in chromosome order from 1 to the sex chromosomes. The p or short arm on each chromosome is followed by the q or long arm. The cbs algorithim recursively split chromosomes into segments based on the maximum t statistic estimated by each permutation (re Mathworks.com.)

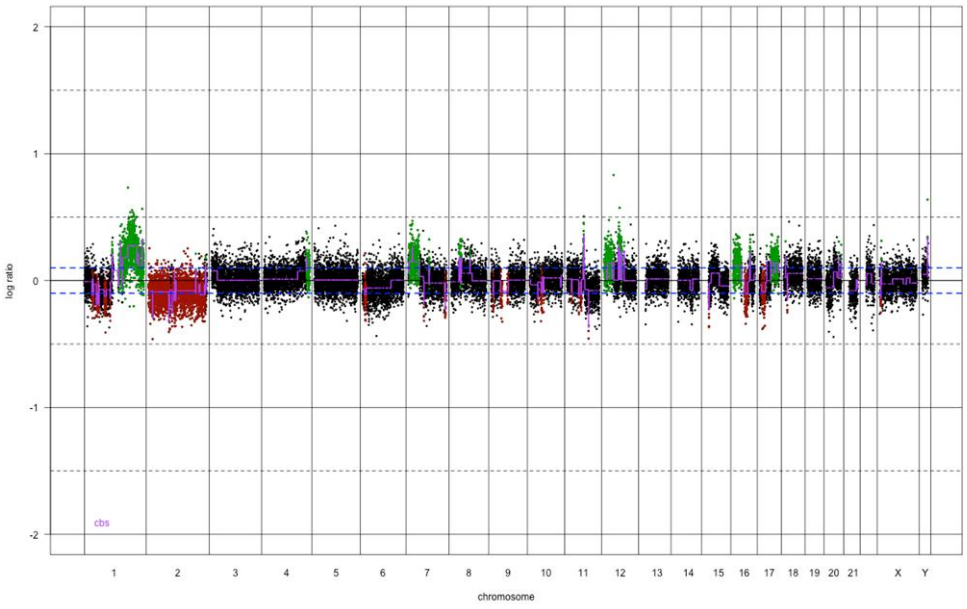

Figure 5.25 and 5.26 show the aCGH plot of the experiments when Native ZR75-1 cells are used as a reference sample and 25nM and 50nM DOCR ZR75-1 as test samples. There are areas of loss in 7q, 12p and 16q in the two highest resistance levels and there is a small common region of gain in the telomeric region of chromosome 20.

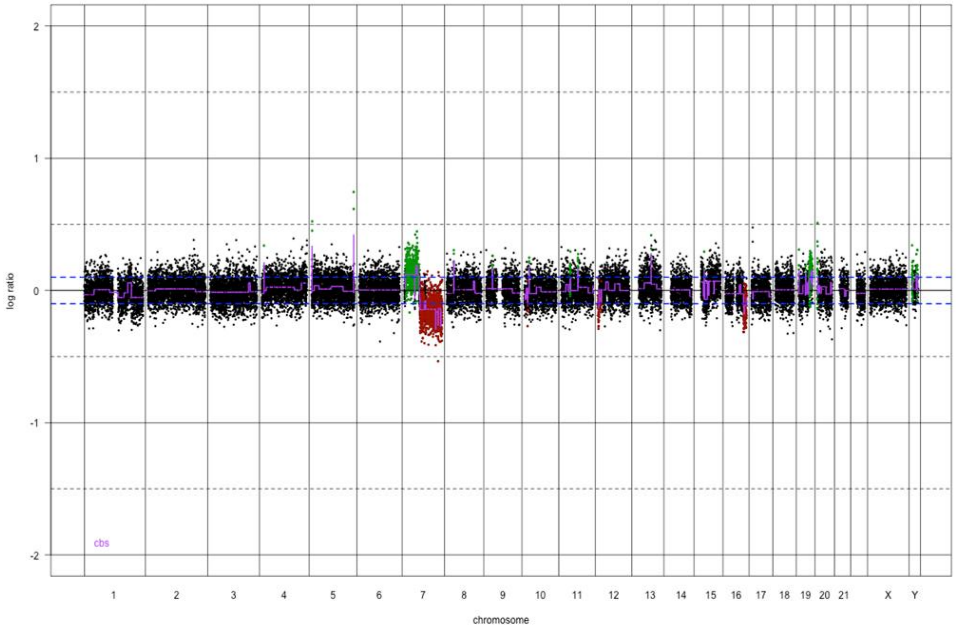


**Figure 5.25 ZR75-1 native vs. 25nM DOCR** This plot charts cbs Log2Ratios of test to reference signal intensity from BAC clones in an aCGH experiment using DNA from pooled female blood as a reference sample and DNA from 25nM DOCR ZR75-1 cells as a test sample. Navy dots represent BAC clones which remain unchanged, the green dots represent the BAC clones in which there is an area of gain on the genome, and the red dots represent the BAC clones in which there is an area of loss of the genome. The Log2ratio is measured on the Y axis and on the X axis the genome runs in chromosome order from 1 to the sex chromosomes. The p or short arm on each chromosome is followed by the q or long arm. The cbs algorithim recursively split chromosomes into segments based on the maximum t statistic estimated by each permutation (re Mathworks.com.)

The data obtained from the ZR75-1 PACR and DOCR plots was then compared and it was observed that there was loss in 7q, 12p and 16q common to both PACR and DOCR samples.

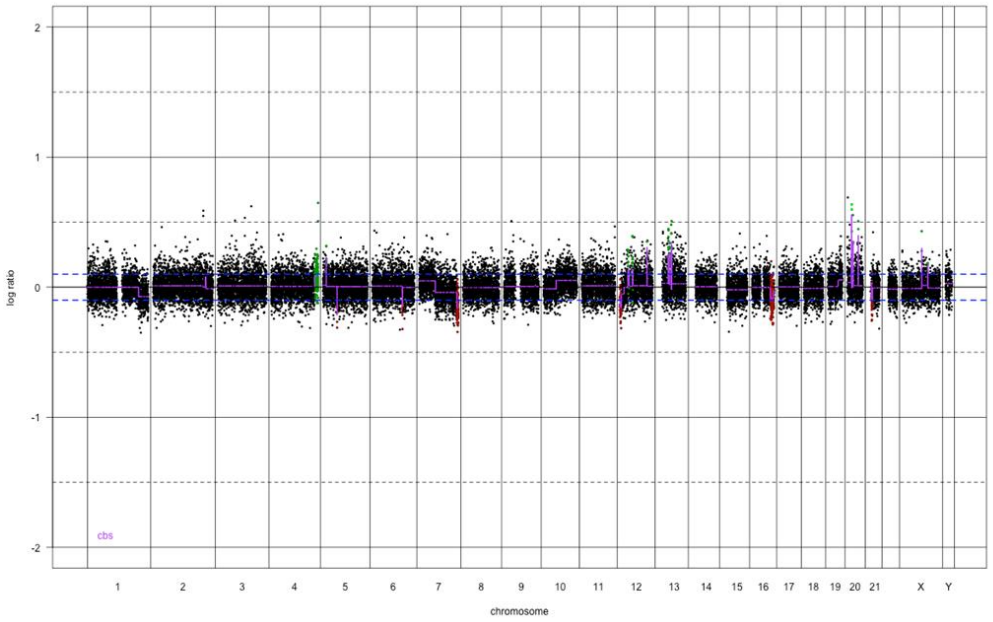


**Figure 5.26. ZR75-1 Native vs. 50nM DOCR** This plot charts cbs Log2Ratios of test to reference signal intensity from BAC clones in an aCGH experiment using DNA from pooled female blood as a reference sample and DNA from 50nM DOCR ZR75-1 cells as a test sample. Navy dots represent BAC clones which remain unchanged, the green dots represent the BAC clones in which there is an area of gain on the genome, and the red dots represent the BAC clones in which there is an area of loss of the genome. The Log2ratio is measured on the Y axis and on the X axis the genome runs in chromosome order from 1 to the sex chromosomes. The p or short arm on each chromosome is followed by the q or long arm. The cbs algorithim recursively split chromosomes into segments based on the maximum t statistic estimated by each permutation (re Mathworks.com.)

**5.1.c. Collating Data from aCGH experiments using taxane resistant cell lines.**

Finally, all the aCGH data was collated, summarised it and constructed table 5.1. The data was then combined from the two set of MDA-MB-231 PACR experiments and identified the areas of interest common to both groups. Both taxane resistant ZR75-1 cell lines were included. Table 5.1 shows the areas of extending loss and gain, and any areas of deletion or amplification.

| Cell line | Extending Loss | Extending Gain | Deletion | Amplification |
|---|---|---|---|---|
| **MDA-MB-231 PACR** | 1p36.13-q44, 6p25.3-q12, 8p, 10p,19q, X Chr. | 2p25.3-23.3, 3p24.3-q13.3, 4p16.1-q12, 5q14.3-q31.1, 8q21.13-24.3, 11q15.1-q25, centromeric 12, and centromeric 14. | 6p21.1 (only in 5 and 25nM PACR.) 2q13, 15q11,2 and 16 q11.2 regions of the 50nM PACR cells. | 6p21.1 25nM PACR cells++. 1q32.3, 4q21.21-21.22, 8p12, 8p11.21, 11q13.2, 12q14.1, 12q14.2, 12q15, 15q11.2 and 15q22.2-q22.3 of 50nM PACR cells+++. |
| **ZR75-1 PACR** | 1q, 3p, 7q*, 10p 12p*, 15p, 16q*. | None | None | None |
| **ZR75-1 DOCR** | 7q**, 12p** and 16q** | None | None | None |

**Table 5.1.** Common area of loss, gain, deletion and amplification in three cell lines: MDA-MB-231 PACR, ZR75-1 PACR and DOCR cell lines at three resistance levels 5nM, 25nM and 50nM when compared to their native line, identified using aCGH.

+ Only in 5 and 25nM PACR MDA-MB-231
++ Only in 25nM PACR MDA-MB-231
+++ only in the 50nM PACR MDA-MB-231
*Regions extend from 5, 25 to 50nM, the others are in the 25 and 50nM alone.
**Regions are common to the ZR75-1 PACR and DOCR cells.

## 5.2. Illumina based expression array profiling of Taxane Resistant Cell lines.

Expression profiling using mRNA from cell lines or whole tumours can provide valuable information on pathways and individual gene which are altered during drug treatment or, in this case during acquisition of drug resistance. Illumina microarrays were selected for these experiments because high quality data and high reproducibility ($r^2$ value = 0.99) is possible due to 50mer probes and 100% array QC. They also require a very low samples input of only 50-100g RNA, have a high yield and are low cost per sample. The same platform could also be used for analysis of both the cell line and the tumour DNA (chapter 6.)

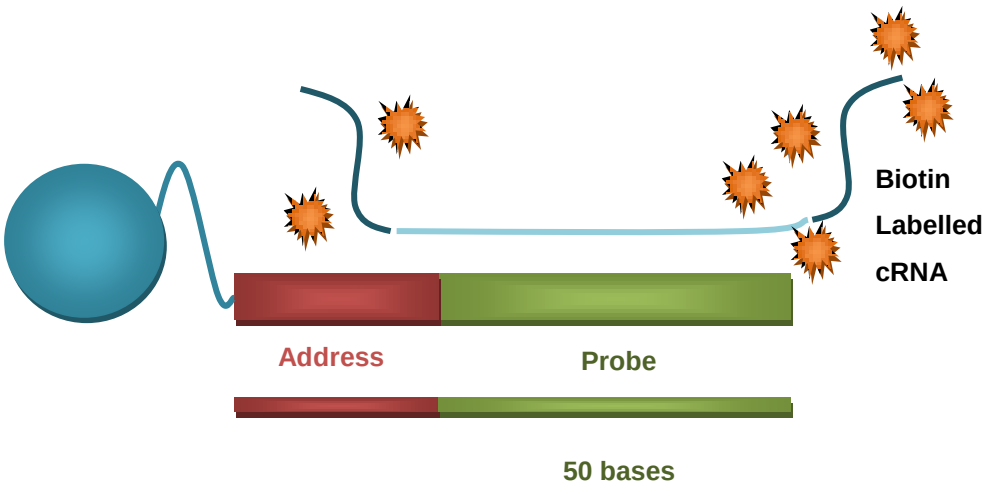


**Figure 5.27.** Direct Hybridisation Assay overview (adapted from http://www.lifesciences.sourcebioscience.com.) A 50 base gene-specific probe linked to short address. This probe is hybridised to labelled nucleic acid derived from total RNA.

The process of the illumina gene expression involves a first and second strand reverse transcription step, followed by a single IVT amplification which incorporates biotin labelled nucleotides. This is followed by array hybridisation, washing, blocking and streptavidin Cy3 binding.

### 5.2a Illumina profiling of paclitaxel resistant MDA-MB-231 cells.

Analysis of the illumina data obtained from the MDA-MB-231 PACR cells began by conducting a simple pairwise comparison between the native cells and each of the resistant cell lines and observing how many genes are dysregulated with increasing resistance to taxane exposure. Methods utilised for these experiments are detailed in section 2.3.a.i-2.3.c.iv RNA was extracted using the qiagen RNeasy kit and amplified using the total prep kit from Ambion. Samples were then run on the human Ref 8 version 2 illumina microarray chips. Figure 5.28 shows the number of genes dysregulated between native and taxane resistant cell lines ($p$ value of $\leq$ 0.001.) When RNA from the 5nM PACR MDA-MB-231 cells was compared to the RNA from the

corresponding native cells 25 genes were dysregulated (re leftmost bar fig 5.28). 225 genes are dysregulated when RNA from the 25nM PACR cells is compared to the RNA from the native cells (central bar fig 5.28). Finally, when comparing RNA from the 100nM PACR cells to the natives, 425 genes were dysregulated (re. rightmost bar 5.28). This shows a significant and stepwise increase in mRNA dysregulation with increasing paclitaxel resistance.

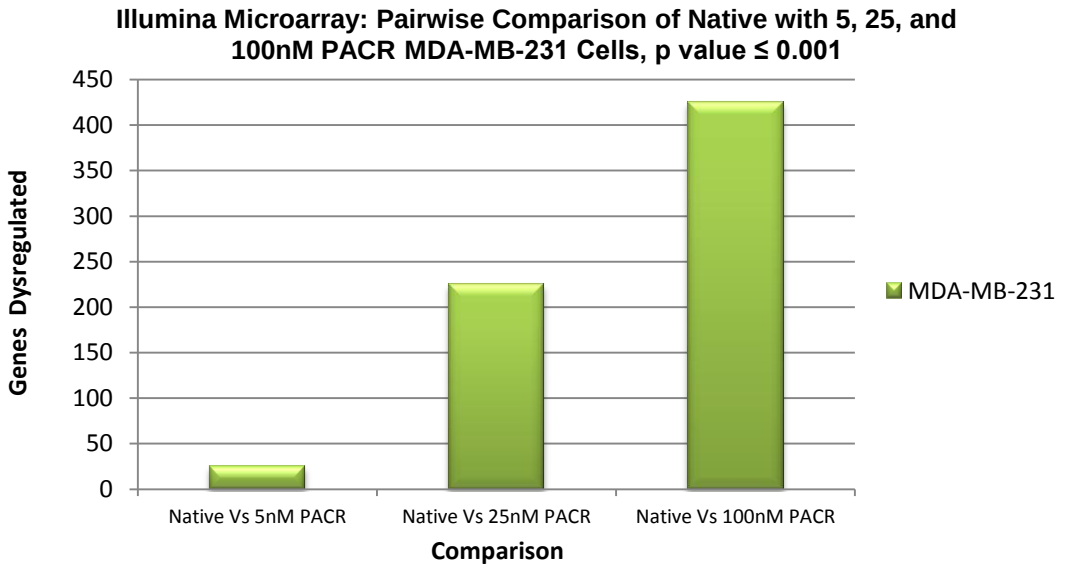


**Figure. 5.28** This figure shows a comparison between RNA taken from each of the Paclitaxel resistant MDA-MB-231 cell lines and RNA taken from their respective native cells. RNA was extracted using the qiagen RNeasy kit and amplified using the total prep kit from Ambion. Samples were then run on the human Ref 8 version two illumina microarray chips.

All the genes that were dysregulated when RNA from each of the paclitaxel resistant cell lines was compared to the native were compiled and constructed into a Venn diagram according to their resistance status (figure 5.29). The red circle contains the genes that are dysregulated in the 5nM PACR cells and not in the native cells. The blue circle encapsulates genes dysregulated in the 25nM PACR cells and not in the natives. Finally, the green circle contains genes that are dysregulated in the 100nM PACR cells and not in the natives.

There are 4 genes that are solely dysregulated in the 5nM PACR cells and not the natives. 7 genes are dysregulated in both the 5nM and 25nM PACR cells and not the natives. 91 genes are dysregulated solely in the 25nM PACR group and not in the natives. 109 genes are dysregulated in both the 25nM and 100nM PACR compared to the native cells. There are 287 genes that are dysregulated only in the 100nM and not the natives. Reassuringly there is only one gene that is commonly dysregulated in the 5nM and the 100nM PACR cells and not in the native cells. It is important to consider that there are 91 genes that are dysregulated in the 25nM PACR cell line

that are not dysregulated in the 5nM and 100nM PACR cell lines which suggests that these genes are not related to taxane resistance mechanisms.

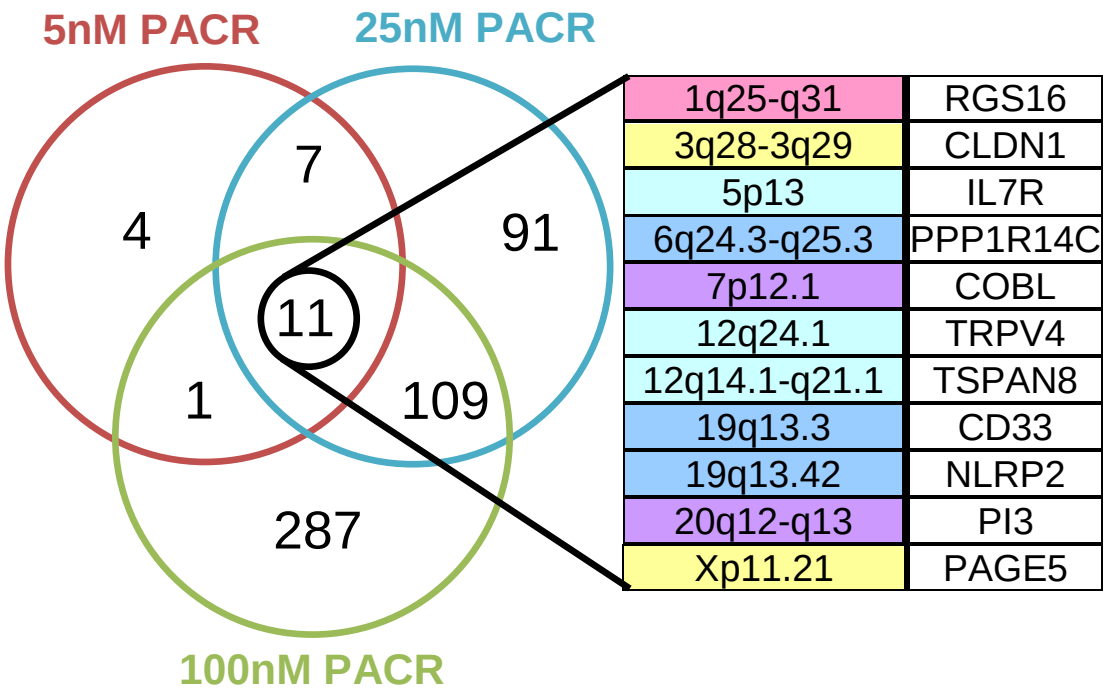


**Figure 5.29.** This Venn diagram consists of three overlapping circles encapsulating each of the 425 genes dysregulated in the paclitaxel resistant MDA-MB-231 cells and not their native sensitive line from which they originated.

The Venn diagram shows an increase in the number of dyregulated genes that are shared across "neighbouring" resistance groups and not in the natives. Across all three resistance groups there are a total of eleven genes dysregulated compared to the native cells. These eleven genes and their cytogenetic locations are detailed in the two columns on the right hand side of figure. The expression level of these eleven genes has also been expressed as individual line graphs created using the illumina Gui programme[226]. These graphs are shown in figure 5.30.

**5.2ai Genes dyregulated in all paclitaxel resistant MDA-MB-231 cell lines when compared to the native line: candidates for identification of mechanisms of resistance.**

11 genes were identified as candidates for promoting paclitaxel resistance based on the analysis described above.

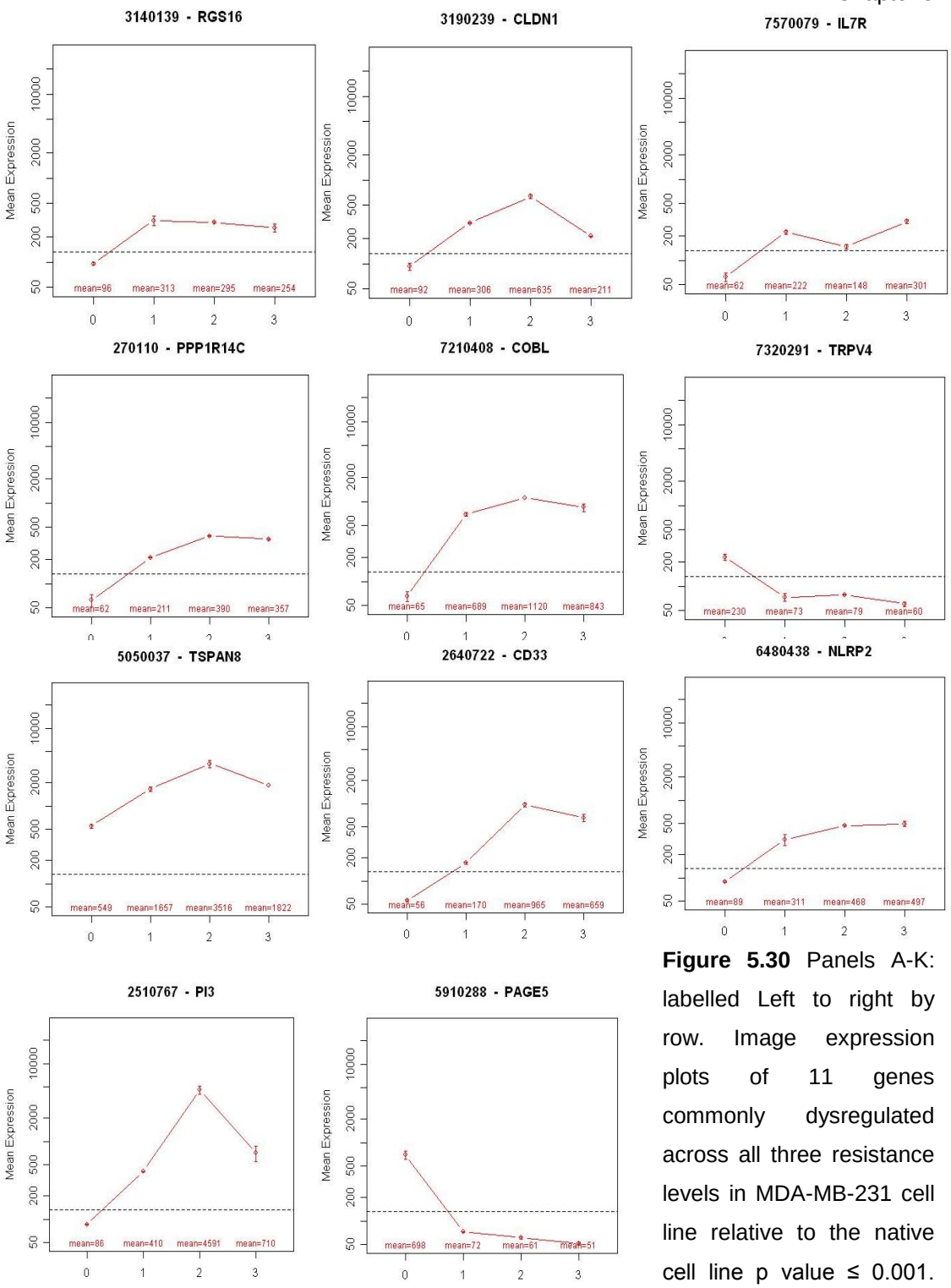


**Figure 5.30** Panels A-K: labelled Left to right by row. Image expression plots of 11 genes commonly dysregulated across all three resistance levels in MDA-MB-231 cell line relative to the native cell line p value ≤ 0.001. The Y axis is a logarithmic scale of the mean expression of each gene. The X axis from 0 – 3 designates the native, 5nM, 25nM and 100nM PACR samples respectively in duplicate. On row one A-C left to right, **RGS16**, **CLDN1** and **IL7R**. On row two D-F left to right are the plots for, **PPP1R14C**, **COBL** and **TRPV4**. On row three G-I left to right are the plots for, **TSPAN8, CD33** and **NLRP2**. On the fourth row J-K are plots for **PI3** and **PAGE5**.

The *RGS* family, comprising 22 homologues of proteins, plays a role in cellular proliferation, differentiation, membrane trafficking, and embryonic development through the involvement of the mitogen-activated protein kinase signalling pathway[227] RGS16 or retinally abundant regulator of G protein signalling has been identified as a prognostic marker in colorectal cancer. Patients expressing high levels of RGS16 had and a worse overall survival rate than low expressers. Previous studies have shown that a number of breast cancers have mutations in RGS16 and that shRNA-mediated extinction of RGS16 augmented cell growth. In addition they found that loss of RGS16 in some breast tumours has been shown to enhance PI3K signalling elicited by growth factors and thereby to promote proliferation and TKI evasion downstream of HER activation[228].

In Panel A figure 5.30 it can be seen that expression of RGS16 increases with increased degree of paclitaxel resistance in the MDA-MB-231 cells. The RGS16 gene has TP53 binding sites located in intron 3 and the 3' UTR, and the TP53 tumor suppressor induces RGS16 transcription[229]. MDA-MB-231 native cells have high levels of mutant p53. It would be pertinent to consider how the p53 status might change with increasing paclitaxel resistance in the MDA-MB-231 cells. However, in reference to this data, the picture seems unclear when considering the breast cancer data, perhaps in future studies it would be pertinent to look at the RGS16 mutation status. In one study the promoter region of RGS16 was found to be methylated in 10% of the tumours investigated[229]. There are plans to run DNA from each of these cell lines on illumina methylation chips in the future.

CLDN1 expression is increased in PACR cell lines (2-6 fold above controls) compared to the native cell lines although the highest level of resistance the expression of CLDN1 fell relative to 25nM PACR cells (re figure 5.30, panel B.) One study found that claudins 1 and 4 were significantly higher in the basal-like breast tumour subtype of breast cancers (ER-ve, Her-2-ve, EGFR+ve, CK5/6+ve)[230]. MDA-MB-231s are thought to represent this tumour type[199]. This poses a question – does the "basalness" of the MDA-MB-231 cells change with paclitaxel resistance? Ultimately, the lack of consistency in the pattern of gene expression as paclitaxel resistance increases in the MDA-MB-231 cells suggests that it may not be the most promising member of the eleven commonly dysregulated genes, however, this data has been validated using qPCR, the details of which are noted later in this section.

IL7R, (interleukin 7 receptor) expression increases as paclitaxel resistance increases but there is a slight dip in expression level at the 25nM PACR level, previously designated as the most clinically relevant (re figure 5.30 panel C.) In addition, although there is data to suggest a link between IL7R and other cancers there is very little data linking it specifically to breast cancer. This pattern of expression and lack of data relevant to cancer and drug resistance mechanisms

suggests that this gene might be slightly less interesting to investigate further, however, it has been validated it using qPCR further on in this section.

PPP1R14C also know as KEPI shows a progressive and consistent increase in gene expression level as paclitaxel resistance increases in the MDA-MB-231 paclitaxel resistant cell lines (re figure 5.30 second panel D.) KEPI is a protein kinase C-potentiated inhibitory protein for type 1 Ser/Thr protein phosphatases, there is very little data published regarding this protein and very little in relation to breast cancer[310]. Published data investigating the expression levels of KEPI showed very little or no gene or protein expression of KEPI in a panel of cell lines including MDA-MB-231 cell lines and KEPI has been implicated in regulating the EGR1 tumour suppressor via MEK-ERK MAPK pathway activation[231].

COBL or Cordon bleu protein increases steadily as paclitaxel resistance increases (figure 5.30 2nd line Panel E.) Although the function of this protein is at present unknown, studies in renal cell carcinoma have shown that it is regulated by the tissue specific transcription factor HNF4α[232, 311, 317]. This was shown by generating HEK293 cells which conditionally expressed wt or mutant HNF4α and observing any genes that were upregulated as a consequence. HNF4α has also been shown to regulate the activity of CYP450[233].

Cytochrome p450s are enzymes known to be involved in taxane metabolism. The sometimes erratic and unpredictable pharmacokinetic behaviour of docetaxel can limit its use[234]. This is because there is a substantial variability in pharmacokinetic behaviour between different individuals; even in patients with normal hepatic function, drug clearance can vary by up to ten fold[235]. It has been shown that decreasing docetaxel clearance can increase the chances of patients suffering from grade 4 neutropenia by over fourfold[236]. In patients with NSCLC it has been demonstrated that docetaxel exposure can predict tumour time to progression (TTP)[237]. This unpredictable nature can limit the use of docetaxel and one theory suggests that this occurs as a result of the drug's dependence on cytochrome P450 3A4 (CYP3A4)–mediated metabolism for inactivation[233]. In addition the cytochrome p450 member CYP1B1 has been shown to be increased in expression level in the paclitaxel resistant MDA-MB-231 cell lines (re figure. 5.31, panel D.) Marsh and colleagues looked at a series of polymorphisms in genes associated with the transport and metabolism of paclitaxel and found that patients homozygous for the CYP1B1*3 allele had a significantly increased PFS ($p$=0.037) compared to those with a minimum of one valine allele. The authors postulated that this may reflect altered paclitaxel metabolism although the effect was found to be independent of paclitaxel clearance. However, it is important to point out that this study was carried out on a relatively small cohort of patients (only 93) and that patients were additionally treated with doxorubicin and cyclophosphamide. The authors also highlighted the role of CYP1B1 in oestrogen metabolism and suggested that this relationship

may partly influence the chance of developing paclitaxel resistant or invasive breast cancer in patients carrying the CYP1B1*3 allele.

Subsequently, members of the same group went on to investigate a similar panel of polymorphisms in a group of genes identified as playing a potential role in paclitaxel resistance. They observed a much larger group of patients (914) but this time looked at ovarian tumours and found no clear association with outcome and toxicity with the CYP1B1 genotypes studied[238].

The association between CYP1B1 expression and paclitaxel remains unclear, yet intriguing. This may warrant further investigation, particularly into unknown factors such as oestrogen expression that may by modulated by CYP1B1 expression and may consequently effect paclitaxel sensitivity.

The expression of TRPV4 is reduced in the paclitaxel resistant MDA-MB-231 cells when compared to the native cell line (re figure 5.30 Panel F.) The TRPV4 protein is a $Ca^{2+}$ permeable, non-selective cation channel which is thought to play a role in regulating systemic osmotic pressure and is regulated by a calmodulin-dependent negative feedback mechanism[239]. TRPV4 can be activated by changes in heat, pH, protons, lipids, citrate and phorbol esters and has been shown to be associated with mechanical hyperalgesia induced by paclitaxel[239]. This seems to suggest that this increase in TRPV4 may occur as a result of treatment with paclitaxel rather than to be indicative of paclitaxel resistance *per se*.

TSPAN8 is increasingly expressed in paclitaxel resistant MDA-MB-231 cell lines, however at the highest level of resistance the expression is slightly lower (figure 5.30 third line, panel G.) The tetraspanin family member TSPAN13 also shows a similar pattern to TSPAN8 in terms of increasing expression level with increasing paclitaxel resistance in MDA-MB-231 cells (Re. Fig 5.31 panel K.) These TSPANS are cell surface proteins which are involved in growth, motility, cell development and activation. Interestingly, TSPAN13 (also known as NET-6) has been recently identified as a potential tumour suppressor gene. In a paper by Huang *et al* they identified that the MDA-MB-231 cell line expressed TSPAN13 at a particularly low level. They transfected a GFP-TSPAN13 construct into MDA-MB-231 cells and observed the resulting phenotypic changes[223]. Cells with transfected TSPAN13 had elevated antiproliferative activity *in vitro* and *in vivo*, due to increased apoptosis and exibited reduced anchorage, independent growth and invasion[223]. Although this does not seem to directly influence taxane resistance mechanisms, it does suggest that these paclitaxel resistant MDA-MB-231 cell lines may have these same phenotypic changes as a result of increased TSPAN13 expression. This may be of particular interest when considering the xenograft experiments.

CD33 is a transmembrane receptor expressed on cell of myeloid lineage or on some lymphoid cells[240]. The expression of CD33 increases with increasing paclitaxel resistance (re. Figure 5.30 panel H.) CD33 plays a role in the immune response and there is a slightly inconsistent pattern of increasing expression with increasing paclitaxel resistance however it may be another intriguing potential biomarker of resistance.

NLRP2 expression consistently increased with increasing paclitaxel resistance (re. Figure 5.30 Panel I.) There is very little data surrounding the function of NLRP2 protein although it has been associated with the activation of CASP1 and toll-like receptors[241]. This association with these aspects of the inflammasome and the lack of any previously published data suggesting any association of NLRP2 with drug resistance mechanisms implies that this protein may be a novel candidate as a biomarker of taxane resistance.

PI3 (also known as elafin) is found consistently expressed in normal mammary epithelial tissue, but is usually down-regulated in most breast cell lines[242]. In the cell lines used in these experiments PI3 expression increases with paclitaxel resistance at the low levels of resistance: 5 and 25nM PACR and then falls again dramatically at the highest resistance level of 50nM PACR but remains 8-10 fold higher in the native (re figure 5.30 panel J.) This lack of consistency in the progression of increasing expression with increasing paclitaxel resistance suggests that PI3 is perhaps a less likely appropriate candidate for a biomarker of taxane resistance than some other, yet this pattern is intriguing enough to warrant further research.

Expression of PAGE 5 is much higher in the native MDA-MB-231 cell line than in the 5, 25, and 50nM PACR cell line and it shows a progressive and consistent reduction in expression as paclitaxel resistance increases (re figure 5.31 panel K.) This pattern would suggest that PAGE5 could possibly be a biomarker of taxane sensitivity rather than resistance. Very little is known about PAGE-5, it is a member of the GAGE family which has shown to be expressed in a number of tumours and in foetal and reproductive tissues (re gene cards.)

We looked at the group of genes that were dysregulated at all three resistance levels when compared to the native cell line ($p$ value $\leq 0.001$.) In addition the genes which showed a consistent progression in increasing or decreasing expression with paclitaxel resistance with a $p$ value $\leq 0.001$ in one or more resistance level and a $p$ value$\leq 0.005$ for the other resistance levels were investigated. Image expression plots of these genes are detailed in figure 5.4. The genes illustrated in figures 5.30 and 5.31 were selected for further investigation using quantitative PCR which is detailed in section 5.3.

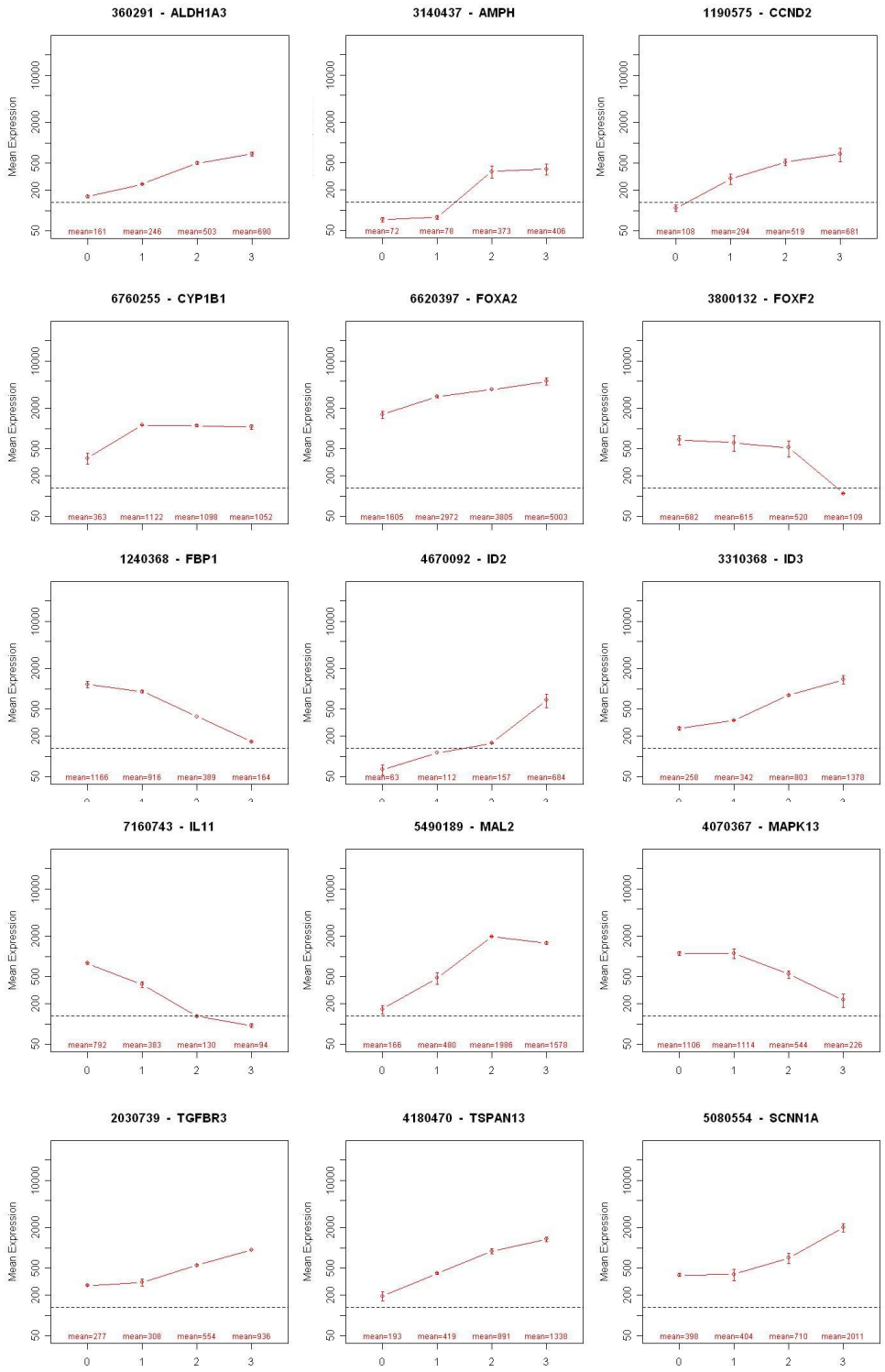


**Figure 5.31** Image expression plots of select genes commonly dysregulated across all three resistance levels in MDA-MB-231 cells relative to their native cell lines. In this instance the p value at one or more of the resistance levels is ≤ 0.001 and at ≤ 0.005 in the other samples. The Y axis is a logarithmic scale of the mean expression of each gene. The X axis from 0-3 designates the native, 5nM, 25nM and 100nM PACR samples respectively, in duplicate. Labelled Panels A – O Left to right by row.

**5.2.a.ii MDA-MB-231 PACR heat maps generated from illumina data.**

The data generated from the illumina experiments was used to create heat maps using the DAVID online tool. They were constructed from genes dysregulated between native and taxane resistant cell lines with a *p* value of ≤ 0.001. The left hand panel of figure 5.32 shows the entirety of the heat maps generated from the illumina data which can be used as a reference. The other four panels on this figure show genes with highest expression levels in the native and low level resistance cell lines that reduce in expression as paclitaxel resistance increases.

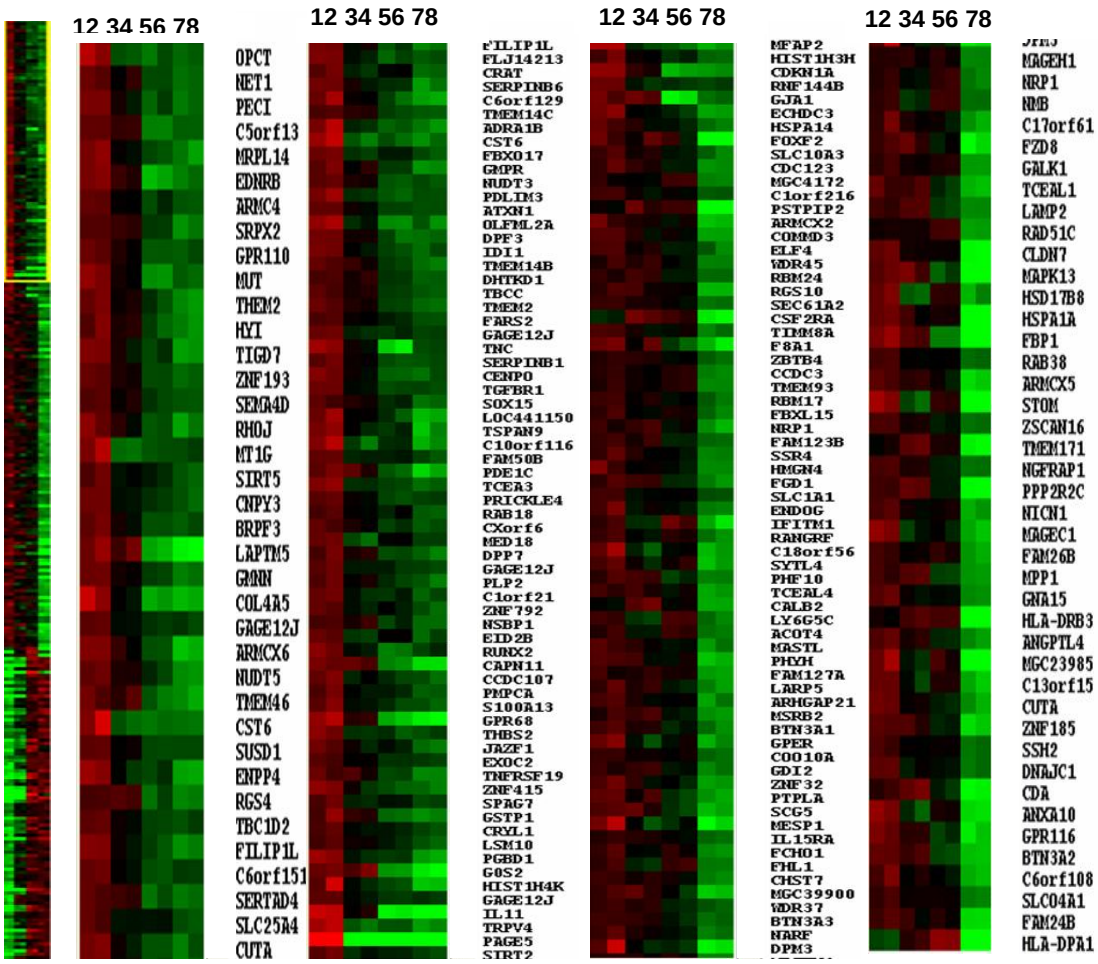


**Figure 5.32** Heat map on the left shows the entire heat map as a reference. The 4 larger heatmaps represent part of the total heat map showing genes that go down in expression with increasing paclitaxel resistance using the native samples as a reference. Along the top edges numbered 1 to 8, sample 1 and 2 are the native cells, sample 3 and 4 are the 5nM PACR cells, sample 5 and 6 are the 25nM PACR cells and sample 7 and 8 are the 100nM PACR MDA-MB-231 cells. On the RHS of each heatmap are listed the gene names. Red boxes represent genes with high gene expression levels and green boxes represent genes with low gene expression levels.

Figure 5.33 illustrates the other part of the heat map that shows genes with lowest expression levels in the native and low level resistance cell lines that increase in expression as paclitaxel resistance increases.

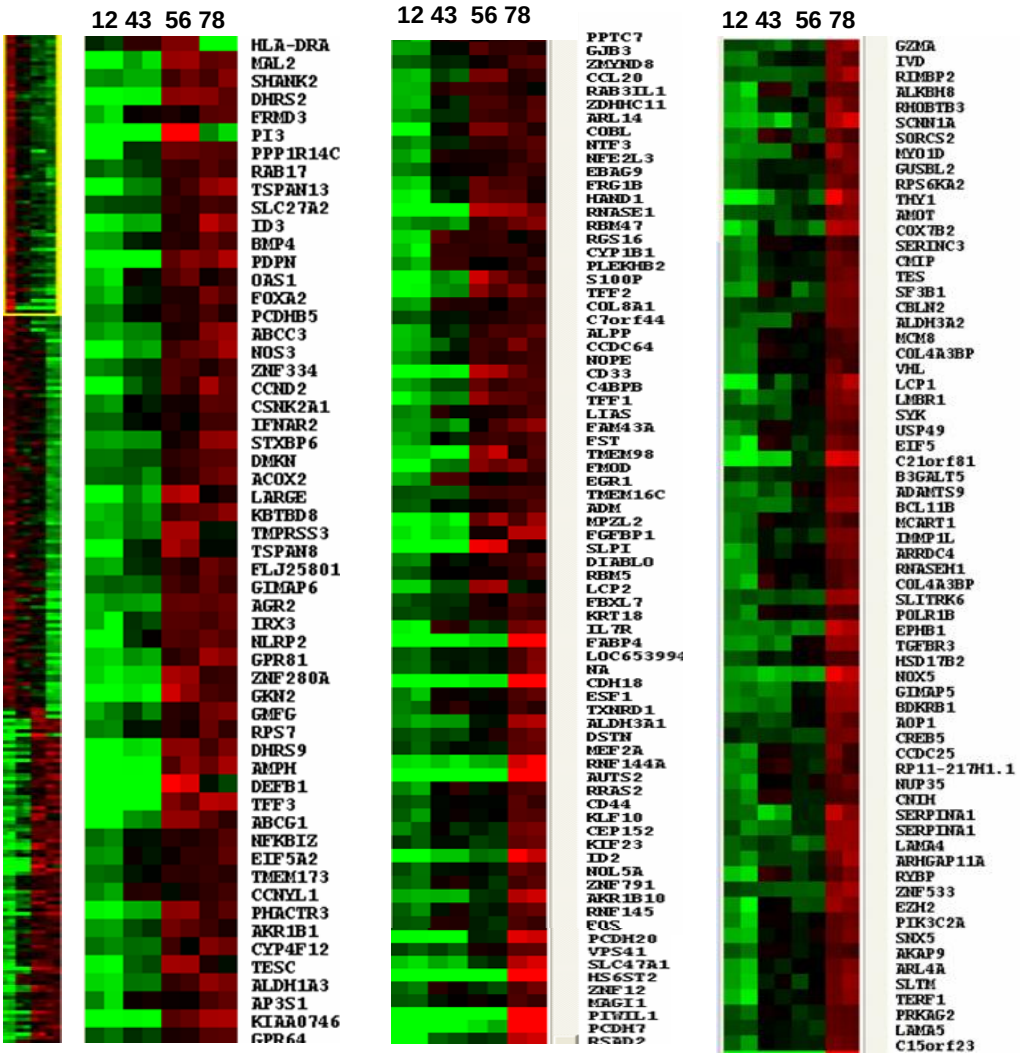


**Figure 5.33**. Heat map on the left shows the entire heat map as a reference. The 4 larger heatmaps represent part of the total heat map showing genes that go up in expression with increasing paclitaxel resistance using the native samples as a reference. Along the top edges numbered 1 to 8, sample 1 and 2 are the native cells, sample 3 and 4 are the 5nM PACR cells, sample 5 and 6 are the 25nM PACR cells and sample 7 and 8 are the 100nM PACR MDA-MB-231 cells. On the RHS of each heatmap are listed the gene names. Red boxes represent genes with high gene expression levels and green boxes represent genes with low gene expression levels.

## 5.3. Analysis of taxane resistant cell lines using quantitative real time PCR.

A quantitative analysis was conducted of selected genes that were identified in the genome wide transcriptomic screen using qPCR to investigate how the expression levels of these gene changes with increasing paclitaxel resistance and to confirm expression patterns identified using illumina arrays.

One group of 11 genes was identified that were dyregulated in all 3 of the PACR MDA-MB-231 cell lines when compared to the native line (*p* value ≤ 0.01 re figure 5.30.)

A further 15 genes which were dysregulated in all three PACR MDA-MB-231 cell lines with at least one of the cell lines having a p value ≤ 0.00.1 and the rest with a p value ≤ 0.005 were also identified. These genes were selected on the basis that they showed a consistent pattern of progressive increase or decrease in expression with increasing taxane resistance.

Finally a further four genes were selected by conducting a comprehensive literature search as well as well as a comparison of the transcriptomic and genomic data.

The gene Aurora Kinase A was included as it is located in a region of gain in the highest resistance levels in the MDA-MB-231 100nM PACR cells and also showed higher expression in only the MDA-MB-231 100nM PACR cells on the illumina array (*p value* = 0.005.) Aurora Kinase A has been shown to be involved in tumour development and progression and overexpression is estimated to occur in 12 and 62% of breast and colon cancers[159]. It is involved in centrosome function, spindle assembly, MT formation and stablilisation[243].

MDR1 (ABCB1) gene was included as it is an important factor to consider when looking at drug resistance. MDR-1 encodes p-glycoprotein which increases drug efflux out of a cell leading to drug resistance by reducing the intracellular levels of the drug. Paclitaxel is a known substrate of p-gyp and binds to it, activating one of the ATP binding domains and causing a conformational change in p-gyp which leads to drug being released into the intracellular space[149,244,245].

The third gene identified was Stathmin which is involved in the regulation of microtubules and is often expressed in cell lines with mutant p53 that have decreased binding of paclitaxel[147]. RNA interference of stathmin has been shown to induce polymerisation of microtubules and resensitise paclitaxel resistant cells[246]. In the cell lines generated in these experiment the resistant line had reduced gene expression compared to the native lines and it was located in an area of loss in the resistant lines (1p36.11.)

The fourth and final gene belonging to this group is the transcription factor YY1 which plays a role in taxane response in epithelial ovarian cancer[247]. Knockdown of YY1 resulted in increased taxane resistance. The cell line transcriptomic data showed increased YY1 expression at the highest resistance level in the MDA-MB-231 cells and increased expression of RYBP a protein that binds YY1 in all three paclitaxel resistant MDA-MB-231 cell lines compared to the native cells.

For the purposes of the qPCR experiments to validate the chosen panel of genes from the transcriptomic and genomic experiments, cell lines were grown up as described in section in 2.3.f.iii. RNA was extracted and quantified according to 2.1.a.i and 2.1.a.ii and the qPCR was carried out according to section 2.3.d.i.

### 5.3.a. qPCR analysis of MDA-MB-231 cell lines.

Figure 5.34 shows a heat map of qPCR data using the MDA-MB-231 PACR cell lines. Each cell line is listed down the left hand side of the heatmap, MDA-MB-231 Native cells are listed as 231 Native, and the 5nM, 25nM and 50nM PACR MDA-MB-231 cells are listed as 231 PACR1, 231 PACR 2 and 231 PACR 3 respectively. The data is normalised to the native cell line. High expression is shown by the bright red boxes, unchanged expression is shown by the black boxes and low expression is shown in green and the white boxes represent samples that failed the run with that particular primer.

The heat map shows increased expression of the following genes in the higher resistance levels: SCN11A, FOXA2, TGFBR3, CCND2, ID3, MAL2, NLRP2, PPP1R14C, RGS16, TSPAN13, CD33, ID2, PI3, TSPAN8, ALDH1A3 and AMPH. Levels of MDR1 seem to increase at the low level of resistance, reduce again at the middle level of resistance and then increase again at the highest level of resistance. The following genes have high expression in the native and 5nM PACR cells and lower expression in the 25nM and 50nM PACR cells: IL7R, AURKA, IL11, MAPK13, FOXF2, COBL and FBP1.

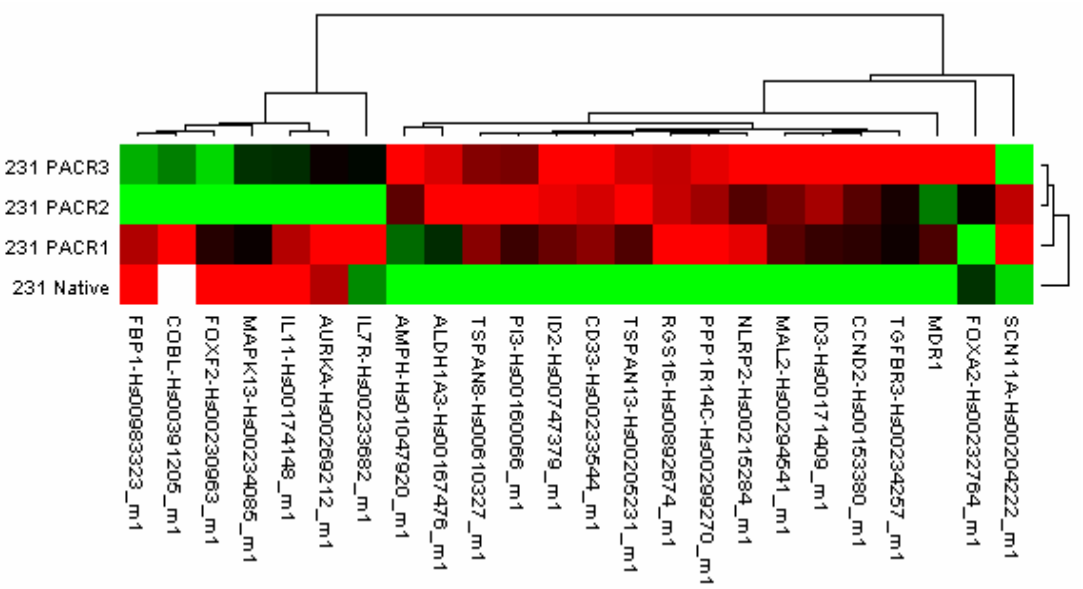


**Figure 5.34** Heat maps of gene expression levels in a select panel of genes detected with qPCR using RNA extracted from MDA-MB-231 native and PACR cell lines. Native cells lines are used as a control to compare the gene expression levels of the PACR cell lines. Green boxes denote samples where expression levels are low and the red boxes denote samples where expression levels are high. The black boxes denote samples where the expression level is unchanged. 231 PACR1 samples denote the samples from 5nM PACR MDA-MB-231 cell line RNA. The 231 PACR2 samples denote the samples from 25nM PACR MDA-MB-231 cell line RNA. The 231 PACR3 samples denote the samples from 50nM PACR MDA-MB-231 cell line RNA.

The heat map is valuable however, to dissect this data further, the qPCR data was constructed into a bar chart (figure 5.35.) Figure 5.35 shows the log10 of RQ value (relative quantity) of expression of each gene investigated in the qPCR experiment using the MDA-MB-231 native and PACR samples (in quadruplicate.) The data is normalised to the native samples (RQ value = 1 and the log10 of 1 is 0.) There are error bars added to each data point, the error bars are calculated from the maximum and minimum RQ values. Each of the genes is listed along the x axis. Missing bars on the graph represent the primers that failed after repeated runs. The 5nM PACR samples are represented by the dark green bar, the 25nM PACR samples are represented by the mid green bar and the 50nM PACR samples are represented by the light green bar.

The following genes have reduced expression in the PACR samples compared to the native cell line: AURKA, FBP1, FOXF2, IL11, MAPK13. FOXA2 shows very little deviation in expression compared to the native cell line. The following genes show increased expression in the PACR cell line compared to the native: ALDH1A3, AMPH, CCND2, CD33, ID2, ID3, MAL2, MDR1, NLRP2, PI3, PPP1R14C, RGS16, SCN11A, TGFBR3, TSPAN13 and TSPAN8. Of the genes that have

increased expression in the PACR compared to the native cells, the genes that increase with increasing paclitaxel resistance or achieve a "plateau" of consistent expression in the PACR compared to the native cell are as follows: ALDH1A3, AMPH, CCND2, CD33, ID2, ID3, MAL2, NLRP2, PPP1R14C, RGS16, TGFBR3, TSPAN8 and TSPAN13.

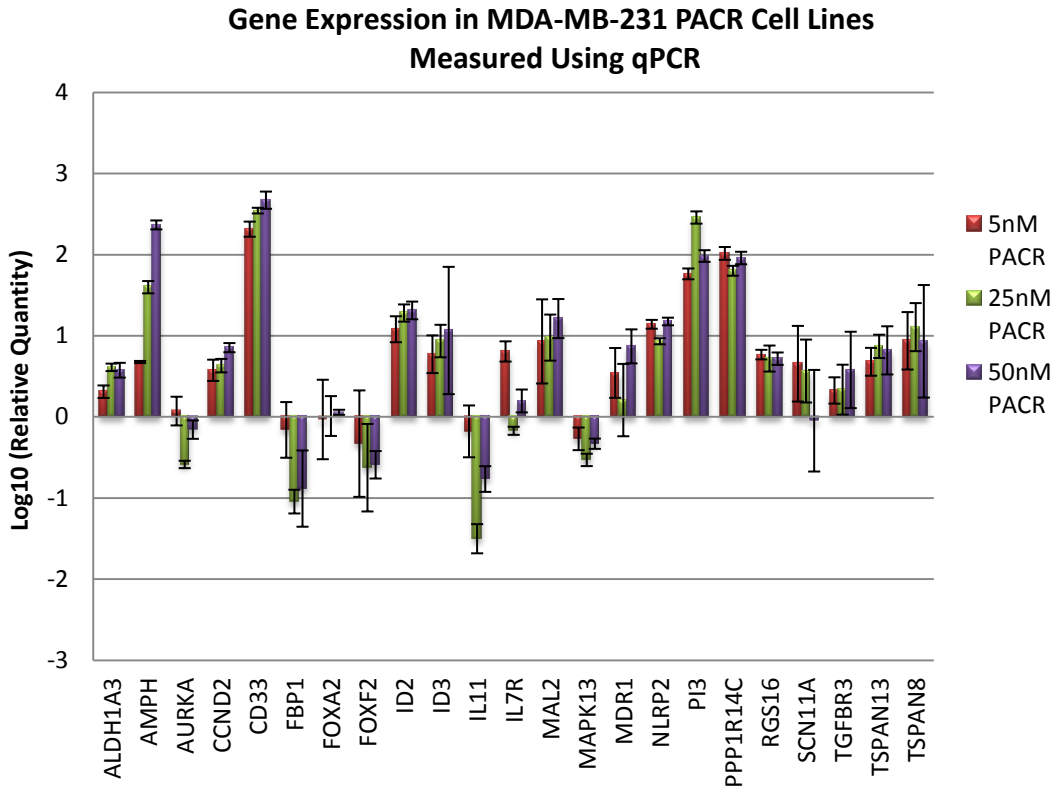


**Figure 5.35** Gene expression levels of paclitaxel resistant MDA-MB-231 cell lines measured by qPCR. The X axis lists each gene alphabetically. The Y axis lists the Relative Quantity of expression to Log10. Each expression level of the PACR cell lines is normalised to the expression in the native cell lines – the relative quantity in the native cells is 1 and so is 0 at log10. The darkest green bar represents the expression level of the 5nM PACR cell lines, the mid green bar represents the expression level of the 25nM PACR cell lines and the lightest green bars represent the expression level of the 50nM PACR cell lines. The error bars represent the maximum and minimum RQ values of the expression levels of each gene.

The taxanes have been shown to be particularly effective in the ER negative population of patients and ER negative cell lines are more sensitive to paclitaxel than ER positive ones[248]. One study by Tabuchi *et al* suggested that ER status influenced chemosensitivity to paclitaxel via regulation of members of the Bcl-2 family[248]. It therefore seems pertinent to investigate ER status in the panel of taxane resistant cell lines. These qPCR experiments were conducted in separate runs to the main qPCR experiments so the data is presented separately.

Firstly, ER expression was measured in the MDA-MB-231 Native, 5nM, 25nM and 50nM PACR cell lines (re green bars figure 5.36.) Figure 5.36 shows the fold change in expression of the PACR MDA-MB-231 cell lines when normalised to a native background. Even though the expression of ER in the 5nM PACR cell line is still low, expression of ER in the 25nM PACR cells is double that of the native cells and in the 50nM PACR cells it is 5 times that of the native cells.

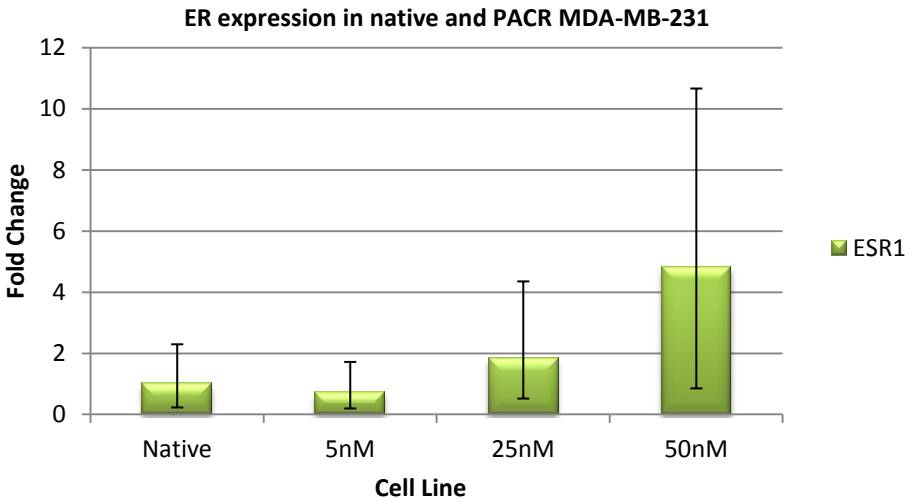


**Fig 5.36.** The Y axis measures the Fold change in ER expression level. The X axis shows each of the MDA-MB-231 cell lines: Native, 5nM, 25nM and 50nM PACR. Error bars are min and max RQ value.

### 5.3.b. qPCR analysis of ZR75-1 cell lines.

The same series of experiments was then performed on the ZR75-1 PACR and DOCR cell lines. Figure 5.37 shows a heat map of the combined qPCR data of the ZR75-1 PACR and DOCR cell lines. Each cell line is listed down the left hand side of the heatmap, ZR75-1 Native cells are listed as ZR75-1 Native, and the 5nM, 25nM and 50nM PACR and DOCR ZR75-1 cells are listed as ZR75-1 PACR1/DOCR1, ZR75-1 PACR2/DOCR 2 and ZR75-1 PACR3/DOCR 3 respectively.

As with previous experiments the data is normalised to the native cell line, high expression is shown by the bright red boxes, unchanged expression is shown by the black boxes and low expression is shown in green and the white boxes represent samples that failed the run with that particular primer, even after repeat runs. The clustering in this heatmap shows a less clear separation than is shown in the MDA-MB-231 heat map and 11 of the data points are missing. It is especially difficult to interpret this heat map as the cell lines listed down the left hand side are not listed in order of increasing taxane resistance. This is because the data will be skewed by any genes that do not increase or decrease consistently with increasing taxane expression, i.e. the majority of genes in this case.

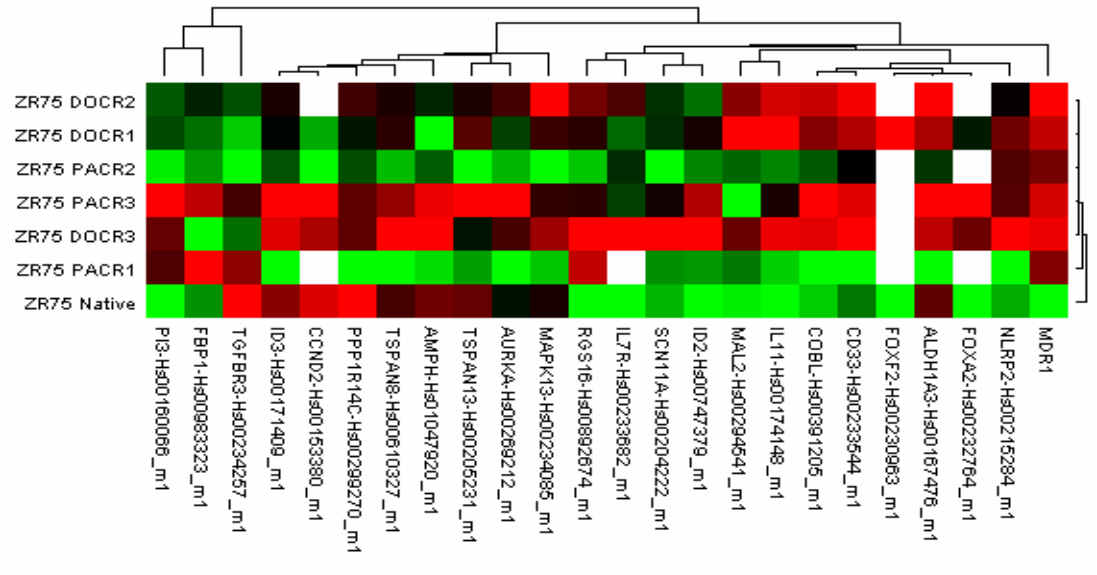


**Figure 5.37** Heat maps of gene expression levels in a select panel of genes detected with qPCR using RNA extracted from ZR75-1 Native, PACR and DOCR cell lines. Native cells lines are used as a control to compare the gene expression levels of the PACR and DOCR cell lines. Green boxes denote samples where expression levels are low and the red boxes denote samples where expression levels are high. The black boxes denote samples where the expression level is unchanged.

**5.3.b.ii qPCR analysis of ZR75-1 PACR cell lines.**

This data was then constructed into a bar graph to dissect the progression of gene expression in each gene in the ZR75-1 PACR cells (figure 5.38.) Figure 5.38 which again shows the log10 of RQ value (relative quantity) of expression of each gene investigated in the qPCR experiment using the ZR75-1 native and PACR samples (in quadruplicate.) The data is normalised to the native samples (RQ value = 1 and the log10 of 1 is 0.) Each of the genes is listed along the x axis. Missing bars on the graph represent the primers that failed after repeated runs. There are error bars added to each data point, the error bars are calculated from the maximum and minimum RQ values. The error bars are much larger for the ZR75-1 native and PACR cell lines than the MDA-MB-231 native and PACR, and more of the primers failed with the ZR75-1 PACR samples than with the MDA-MB-231 PACR samples. The 5nM PACR samples are represented by the blue bar, the 25nM PACR samples are represented by the red bar and the 50nM PACR samples are represented by the green bar. The most consistent pattern shown in the ZR75-1 PACR cell lines is the increased expression of MDR1 in the native. There is also increased expression of ID2. However, it is important to point out that there are large error bars for a number of the samples and a number of the primers failed for certain cell lines.

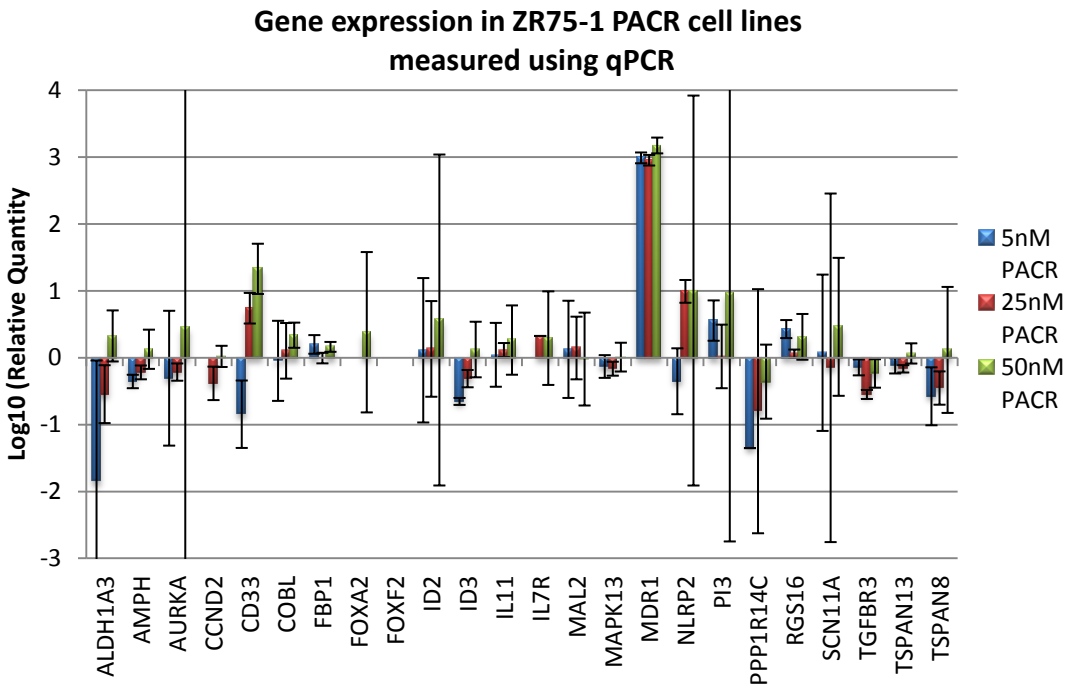


**Figure 5.38** Gene expression levels of paclitaxel resistant ZR75-1 cell lines measured by qPCR. The X axis lists each gene alphabetically. The Y axis lists the Relative Quantity of expression to Log10. Each expression level of the PACR cell lines is normalised to the expression in the native cell lines – the relative quantity in the native cells is 1 and so is 0 at log10. The blue bar represents the expression level of the 5nM PACR cell lines, the red bar represents the expression level of the 25nM PACR cell lines and the green bars represent the expression level of the 50nM PACR cell lines. Error bars represent maximum and minimum RQ values of the expression levels of each gene.

ER expression was then measured in the ZR75-1 PACR and DOCR cell lines. The turquoise bars shown in figure 5.39 show the fold change in expression of ER in the native, 5, 25, and 50nM PACR cell lines. There is very little change in ER expression with increasing paclitaxel resistance in the ZR75-1 cells and there is no consistent pattern of increased or decreased expression with increasing resistance.

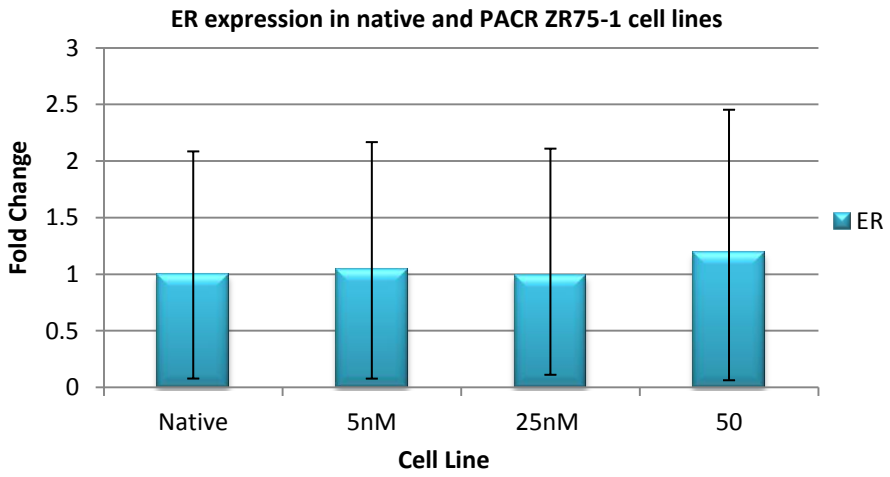


**Fig 5.39.** The Y axis measures the Fold change in ER expression level. The X axis shows each of the ZR75-1 cell lines: Native, 5nM, 25nM and 50nM PACR. Error bars are min and max RQ value.

### 5.3.b.ii qPCR analysis of ZR75-1 DOCR cell lines.

The ZR75-1 DOCR data was then constructed into a bar graph to dissect the progression of gene expression in each gene in the ZR75-1 DOCR cells (figure 5.40.) Figure 5.40 again shows the log10 of RQ value (relative quantity) of expression of each gene investigated in the qPCR experiment using the ZR75-1 native and DOCR samples (in quadruplicate.) The data is normalised to the native samples (RQ value = 1 and the log10 of 1 is 0.) Each of the genes is listed along the x axis. Missing bars on the graph represent the primers that failed after repeated runs. There are error bars added to each data point, the error bars are calculated from the maximum and minimum RQ values. The error bars are much larger for the ZR75-1 DOCR cell lines than the MDA-MB-231 but many are smaller than for the ZR75-1 PACR cell lines. In addition more of the primers failed with the ZR75-1 DOCR samples than with the MDA-MB-231 PACR samples, but less failed than in the ZR75-1 PACR.

The 5nM DOCR samples are represented by the blue, the 25nM DOCR samples are represented by the red bar and the 50nM DOCR samples are represented by the green.

Some genes showed a very similar expression level in the ZR75-1 DOCR cell lines as the ZR75-1 native cell lines namely AMPH, ALDH1A3, FBP, FOXA2 FOXF2, ID3, MAPK13, TSPAN8 and TSPAN13. Two genes show a lower expression level in the DOCR ZR75-1 cell lines than in the ZR75-1 native cell lines, PPP1R14C and TGFBR3. The following genes show higher expression in the ZR75-1 DOCR cell lines than in the ZR75-1 native cell line: CD33, COBL, ID2, IL11, IL7R, MAL2, MDR, NLRP2, PI3, and SCN11A.

Of the genes that have increased expression in the DOCR compared to the native cells, the genes that increase with increasing docetaxel resistance or achieve a "plateau" of consistent expression in the DOCR compared to the native cell are as follows: CD33, COBL, IL11, MDR1, PI3, SCN11A. The most robust data from this figure showing the highest change in expression relative to the Native and the lowest variation among replicates is for CD33 and MDR-1.

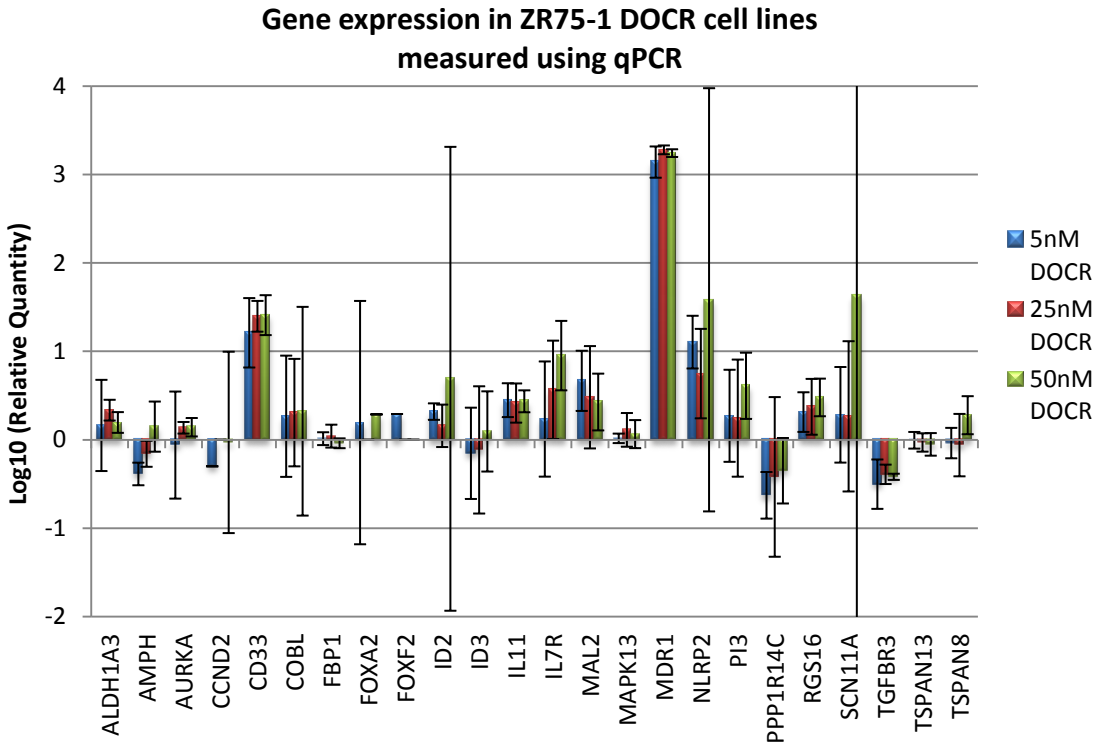


**Figure 5.40** Gene expression levels of docetaxel resistant ZR75-1 cell lines measured by qPCR. The X axis lists each gene alphabetically. The Y axis lists the Relative Quantity of expression to Log10. Each expression level of the PACR cell lines is normalised to the expression in the native cell lines – the relative quantity in the native cells is 1 and so is 0 at log10. The blue bar represents the expression level of the 5nM PACR cell lines, the red bar represents the expression level of the 25nM PACR cell lines and the green bars represent the expression level of the 50nM PACR cell lines. The error bars represent the maximum and minimum RQ values of the expression levels of each gene.

Finally, the ER expression was measured in the ZR75-1 DOCR cell lines. The orange bars shown in figure 5.42 show the fold change in expression of ER in the native, 5, 25, and 50nM DOCR cell lines.

There is a slight change in ER expression in the 5nM and 25nM DOCR cell lines compared to the ZR75-1 native cells, and there is only a very small increase in expression of ER in the 50nM

DOCR cell lines when measured against the same ZR75-1 native background. Again there is no consistent pattern of increase or decrease of ER expression with increasing docetaxel resistance in the ZR75-1 cell lines.

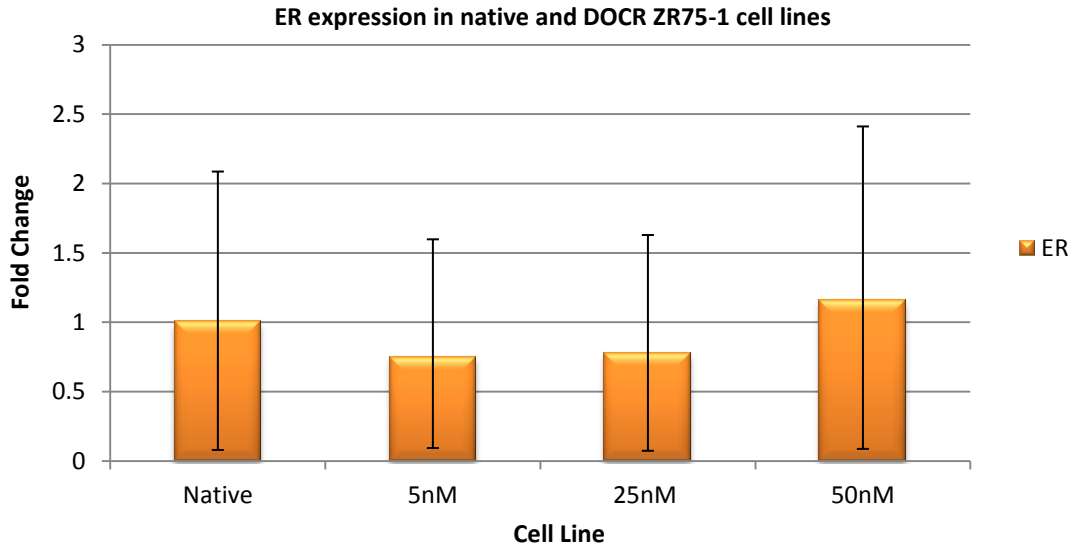


**Fig 5.41.** The Y axis measures the Fold change in ER expression level. The X axis shows each of the ZR75-1 cell lines: Native, 5nM, 25nM and 50nM DOCR. Error bars are min and max RQ value.

This data reinforces the theory that ER status influences paclitaxel sensitivity and resistance as it has already be determined that that the ER negative MDA-MB-231 native cells are more sensitive to paclitaxel than the ER positive ZR75-1 native line (re chapter 3). This data suggests that ER expression increases with increasing paclitaxel resistance in an ER negative cell line where as ER status remains unchanged in already ER positive cell lines with increasing taxane resistance. However, it is important to bear in mind that it is unusual to see increasing ER expression in an ER negative line.

### 5.3.c. Combined heat map of q-PCR Data

The MDA-MB-231 and ZR75-1 heat maps were then combined with one another, still both normalised to their respective native expression level, and then observed how the gene expression levels clustered with the cell lines (ref fig 5.42.) There is a much clearer separation of clusters in the combined heat map. Generally where expression is high in the MDA-MB-231 cell lines it is low in the ZR75-1 cell lines and vice versa. This shows that the MDA-MB-231 and the ZR75-1 cell lines express significantly different genes to one another as they become resistant to taxanes.

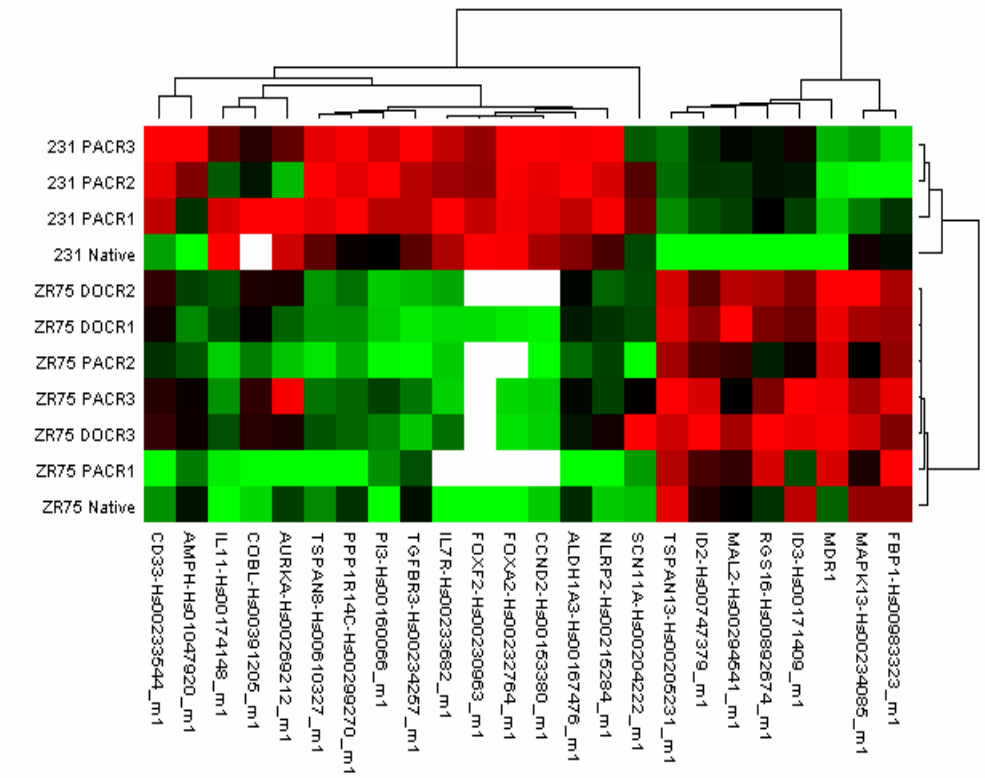


**Figure 5.42** Combined Heat maps of gene expression levels in a select panel of genes detected with qPCR using RNA extracted from MDA-MB-231 native and PACR, ZR75-1 Native PACR and DOCR cell lines Native cells lines are used as a control to compare the gene expression levels of the taxane resistant cell lines. Green boxes denote samples where expression levels are low and the red boxes denote samples where expression levels are high. The black boxes denote samples where the expression level is unchanged.

## 5.4. Illumina Profiling of MDA-MB-231 PACR and ZR75-1 PACR and DOCR Cell lines.

After the initial illumina experiments using only the MDA-MB-231 cell lines the complete panel of taxane resistant breast cell lines was investigated, which is detailed in section 2.3.a.i – 2.3.c.iv. I am very grateful to Dr. Andy Sims for helping me analyse the resulting data.

The resulting data was analysed using R (a statistical language for computing statistical analyses) and represented it as the heat maps shown below in figure 5.43. Both panel A and B show each of the samples clustered according to similarity in gene expression of the clones on the array. The tree dendrogram shows the relationships between samples. Panel A on the left shows the data pre-normalisation and panel B on the right shows the data post normalisation.

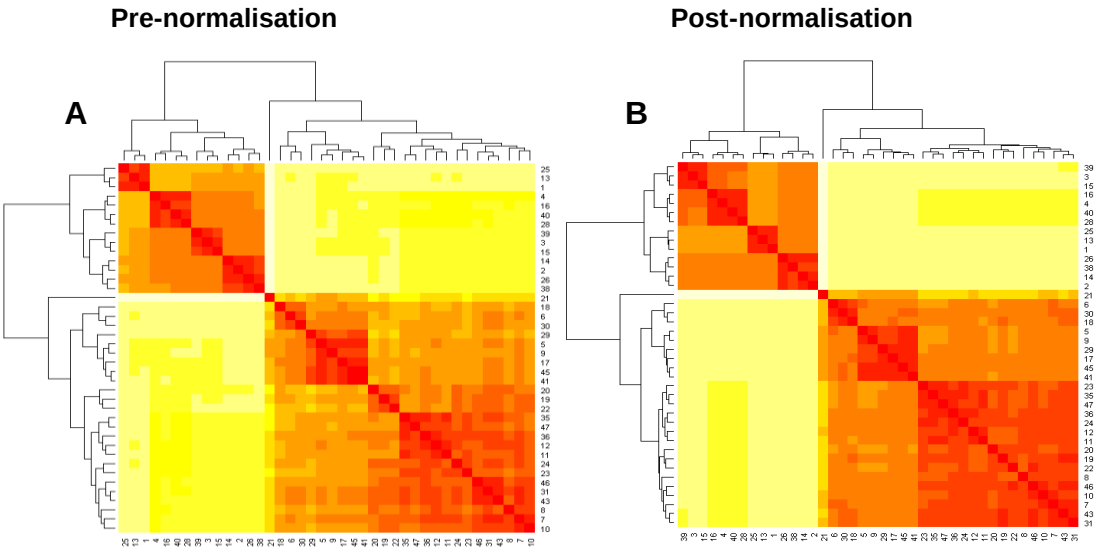


**Figure 5.43** Panels A and B shows heat maps of the illumina data from the entire panel of taxane resistant cell lines before and after normalisation methods using R. Along the right hand and the bottom edges of both of the heat maps are each of the samples and along the left hand and top edge hierarchical tree clustering linking the most similar clones. The red and orange boxes indicate clones on the array where samples have the highest similarity and the pale yellow and white boxes represent the samples with the least similarity

Figure 5.44 shows the same data pre and post normalisation (Panel A pre, Panel B post) represented as box plots of microarray signal intensity. Figure 5.43 and 5.44 show that the data were effectively normalised using these methods.

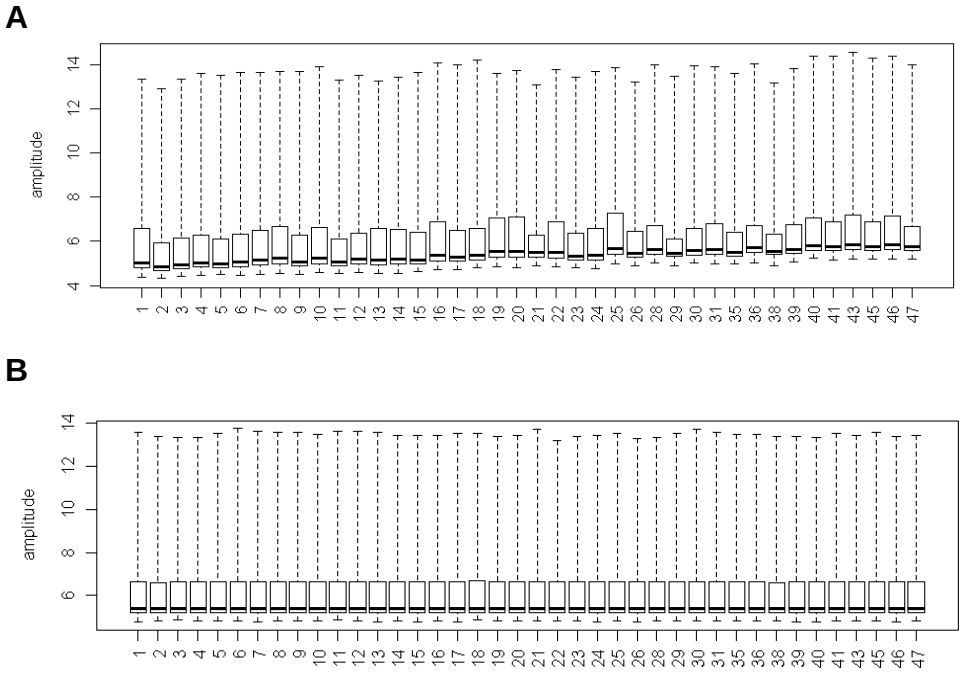


**Figure 5.44**. Panels A and B are box plots of microarray signal amplitude intensity of the cell line illumina data pre and post normalisation.

Panel A of figure 5.45 (next page) shows all 24,527 probes on the array, represented as another heat map. This time the heat map is labelled with which taxane resistant cell line each sample is taken from. This is listed down the right hand side of the heat map. This shows that MDA-MB-231 and ZR75-1 cell lines cluster together separately, the PACR and DOCR cell lines tend to cluster with one another within their own cell line and the replicates at one resistance level tend to cluster together.

Each of the eleven cell lines were run in quadruplicate and the ZR75-1 native line was run in quadruplicate to provide separate groups of replicates to compare to both the PACR and the DOCR cell lines. The following samples did not provide sufficient quality of data to be analysed: MDA-MB-231 Native MDA-MB-231 25nM PACR, ZR75-1 Native, ZR75-1 5nM PACR, ZR75-1 50nM PACR x 2, ZR75-1 5nM DOCR and 50nM DOCR. These 8/48 samples failed QA and so were rejected.

Multidimensional Scaling (MDS) is used to observe dissimilarities between data, shown in panel B of figure 5.45.

The ZR75-1 samples cluster together and the MDA-MB-231 samples cluster together. The Native MDA-MB-231 samples cluster together (scarlet rhombuses), the 5nM and 25nM PACR MDA-MB-231 cluster close together (dark red and orange triangles) and the MDA-MB-231 50nM PACR cells form a third cluster (yellow triangles.) The ZR75-1 Native samples forms a distinct cluster (navy rhombuses), with one outlying sample – indicated by green arrow. The ZR75-1 samples form a cluster close to this cluster (dark blue triangles.) The 25nM and 50nM (mid blue and light turquoise triangles) PACR, 5nM, 25nM, and 50nM DOCR (dark blue, mid blue and light turquoise squares) samples form a more disparate cluster with one another.

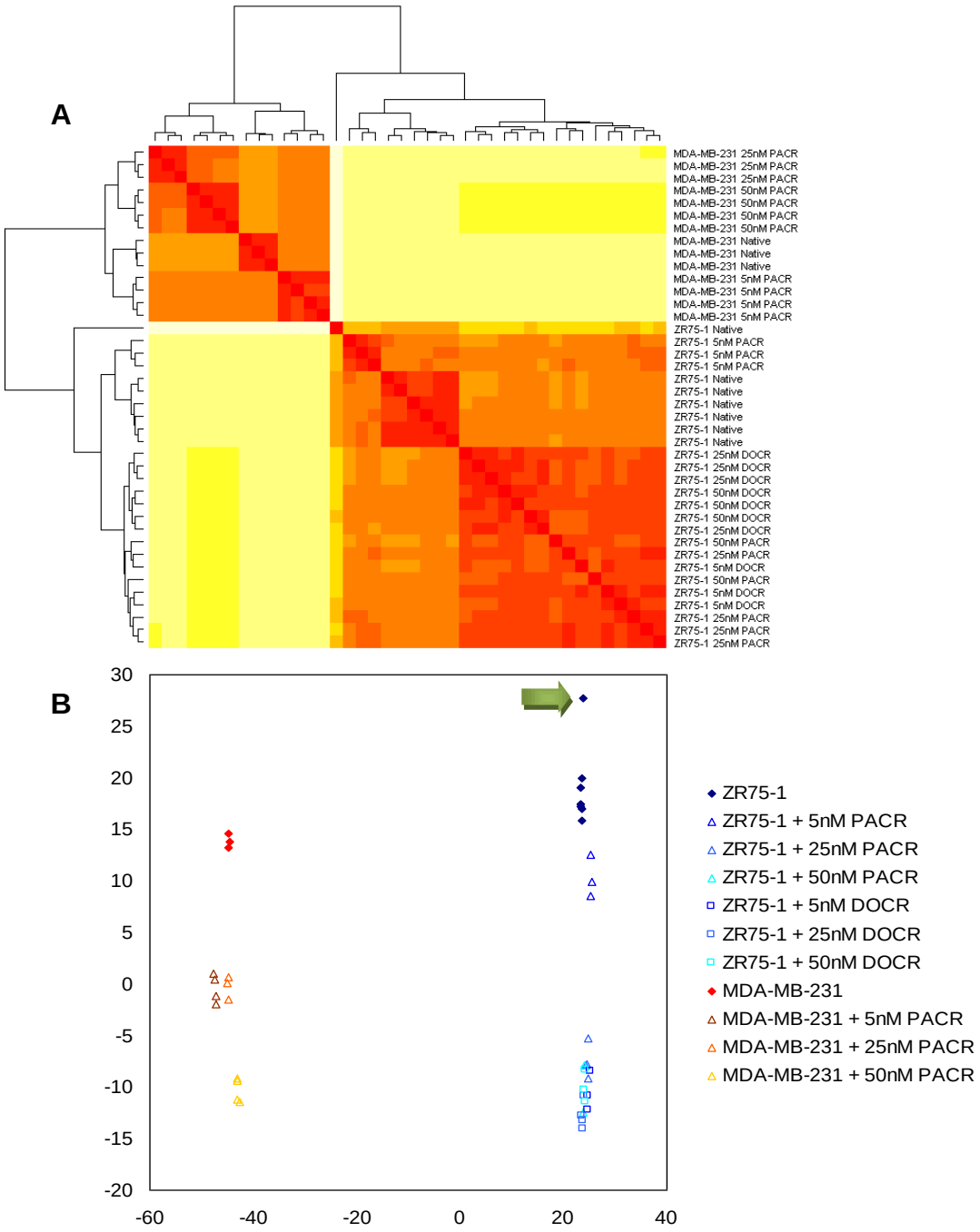


**Figure 5.45** Panel A: all 24527 probes on array represented as heat map, each sample listed down RHS. Panel B: MDS plot of all samples to observe dissimilarities between data. Native MDA-MB-231 samples: scarlet rhombuses, 5nM PACR MDA-MB-231: dark red triangles. 25nM PACR MDA-MB-231: orange triangles.) MDA-MB-231 50nM PACR cells: yellow triangles. ZR75-1 Native samples: navy rhombuses (one outlying sample, indicated by green arrow.) ZR75-1 5nM PACR: dark blue triangles. ZR75-1 25nM PACR cells: mid blue triangle. ZR75-1 50nM PACR: light turquoise triangles. ZR75-1 DOCR: dark blue square. ZR75-1 25nM DOCR: mid blue squares. ZR75-1 50nM DOCR: light turquoise squares.

The next two figures 5.46 and 5.47 show a heat map of the 200 most variable genes divided into two parts, so the gene names shown down the right hand side of the heat map were large enough to be read from the page.

Figure 5.46 is the top half of the heat map and figure 5.47 is the bottom half of the heat-map. The heat map separates the two cell lines MDA-MB-231 and ZR75-1 very clearly according to ER status. The hierarchical clustering separates the native from the taxane resistant cell lines and replicates cluster together. The ZR75-1 PACR cell lines separate from the DOCR lines. The higher resistance level cell lines (25nM and 50nM DOCR) cluster together. The lowest resistance level the 5nM PACR cell line clusters separately.

Figures 5.46 and 5.47 show the pathway to resistance is different in the MDA-MB-231 and ZR75-1 cell lines and that PACR is different from DOCR in the ZR75-1 cell lines. This is a very important conclusion which is supported by what has been observed in the aCGH, and qPCR experiments. This also agrees with work conducted locally in Edinburgh which suggests that there is a diversity of resistance pathways to endocrine therapy[249].

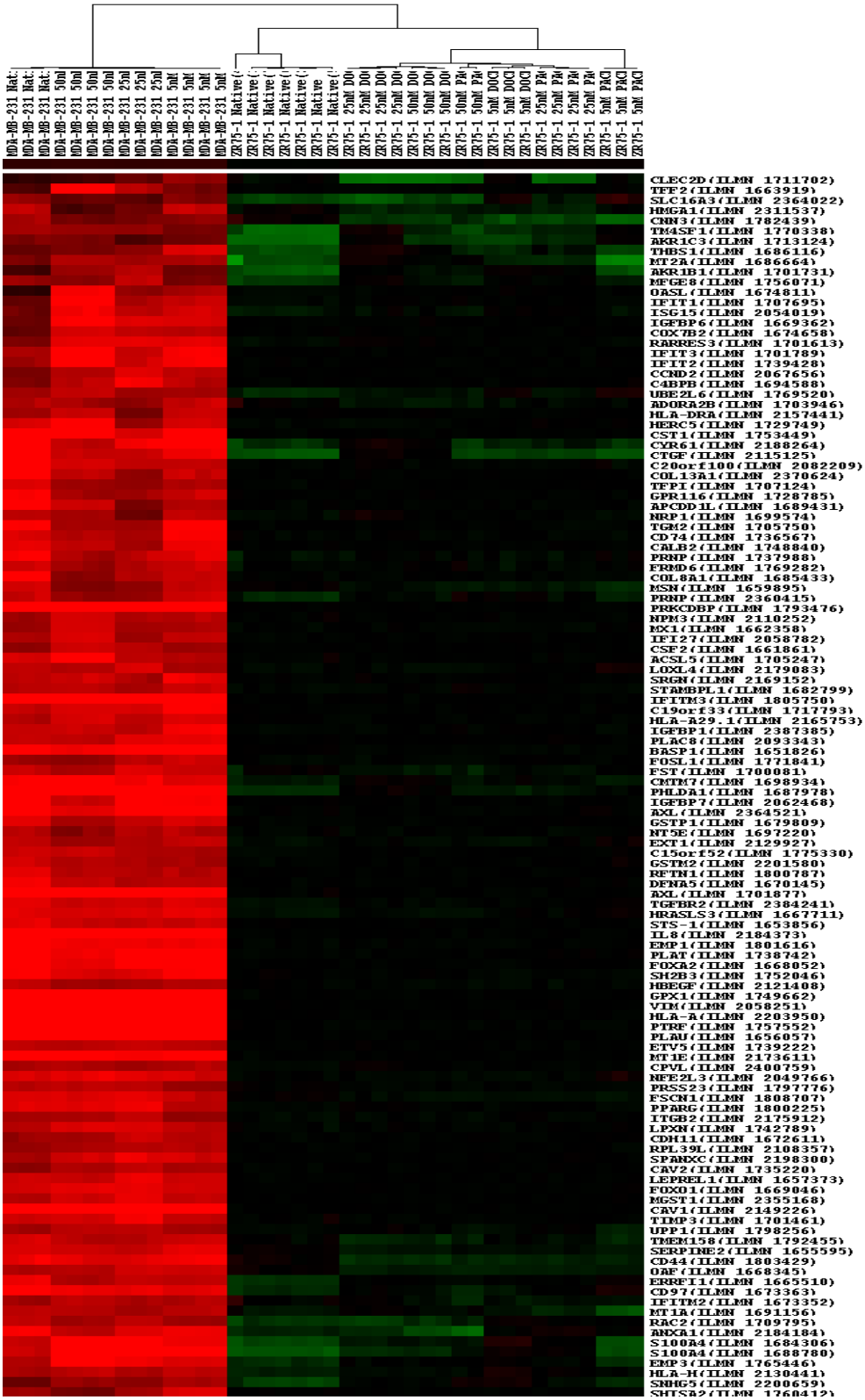


**Figure 5.46** Upper half of heat map showing the top 200 most variable genes obtained from the illumina experiments using all 11 taxane resistant cell lines. Red boxes indicate high expression and green boxes indicate low expression.

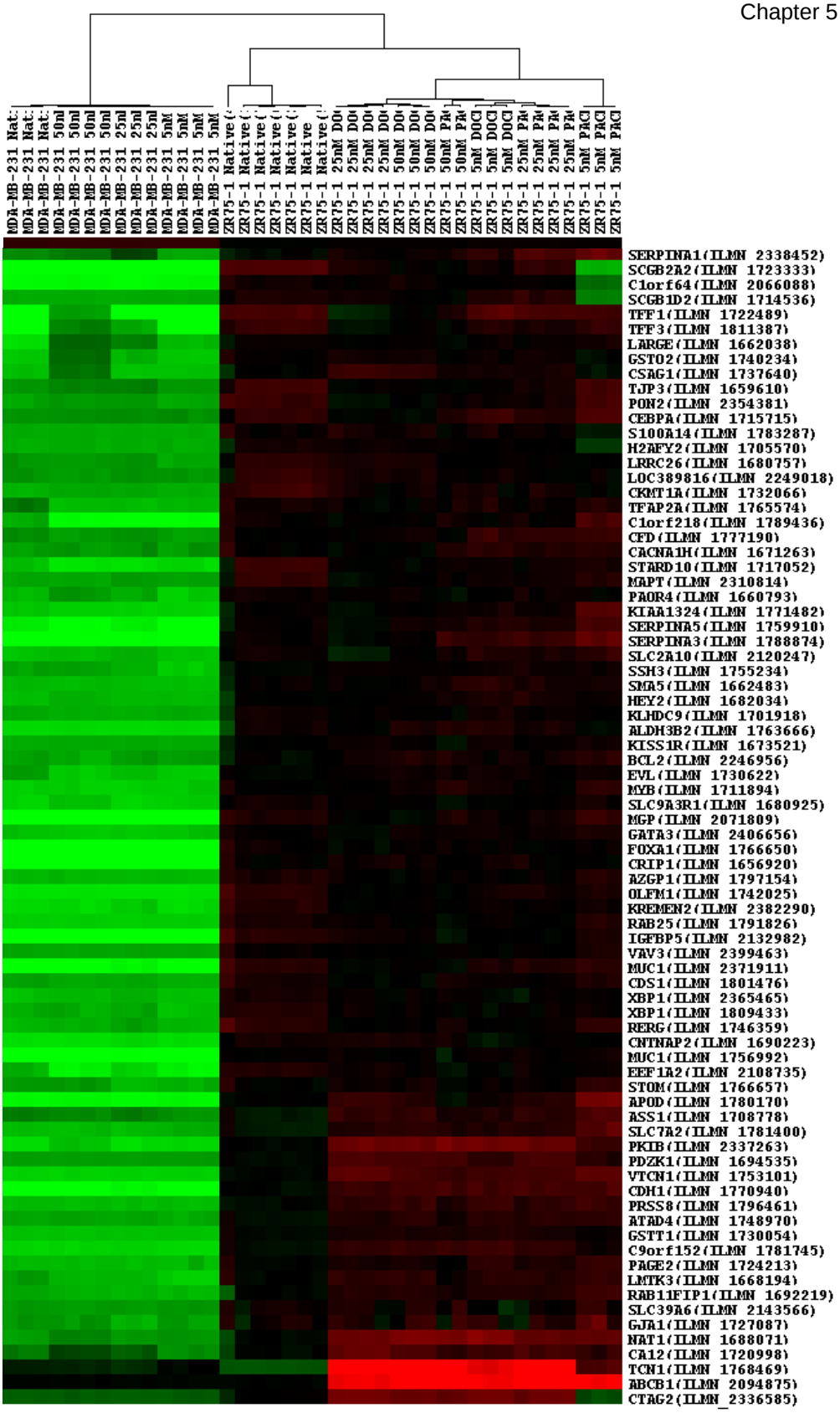


**Figure 5.47** Lower half of the heat map showing the top 200 most variable genes obtained from the illumina experiments using all 11 taxane resistant cell lines. Red boxes indicate high expression and green boxes indicate low expression.

The overlap was observed between cell lines of the top 200 genes changed at the highest resistance level: 50nM treatment, from this created heat maps and Venn diagram shown in figure 5.48.

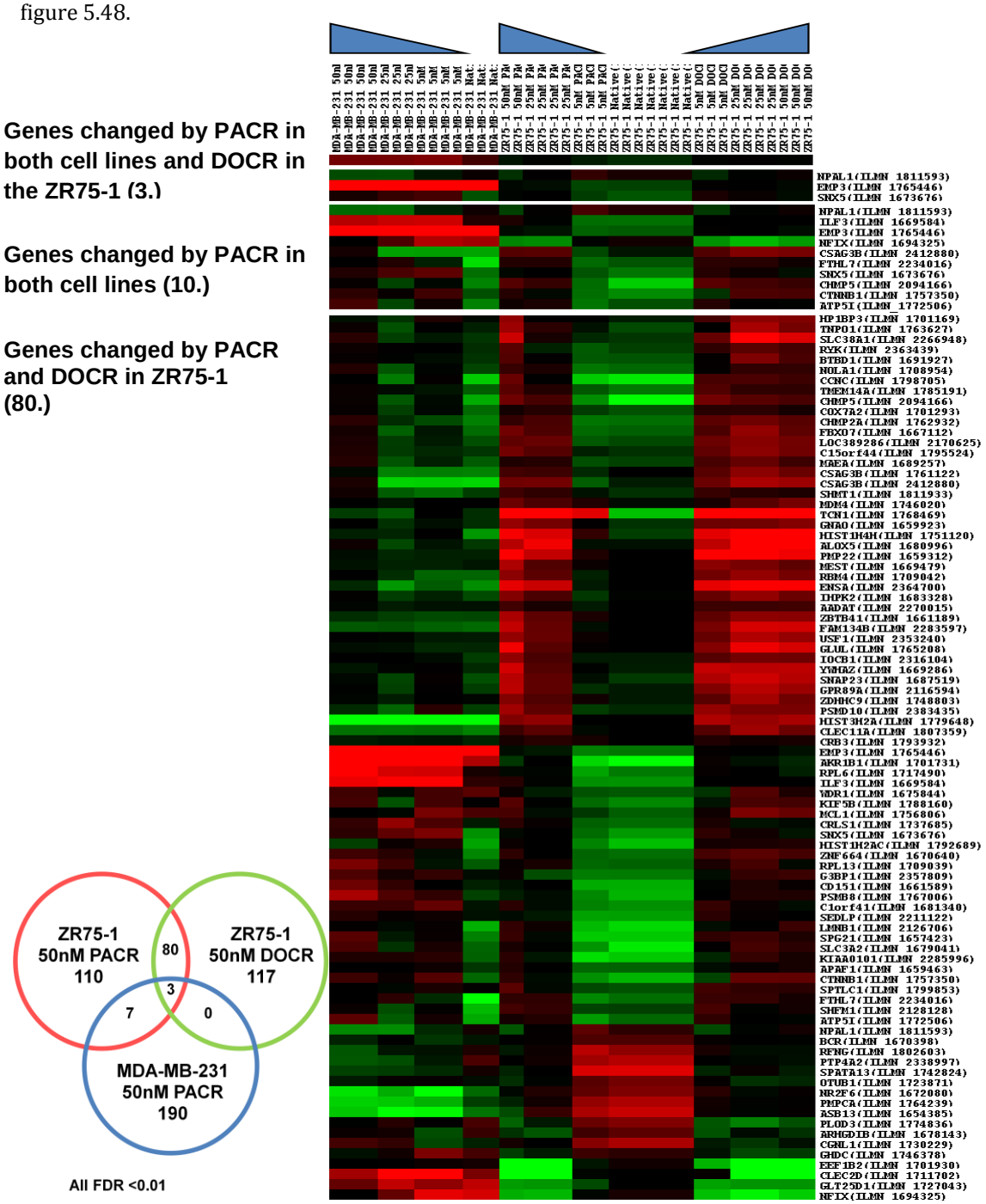


**Figure 5.48**.On the right hand side of the figure are heat maps of the overlap of the top 200 genes identified using illumina microarrays at the highest resistance level of 50nM in all three taxane resistant cell lines. Genes are listed down the right hand side of the heat map. Red represents high expression and green low expression. On the left of the figure is the data represented in a Venn diagram.

This same approach was adopted to look at the overlap between cell lines, this time in the top 500 most variable genes (figure 5.49.) The data is summarised in the Venn Diagram which shows that there are 33 genes changed by PACR in both cell lines and DOCR in the ZR75-1, there are 17 genes changed by PACR in both cell lines and there are 20 genes changed by PACR in the MDA-MB-231s and by DOCR ZR75-1.

**Genes Changed by PACR in both cell lines and DOCR in ZR75-1 (33.)**

**Gene changed by PACR in both cell lines (17.)**

**Genes changed by PACR in MDA-MB-231s and DOCR in ZR75-1 (20.)**

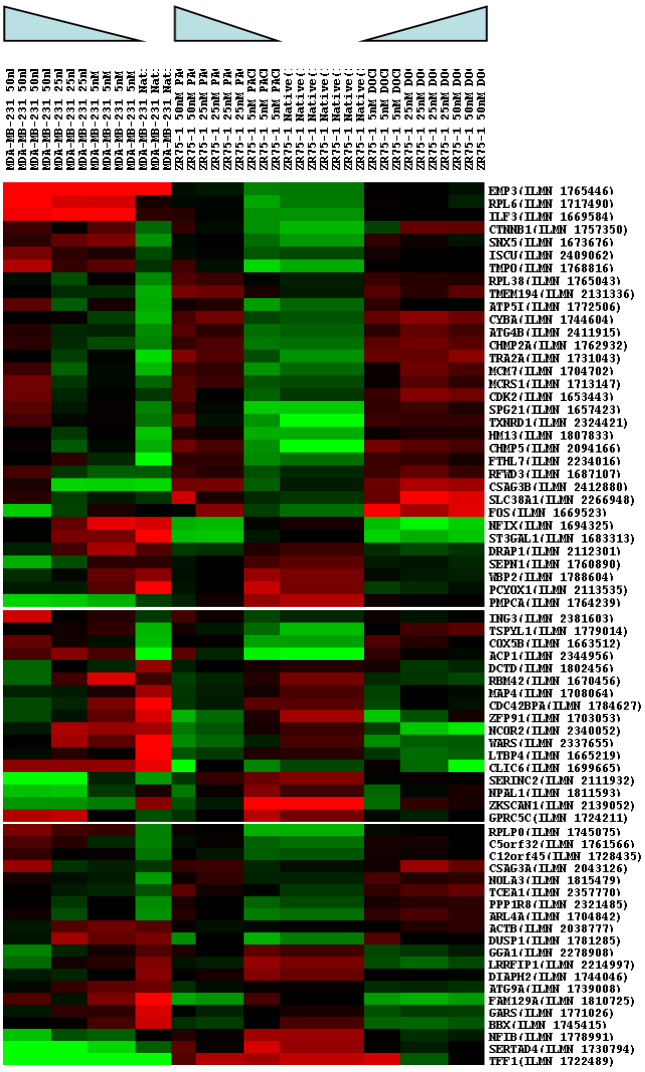


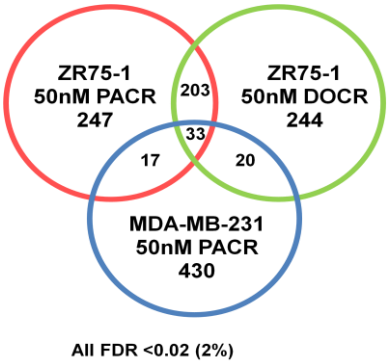


**Figure 5.49** On the right hand side of the figure are heat maps of the overlap of the top 500 genes identified using illumina microarrays looking at the highest resistance level of 50nM in all three taxane resistant cell lines. Genes are listed down the right hand side of the heat map. Red represents high expression and green low expression. On the right hand side of the figure is the data represented in a Venn diagram.

When comparing the 200 most highly differentially expressed genes in ZR75-1 cells resistant to either 50nM paclitaxel or docetaxel, with those identified in MDA-MB-231 cells resistant to 50nM paclitaxel a total of 507 different genes were identified. Only 10 (2.5%) of gene were identified in common between MDA-MB-231 and ZR75-1 cells resistant to the same drug, paclitaxel versus 380 genes which were not common between these cell lines. More genes (83) were identified which were common to PACR vs. DOCR ZR75-1 cells, however a further 234 genes were identified which were distinct between the two cell lines. Only 3 genes were identified in all three cell lines.

Extending this list to the top 500 most differentially expressed genes in each cell line did not dramatically alter this finding (see figure 5.49.) Only 50 (5.2%) genes were identified in common between ZR75-1 and MDA-MB-231 cells even though both cell lines were resistant to 50nM paclitaxel. More genes, 236 (31%) were now commonly identified in ZR75-1 cells resistant to either paclitaxel or docetaxel, but 528 genes were identified which were not common between these cell lines.

It appears that different molecular alterations drive resistance depending on the parental cell lines, and that resistance within a single cell line to different taxanes may also be driven by different pathways. In this context it is noteworthy to remember that MDA-MB-231 DOCR cell lines could not be derived successfully.

Table 5.5 shows the pathways identified by this method in the ZR75-1 50nM DOCR cell line. Table 5.2 illustrates the point that differing numbers of replicates using microarray technology can affect the number of genes consistently expressed when using the same constant false discovery rate threshold. This is an important factor to consider when looking at any microarray data using multiple replicates.

| **FDR set at 0.02** | **Replicates** |
|---|---|
| MDA-MB-231 50nM PACR | 7432 (3 vs 4) |
| ZR75-1 50nM PACR | 487 (2 vs. 7) |
| ZR75-1 50nM DOCR | 3725 (3 vs. 7) |
| **FDR set at 0.03** | **Replicates** |
| MDA-MB-231 50nM PACR | 10 genes (3 vs. 3) |
| ZR75-1 50nM PACR | 6508 (4 vs. 7) |
| ZR75-1 50nM DOCR | 5627 (3 vs. 7) |

**Table 5.2** Differing numbers of replicates affect the numbers of genes consistently expressed at a single FDR threshold.

**5.4.b. Kegg Pathway Analysis of illumina data using taxane resistant cell lines.**

A KEGG database analysis was conducted on the top 500 most variable genes at the highest resistance level to identify any common pathways dysregulated in the MDA-MB-231 PACR, ZR75-1 PACR and ZR75-1 DOCR cell lines when compared to their native line. Table 5.3 shows the pathways identified by this method in the MDA-MB-231 50nM PACR cell line, the table lists each of the pathways, the genes involved in the pathway, the *p* value and the false discovery rate observed in each analysis. They are listed in order of the most significant to least significant.

| Term | Genes | *P* Value | FDR |
|---|---|---|---|
| **hsa03010:Ribosomes** | RPL41 RPL6 RPL0 RPL26 RPL15A RPS38 RPS21 RPS7 RPS24 RPL29. | 0.001 | 2 |
| **hsa04510:Focal Adhesion** | ACTB ITGA2 ACTN1 ITGB5 ITGA3 BIRC3 COL5A1 CTNNB LAMB3 PAK2 CCND2 COL6A3 VEGFA SHC1 | 0.01 | 1 |
| **hsa04142:lysosome** | NPC1 LAPTM5 AP1G1 LGMN PPT2 NEU1 CTSB GGA1 FUCA1 | 0.04 | 35 |
| **hsa05412:Arrythmogenic right ventricular cardiomyopathy (ARVC)** | ACTB ATP2A2 ITGB5 ITGA2 ACTN1 ITGA3 CTNNB1 | 0.04 | 35 |
| **hsa00970:Aminoacyl tRNA biosynthesis** | WARS YARS DARS AARS GARS | 0.04 | 41 |
| **hsa05215:prostate cancer** | HSP90AB1 CREB1 CREB3L2 CREB3L3 CDK2 GSTP1 CTNNB1 | 0.07 | 57 |

**Table 5.3** Kegg pathway analysis of MDA-MB-231 50nM PACR cell lines from the top 500 most variable genes determined from illumina data. Column one shows each pathway and column two shows the genes in this pathway. Column three is the *p* value used in the analysis and column four is the FDR observed in the analysis. Note by entering the hsa code into the KEGG pathway database online one can obtain extensive additional information on each pathway.

Table 5.4 shows the pathways identified by this method in the ZR75-1 50nM PACR cell line.

| Term | Genes | P Value | FDR |
|---|---|---|---|
| **hsa00051: fructose & mannose metabolism** | ALDOA SORD PFKL AKR1B1 HK1 PMM2 | 0.004 | 4 |
| **hsa04330:Notch signalling** | CTBP1 PSEN1 MAML1 RFNG RBPJ NCOR2 | 0.01 | 16 |
| **hsa03040:spliceosome** | NCBP2 HNRNPA3 DHX38 NHP2L1 TRA2A ZMAT2 PQBP1 HSPA1B1 SNRPF | 0.04 | 41 |
| **hsa00052:galactose metabolism** | GALK2 PFKL AKR1B1 HK1 | 0.05 | 43 |
| **hsa04115:p53 signalling pathway** | EI24 CDKN2A CASP8 APAF1 MDM4 CDK2 | 0.06 | 52 |
| **hsa05010:Alzheimer's** | COX7A2 GNAQ PSEN1 CASP7 CASP8 COX8A ATP5G2 APAF1 ATP5G1 COX5B | 0.07 | 57 |

**Table 5.4.** Kegg pathway analysis of ZR75-1 50nM PACR cell lines from the top 500 most variable genes determined from illumina data. Column one shows each pathway and column two shows the genes in this pathway. Column three is the *p* value used in the analysis and column four is the FDR observed in the analysis. Note by entering the hsa code into the KEGG pathway database online one can obtain extensive additional information on each pathway.

Table 5.5 shows the pathways identified by this method in the ZR75-1 50nM DOCR cell line.

| Term | Genes | *P* Value | FDR |
|---|---|---|---|
| **hsa04210:Apoptosis** | AKT1 CASP9 CASP7 BAX CASP8 PPP3R1 APAF1 PRKACB TRADD | 0.006 | 7 |
| **hsa03010:Ribosome** | RPS29 RPL13 RPL6 RPLP0 RPL21 RPL27A RPL27 RPL4 RPL38 | 0.006 | 7 |
| **hsa05130:Pathogenic E.coli infection** | ACTB CTTN YWHAZ TUBB6 ARCP4 ITGB1 CTNNB1 | 0.009 | 10 |
| **hsa05222:Small cell lung cancer** | AKT1 MAX CASP9 PIAS4 RB1 APAF1 ITGB1 CDK2 | 0.02 | 18 |
| **hsa04115:p53 signalling** | CASP9 BAX CASP8 APAF1 MDM4 THBS1 CDK2 | 0.02 | 33 |
| **hsa00051:Fructose and Mannose metabolism** | ALDOA SORD PFKL AKR1B1 HK1 | 0.02 | 34 |

| | | | |
|---|---|---|---|
| **hsa05014:Amyotrophic lateral sclerosis (ALS)** | CASP9 BAX PPP3R1 CCS APAF1 DAXX | 0.03 | 37 |
| **ATP5Jhsa050101: Alzheimer's** | APP COX7A2 GNAQ CASP9 CASP8 CASP7 PPP3R1 ATP5G2 APAF1 ATP5G1 ATP5J | 0.03 | 34 |
| **hsa00052:Galactose metabolism** | GALK2 PFKL AKR1B1 HK1 | 0.05 | 45 |
| **hsa00920:Sulphur metabolism** | SULT1A1 SULT1A3 BPNT1 | 0.05 | 48 |
| **hsa05200:pathways in cancer** | CTBP1 BCR VHL RB1 NFKB2 ITGB1 CDK2 CTNNB1 TPM3 AKT1 FOS MAX PIAS4 CASP9 JUN BAX CASP8 | 0.06 | 50 |
| **hsa04120:ubiquitin mediated proteolysis** | UBE23E UBE2D3 UBE2Z PIAS4 NEDD4 VHL UBE2I HERC3 UBE2E1 | 0.07 | 58 |
| **hsa04662:B cell receptor signalling pathway** | AKT1 PTPN6 BCL10 FOS JUN PPP3R1 | 0.09 | 67 |
| **hsa04520:adherens junction** | ACTB PTPN6 TJP1 CSNK2A1 SORBS1 CTNNB1 | 0.09 | 71 |

**Table 5.5** Kegg pathway analysis of ZR75-1 50nM DOCR cell lines from the top 500 most variable genes determined from illumina data. Column one shows each pathway and column two shows the genes in this pathway. Column three is the *p* value used in the analysis and column four is the FDR observed in the analysis. Note by entering the hsa code into the KEGG pathway database online one can obtain extensive additional information on each pathway.

Each of the Kegg pathway analyses was then compared to one another to identify common pathways. The following common pathways were identified which have been highlighted in corresponding colours on each table.

- **hsa03010:Ribosomes** (MDA-MB-231 PACR *p* value ≤ 0.001, FDR=2: ZR75-1 DOCR *p* value ≤ 0.006, FDR=7.) Common to MDA-MB-231 PACR and ZR75-1 DOCR.
- **hsa00051:Fructose and Mannose metabolism** (ZR75-1 PACR *p* value ≤ 0.004, FDR=4: ZR75-1 DOCR *p* value ≤ 0.02 FDR=34.) Common to both ZR75-1 PACR and DOCR.
- **hsa00052:Galactose metabolism** (ZR75-1 PACR *p* value ≤0.05 FDR=43: ZR75-1 DOCR *p* value ≤0.05 FDR=45.) Common to both ZR75-1 PACR and DOCR.
- **hsa04115:p53 signalling** (ZR75-1 PACR *p* value ≤ 0.06 FDR=52: ZR75-1 DOCR *p* value ≤0.02 FDR=33.) Common to both ZR75-1 PACR and DOCR.

This is encouraging as there is only one pathway in common between the MDA-MB-231 and ZR75-1 cell line and there are three in common between the two taxane resistant ZR75-1 cell lines.

In addition it was noted that in the PACR MDA-MB-231 cell line alone there was increased variability in gene expression of members of the Focal adhesion pathway. The focal adhesion pathway is involved in cell motility, proliferation, differentiation and anchorage. This may be pertinent in terms of the mouse xenograft experiments (chapter 4) in which it was determined that the MDA-MB-231 PACR cell lines failed to establish as xenografts. It is an intriguing prospect that the failure of the MDA-MB-231 PACR cell line to form xenografts may be explained by a dysregulation in focal adhesion pathways.

An extensive genomic and transcriptomic analysis of the 3 taxane resistant breast cancer cell lines was conducted and this data was validated using qPCR. A panel of genes that are potential biomarkers of taxane resistance has been identified as have pathways of interest in this context. These investigations have allowed it to be determined that differing molecular alterations drive resistance depending on the parental cell lines and that resistance within a single cell line to differing taxanes may be driven by differing pathways. These theories are reiterated by the fact that the MDA-MB-231 failed to become resistant to docetaxel.

The cell lines have been investigated in terms of DNA with the aCGH experiments and RNA with the transcriptomic arrays and qPCR. These experiments were subsequently investigated and validated by looking at protein levels using western blotting.

## 5.5. Western blotting of lysates from taxane resistant cell lines.

After investigating the panel of taxane resistant cell lines, using both transcriptomic and genomic means and validating some of this data using qPCR an investigation into how taxane resistance impacts the expression of certain proteins was conducted. A panel of common breast cancer biomarkers was investigated: EGFR, HER2, HER3, and ERα using Western blotting. MDR1 was included to investigate whether the multidrug resistant phenotype was perpetuated in the cell lysates from the taxane resistant cell lines and the three other genes identified from the literature search, namely Aurora Kinase A, Stathmin and YY1.

Cell lines were grown up according to section 2.1f.vi Lysates were then harvested according to section 2.3.f.i and then run on western blots according to 2.3.f.ii-2.3.f.viii.

Expression of ERα protein is not detected in the MDA-MB-231 native and PACR cell lines. There are similar levels of ERα protein expression in the ZR75-1 native, 5nM, and 50nM DOCR cell lines. There is a similar low level expression in the 25nM DOCR and 25nM PACR ZR75-1 cell

lines and there is slightly higher expression in the ZR75-1 5nM and the 50nM PACR cell lines. Again this lack of consistency with increasing or decreasing ERα expression with increasing taxane resistance suggests that ERα protein expression is unlikely to be a marker of taxane resistance in the taxane resistant cell lines. This result is disappointing in the context of the qPCR in the MDA-MB-231 cell lines which showed a marked increase in gene expression of ER.

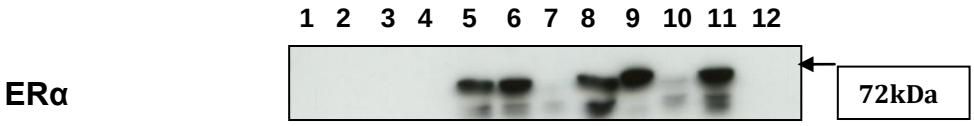


**Figure 5.50** Western blot of ERα expression in taxane resistant cell lines. Lysates from the following cell line were loaded into lanes 1 to 11 as follows. Lane 1: MDA-MB-231 Native, Lane 2: MDA-MB-231 5nM PACR, Lane 3 MDA-MB-231 25nM PACR, Lane 4 MDA-MB-231 50nM PACR, Lane 5: ZR75-1 Native, Lane 6: ZR75-1 5nM DOCR Lane 7: 25nM DOCR, Lane 8: ZR75-1 50nM DOCR Lane 9: ZR75-1 5nM PACR, Lane 10: ZR75-1 25nM PACR, Lane 11: ZR75-1 50nM PACR. The ERα band is detected at 68kDa. (ERα ab - santa cruz - sc-8002, diluted at 1:1000.)

Figure 5.51 shows the expression of EGFR (HER1) in the panel of taxane resistant cell lines. There seems to be increased expression of EGFR1 protein in PACR MDA-MB-231 cells compared to the native line, although there is no consistent pattern of increase in expression with increasing resistance. There is no EGFR1 expression detected in any of the ZR75-1 native, PACR or DOCR cell lines. This lack of consistency with increasing or decreasing EGFR expression with increasing taxane resistance suggests that EGFR1 expression is not a marker of taxane resistance in these cell lines.

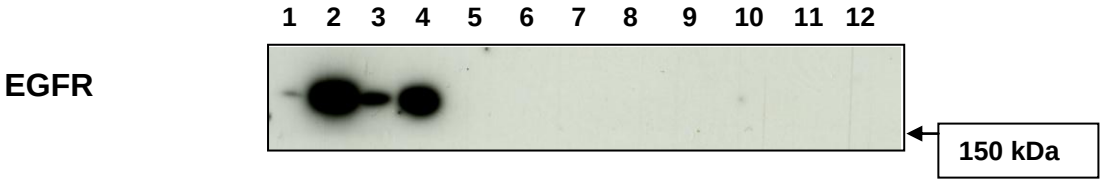


**Figure 5.51** Western blot of EGFR (HER1) expression in taxane resistant cell lines. Lysates from the following cell line were loaded into lanes 1 to 11 as follows. Lane 1: MDA-MB-231 Native, Lane 2: MDA-MB-231 5nM PACR, Lane 3 MDA-MB-231 25nM PACR, Lane 4 MDA-MB-231 50nM PACR, Lane 5: ZR75-1 Native, Lane 6: ZR75-1 5nM DOCR Lane 7: 25nM DOCR, Lane 8: ZR75-1 50nM DOCR Lane 9: ZR75-1 5nM PACR, Lane 10: ZR75-1 25nM PACR, Lane 11: ZR75-1 50nM PACR. The EGFR band is detected at 170kDa. EGFR antibody (santa cruz sc-03) was diluted at 1:1000.

Her2 expression was looked at in the panel of cell lines (re figure 5.52.) In the TACT trial the patients that benefited the most from the addition of a taxane to their therapy were ER-ve and HER2+ve[117]. This suggests that HER2 status may play a role in the taxane resistance which can be investigated in the cell lines.

There was no HER2 expression detected in the MDA-MB-231 native and PACR cell lines. There is increased expression of HER2 protein in the native, 5nM and 50nM DOCR cell lines and no expression is seen in the 5nM DOC cell lines. No HER 2 expression was seen in the PACR ZR75-1 cell lines. Again a lack of consistency with increasing or decreasing HER2 expression with increasing taxane resistance suggests that HER2 expression is not a marker of taxane resistance in the cell lines.

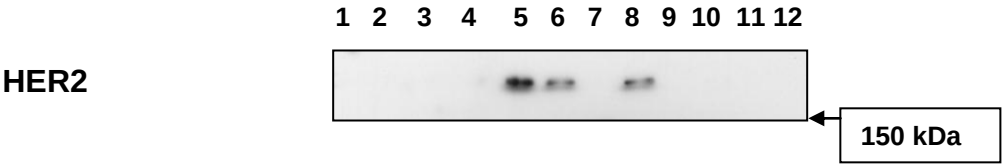


**Figure 5.52** Western blot of HER2 (ERBB2) expression in taxane resistant cell lines. Lysates from the following cell line were loaded into lanes 1 to 11 as follows. Lane 1: MDA-MB-231 Native, Lane 2: MDA-MB-231 5nM PACR, Lane 3 MDA-MB-231 25nM PACR, Lane 4 MDA-MB-231 50nM PACR, Lane 5: ZR75-1 Native, Lane 6: ZR75-1 5nM DOCR Lane 7: 25nM DOCR, Lane 8: ZR75-1 50nM DOCR Lane 9: ZR75-1 5nM PACR, Lane 10: ZR75-1 25nM PACR, Lane 11: ZR75-1 50nM PACR. The Her2 band is detected at 185kDa. (Her2 ab - cell signalling - 2165 – diluted at 1:1000.)

No HER3 expression is detected in the MDA-MB-231 native and PACR cell lines (re fig 5.53). A moderate level of HER3 was expressed in the native and 5nM DOCR cell lines, there was no expression seen in the 25nM DOCR cell line and a low level of expression was seen in the 50nM DOCR cells. ZR75-1 cell resistant to 5nM paclitaxel show a large increase in expression when compared to the native line and the 25nM PACR and 50nM PACR ZR75-1 cell lines have low level and no expression of HER3 respectively.

This lack of consistency with increasing or decreasing HER3 expression with increasing taxane resistance suggests that HER3 expression is unlikely to be marker of taxane resistance in the cell lines.

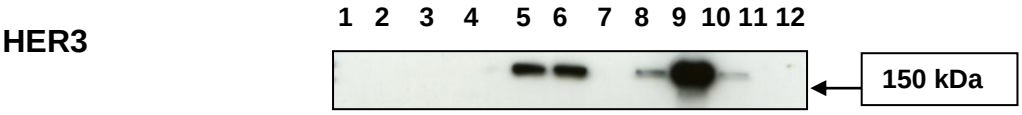


**Figure 5.53** Western blot of HER3 expression in taxane resistant cell lines. Lysates from the following cell line were loaded into lanes 1 to 11 as follows. Lane 1: MDA-MB-231 Native, Lane 2: MDA-MB-231 5nM PACR, Lane 3 MDA-MB-231 25nM PACR, Lane 4 MDA-MB-231 50nM PACR, Lane 5: ZR75-1 Native, Lane 6: ZR75-1 5nM DOCR Lane 7: 25nM DOCR, Lane 8: ZR75-1 50nM DOCR Lane 9: ZR75-1 5nM PACR, Lane 10: ZR75-1 25nM PACR, Lane 11: ZR75-1 50nM PACR. The Her3 band is detected at 148kDa. (HER 3 clone 2F12 ab – neomarkers - MS-201-P – diluted at 1:1000.)

Protein expression of Aurora Kinase A was measure in the cell lines as it has been implicated as a potential marker of taxane resistance[159]. (Re. figure 5.54)

Multiple Splice variants of Aurora A have been identified that are between 40 and 50kDa in size. As it can autophosphorylate under certain conditions such as stress, these extra bands could be post-translational modifications[250], or they could be alternatively spliced trancsripts. There does not seem to be a consistent pattern of increasing Aurora Kinase A expression with increasing taxane resistance in the cell lines. This suggests that Aurora Kinase A is a less likely candidate for taxane resistance in the cell lines.

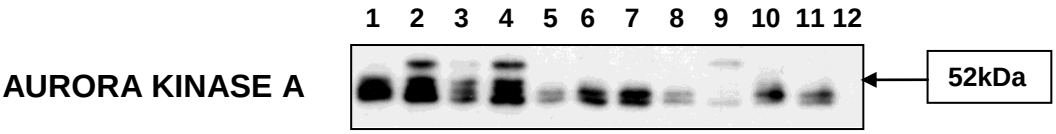


**Figure 5.54**. Western blot of AURKA expression in taxane resistant cell lines. Lysates from the following cell line were loaded into lanes 1 to 11 as follows. Lane 1: MDA-MB-231 Native, Lane 2: MDA-MB-231 5nM PACR, Lane 3 MDA-MB-231 25nM PACR, Lane 4 MDA-MB-231 50nM PACR, Lane 5: ZR75-1 Native, Lane 6: ZR75-1 5nM DOCR Lane 7: 25nM DOCR, Lane 8: ZR75-1 50nM DOCR Lane 9: ZR75-1 5nM PACR, Lane 10: ZR75-1 25nM PACR, Lane 11: ZR75-1 50nM PACR. Band detected at 46KDa. (abcam – ab13824, 4.3µl in 10ml.)

No MDR-1 protein expression is seen in the MDA-MB-231 native, 5nM, 25nM or 50nM PACR cell lines (re figure 5.54.) There is a large increase in MDR1 protein expression in all six taxane resistant ZR75-1 cell lines and no expression of the protein is seen in the ZR75-1 native line which concurs with what was observed in the transcriptomic and qPCR data (figure 5.55.)

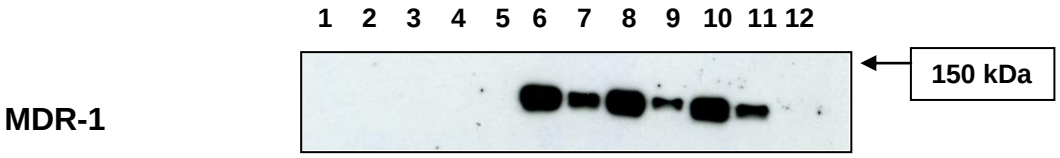


**Figure 5.55** Western blot of Mdr1 expression in taxane resistant cell lines. Lysates from the following cell line were loaded into lanes 1 to 11 as follows. Lane 1: MDA-MB-231 Native, Lane 2: MDA-MB-231 5nM PACR, Lane 3 MDA-MB-231 25nM PACR, Lane 4 MDA-MB-231 50nM PACR, Lane 5: ZR75-1 Native, Lane 6: ZR75-1 5nM DOCR Lane 7: 25nM DOCR, Lane 8: ZR75-1 50nM DOCR Lane 9: ZR75-1 5nM PACR, Lane 10: ZR75-1 25nM PACR, Lane 11: ZR75-1 50nM PACR. The Mdr-1 band is detected at 141kDa. (santa cruz – sc13131 – diluted at 1:1000.)

Overexpression of stathmin has been implicated in taxane resistance as it has been shown to override the mitotic spindle assembly checkpoint inducing resistance[147,246,251]. Stathmin was identified as a potential taxane resistant marker in the array work and from a literature search, however the primer for q-PCR failed to work. Expression of stathmin protein seems to be fairly even in all native and taxane resistant cell lines (figure 5.56.)

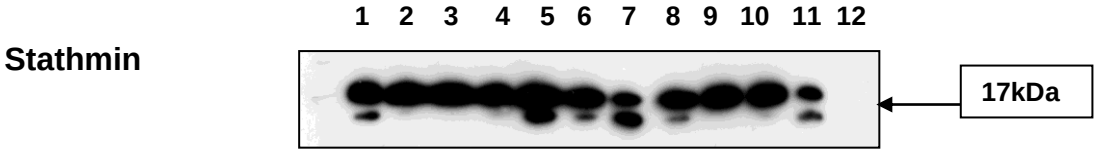


**Figure 5.56**. Western blot of Stathmin expression in taxane resistant cell lines. Lysates from the following cell line were loaded into lanes 1 to 11 as follows. Lane 1: MDA-MB-231 Native, Lane 2: MDA-MB-231 5nM PACR, Lane 3 MDA-MB-231 25nM PACR, Lane 4 MDA-MB-231 50nM PACR, Lane 5: ZR75-1 Native, Lane 6: ZR75-1 5nM DOCR Lane 7: 25nM DOCR, Lane 8: ZR75-1 50nM DOCR Lane 9: ZR75-1 5nM PACR, Lane 10: ZR75-1 25nM PACR, Lane 11: ZR75-1 50nM PACR. Band is detected at 19KDa (abcam - ab52630 1:50000.)

The transcription factor YY1 has been shown to increase resistance to taxanes when knocked down, suggesting that it may be a potential marker of taxane sensitivity[247]. However, intriguingly in the PACR MDA-MB-231 cell lines there is a marked increase in expression of YY1 when compared to the native lines. This pattern is not seen in either of the taxane resistant ZR75-1 cell lines, suggesting that this potential taxane resistant biomarker may be exclusive in the MDA-MB-231 line (figure 5.57.)

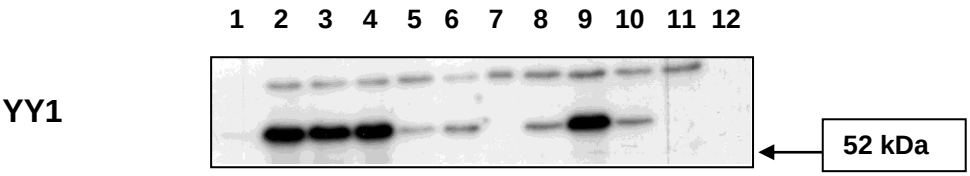


**Figure 5.57**. Western Blot of YY1 in taxane resistant cell lines. Lysates from the following cell line were loaded into lanes 1 to 11 as follows. Lane 1: MDA-MB-231 Native, Lane 2: MDA-MB-231 5nM PACR, Lane 3 MDA-MB-231 25nM PACR, Lane 4 MDA-MB-231 50nM PACR, Lane 5: ZR75-1 Native, Lane 6: ZR75-1 5nM DOCR Lane 7: 25nM DOCR, Lane 8: ZR75-1 50nM DOCR Lane 9: ZR75-1 5nM PACR, Lane 10: ZR75-1 25nM PACR, Lane 11: ZR75-1 50nM PACR. Band detected at 58 KDa. (abcam - ab 43058, diluted 8.3µl in 5ml)

Figure 5.58 show the β-Actin loading control blots for each of the blots shown in figures 5.49-5.56. The blots show even loading of protein in all lanes.

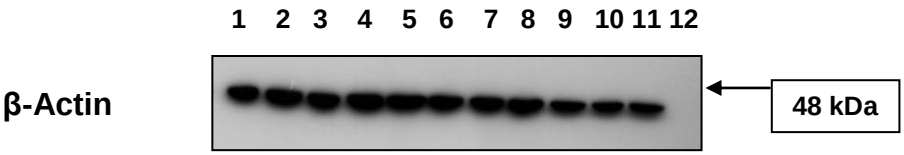


**Figure 5.58** Western blot of β-Actin expression in taxane resistant cell lines. β-Actin is used as a loading control. Lysates from the following cell line were loaded into lanes 1 to 11 as follows. Lane 1: MDA-MB-231 Native, Lane 2: MDA-MB-231 5nM PACR, Lane 3 MDA-MB-231 25nM PACR, Lane 4 MDA-MB-231 50nM PACR, Lane 5: ZR75-1 Native, Lane 6: ZR75-1 5nM DOCR Lane 7: 25nM DOCR, Lane 8: ZR75-1 50nM DOCR Lane 9: ZR75-1 5nM PACR, Lane 10: ZR75-1 25nM PACR, Lane 11: ZR75-1 50nM PACR. (β-Actin band is detected at 42kDa.)

**5.6. Summary of Data from aCGH, transcriptomic microarray, qPCR and Western data.**

All the genomic and transcriptomic array, q-PCR and western data from each cell line was then constructed into three tables (table 5.5-5.7.)

| Gene Name | Gene Location | Lost or Gained (aCGH) | ↑ or ↓ with ↑ PACR? (ILMN) | ↑ or ↓ with ↑PACR? (qPCR) | ↑ or ↓ with ↑ PACR? (Prot) |
|---|---|---|---|---|---|
| 1. CD33 | 19q13.3 | L | ↑ | ↑ | N/A |
| 2. COBL | 7q12.1 | ↔ | ↑ | PF | N/A |
| 3. CLDN1 | 3q28-9 | ↔ | ↑ | PF | N/A |
| 4. IL7R | 5p13 | ↔ | ↑ | ↔ | N/A |
| 5. NLRP2 | 19q13.42 | L | ↑ | ↑ | N/A |
| 6. PAGE5 | Xp11.21 | L | ↓ | PF | N/A |
| 7. PI3 | 20q12-13 | ↔ | ↑ | ↑ | N/A |
| 8. PPP1R14C | 6q24.3-25.3 | ↔ | ↑ | ↑ | N/A |
| 9. TRPV4 | 12q24.1 | ↔ | ↓ | PF | N/A |
| 10. TSPAN8 | 12q14.1-21.1 | G* | ↑ | ↑ | N/A |
| 11. RGS16 | 1q25-q31 | ↔ | ↑ | ↑ | N/A |
| | | | | | |
| 1. ALDH1A3 | 15q26.3 | ↔ | ↑ | ↑ | N/A |
| 2. AMPH | 7p14-p13 | ↔ | ↑ | ↑ | N/A |
| 3. CCND2 | 12p13 | G | ↑ | ↑ | N/A |
| 4. CYP1B1 | 2p21 | ↔ | ↑ | PF | N/A |
| 5. FBP1 | 9q22.3 | ↔ | ↓ | ↓ | N/A |
| 6. FOXA2 | 20p11 | ↔ | ↑ | ↔ | N/A |
| 7. FOXF2 | 6p25.3 | L | ↓ | ↓ | N/A |
| 8. ID2 | 2p25 | G | ↑ | ↑ | N/A |
| 9. ID3 | 1p36.13-12 | L | ↑ | ↑ | N/A |
| 10. IL11 | 19q13.3-4 | L | ↓ | ↓ | N/A |
| 11. MAL2 | 8q23 | G | ↑ | ↑ | N/A |
| 12. MAPK13 | 6p21.31 | ↔ | ↓ | ↓ | N/A |
| 13. TGFBR3 | 1p33-p32 | ↔ | ↑ | ↑ | N/A |
| 14. TSPAN13 | 7p12.1 | ↔ | ↑ | ↑ | N/A |
| 15. SCN11A | 12p13 | ↔ | ↑ | ↔ | N/A |
| | | | | | |
| 1. ER | 6q25.1 | ↔ | ↔ | ↑ | ↔ |
| 2. EGFR | 7p11.2-q12 | ↔ | ↑ | N/A | ↑ |
| 3. HER-2 | 17q11.2-q12 | ↔ | ↔ | N/A | ↔ |
| 4. HER-3 | 12q13 | ↔ | ↔ | N/A | ↔ |
| 5. AURKA | 20q13 | G** | ↑** | ↔ | ↔ |
| 6. MDR-1 | 7q21.12 | ↔ | ↔ | ↑ | ↔ |
| 7. STATHMIN | 1p36.11 | L | ↓ | PF | ↔ |
| 8. YY-1 | 14q | ↔ | ↑ | PF | ↑ |

**TABLE 5.5.** Summary - MD-MB-231, genomic, transcriptomic, qPCR, Western data. C1: Gene, C2: Gene Location, C3: aCGH, C4:Illumina microarray, C5: Westerns. Genes 1-11: dysregulated in all PACR MDA-MB-231 cell lines. Genes 1-14: Genes with consistent patterns of ↑ **or** ↓ with ↑ PACR, Genes 1-8 determined by extensive literature search. **G**= Gain, **L**=Lost. ↑ **=** increased, ↓ = decreased, ↔ = unchanged or variable with ↑, **N/A** = Not assessed, **PF**: Primer Failed or unavailable. * If gained (**G**) is amplified, if lost (**L**) is deleted. ** = Only in MDA-MB-231 100nM PACR.

| Gene Name | Gene Location | Lost or Gained (aCGH) | ↑ or ↓ with ↑ PACR ILMN? | ↑ or ↓ with ↑ PACR qPCR? | ↑ or ↓ with ↑ PACR Protein? |
|---|---|---|---|---|---|
| **1. CD33** | **19q13.3** | ↔ | **N/A** | ↔ | **N/A** |
| **2. COBL** | **7q12.1** | **L** | **N/A** | ↔ | **N/A** |
| **3. CLDN1** | **3q28-9** | ↔ | **N/A** | **PF** | **N/A** |
| **4. IL7R** | **5p13** | ↔ | **N/A** | ↔ | **N/A** |
| **5. NLRP2** | **19q13.42** | ↔ | **N/A** | ↔ | **N/A** |
| **6. PAGE5** | **Xp11.21** | ↔ | **N/A** | **PF** | **N/A** |
| **7. PI3** | **20q12-13** | ↔ | **N/A** | ↔ | **N/A** |
| **8. PPP1R14C** | **6q24.3-25.3** | ↔ | **N/A** | ↔ | **N/A** |
| **9. TRPV4** | **12q24.1** | ↔ | **N/A** | **PF** | **N/A** |
| **10. TSPAN8** | **12q14.1-21.1** | ↔ | **N/A** | ↔ | **N/A** |
| **11. RGS16** | **1q25-q31** | **L** | **N/A** | ↔ | **N/A** |
| | | | | | |
| **1. ALDH1A3** | **15q26.3** | ↔ | **N/A** | ↔ | **N/A** |
| **2. AMPH** | **7p14-p13** | ↔ | **N/A** | ↔ | **N/A** |
| **3. CCND2** | **12p13** | **L** | **N/A** | ↔ | **N/A** |
| **4. CYP1B1** | **2p21** | ↔ | **N/A** | **PF** | **N/A** |
| **5. FBP1** | **9q22.3** | ↔ | **N/A** | ↔ | **N/A** |
| **6. FOXA2** | **20p11** | ↔ | **N/A** | ↔ | **N/A** |
| **7. FOXF2** | **6p25.3** | ↔ | **N/A** | ↔ | **N/A** |
| **8. ID2** | **2p25** | ↔ | **N/A** | ↔ | **N/A** |
| **9. ID3** | **1p36.13-12** | ↔ | **N/A** | ↔ | **N/A** |
| **10. IL11** | **19q13.3-4** | ↔ | **N/A** | ↔ | **N/A** |
| **11. MAL2** | **8q23** | ↔ | **N/A** | ↔ | **N/A** |
| **12. MAPK13** | **6p21.31** | ↔ | **N/A** | ↔ | **N/A** |
| **13. TGFBR3** | **1p33-p32** | ↔ | **N/A** | ↔ | **N/A** |
| **14. TSPAN13** | **7p12.1** | ↔ | **N/A** | ↔ | **N/A** |
| **15. SCN11A** | **12p13** | **L** | **N/A** | ↔ | **N/A** |
| | | | | | |
| **1. ERα** | **6q25.1** | ↔ | **N/A** | ↔ | ↔ |
| **2. EGFR** | **7p11.2-q12** | ↔ | **N/A** | **N/A** | ↔ |
| **3. HER-2** | **17q11.2-q12** | **L** | **N/A** | **N/A** | ↔ |
| **4. HER-3** | **12q13** | ↔ | **N/A** | **N/A** | ↔ |
| **5. AURKA** | **20q13** | ↔ | **N/A** | ↔ | ↔ |
| **6. MDR-1** | **7q21.12** | ↔ | ↑ | ↑ | ↑ |
| **7. STATHMIN** | **1p36.11** | ↔ | **N/A** | **N/A** | ↔ |
| **8. YY-1** | **14q** | ↔ | **N/A** | **N/A** | ↔ |

**TABLE 5.6.** Summary – ZR75-1 PACR, genomic, transcriptomic, qPCR, Western data. C1: Gene, C2: Gene Location, C3: aCGH, C4:Illumina microarray, C5: Westerns. Genes 1-11: dysregulated in all PACR MDA-MB-231 cell lines. Genes 1-14: Genes with consistent patterns of ↑ or ↓ with ↑ PACR, Genes 1-8 determined by extensive literature search. **G**= Gain, **L**=Lost. ↑ **=** increased, ↓ = decreased, ↔ = unchanged or variable with ↑, **N/A** = Not assessed, **PF**: Primer Failed or unavailable.

| Gene Name | Gene Location | Lost or Gained (aCGH) | ↑ or ↓ with ↑ DOCR ILMN? | ↑ or ↓ with ↑ DOCR qPCR? | ↑ or ↓ with ↑ DOCR Protein? |
|---|---|---|---|---|---|
| 1. CD33 | 19q13.3 | ↔ | N/A | ↑ | N/A |
| 2. COBL | 7q12.1 | L | N/A | ↑ | N/A |
| 3. CLDN1 | 3q28-9 | ↔ | N/A | PF | N/A |
| 4. IL7R | 5p13 | ↔ | N/A | ↑ | N/A |
| 5. NLRP2 | 19q13.42 | ↔ | N/A | ↑ | N/A |
| 6. PAGE5 | Xp11.21 | ↔ | N/A | PF | N/A |
| 7. PI3 | 20q12-13 | ↔ | N/A | ↑ | N/A |
| 8. PPP1R14C | 6q24.3-25.3 | ↔ | N/A | ↔ | N/A |
| 9. TRPV4 | 12q24.1 | ↔ | N/A | PF | N/A |
| 10. TSPAN8 | 12q14.1-21.1 | ↔ | N/A | ↔ | N/A |
| 11. RGS16 | 1q25-q31 | ↔ | | | |
| | | | | | |
| 1. ALDH1A3 | 15q26.3 | ↔ | N/A | ↔ | N/A |
| 2. AMPH | 7p14-p13 | ↔ | N/A | ↔ | N/A |
| 3. CCND2 | 12p13 | L | N/A | ↔ | N/A |
| 4. CYP1B1 | 2p21 | ↔ | N/A | PF | N/A |
| 5. FBP1 | 9q22.3 | ↔ | N/A | ↔ | N/A |
| 6. FOXA2 | 20p11 | ↔ | N/A | ↔ | N/A |
| 7. FOXF2 | 6p25.3 | ↔ | N/A | ↔ | N/A |
| 8. ID2 | 2p25 | ↔ | N/A | ↑ | N/A |
| 9. ID3 | 1p36.13-12 | ↔ | N/A | ↔ | N/A |
| 10. IL11 | 19q13.3-4 | ↔ | N/A | ↑ | N/A |
| 11. MAL2 | 8q23 | ↔ | N/A | ↑ | N/A |
| 12. MAPK13 | 6p21.31 | ↔ | N/A | ↔ | N/A |
| 13. TGFBR3 | 1p33-p32 | ↔ | N/A | ↔ | N/A |
| 14. TSPAN13 | 7p12.1 | ↔ | N/A | ↔ | N/A |
| 15. SCN11A | 12p13 | L | N/A | ↑ | N/A |
| | | | | | |
| 1. ERα | 6q25.1 | ↔ | N/A | ↔ | ↔ |
| 2. EGFR | 7p11.2-q12 | ↔ | N/A | N/A | ↔ |
| 3. HER-2 | 17q11.2-q12 | ↔ | N/A | N/A | ↔ |
| 4. HER-3 | 12q13 | ↔ | N/A | N/A | ↔ |
| 5. AURKA | 20q13 | ↔ | N/A | ↔ | ↔ |
| 6. MDR-1 | 7q21.12 | ↔ | ↑ | ↑ | ↑ |
| 7. STATHMIN | 1p36.11 | ↔ | N/A | N/A | ↔ |
| 8. YY-1 | 14q | ↔ | N/A | N/A | ↔ |

**TABLE 5.7.** Summary – ZR75-1 DOCR, genomic, transcriptomic, qPCR, Western data. C1: Gene, C2: Gene Location, C3: aCGH, C4: Illumina microarray, C5: Westerns. Genes 1-11: dysregulated in all PACR MDA-MB-231 cell lines. Genes 1-14: Genes with consistent patterns of **c** or ↓ with ↑ PACR, Genes 1-8 determined by extensive literature search. **G**= Gain, **L**=Lost. ↑ **=** increased, ↓= decreased, ↔ = unchanged or variable with ↑, **N/A** = Not assessed, **PF**: Primer Failed or unavailable.

# Chapter 6

## Results:

### Illumina Gene Expression data from Frozen Tissue from the LAPATAX trial

## 6.1 A transcriptomic analysis of material from the LAPATAX trial using illumina arrays.

Tumour material from the LAPATAX trial was provided for extraction and expression on illumina arrays. Details of the dose escalation phase and phase II study of the LAPATAX trial are detailed in figure 6.1 and 6.2 respectively. Further information on how samples were received and stored, extracted amplified and hybridised to the illumina arrays are detailed in section 2.4.

Having clinical material available from the LAPTAX trial allowed it to be determined whether what was observed *in vitro* in the taxane resistant cell lines mirrored what occurs *in vivo* in breast tumours treated with taxanes.

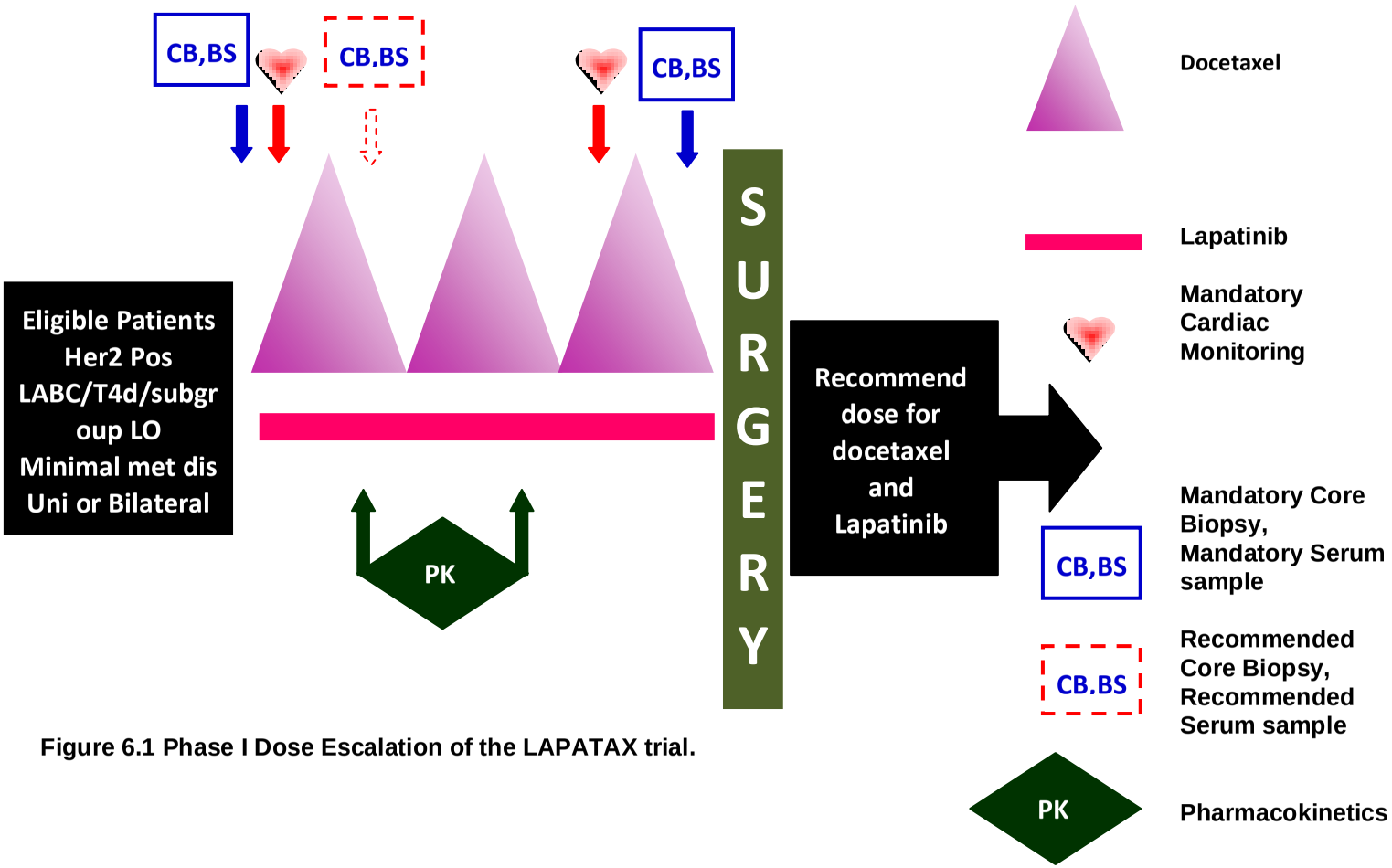


**Figure 6.1 Phase I Dose Escalation of the LAPATAX trial.**

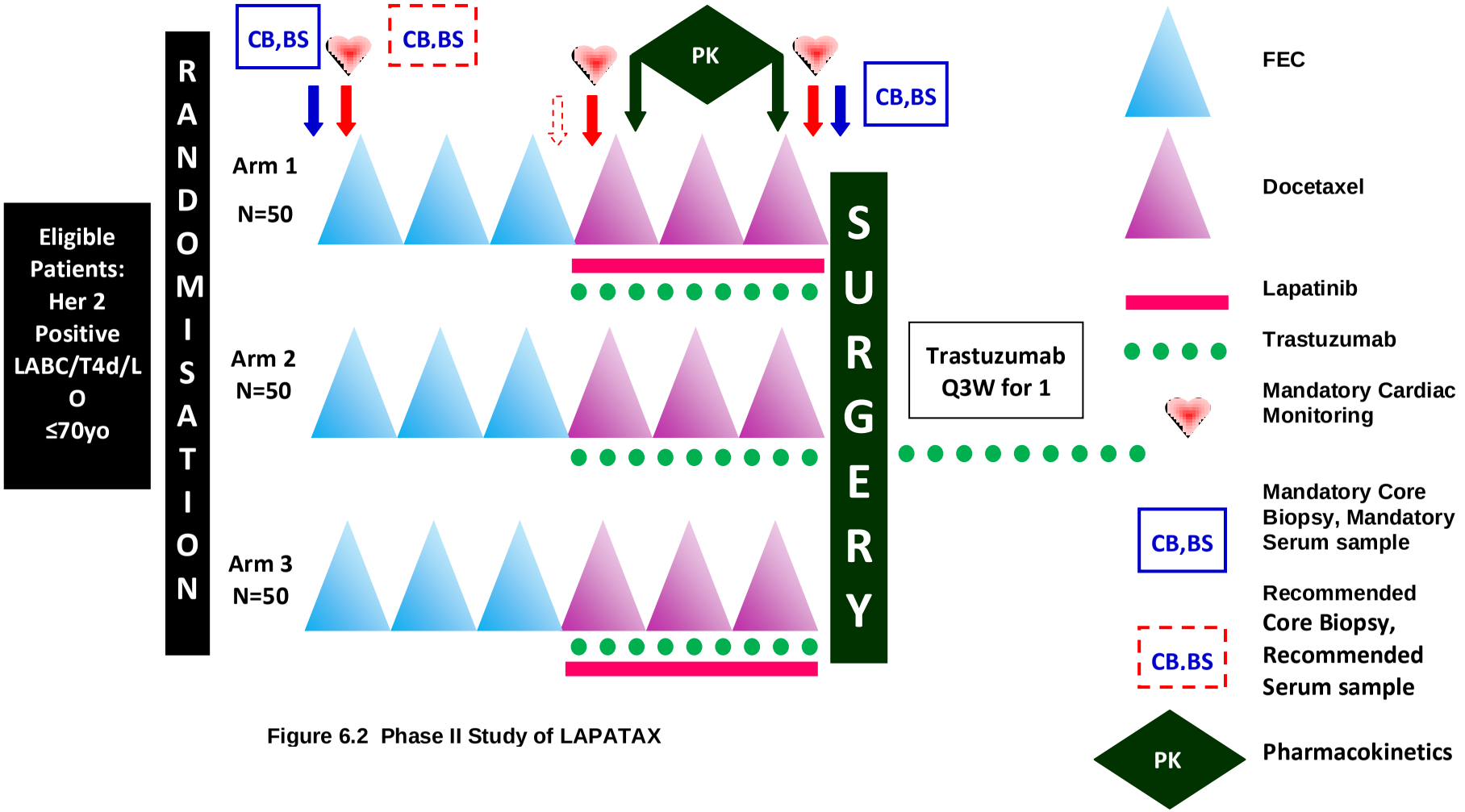


Figure 6.2 Phase II Study of LAPATAX

A total of 32 tumour samples were received from the LAPATAX trial. 22 of these samples were matched pairs of pre and post treatment samples. Of these samples 19 pre samples and 10 post samples were successfully extracted, amplified and hybridised to the array. There were 9 matched pre and post pairs.

The successfully extracted samples are shown in table 6.1 below. 3 UHRRs in duplicate were included as controls for the experiment. The matched pairs of pre and post samples are the most interesting and valuable to the investigation as they allowed the changes in gene expression to be tracked with taxane treatment.

| Pre sample | Post sample |
|---|---|
| **Pre 1** | **Post 1** |
| **Pre 2** | **Post 2** |
| **Pre 3** | **Post 3** |
| **Pre 4** | **Post 4** |
| **Pre 5** | **Post 5** |
| **Pre 6** | **Post 6** |
| Pre 7 | |
| **Pre 8** | **Post 8** |
| **Pre 9** | **Post 9** |
| Pre 10 | |
| Pre 11 | |
| Pre 12 | |
| Pre 13 | |
| Pre 14 | |
| Pre 15 | |
| Pre 16 | |
| **Pre 17** | **Post 17** |
| Pre 18 | |
| Pre 19 | |
| | Post 20 |

**Table 6.1.** This table lists the samples from the LAPATAX trial that were successfully extracted, amplified and hybridised to illumina arrays. Samples with both pre and post pairs are highlighted in bold.

The resulting data was analysed using R (with the help of Andy Simms.) Figure 6.3 shows box plots of un-normalised (top) and normalised data (bottom) using the amplitude of the signal on the illumina represented as box plots. This normalisation allowed any chip to chip variation to be corrected. These normalisation methods make the data more robust.

## Pre-normalisation

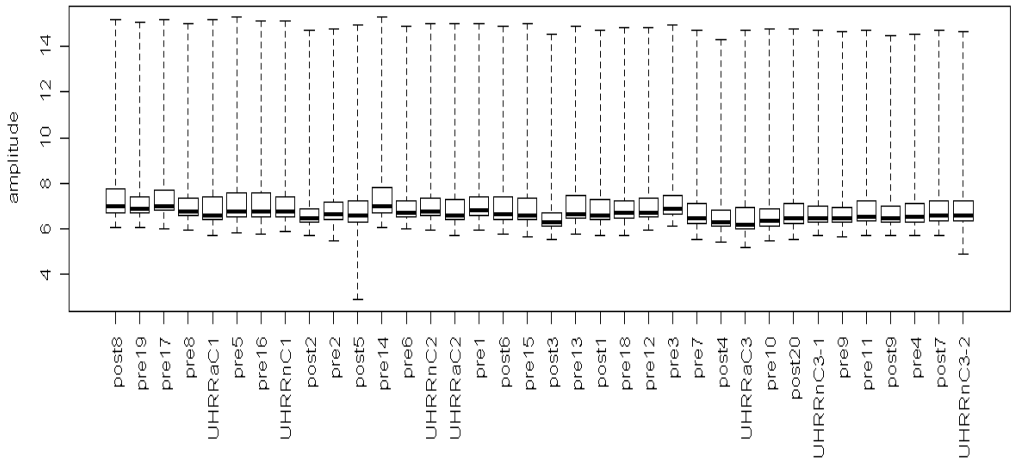


## Post-normalisation

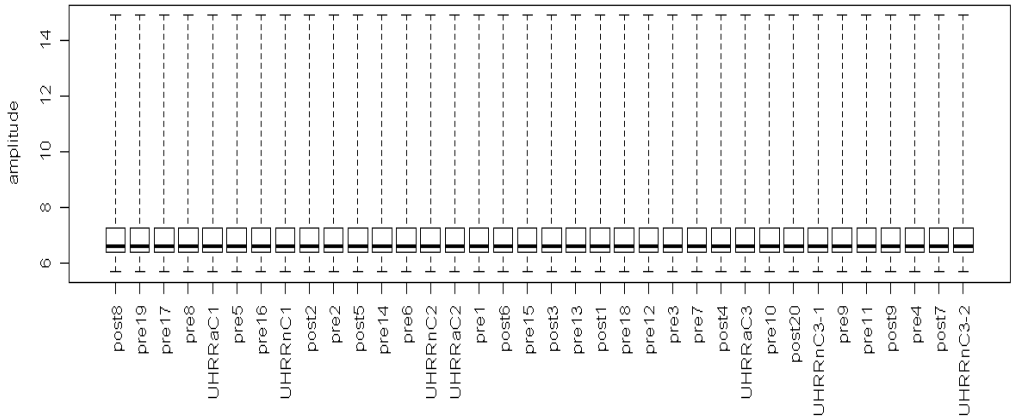


**Figure 6.3.** Box plots of signal intensity amplitude from illumina microarrays using samples from the LAPATAX trial. Top panel represents un-normalised data and the bottom panel represents the normalised data.

Figure 6.4 shows the entire panel of normalised data from the LAPATAX trial including the 3 UHRR controls in duplicate. UHRRs are used as interbatch calibrators to allow the generation of

more robust gene expression profiles[252]. The replicates of each of the UHRRs cluster together. UHRRs replicates were run on separate chips and in separate runs, so this clustering suggests that there is no evidence of clustering of samples according to which batch/chips the samples were run on.

The post samples formed three clusters, two of which cluster near one another. The pre samples formed three clusters, two of which are near one another, although there is one outlying sample: pre8.

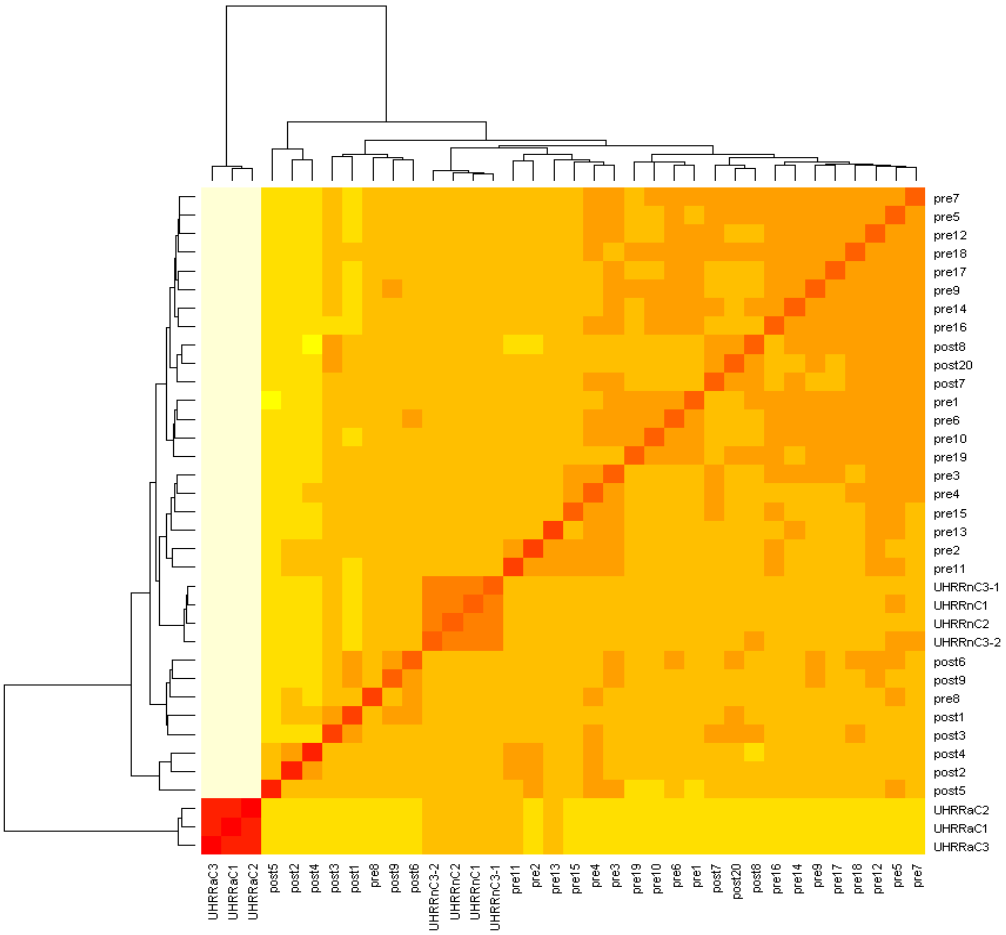


**Fig 6.4**. Heat map of illumina data using material from the LAPATAX trial, normalised using R. Along the right hand and the bottom edges the heat maps are each of the samples and along the left hand and top edge hierarchical tree clustering linking the most similar clones. The red and orange boxes indicate clones on the array where samples have the highest similarity and the pale yellow and white boxes represent the samples with the least similarity.

Figure 6.5 shows the heat map of normalised LAPATAX data excluding the UHRR samples. The LAPATAX samples formed the same clusters.

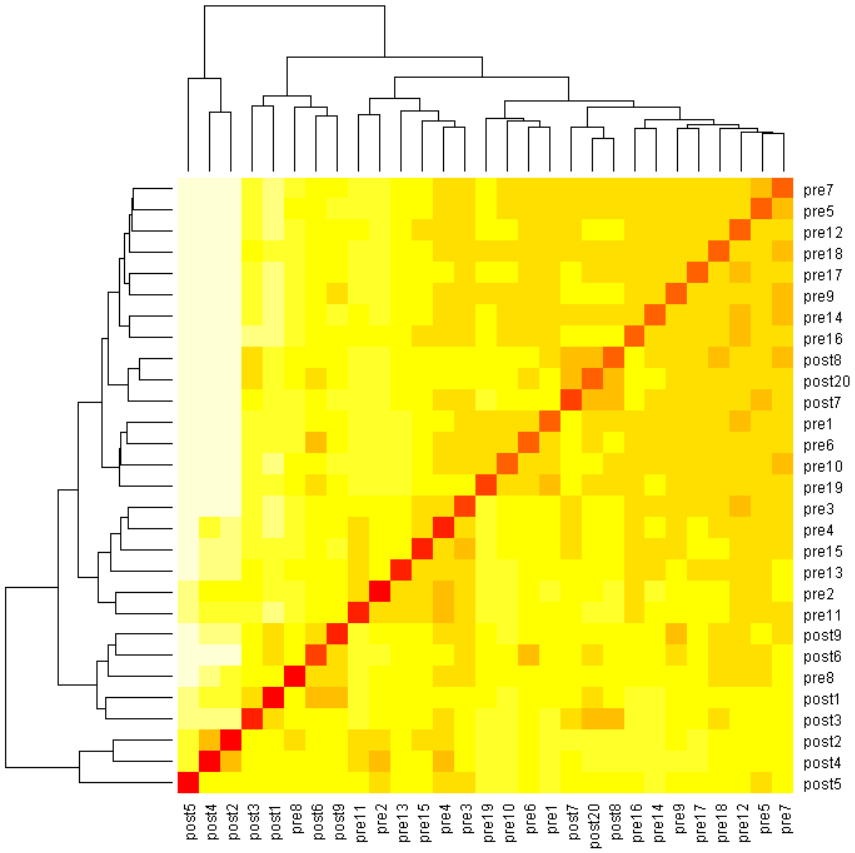


**Fig 6.5**. Heat map of illumina data using material from the LAPATAX trial, normalised using R. This heat map excludes the UHRR replicate control samples. Along the right hand and the bottom edges the heat maps are each of the samples and along the left hand and top edge hierarchical tree clustering linking the most similar clones. The red and orange boxes indicate clones on the array where samples have the highest similarity and the pale yellow and white boxes represent the samples with the least similarity.

Figure 6.6 shows two multidimensional scaling plot using the 500 most variable genes detected using the LAPATAX samples on the illumina arrays. The MDS plots show the dissimilarities between samples. The left hand plot shows the three chips used in the illumina experiment and how each of the twenty nine samples are dispersed over the three chips in terms of their

dissimilarity to one another. Samples on chips one are shown by the navy rhombuses, samples on chip two are shown by the pink squares and samples on chip three are shown by the green triangles. The samples do not cluster according to according to what chip they were run on so it can be concluded that the normalisation methods have eliminated any chip to chip variation.

The MDS plot on the right hand side of figure 6.6 show the same samples, this time labelled according to whether they are pre or post treatment. The pre samples are shown as navy rhombuses and the post samples are shown as pink squares. The pre and post samples tend to cluster together separately.

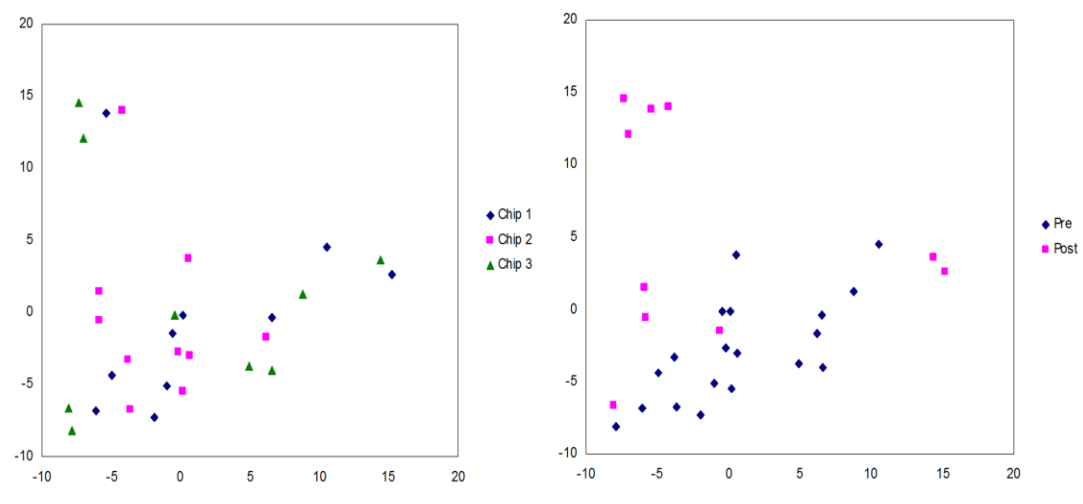


**Figure 6.6.** Multidimensional scaling plots using the 500 most variable genes identified using the LAPATAX samples on the illumina microarrays. The left hand plot shows each of the 29 samples on the three chips. Chip 1 – Navy rhombuses, Chip2 – Pink squares, Chip 3 – Green Triangles. The right hand plot shows the same samples showing whether they were pre or post treatment. Pre samples Navy rhombuses, Post samples – pink squares.

Figure 6.7 shows a heat map of the 500 most variable genes identified using the LAPATAX samples on the illumina arrays. ESR1 and TFF1/2 were identified as the genes showing the highest degree of variability across the panel of samples.

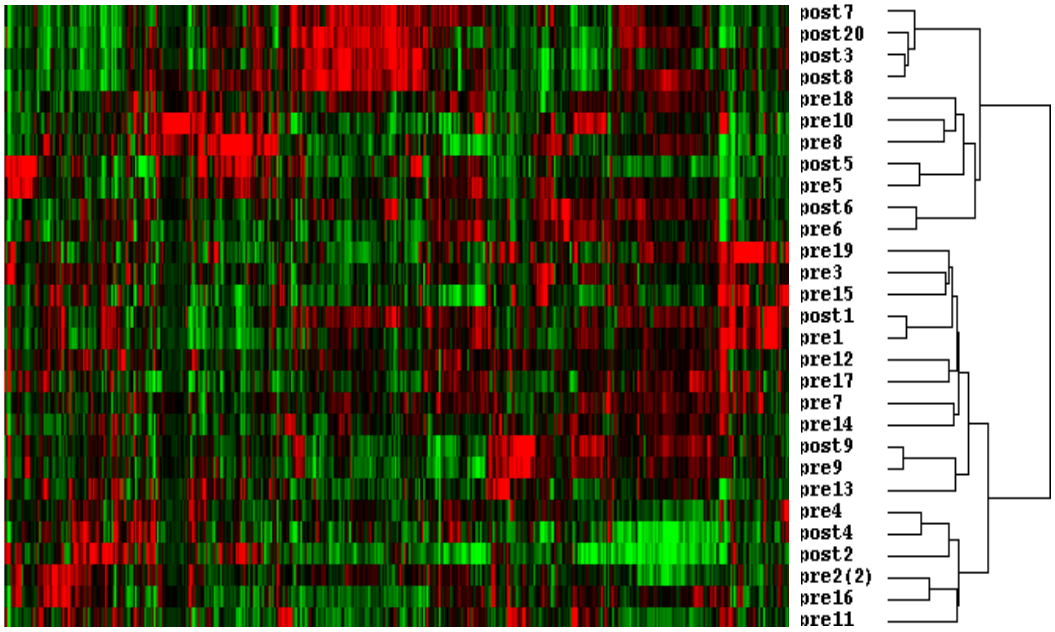


**Figure 6.7** Heat map of the 500 most variable genes identified using the 29 samples from the LAPATAX trial on the illumina arrays. The clusters are shown on the right hand side of the diagram. Red areas show high expression of a particular gene in a particular sample and green areas show low expression of a particular gene in a particular sample.

A SAM analysis was then conducted upon the data. A score was assigned to each gene which was calculated according to the change in gene expression relative to the SD of repeated measurements, this was then used to calculate a false discovery rate[253]. A SAM (significance analysis of microarrays) analysis is a statistical technique which identifies significant genes by carrying out gene specific t tests to ascertain the strength of the relationship between gene expression and a response variable[254,255]. When using only two groups of samples; pre and post treatment the SAM analysis is performed using a t test like statistic for each probe on the array. Two plots resulting from the SAM analysis are shown in figure 6.8.

The plot on the left hand side of figure 6.8 shows how the FDR in the experiment falls as Δ (the change in gene expression) increases. The plot on the right hand side of figure 6.8 shows the Δ (change in gene expression) versus the number of significant genes. As the Δ (change in gene expression) increases the number of significant genes decreases.

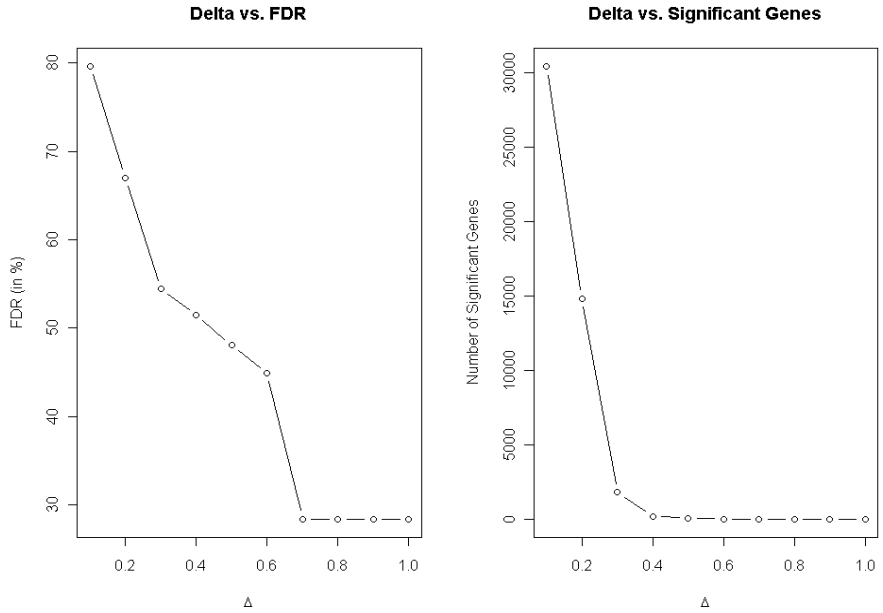


**Figure 6.8**. SAM analysis conducted on the data set of samples from the LAPATAX trial expressed on illumina arrays. The circles punctuated along the line on the graph increase with 0.1 each time. The plot on the right shows Δ (change in expression) plotted along the X axis against the FDR or False discovery rate up the Y axis. The plot on the right hand side shows Δ (change in gene expression level) on the X axis versus the number of genes.

Figure 6.9 shows each of the 9 paired samples (9 pre and post pairs) FDR vs. number of differentially expressed genes. As the differentially expressed genes increases, FDR increases.

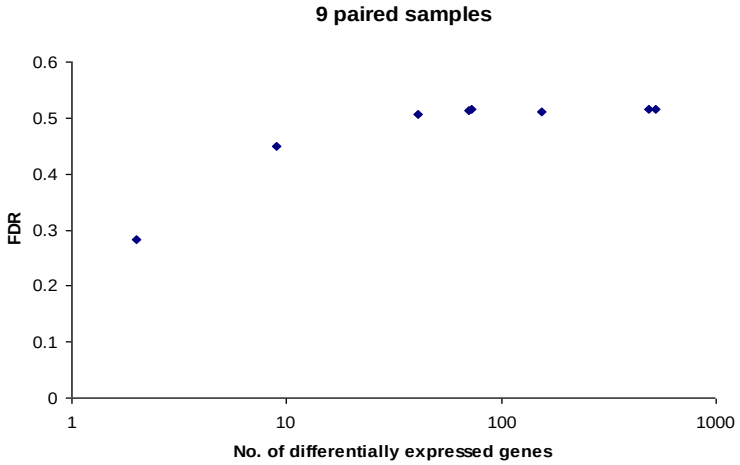


**Figure 6.9.** Sam analysis: plot shows The FDR up the Y axis Versus the No. of differentially expressed genes along the axis. The 9 paired samples (with both pre and post samples)

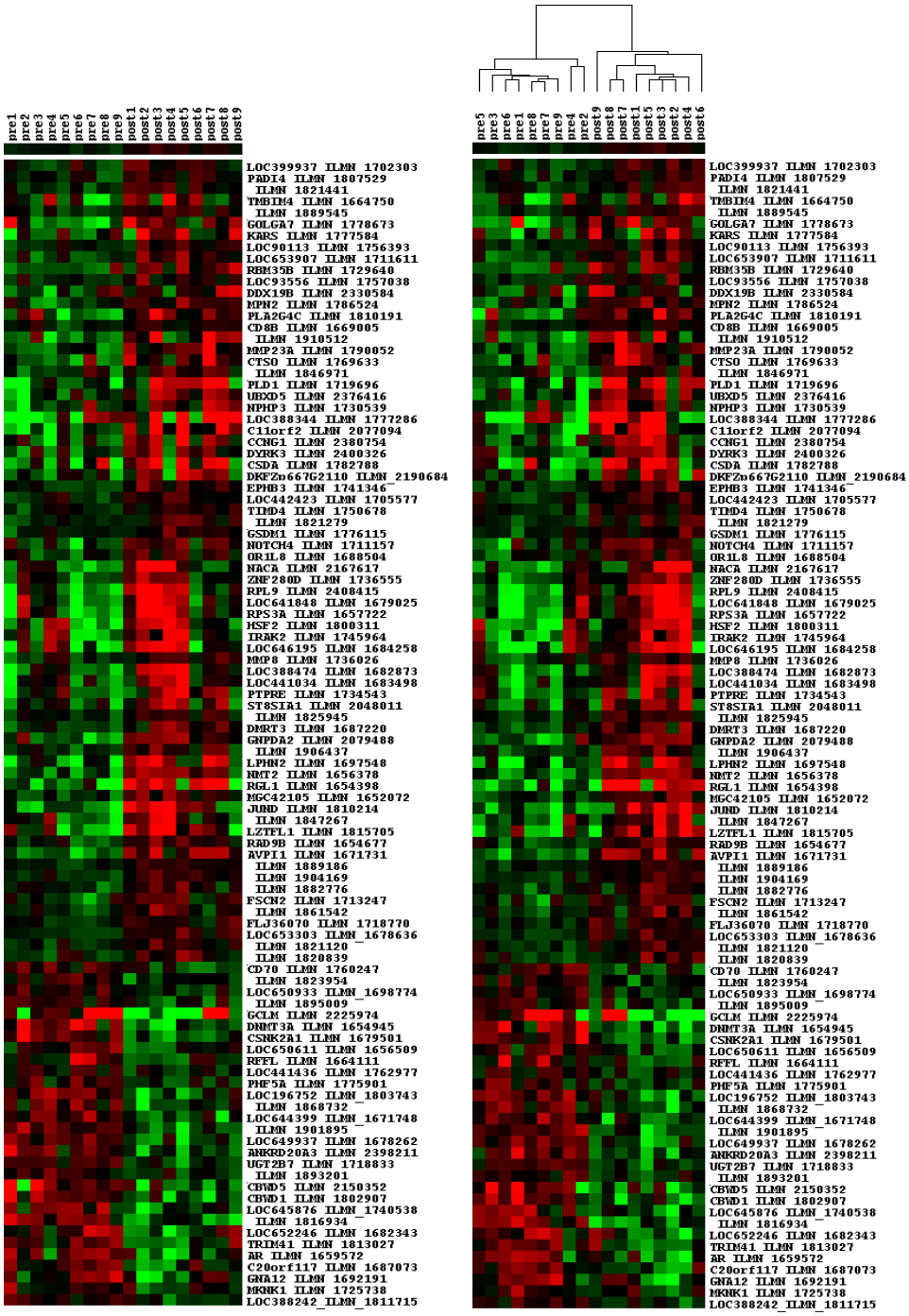


**Figure 6.10** Heatmaps of the 9 paired pre and post samples from the LAPATAX trial. The heat map on the left is the heat map shown without the cluster dendrograms; from left to right the samples are listed in numerical order, with the pre samples first followed by the post samples. The heat map on the right shows the same data with the cluster denodrograms. The red boxes show genes with high expression and the green boxes show genes with low expression. The black boxed show genes where the expression remains unchanged. Each of the genes are listed down the right hand side of each heat map listing either the gene name or the illumina probe number.

Figure 6.10 shows the heat maps of the 9 paired samples (pre and post pairs) from the LAPATAX trial. The heat map on the left shows each of the samples un-clustered listed in numerical order and the heat map on the right shows the same set of samples clustered according to their similarity to one another. The pre samples and the post samples cluster together separately.

There are areas in the heat map in which most of the pre samples are high expressers and most of the post samples are low expressers of particular genes and vice versa. However, the borders between high and low expression in the pre and post samples were not always clearly delineated.

Figure 6.11 shows a heat map including all 29 samples from the LAPATAX trial on the illumina array. The samples are clustered with dendrograms. All the post samples cluster with one another and all the pre samples apart from two: pre 13 and pre 18. Pre 13 and pre 18 both form another cluster with one post sample and this cluster is a part of a large cluster of post samples. However, the two pre samples in the post cluster do cluster towards the “pre side” of the heat map.

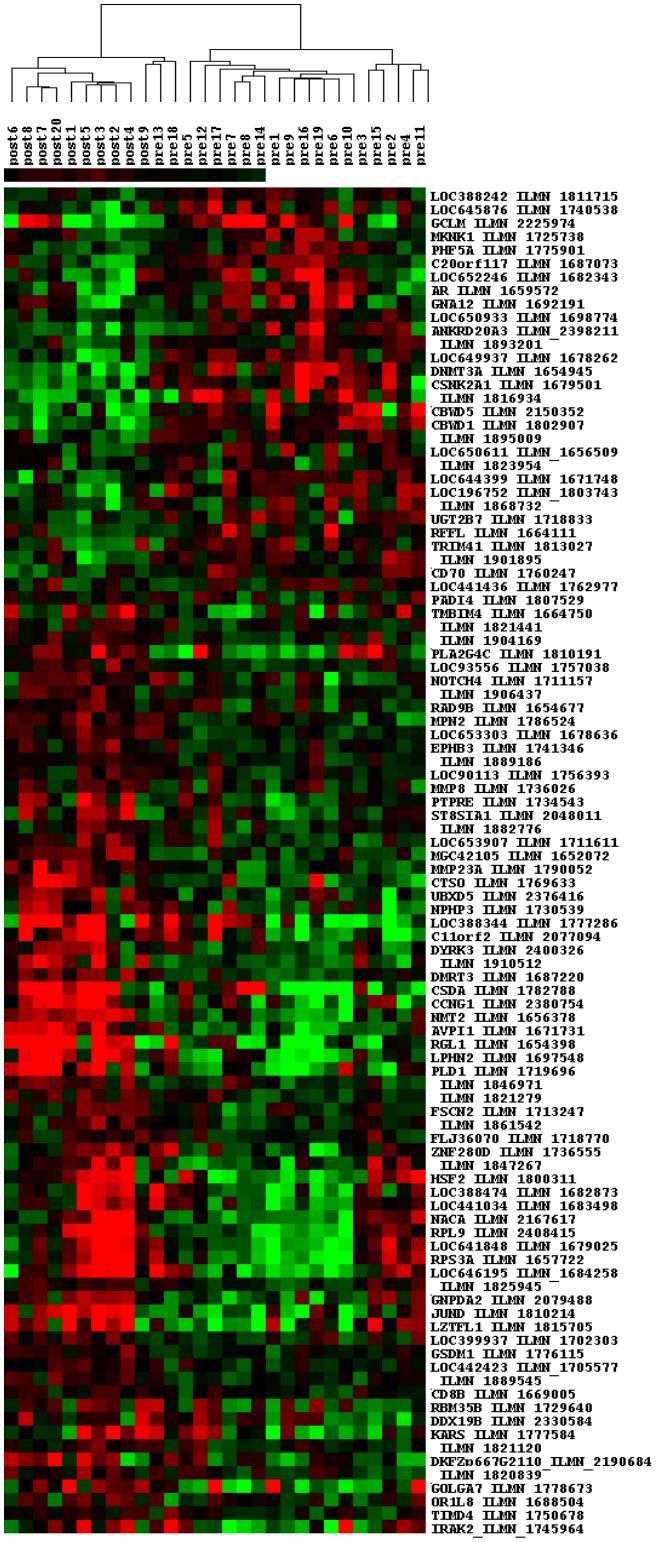


**Figure 6.11** Shows a heat map of the entire data set from the 29 samples from the LAPATAX trial using illumina microarrays. The red boxes show genes with high expression and the green boxes show genes with low expression. The black boxed show genes where the expression remains unchanged. Each of the genes are listed down the right hand side of each heat map, listing either the gene name or the illumina probe number.

Finally, the 9 matched pairs of pre and post samples were looked at and heat maps that mapped the changes between the pre and the post samples were constructed. These changes are shown in the heat map in 6.12. Genes that were of interest were those that showed a consistent pattern of change in gene expression.

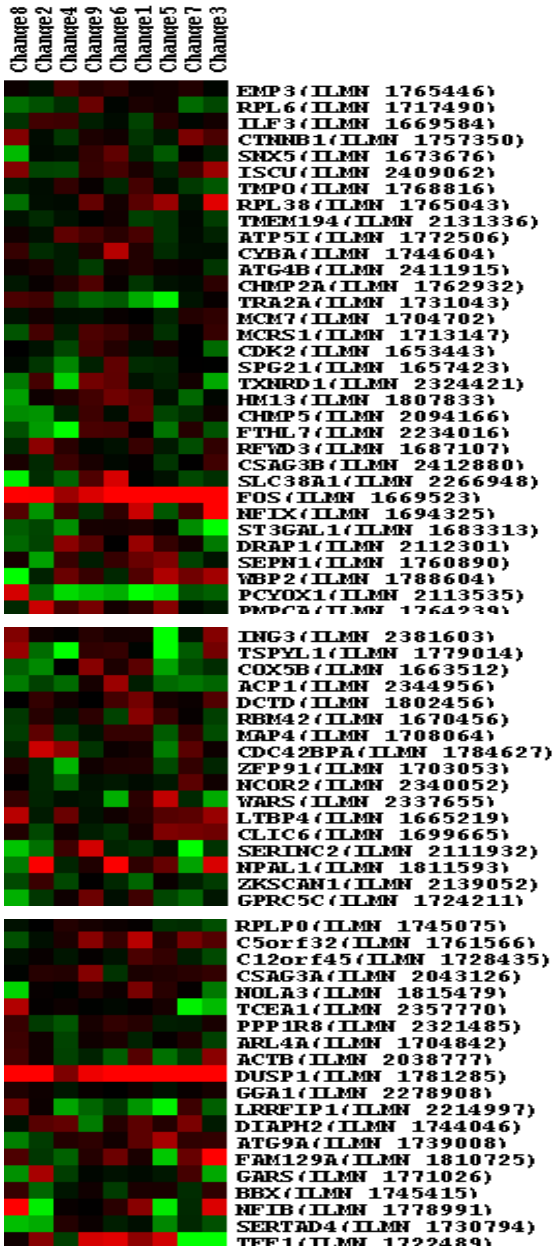


**Figure 6.12** Clustered heat maps of change in gene expression in 9 matched pre and post treatment pairs from the LAPATAX trial. Genes listed down the right handside with illumina probe number. High gene expression is shown by the red boxes, low gene expression is shown by the green boxes and black boxes are where expression remains unchanged

Figure 6.12 does not show the entirety of the heat map of all the most variable genes detected on the array. The three segments relate to other heat maps from illumina data using RNA from the panel of 11 taxane resistant cell lines which are shown together in figure 6.13.

## 6.2 Assessment of gene ontological pathways identified in taxane treated clinical samples from the LAPATAX trial.

The gene ontological pathways involved in the genes identified with taxane treatment in the LAPATAX samples were investigated[256]. The DAVID online resource was utilised to perform a gene functional classification on the LAPATAX gene lists[256] the gene list identified in figure 6.10 which shows the gene changed in the LAPATAX samples following treatment was used and analysed with DAVID to categorise the genes in to functionally similar groups. The gene functional analysis was performed on the gene list from figure 6.10 using a medium classification stringency level and identified 2 gene groups shown in table 6.2. and 6.3.

An enrichment score was determined for the two groups of genes which ranks the biological significance of each gene group. The enrichment score is determined by ascertaining the geometric mean of the *p* values of each member in the gene cluster using a –log scale.

| Gene Group 1:Kinases | ILMN_Probe |
|---|---|
| Serine/threonine kinase protein NIM1 | 1652072 |
| Casein kinase 2 | 1679501 |
| EPH receptor B3 | 1741736 |
| COBW domain containing 5 | 2150352/1802907 |
| MAP kinase interacting serine/threonine kinase 1 | 1725738 |
| COBW domain containing 6 | 1802907 |
| Dual Specificity tyrosine phosphorylation regulated kinase 3 | 2400326 |

**Table 6.2.** Gene group 1 from gene list in figure 6.10 using 9 paired samples from LAPATAX trial, Enrichment score is 1.2.

| Gene Group 2: Ribosomes | ILMN_Probe |
|---|---|
| Ribosomal protein L7a | 1682873/1683498 |
| Ribosomal protein L9 | 2408415 |
| Ribosomal Protein L13 | 1777286 |
| Ribosomal Protein S3A | 1657722 |

**Table 6.3.** Gene group 2 from gene list in figure 6.10 using 9 paired samples from LAPATAX trial. Enrichment score is 1.1.

The same analysis tool was then used with the combined gene list from the LAPATAX data and the gene list from the taxane resistant cell lines (this is detailed in figure 6.13) and identified 5 gene clusters shown in table 6.4-6.8.

| Gene Group 1: Ribonucleolar | ILMN_Probe |
|---|---|
| T-SPY like | 1779014 |
| ADP-ribosylation factor-like 4A | 1704842 |
| Microspherule protein 1 | 1713147 |
| NOP10 ribonucleoprotein homologue (yeast) | 18155479 |

**Table 6.4**. Gene group 1 from gene list in figure 6.13 using 9 paired samples from LAPATAX trial. Enrichment score is 2.4.

| Gene Group 2: Regulation of transcription | ILMN_Probe |
|---|---|
| Zinc finger with KRAB and SCAN domains 1 | 2139052 |
| Nuclear factorI/X (CCAAT-binding transcription factor) | 1694325 |
| Bobby-sox homologue (drosophila) | 1745415 |
| DR-1-associated protein 1 (negative cofactor 2 alpha) | 2112301 |
| Transcription elongation factor A (SII) | 2357770 |
| Leucine rich repeat (inFLII) interacting protein 1 | 2214997 |
| Nuclear factor I/B | 1778991 |
| Interleukin enhancer binding factor 3, 90kDa | 1669584 |
| Nuclear receptor co-repressor 2 | 2340052 |

**Table 6.5.** Gene group 2 from gene list in figure 6.13 using 9 paired samples from LAPATAX trial. Enrichment score is 1.8.

| Gene Group 3: Ribosomes | ILMN_Probe |
|---|---|
| Ribosomal protein L6 | 17171490 |
| Ribosomal protein L38 | 1765043 |
| Ribosomal protein Large | 1745075 |

**Table 6.6**. Gene group 3 from gene list in figure 6.13 using 9 paired samples from LAPATAX trial. Enrichment score is 1.8.

| Gene Group 4: Endosomes | ILMN_Probe |
|---|---|
| Golgi associated γ adaptin ear containing ARF binding protein 1 | 2278908 |
| Chromatin modifying protein 5 | 2094166 |
| Chromatin modifying protein 2 A | 1762932 |

**Table 6.7**. Gene group 4 from gene list in figure 6.13 using 9 paired samples from LAPATAX trial. Enrichment score is 1.5.

| Gene Group 5: Membranes | ILMN_Probe |
|---|---|
| NIPA like domain containing 1 | 1811593 |
| Epithelial membrane protein 3 | 1765446 |
| G-protein couples receptor family C group 5 member C | 1724211 |
| ATG9 autophagy | 1739008 |
| Histocompatability (minor) 13 | 1807833 |
| Serine incorporator 2 | 2111932 |
| Transmembrane protein 194A | 2131336 |

**Table 6.8**. Gene group 5 from gene list in figure 6.13 using 9 paired samples from LAPATAX trial. Enrichment score is 0.02.

In conclusion, 2 functional gene groups were identified from the list of most highly differentiated genes in the 9 paired samples from LAPATAX trial following treatment: a group of kinases and a group of genes involved in the ribosome. When combining the list of changed genes from the 9 paired samples from the LAPATAX trial and the genes identified at the highest level of taxane resistance in the panel of taxane resistant cell lines 5 functional gene groups were identified: a group of ribonuclear proteins, transcriptional regulators, Ribosomal, Endosomal and membrane proteins.

The same two gene lists were then used to construct a combined heat map and identify highly differentiated genes that were commonly dysregulated in the LAPATAX samples following treatment and the panel of taxane resistant cell lines at the highest taxane dose (50nM.)

## 6.3. Comparing data from the LAPATAX trial with data obtained from the transcriptomic analysis of the taxane resistant cell lines.

The data obtained from the LAPATAX trial was then investigated in the context of the transcriptomic experiments that were conducted using the panel of taxane resistant cell lines. A heat map was constructed using the data from section 5.4 (figure 5.49) and the illumina data from the LAPATAX trial. We compared the heat map looking at the overlap of the top 500 most

variable genes changed by 50nM treatment to the heat map with each of the 9 paired pre and post samples - un-clustered (according to similarity in gene expression levels), and the heat map that detailed the changes in gene expression in the 9 pairs post treatment.

The heat map using the data cell line illumina data recorded in section 5.4 (figure 5.49) and reproduced in figure 6.13 is split into three sections. The top section shows the overlap in the top 500 most variable genes changed by PACR treatment in both the MDA-MB-231 and ZR75-1 cell lines and by DOCR in the ZR75-1 alone. There are 33 genes in this section of the heat map. The middle section of the cell line heat map shows the overlap of the top 500 most variable genes that are changed by PACR in both the MDA-MB-231 and ZR75-1 cell lines. There are 17 genes in this section of the heat map. The bottom section of the cell line heat map shows the 500 most variable genes changed by PACR in the MDA-MB-231 cell line and DOCR in the ZR75-1. The cell line heat map was aligned with the corresponding parts of the heat map of un-clustered paired samples from the LAPATAX trial and the heat map mapping the changes between pre and post samples.

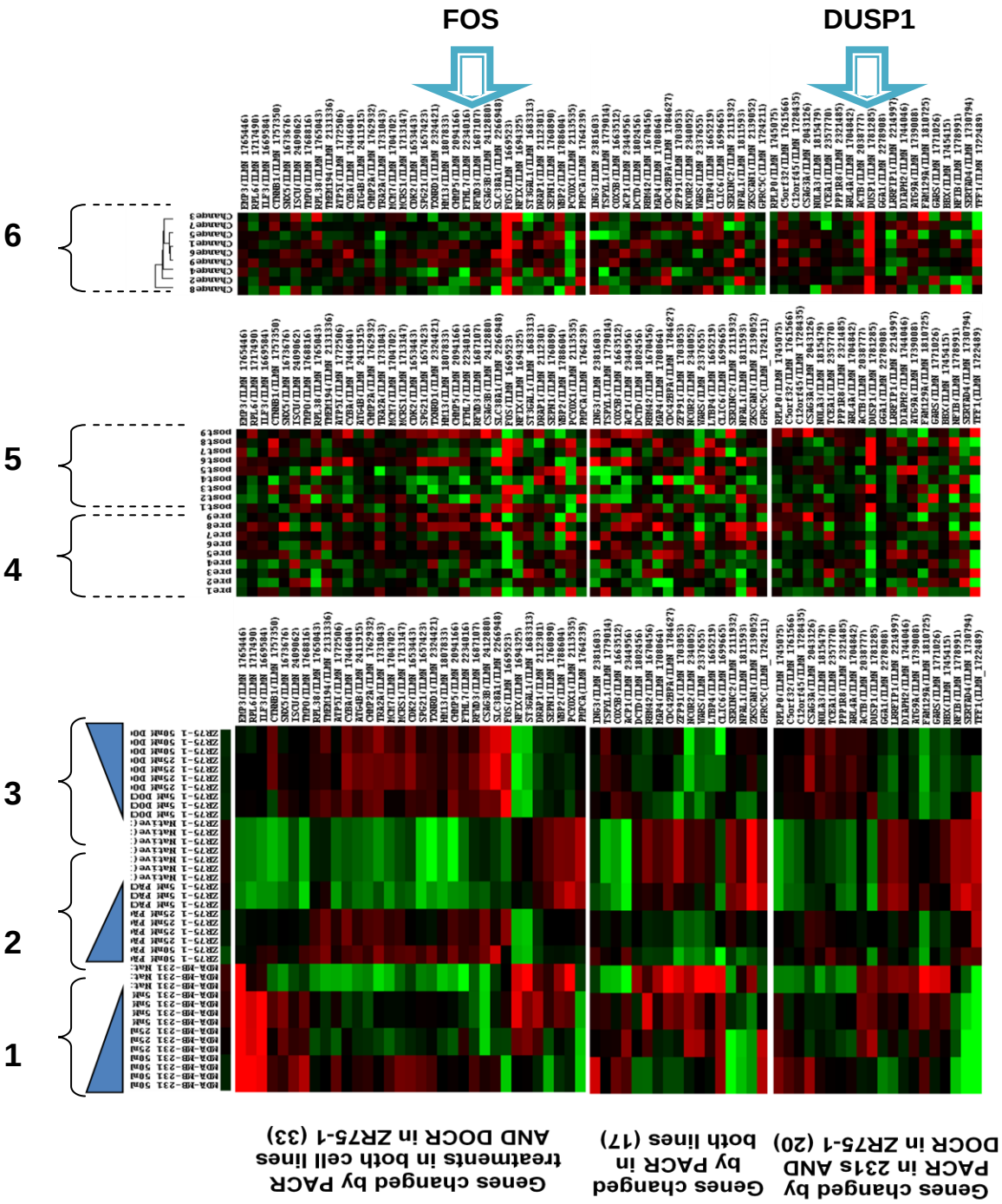


**Figure 6.13** 70 **o**verlapping genes of top 500 most variable genes in the taxane resistant cell lines at highest level of resistance (section 1-3), 9 paired samples unclustered (pre = section 4 and post section = 5), and the changes in gene expression from pre to post treatment (changes = section 6) from LAPATAX trial. Blue triangles show < taxane resistance level in cell lines with lowest level at the acute angled end. MDA-MB-231 cell lines (section 1), followed by the ZR75-1 PACR (section 2) and DOCR cell lines (section 3.) Genes are listed along the top edge of each heatmap. Red = high expression, green = low expression, black = unchanged expression level. Blue arrows indicate genes of interest – FOS and DUSP1.

## 6.4 Genes of interest identified by comparing data from the LAPATAX trial with data obtained from the transcriptomic analysis of the taxane resistant cell lines.

In figure 6.11 the large blue arrows indicate two genes of interest: FOS and DUSP1. These genes were selected as they show a consistent increase in expression in the 9 paired LAPATAX samples following treatment. These two genes were also found to be highly differentially expressed in the taxane resistant cell lines at the highest level of resistance 50nM. FOS is highly differentially expressed in all three of the taxane resistant cell lines at 50nM and DUSP1 is differentially expressed in the PACR MDA-MB-231 cells and the DOCR ZR75 cells

FOS (illumina probe number: 1669523) is one of the top 500 most variable genes overlapping in all three taxane resistant cell lines. Expression of FOS is higher in the MDA-MB-231 native and 5nM PACR cell lines than in the 25nM and 50nM PACR cell lines. In the ZR75-1 cell lines, expression of FOS is low on the native and 5nM PACR cells and higher in the 25nM and 50nM PACR and 5nM, 25nM and DOCR cells. There is increased expression of FOS in all 9 of the post treatment paired samples from the LAPATAX trial.

FOS is also known as FBJ osteosarcoma viral oncogene homologue, c-FOS or G0/G1 switch regulatory protein, it is located on 14q24.3 (www.genecards.org) which is very close to a region of loss in the MDA-MB-231 50nM. FOS is part of the AP-1 (activator protein 1) transcription factor dimeric complex which in addition contains member of the JUN, ATF and MAF families[257]. AP1 was identified over twenty years ago[258] and retroviral homologues of a number of components of AP-1, including FOS protein were discovered over 25 years ago[259]. c-FOS the human homologue of the viral oncoprotein v-FOS and, when over-expressed in mice it has been shown to cause osteosarcoma via the transformation of chondroblasts and osteoblasts[260,261].

AP-1 has been shown to regulate genes involved in cell proliferation, differentiation, apoptosis, and tumour invasion and can exert both oncogenic and antioncogenic effects by regulating its dimer composition, transcription, post-translational modification and interactions with other proteins[257]. As such it has been suggested that AP-1 may be a potential target for anticancer therapy[257]. One example of how components of AP-1 can function both oncogenically and anti-oncogenically in is that deletion of the oncogene C-Fos in Trp53 null mice cause the formation of high penetrance rhabdomyosarcomas, a tumour that is on very rarely seen in Trp53 mice[257].

c-FOS has been shown to cause the loss of polarity in mammary epithelial cells and induce EMT and in addition has been shown to promote invasive growth in collagen gels in vitro[262]. This behaviour has also been replicated *in vivo* as the progression of chemically induced papillomas to invasive squamous-cell carcinomas is impaired in c-Fos-deficient mice[263].

In prostate cancer cell lines, AP-1 has been implicated in the development of Androgen independent Prostate Cancer (AIPC) [264-269]. Formation of c-Jun/c-Jun or c-Jun/c-Fos dimers is activated via the phosphorylation of c-jun which is thought to be mediated by MAPK or protein kinase C[264].

DUSP1 (illumina probe: 1781285) is also one of the top 500 most variable gene overlapping the MDA-MB-231 50nM PACR and the ZR75-1 DOCR cell lines. There is low expression of DUSP1 in the ZR75-1 native, 5nM, 25nM and 50nM PACR cell lines and higher expression in the 5nM, 25nM and 50nM DOCR cells. There is higher expression of DUSP1 MDA-MB-231 native, 5nM, and 25nM PACR cells than in the MDA-MB-231 50nM PACR cells. There is increased expression of DUSP1 in all 9 of the post treatment paired samples from the LAPATAX trial.

DUSP1 (also known as MKP-1) is a dual specific phosphatase shown to regulate activity of MAPKs and is overexpressed in up to 80% of breast cancers including carcinoma *in situ* and metastatic carcinoma[270,271]. DUSP-1 has been implicated as a mediator of chemoresistance in breast cancer[272]. A paper by Small *et al* showed that overexpression of DUSP-1 has been shown to enhance the viability of breast cancer cell lines treated with paclitaxel, the anthracycline, doxorubicin and the alkylating agent, mechlorethamine[272].

Activation of glucocorticoid receptor with dexamethasone has been shown to induce expression of DUSP-1 and inhibit paclitaxel associated MAPK activation, contributing the survival of breast cancer cell lines[273]. The taxane resistant MDA-MB-231 also showed reduced expression of MAPK13 (re figures 5.31.) MAPK13 encodes p38δ MAPK, a component of the p38 MAPK family[274]. Another closely related member of this family, p38α has been implicated to be inhibited by the activity of DUSP1[274]. p38α has been suggested as a potential tumour suppressor gene as it has been shown to negatively regulate the progression of the cell cycle and induce apoptosis[275-277]. However, it has also been implicated as being involved in invasion, inflammation and angiogenesis, all of which play a role in the progression of cancer[274].

Intriguingly, in NSCLC DUSP-1 has been shown to enhance angiogenesis and promote metastasis and invasion[278]. In NSCLC H460 disruption of DUSP1 inhibited the ability of the cells to invade in matrigel, induce metastasis via tail vein injection and grow tumours in nude mice[278]. This is particularly interesting in the context of the MDA-MB-231 cell lines which showed decreased DUSP1 expression as paclitaxel resistance increased and the PACR MDA-MB-231 cell lines failed to grow as tumour xenografts in mice where the native cell succeeded (re figure 4.1-4.4.)

## 6.5 Potential Limitations of the transcriptomic analysis of data from the LAPATAX trial and the panel of taxane resistant cell lines.

Although the information that was gleaned regarding taxane resistance from observing the overlap of dysregulated genes in the panel of taxane resistant cell lines and from the LAPATAX trial is certainly intriguing, it is important to consider the limiting factors of this study.

The material available from the LAPATAX was limited; only 29 samples including 9 matched pre and post pairs. The trial samples were treated with docetaxel and the cell lines available were either docetaxel or paclitaxel, in addition the LAPATAX samples were also treated with lapatinib (dual tyrosine kinase inhibitor which acts on the HER2 growth receptor pathway[279]). Initially the trial samples that were made available were going to be from the phase II study, but due to a delay in the trial we were provided with samples from the dose escalation phase. This meant that the doses of docetaxel and lapatinib varied from sample to sample. Finally, although the LAPATAX samples were all HER2+ve, they were of mixed ER status.

Bearing in mind these pragmatic considerations it is important not underestimate the value of this clinical material. The LAPATAX samples have allowed the *in vitro* investigation to be brought into an *in vivo* setting and gain insight into the clinical behaviour and relevance of the model lines.

# Chapter 7

## Discussion

## 7.1 Mechanisms of resistance

Cancer is a complex group of heterogenic diseases that arise from uncontrolled growth resulting from accumulating mutations and epigenetic modifications in tumour suppressors and oncogenes[280,281]. Drug resistance can be de novo or acquired and the resistance can occur by a number of different mechanisms. Cancer cells can have a growth advantage over normal cells and as a consequence cancers cell can be clonally selected. This clonal selection goes hand in hand with a high mutation rate and the tumour environment selects variants of mutated tumour cells by favouring their growth[282]. Like tumourigenesis, the development of drug resistance evolves in a complex manner over a number of stages and both tumourigenesis and drug resistance show as strong association with genomic instability[316].

In a paper by Blagosklonny it was postulated that there are four different resistance mechanisms which were described as[282]; non-oncogenic resistance, oncogenic shift, conditionally non-oncogenic resistance and oncogenic resistance.

Non-oncogenic resistance is describes where natural processes such as metabolic pathways or efflux pumps may reduce drug response in cells with high levels of these proteins. For example when cytotoxic agents are expelled from cells using the efflux pump p-gyp (mdr-1) (figure 7.1), the growth arrest or death of the cell is avoided due to non-oncogenic resistance. In the case of p-glycoprotein (mdr-1) this is regarded as “non-specific” resistance via a non-oncogenic mechanism since multiple drugs are transported via the p-glycoprotein pump. Where altered expression of genes for example tubulin, lead to resistance specific to a class of drugs (taxane) this is regarded as specific resistance Oncogenic resistance is illustrated in figure 7.1 and, in the context of paclitaxel resistance in figure 7.2.

In some circumstances resistance mechanism can shift from non-oncogenic to oncogenic, this is termed, oncogenic shift[282]. An example of oncogenic shift is detailed in a study by Giannnakakou[140]. Paclitaxel resistant ovarian cancer cells which were resistant as a result of overexpression of p-gyp were cultured with paclitaxel and a p-gyp antagonist verapamil (figure 7.2), and in the process developed another mechanism of resistance by acquiring tubulin mutations[140]. Figure 8.2 shows that oncogenic shift can occur as a result of overexpression of components of cell death causing cells to become resistant to paclitaxel even if the drug successfully binds tubulin. Paclitaxel can still exert mitotic arrest even when the cell is resistant to paclitaxel via the overexpression of BCR-ABL, AKT or BCL-$A_L$[283] (figure 7.2.)

Conditionally non-oncogenic resistance can occur when the same genetic mutation occurs in differing cellular contexts[282]. For example the loss of p53 has actually been shown to cause a tumour inhibitory effect in transgenic mice that express epidermal targeted v-$ras^{Ha}$, v-fos or

human transforming growth factor α[284]. The cells achieve this by eliminating requirement for a "normal" oncogenic response to v-Ras by stopping the p53 induced apoptotic mechanism and thereby removing the selective pressure for this response.

Methods of oncogenic resistance are illustrated in figure 7.1 and in the context of paclitaxel resistance in figure 7.2. Oncogenic resistance is where signalling pathways that manage cell growth and proliferation are disrupted in a way that can increase cell cycling as opposed to growth inhibition for example when suppression of apoptosis occurs via the activation of oncogenes.

It is important to consider that some mechanisms of resistance can be nonspecific such as overexpression of p-gyp/mdr1 while others are specific for example tubulin modification, altered expression of tubulin isotypes and post translational modifications of [246,251,244,285-287]. Additionally it is important to consider that one component of molecular pathways may affect resistance in more than one way, for example the p53 regulated protein stathmin (MAP4.[246]). Overexpression of stathmin decreased microtubule polymerisation and hence binding of paclitaxel and cells that over expressed stathmin were also found to be more likely to enter G2 but less likely to enter M phase than cells that did not overexpress it[246]. It is also notable to consider that resistance is not always mechanistically "on or off"; resistance levels are effectively on a scale that must always be considered in the context of other cell lines or tissues that they may be compared with.

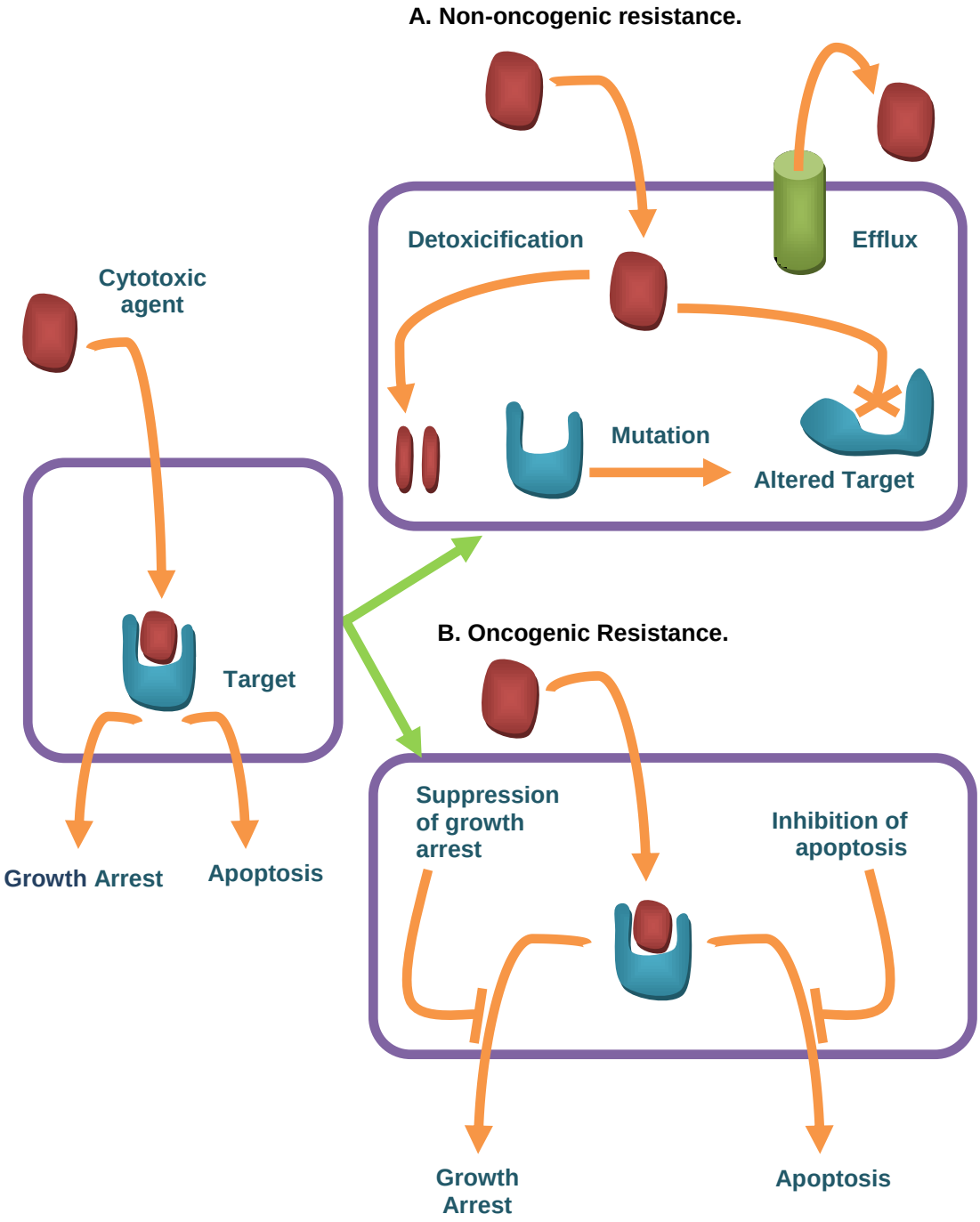


**Figure 7.1**.Reproduced and adapted from Blagosklonny[282]. 2 mechanisms of resistance: non oncogenic or oncogenic. Oncogenic mechanisms: Expression of a pump, detoxicification of an agent, mutation or amplification of a target can render a cell resistant to cytotoxic or cytostatic agents, without leading to cancer, this may even prevent cancer in some circumstances – e.g. pumping a DNA damaging agent out of a cell. Oncogenic resistance: When the activation of pathways of cell proliferation and suppression of apoptosis (alteration of tumour suppressors/oncogenes) confers resistance to the growth inhibitory carcinogenic environment, this eventually leads to uncontrolled malignant growth.

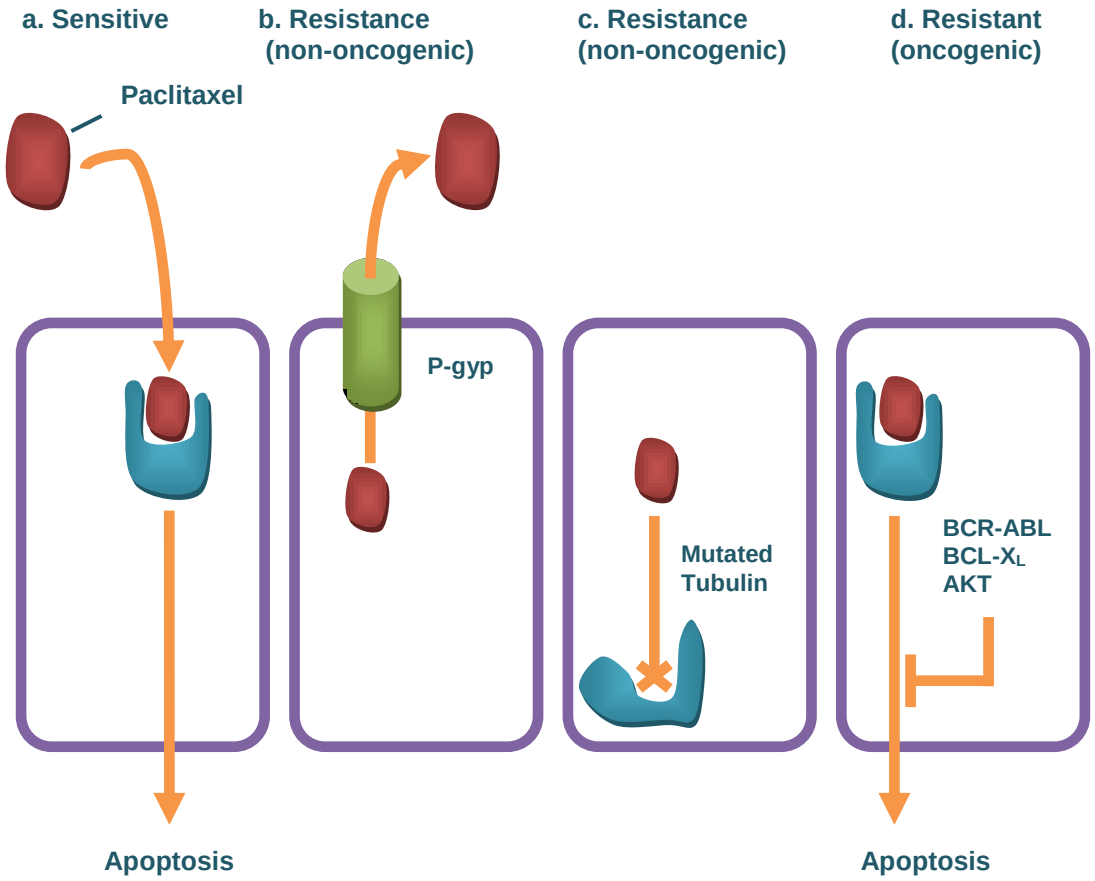


**Figure 7.2**. Reproduced and adapted from Balgosklonny[282]. Development of non-oncogenic or oncogenic resistance to an antimicrotubule agent – Paclitaxel **a**. Paclitaxel binds microtubules and arrests cell in mitosis, causing apoptosis. **b.** Expression of p-gyp/mdr1 which pumps paclitaxel out of the cell, prevents interaction of the drug with its target (non-oncogenic resistance) **c.** Mutation of tubulin prevents interaction of the drug with its target (non-onogenic.) **d.** Suppression of apoptosis by activation of activation (for examples, by formation of the fusion proteins BCR-ABL, or overexpression of AKT or BCL-XL) although Paclitaxel binds microtubules and causes mitotic arrest, apoptosis does not occur (oncogenic resistance.)

The paradigm of drug resistance is complex and can evolve constantly. Resistance to the taxanes is proving to be a considerable problem in the treatment of breast and other cancer types. By elucidating possible mechanisms of resistance it may be possible to gain a better understanding of how one might identify patients that will or will not respond to taxane based therapy and it may help pin point targets that can be used to reverse taxane resistance.

## 7.2 Characterisation of taxane resistant cell lines: Cell growth and the cell cycle.

To investigate potential mechanisms of taxane resistance taxane resistant cell line models were generated. Initially a panel of five cell lines was investigated: BT20, BT474, MDA-MB-231, MDA-MB-453 and ZR75-1. Cells were treated with either paclitaxel or docetaxel in low dose and gradually increased this dose in incremental steps.

Two of the panel of five cell lines went on to develop resistance to taxanes, the MDA-MB-231 cell developed resistance to paclitaxel and the ZR75-1 cells developed resistance to paclitaxel and docetaxel. When the BT20, BT474 and MDA-MB-453 cells failed to become resistant to paclitaxel or docetaxel the initial dose was dropped to 0.5nM but the cells still failed to grow in the presence of the drug. It would be pertinent to consider in future studies why these cell lines failed to grow in the presence of paclitaxel or docetaxel, perhaps if the initial doses had been lowered further the experiment may have succeeded. Interestingly, BT20 cells transfected to overexpress the p53 regulated gene stathmin have shown to be resistant to paclitaxel unlike their parent cell lines[244]. In future work it would be valuable to look at the changes detected in the taxane resistance cell line and compare them to the cell lines that failed to generate resistance as well as to their parent cell line.

After consulting with a clinician it was established that the 25nM PACR cells were the most clinically relevant dose to investigate. A suboptimal dose of 5nM and a superoptimal dose of 100nM were included in the experiments and the native cells were included as a negative control.

In addition, the MDA-MB-231 cell line failed to become resistant to docetaxel. This may have been hindered by the fact that the initial literature searches indicated that docetaxel was roughly twice as potent as paclitaxel where as more recent searches suggested that difference in potency was in a range between two and four fold between the two taxanes[131]. Docetaxel has also been shown to target the S, G2 and M phase of the cell cycle where as paclitaxel affects the mitotic spindle in G2/M[161]. Docetaxel has been show to be highly effective against S phase cells in particular whilst the maximum resistance level on paclitaxel treatment is seen in cells in the initial part of S phase[162].

After successfully generating the taxane resistant cell lines, they were characterised in terms of their growth and cell cycle behaviour on treatment with taxanes. Both the MDA-MB-231 and the ZR75-1 native cell lines were more sensitive to docetaxel than paclitaxel which concurs with previous studies using other cell lines[165].

Initial experiments using the MDA-MB-231 cells were conducted using cell lines of four different resistance levels. The native cells were used as control cells and the 5nM PACR cells were used to investigate low level resistance. The 25nM PACR cells were the most clinically relevant, optimal dose on conducting a literature search and consulting with a clinician. Finally, the 100nM PACR MDA-MB-231 cells were included as a dose that went beyond the optimum. However, when the 100nM PACR cells were grown in culture in the presence of paclitaxel they actually grew better in the presence of the drug than in its absence. This aberrant behaviour is not seen in the clinic and as a consequence it was decided that these cells should be excluded from further study.

Although what appears to be a degree of taxane dependence that is seen in this cell line, is not seen in the clinic, it is seen in other cell lines[286]. The A549-T12 and A549-T24 adenocarcinoma human alveolar basal epithelial cell lines have been isolated and were established as being dependent on paclitaxel for normal growth[286]. A point mutation in α tubulin was identified in these cell lines α379 (Ser to Ser/Arg), however the mutant and wild type allele were both expressed in the cell lines. The region of the mutation on this site is close to the carboxy-terminus, which has been postulated as a binding site for the microtubule associated protein stathmin. These paclitaxel resistant cells have increased expression of stathmin.

As the 100nM PACR cells were excluded from this study, the 50nM PACR cells were used as an alternative as these cells did not exhibit the aberrant paclitaxel dependent behaviour and still provided a comparison that went beyond the optimal clinically relevant dose.

Other research groups have generated taxane resistant cell lines, using alternative methodologies and alternative cell lines. Dumontet *et al* used the MES-SA cell line derived from Sarcomatous elements of the uterine mixed mullerian tumour and exposed the cells to a single dose of 10nM paclitaxel for 7 days [288]. Surviving colonies were found in 12 of the 15 treated populations of cells and 9 of these 12 colonies had clones that retained the paclitaxel resistant phenotype after 2 months of propagation[288]. 4 of the 9 clones were mdr1 positive when measured using qPCR and exhibited a broad cross resistance to vinblastine, doxorubicin, and etoposide. The other 5 clones were mdr1 negative and exhibited cross resistance only to vinca alkaloids, which, like the taxanes, target the microtubule. This confirms that taxane resistance can occur by non-mdr1 mediated mechanisms. Ranganathan *et al* used prostate cancer cell lines and treated them with increasing doses of paclitaxel and found that cells that were selected and maintained at a dose of 10nM were 5 fold resistant to the drug via an mdr-1 independent mechanism[289]. However, Ranganathan *et al* did not look at a panel of different isogenically derived cell lines at a variety of doses.

To develop these taxane resistant cells as xenografts in mice the resistant cells were first grown in the absence of drug long term *in vitro* and then re-challenge the cells with drug. The 25nM PACR cells retained their paclitaxel resistant phenotype after long term growth in the absence of drug.

The same four taxane doses were used for the ZR75-1 PACR and DOCR cells; native, 5nM, 25nM and 50nM. It was established that the ZR75-1 cells were more resistant to both taxanes than the MDA-MB-231 cells and the ZR75-1 native cells were more sensitive to docetaxel than paclitaxel.

How the cell-cycle of the native and taxane resistant cell lines was affected when they were treated with taxane was investigated using flow cytometry cell cycle analysis. When the native MDA-MB-231 cells were treated with paclitaxel they underwent a G2/M block. This block was not seen when the 25nM PACR cells were treated with the same doses of paclitaxel. The same experiment was then conducted using the ZR75-1 Native, PACR and DOCR cells. Unfortunately, the data from the paclitaxel treated ZR75-1 PACR cells, and the docetaxel treated ZR75-1 native and DOCR cells could not be analysed. This may have been because the trypsin used in the Vindelov's protocol did not sufficiently separate the cell into the single cell suspension that is required for running the samples on the FACS Aria scanner. However, the ZR75-1 native paclitaxel treated cells were successfully analysed and at the two highest doses the drug caused a G2/M block. The G2/M block in the ZR75-1 native cells was exerted at higher doses: 25 and 50nM paclitaxel than in the MDA-MB-31 native cells where the G2/M block is first observed at the 10nM Paclitaxel dose. This reiterates what was previously found in the cell count experiments that the ZR75-1 native cells were less sensitive to paclitaxel than the MDA-MB-231 native cells.

Previous studies have shown that docetaxel and paclitaxel affect different stages of the cell cycle with paclitaxel only targeting G2/M whilst Docetaxel targets both S phase and G2/M[131]. Furthermore, individually, the taxanes can exert a dual mechanistic effect on the cell cycle depending on what concentration of drug is used; causing the cells to exit mitosis in more than one way[131]

One study by Hernández-Vargas used synchronised cells and then subjected them to low (2-4nM) or high (100nM) concentrations of docetaxel. The low dose treatment caused a transient arrest and the high dose cause a prolonged arrest in mitosis. The short arrest leads to an aberrant mitosis and aneuploidy whereas the long arrest leads to mitotic slippage and tetraploidy[290].

A dual mechanism of cell cycle response has also been seen with paclitaxel treatment[291]. Low doses of paclitaxel have been shown to inhibit or retard the progression of mitosis and as a consequence alter microtubule dynamics rather than actually increasing polymer mass [292,293]. At higher concentrations of paclitaxel cells become blocked in G2/M phase so that they cannot progress through mitosis. These cells go on to apoptose[291].

This study looked at A549 cell lines and noticed that at low concentrations (<9nM) of paclitaxel the cells undergo abnormal mitosis leading to growth of multinucleated cells. They also found that 15% of the multinucleated cells went on to die after 24Hrs. The mechanism by which this small proportion of cells went on to die was established as being independent of Raf-1[291]. The A59 cells were also treated with high doses of paclitaxel (≥9nM). These cells were blocked in G2/M phase which lead to cell death by a Raf-1 dependent mechanism. Comparing data from different studies using different cell lines and different doses can prove difficult as doses are deemed low or high relative to how sensitive or resistant the individual line is.

The mechanisms of action and targeting of different stages of the cell cycle is dependent upon which cell line is being studied, which taxane is being used and at what dose.

A panel of isogenic taxane resistant cell lines have been successfully generated. It has been shown that the native lines exhibited cell cycle responses in the presence of taxane that concur with published data. Finally, it has been established that these resistant lines escape these cell cycle effects when treated with taxane.

An observation was made that not all of the cell lines became resistant to taxanes and the MD-MB-231 cell lines became resistant to paclitaxel and docetaxel. This suggests that there may be more than one mechanism of taxane resistance occurring in these cell lines.

### 7.3 Mouse xenografts

Experiments were designed to establish the taxane resistant cell lines as xenografts in mice. Although some controversy exists over the true value of xenografts established from cell lines, a number of studies have found them to be a valuable tool for developing a more clinically relevant model of resistance[294,295,219,220]. Although, ideally the most valuable xenograft experiments would use orthotopic xenografts of human tumour tissue from patients that were resistant to a taxane, these cell lines provided a useful and more readily available resource[294,295].

Previously, in the characterisation experiments it was established that that the MDA-MB-231 25nM PACR cells retained the paclitaxel resistant phenotype when grown long term in the

absence of drug. This allowed the xenograft experiments to proceed, with evidence to suggest that the taxane resistance phenotype may also be perpetuated in the absence of drug *in vivo*. Unfortunately, the MDA-MB-231 25nM PACR cells failed to grow as xenografts in mice even after repeated attempts and implanting the cells in 50% matrigel. One possible partial explanation for the failure of the MDA-MB-231 PACR cell lines to establish as xenografts was the increased expression of the cell surface protein TSPAN13. A consistent increase in expression with paclitaxel resistance was observed both in the expression array and qPCR experiments. Although it is important to remember that it may not be likely that the sole reason for the failure of the MDA-MB-231 PACR cells to form xenografts it would be valuable to investigate properties of anchorage, independent growth and invasion in both the native and 25nM PACR MDA-MB-231 cell lines.

A sensible strategy to investigate this would be to grow the cell lines in matrigel and conduct invasion and scratch wound assays. The qPCR data also showed an increase in oestrogen expression in the PACR MDA-MB-231 cell line (figure 5.28). Perhaps it may be worthwhile to observe whether growing the PACR MDA-MB-231 tumours in the presence of oestrogen, by implanting oestrogen pellets at the time of injection would allow the MDA-MB-231 PACR cell line to grow as xenografts. One other method the help establish the MDA-MB-231 25nM PACR cell lines as xenografts would be to attempt to inject cells into the mammary fat pads instead of the flank of the mouse.

As the 25nM PACR cell line failed to establish, the ZR75-1 Native, 25nM PACR and DOCR cell lines were used as an alternative. Due to the time pressure of the project, the experiment had to proceed with establishing the cell lines as xenografts without first growing them long-term *in vitro* in the absence of drug to observe whether the drug resistant phenotype was maintained. All three cell lines established well in 50% matrigel in xenografts and exhibited very similar and rapid patterns of growth to one another. As the ZR75-1 cell lines grew very rapidly, experiments were conducted to establish the appropriate number of cells to implant that would allow enough time for the tumours to grow at a reasonable rate to allow time to treat the tumours with taxane and conduct experiments.

The final experiment used all three cell lines: ZR75-1 Native, 25nM PACR and DOCR and conducted a cross resistance experiment treating each cell line xenograft with each treatment: blank drug vehicle control, paclitaxel and docetaxel. Twice the concentration of paclitaxel as docetaxel was used in these experiments to counteract the fact that docetaxel is roughly twice as potent as paclitaxel[131].

Resulting data from the cross resistance experiment was difficult to interpret because a number of problems were encountered in the experiment. Some animals died during the experiment, some animals were injected subcutaneously and the tumour measurements were not consistently measured by the same member of staff. Another concern is due to the fact that reports of the toxicity of docetaxel and paclitaxel vary. The experiments were restricted by a time pressure and ideally conducting a sister experiment *in vitro* would have been a useful exercise. In addition to this it would have been valuable to conduct the same experiment to check for reversion to the parent phenotype that was conducted in the MDA-MB-231 cells in the ZR75-1 cells as well. Finally it is appropriate to contemplate whether the tumours may still be growing too fast and whether we treated the animals at the correct time. Future experiment will require us to investigate and optimise the dosing schedule and period further.

However, bearing all these factors in mind it is possible to suggest some cautious conclusions from the xenograft experiments. They suggest the natives are sensitive to drug when in the xenograft environment. The DOCR xenografts appear to be resistant to docetaxel but not to paclitaxel which may imply that the PACR xenografts do not maintain their phenotype in vitro. In addition, tumour material was retained from each animal. Half of each tumour was kept in formalin for constructing microarrays for conducting future IHC or FISH analyses and the other half was kept frozen in liquid nitrogen for extraction of RNA, DNA or protein. Tumours will prove to be a useful resource for future experimentation.

In conclusion, isogenically derived PACR and DOCR breast cancer cell lines were developed along with their parental taxane sensitive lines and used them to successfully establish xenografts in mice. As far the author is aware this is the first time that taxane resistant mouse xenografts have been developed in this way. The author is satisfied that a successful model of taxane resistance has been developed and although there are some minor caveats, which have been described, it is believed that this model will allow worthwhile, and clinically relevant information on the mechanisms of taxane resistance to be gleaned. In addition, it was shown that the MDA-MB-231 PACR cell line is modified to the extent that, unlike the parental cell line, they do not grow *in vivo*. This is an intriguing result, some potential mechanisms have been suggested as to why this may have arisen and some potential experiments have been described that may be used to investigate this behaviour further.

Although there were some teething-problems treating the taxane resistant ZR75-1 cell lines with taxane in the cross-resistance experiments some positive indications were gained that certainly the DOCR and possibly the PACR cell lines maintained their taxane resistant phenotype *in vivo*. There may be some cross resistance in the PACR xenografts to docetaxel but it was confirmed that there was no cross-resistance of the DOCR xenografts to paclitaxel. In future

experiments the author aims to optimise and possibly extend the dosing schedule of taxane treatment to maximise the effect of the drug.

## 7.4 Profiling of taxane resistant cell lines

After an extensive characterisation a large genomic and transcriptomic study was conducted upon the cell lines.

A genomic analysis was performed using all eleven cell lines and aCGH. In the first set of experiments DNA from each of the cell lines was compared to DNA from pooled female blood and then in the second set of experiments DNA from each of the resistant lines was compared to DNA from their respective native lines. The following regions of loss extended as paclitaxel resistance increased in the MDA-MB-231 cell lines: 1p36.13-q44, 6p25.3-q12, 8p, 10p, 19q, and X Chr and these regions of gain extended as paclitaxel resistance increased: 2p25.3-23.3, 3p24.3-q13.3, 4p16.1-q12, 5q14.3-q31.1, 8q21.13-24.3, 11q15.1-q25, centromeric 12, and centromeric 14. There were three regions of deletion in the 50nM PACR cells alone: 2q13, 15q11,2 and 16 q11.2 and there were also ten regions of amplification in the MDA-MB-231 50nM PACR cells alone: 1q32.3, 4q21.21-21.22, 8p12, 8p11.21, 11q13.2, 12q14.1, 12q14.2, 12q15, 15q11.2 and 15q22.2-q22.3 In the ZR75-1 cell lines there were three regions of loss that extended with increasing taxane resistance in both the PACR and DOCR cells at all resistance levels: 7q, 12p and 16q.

The transcriptomic study began by extracting RNA from the MDA-MB-231, Native, 5nM, 25nM and 100nM PACR cell lines. The RNA was amplified and labelled and hybridised to Illumina arrays. Each of the PACR cell lines were then compared to the native line and established that there were 25, 225 and 425 genes dysregulated respectively. Eleven genes were identified that were commonly dysregulated among all three resistance levels: RGS16, CLDN1, IL7R, PPP1R14C, COBL, TRPV4, TSPAN8, CD33, NLRP2, PI3, and PAGE5. Each of these eleven genes was inputted into the KEGG pathway database and four of the eleven genes obtained a hit. CLDN1 was involved in the pathways of cell adhesion molecules and pathogenic *E. coli* infection. IL7R was involved in cytokine receptor interaction, haematopoietic cell lineage, Jak Stat signalling pathway and primary immunodeficiency. COBL was involved in porphyrin metabolism and metabolic pathways and CD33 was involved in haematopoietic cell lineage. From this it was concluded that there were no clear pathways common to each the eleven genes.

The same set of Illumina experiments was then conducted using the complete panel of eleven cell lines. This time MDA-MB-231 50nM PACR were used instead of the 100nM PACR cell line as it was already established that the 100nM PACR cells exhibited aberrant growth in the presence

of paclitaxel. In this set of experiments the data was analysed using R and constructed heat maps of gene expression were created which allowed us to establish that there was a distinct separation in patterns of gene expression in the three cell lines. The MDA-MD-231 samples clustered separately from the ZR75-1 cell lines according to ER status, the PACR and DOCR ZR75-1 clustered separately and the replicates for each cell line clustered together. The overlap between the cell lines at the highest taxane dose in the top 200 and top 500 gene was investigated. In the top 200 genes, 3 genes overlapped all three cell lines, 7 genes overlapped the MDA-MB-231 PACR and ZR75-11 PACR cell lines, 80 genes overlapped the ZR75-1 PACR and DOCR cell lines and reassuringly no genes overlapped the MDA-MB-231 PACR and ZR75-1 DOCR cell lines. In the top 500 genes, 33 genes overlapped all three cell lines, 17 genes overlapped the MDA-MB-231 and ZR75-1 PACR cell lines, 203 genes overlapped the ZR75-1 PACR and DOCR cell lines and 20 genes overlapped the MDA-MB-231 PACR and ZR75-1 DOCR cell lines. 1

In addition a group of 14 genes was identified that showed a consistent pattern of increasing or decreasing expression with increasing paclitaxel resistance: ALDH1A3, AMPH, CYP1B1, FBP1, FOXA2, FOXF2, ID2, ID3, IL11, MAL2, TGFBR3, TSPAN13, and SCNN1A.

Finally, a further four genes of interest were identified by conducting an extensive literature search in conjunction with the profiling experiments. Because a number of ATP binding cassettes family members have been shown to have increased expression in taxane resistant cells including ABCB1, ABCB4, ABCB11, ABCC2 and ABCC10[243] the author chose to investigate ABCB1 or Mdr1 in the context of the taxane resistant cell lines. Aurora Kinase A, a protein thought to be involved in MT formation and stabilisation, centrosome function and spindle assembly[243] was deemed to be an additional gene of interest and it was decided that this gene should be investigated further. Interestingly AURKA had increased expression only in the 100nM PACR cells. The third gene chosen for investigation was stathmin which has also been identified as being involved in the regulation of microtubules. Stathmin is often highly expressed in cell lines with mutant p53 and these cell lines have decreased binding of paclitaxel[147]. In addition RNA interference of stathmin has been shown to induce polymerisation of microtubules and resensitise paclitaxel resistant cells[246]. In these cell lines the resistant line had reduced gene expression compared to the native lines. Finally the transcription factor YY1 has been shown to play a role in taxane response in epithelial ovarian cancer[247]. Knockdown of YY1 resulted in increased taxane resistance which seemed to contradict the cell line data which showed increased YY1 expression at the highest resistance level in the MDA-MB-231 cells and increased expression of RYBP a protein that binds YY1 in all three paclitaxel resistant MDA-MB-231 cell lines compared to the native cells.

The aCGH was also used to help characterise the four genes discovered by conducting a literature search in conjunction with the transcriptomic experiments. Mdr-1 is located on 7q21.12 and in this region there are no distinct regions of loss or gain in any of the taxane resistant cell lines. Stathmin is located in the region of loss that extends with paclitaxel resistance in the MDA-MB-231 PACR which agrees with the transcriptomic data yet contradicts some published data[147,246]. AURKA is located in the region 20q13-13.2 that is gained only in the MDA-MB-231 100nM PACR cells which concurs with the data found in the transcriptomic experiment. YY1 is located at the telomeric region of chromosome 14 and the aCGH data shows that this region is neither lost nor gained in any of the taxane resistant cell lines.

This data was then verified this data using qPCR. The following genes showed a consistent pattern of decreased expression with increasing paclitaxel resistance: AURKA, FBP1, FOXF2, IL11, MAPK13, however these genes either showed very little deviation in expression compared to the native or had large errors. Another panel of genes showed a consistent pattern of increased expression with increasing paclitaxel resistance: ALDH1A3, AMPH, CCND2, CD33, ID2, ID3, MAL2, NLRP2, PPP1R14C, RGS16, TGFBR3, TSPAN8 and TSPAN13. This data showing the gene with increased expression in the taxane resistant cell lines all concurs with the data discovered using transcriptomic arrays. In the last part of this section ER expression was measured in all three cell lines and showed that although ER expression remains relatively constant in the ER+ve ZR75-1 PACR and DOCR cell lines with increasing taxane resistance. ER expression increases with increasing paclitaxel resistance in the MDA-MB-231 cell lines. ER expression was measured as previous studies have found that patients who are ER –ve have been shown to benefit more from taxane based chemotherapy than those who are ER +ve [296-299].

Finally, the protein levels of some of the genes obtained from the transcriptomic and genomic studies were ascertained using western blotting. A panel of common breast cancer biomarkers EGFR, HER2, HER3 and ERα were investigated. Mdr-1, Aurora Kinase A, Stathmin and YY1 protein expression was also investigated in the same panel of 11 cell lines. The MD-MB-231 showed no MDR-1 expression but the all taxane resistant ZR75-1 cell lines showed increased expression of Mdr-1 protein compared to their native line. The expression of YY1 is increased in all three paclitaxel resistant MDA-MB-231 compared to the native line. This suggests that increase YY1 expression may be a biomarker of taxane resistance and that the ZR75-1 cell lines are multidrug resistant.

In conclusion, it was shown that differing changes in patterns of gene expression in the MDA-MB-231 PACR and the ZR75-1 PAC and DOCR resistant lines. A panel of potential markers of taxane resistance and commonly dysregulated genes and pathways were identified.

## 7.5 LAPATAX

9 pairs matched of pre and post treatment samples were received from the dose escalation phase of the LAPATAX trial. A gene expression profile of these lines was conducted and analysed the resulting data and identified common functional pathways in the sample set. This data was then analysed in conjunction with the gene expression profile obtained from the taxane resistant cell line panel and identified two potential taxane resistance markers that were highly differentially expressed in the cell lines and showed increased expression in all nine paired LAPATAX samples following treatment with a taxane. DUSP1 and FOS were identified as two clinically relevant biomarkers. FOS is of particular interest because it has already be implicated in other mechanisms of drug resistance, namely in the development androgen independent prostate cancer[264-269]. Material from the phase II study of the LAPATAX would have been more valuable than that from the dose escalation phase, however it is important not to underestimate the value of the addition of any clinical material to a largely *in vitro* study.

## 7.6 Future Directions

A valuable and isogenically derived taxane resistant cell line model has been successfully developed. Their cell cycle response on treatment with taxanes in the Native and PACR MDA-MB-231 cell lines and the ZR75-1 native line has been established. In future experiments sister cell cycle analysis experiments using the ZR75-1 PACR and DOCR lines will be conducted.

The taxane resistant model was successfully brought into the *in vivo* setting using mouse xenografts, and the author believes that doing this, using these isogenically derived cell lines is an experimental first. It is important to investigate why the MDA-MB-231 cell lines failed to grown as xenograft tumours in mice by potentially knocking down TSPAN13 using shRNA. Knocking down of TSPAN13 using shRNA may potentially restore the phenotype that allows the native line to grow *in vivo*. The properties of anchorage, invasion and the metastatic potential of these lines will also be investigated using matrigel, invasion and scratch wound assays *in vitro*. Using a ZR75-1 native and taxane resistant cell lines the taxane dosing schedule could be optimised and hopefully extended to maximise the effect of the drug and clarify initial findings from the cross resistance experiment that showed that the DOCR and possibly the PACR cell lines maintained their taxane resistant phenotype.

The transcriptomic and genomic profiling of these cell lines has allowed commonly dyregulated pathways, genes and proteins in the taxane resistant model to be identified. This has allowed a panel of potential markers of resistance to be identified including the transcription factor YY1 in the MDA-MB-231 and mdr1 in the ZR75-1 cell lines. Rituximab has been shown to inhibit the activity of YY1 and perhaps could be tested *in vitro* to see if it exerts a reversion of the taxane resistant phenotype[300,321]. Methylation and proteomic arrays are available and it is hoped that

these cell line samples will be run on these arrays to help complete the "omic" profile of the lines and therefore establish a very comprehensive molecular picture of these cell lines. Mass spectrometry could also be employed to construct a protein screen of the cell line panel and the frozen tissue retained from the xenograft experiments. With advances in the efficiency and reduction in the cost of modern sequencing techniques it is pertinent to consider the possibility of sequencing regions of interest in the genomes of the panel of the taxane resistant cell lines in the future.

Using the gene expression models of taxane resistant cell lines in conjunction with data obtained from the LAPATAX trial two further potential and clinically verified markers were identified showing increased expression following treatment with taxane, namely DUSP1 and FOS, both of which are mechanistically linked via the MAPK pathway. In the future any further clinical material from other trials from patients treated with taxane will be sought to help extend the clinical relevance of this study. Larger study size and information on which patients responded to therapy would help confirm previous findings and elucidate other aspects of the previously established resistance mechanisms. If this type of material were to be made available the expression of the taxane resistance biomarkers in responders and non-responders could be investigated using FISH and IHC.

In future studies the author hopes to knock down some of these biomarkers of taxane resistance using shRNA to see if sensitivity can be restored in the cells lines. If successful it would also be interesting to see if this phenotype was retained when tumours from the shRNA knock down cells were grown as xenografts in mice. Initial shRNA candidates would be FOS and DUSP1 as these both have shown to have clinical relevance, in addition it would be pertinent to consider the group of eleven commonly dysregulated genes in the paclitaxel resistant MDA-MB0231 cell lines.

A literature search was conducted and identified potential inhibitors of both DUSP1 and FOS, including the quaternary benzo[c]phenanthridine alkaloids (QBA) sanguinarine and chelerythrine[300,301] were identified. In future studies this could be observe *in vitro* if these inhibitors could improve the activity of taxanes in the taxane resistant cell lines. Again, this experiment could be brought in to the *in vivo* experiments using the taxane resistant mouse xenografts and treating animals with a combination of taxane and DUSP/FOS inhibitor to see if they potentiate the action of taxanes.

A number of mechanisms of taxane resistance have already been established and described in the literature[319] including increased expression of efflux pumps and altered expression of mediators of taxane metabolism (CYP3A4), somatic mutations of β-tubulin and changes in β-

tubulin isotype expression, alterations in mediators of microtubules), [150, 233, 141,286], changes in mediators of the cell cycle (HER2, BRCA1 AKT and Aurora A) [304, 152, 153, 163, 302 ,159] and perturbation of apoptotic mechanisms (p53 Bcl-2 and thioredoxin) [133, 248, 303]. The work carried out in this study has identified novel biomarkers and pathways implicated in taxane resistance and the author believes that this has made a significant contribution to the understanding of this subject area.

Finally, a robust model of taxane resistance has been developed *in vitro* which has been characterised extensively. This model has been brought into an *in vivo* setting to better observe how the model may behave clinically and clinically relevant biomarkers of taxane resistance have been identified. Biomarkers of resistance and response are incredibly important for identifying patients that will benefit from a particular therapy and avoiding needlessly treating patients that are unlikely to respond. These biomarkers may be targeted by inhibitor therapies that could be utilised in combination with taxanes in the clinic to improve response rates. This concept of tailored therapy is a crucial paradigm in the struggle against breast cancer and improving patient survival.

# References


1. Sant M, Allemani C, Capoacaccia R, Hakulen T, Aareleid T, Coebergh JW, Coleman MP, Grosclaude P, Martinez P, Martinez C, Bell J, Youngson J, Berrino F and the Eurocare working group. Stage at diagnosis is a key explanation is of differences in breast cancer survival across Europe. International Journal of Cancer (2003.) 106: 416-422.
2. Austoker J, Bankhead C, Forbes JLJ, Atkins L, Martin F, Ross K, Wardle J and Ramirez AJ. Interventions to promote cancer awareness and early presentation: systematic review. British Journal of Cancer (2009.) 101:531-539.
3. Downing A, Prakash, K, Gilthorpe MS, Mikeljevic JS and Forman D. Socioeconomic background in relation to stage at diagnosis, treatment and survival in women with breast cancer. British Journal of Cancer (2007.) 96:836-840.
4. Jack RH, Davis EA and Møller H. Breast cancer incidence, stage, treatment and survival in ethnic groups in South East England. British Journal of Cancer (2009.) 1:545-550.
5. Jørgensen KJ, Zahl PH, and Gøtzsche PC. Breast Cancer mortality in organised mammography screening in Denmark: comparative study. British Medical Journal (2010.) 340:1241-1246.
6. Wald NJ, Law MR, and Duffy SW. Breast cancer screening saves lives. British Medical Journal (2009.) 339:2922.
7. Toikkanen S, Pylkkanen L and Joensuu H. Invasive lobular carcinoma of the breast has better short- and long-term survival than invasive ductal carcinoma. British Journal of Cancer (1997.) 76: 1234-1240.
8. Kuukasjärvi T, Tanner M, Pennanen S, Karhu R, Kallioniemi OP, Isolat J. Genetic Changes in Intraductal Breast Cancer Detected by Comparative Genomic Hybridization. American Journal of Pathology (1997). 150: 1465-1471.
9. Lu YJ, Osin P, Lakhani SR, Di Palma S, Gusterson BA, and Shipley JM. Comparative Genomic Hybridization Analysis of Lobular Carcinoma in Situ and Atypical Lobular Hyperplasia and Potential Roles for Gains and Losses of Genetic Material in Breast Neoplasia. Cancer Research (1998) 58:4721-4727.
10. Buerger H, Simon R, Schäfer KL, Diallo R, Littmann R, Poremba C, van Diest PJ, Dockhorn-Dworniczak B, and Böcker W. Genetic relation of lobular carcinoma *in situ*, ductal carcinoma in situ, and associated invasive carcinoma of the breast. Molecular Pathology (2000.) 53:118-121.
11. Millikan R, Dressler L, Geradts J, and Graham M. The need for epidemiologic studies of in-situ carcinoma of the breast. Breast Cancer Research and Treatment. (1995) 35: 65-67.

12. Giordano SH and Hortobagi GN. Inflammatory breast cancer: clinical progress and the main problems that must be addressed. Breast Cancer Research (2003.) 5:284-288.
13. Schnitt SJ. Classification and prognosis of invasive breast cancer: from morphology to molecular taxonomy. Molecular Pathology (2010.) 23:S60-S64.
14. Weinburg RA. The Biology of Cancer (2007.) 14:588-591.
15. Novak C. A metastatic Switch. Nature Reviews Cancer (2008.) 8:248-249.
16. Malyuchik SS, and Kiyamova RG. Medullary Breast Carcinoma. Experimental Oncology (2008.) 30:96-101.
17. Giordano SH, and Hortobagyi GN. Inflammatory breast cancer: Clinical progress and the main problems that must be addressed. Breast Cancer Research (2003.) 5:284-288.
18. Reis-Filho JS, Milanzi F, Steele D, Savage K, Simpson PT, Nesland JM, Pereira EM, Lakhani SR, and Schmitt FC. Metaplastic breast carcinomas are basal like tumours. Histopathology (2006.) 49:10-21.
19. Marcus E. Paget's disease of the breast. Current treatment options in oncology (2004.) 5:153-160.
20. Sullivan T, Raad RA, Goldberg S, Assaad SI, Gadd M, Smith BL, Powell SN and Taghian AG. Tubular carcinoma of the breast: a retrospective analysis and review of the literature. Breast Cancer Research and Treatment (2005.) 93:199-205.
21. Murad TM, Swaid S, Pritchett P. Malignant and benign lesions of the breast. Human Pathology (1977.) 8:379-390.
22. Patel T, Moreno-Aspitia A, Hume C, Saurel C, Roy V, Perez E. A retrospective review of patients with adenoid cyctic breast cancer treated at Mayo clinic. Cancer Research (2009.) 69:24 Suppl.
23. Monroe AT, Feigenberg SJ, Mendenhall NP. Angiosarcoma after breast-conserving therapy. Cancer. (2003) 97:1832-1840.
24. Myerowitz RL, Pietruszka M, Barnes EL. Primary angiosarcoma of the breast. JAMA (1978.) 239:403.
25. Chen KT, Kirkegaard DD, Bocian JJ. Angiosarcoma of the breast. Cancer (1980.) 46:368–371.
26. Rosen PP. Sarcoma. Rosen's breast pathology. 2nd ed. New York, NY: Lippincott Williams & Wilkins (2001) 813–861.
27. Yap J, Chuba PJ, Thomas R, et al. Sarcoma as a second malignancy after treatment for breast cancer. Int J Radiat Oncol Biol Phys (2002) 52:1231–1237.
28. Cozen W, Bernstein L, Wang F, Press MF, Mack TM. The risk of angiosarcoma following primary breast cancer. Br J Cancer (1999) 81:532–536.
29. Billings SD, McKenney JK, Folpe AL, Hardacre MC, Weiss SW. Cutaneous angiosarcoma following breast-conserving surgery and radiation. Am J Surg Pathol (2004.) 28:781–788.

30. Kuten A, Sapir D, Cohen Y, Haim N, Borovik R, Robinson E. Post irradiation soft tissue sarcoma occurring in breast cancer patients: report of seven cases and results of combination chemotherapy. J Surg Oncol (1985.) 28:168–171.

31. Belkacémi Y, Bousquet G, Marsiglia H, et al. Phyllodes Tumor of the Breast. Int J Radiat Oncol Biol Phys (2007). 70: 492.

32. Tan, PH., et al. Phyllodes Tumors of the Breast The Role of Pathologic Parameters. Am J Clin Pathol (2005.) 123:529-540.

33. Kleer, CG, et al. Pathologic, Immunohistochemical, and Molecular Features of Benign and Malignant Phyllodes Tumors of the Breast. Mod Pathol (2001.)14:185-190

34. Muttarak, M, Lerttumnongtum, P, Somwangjaroen, A, Chaiwun, B, Phyllodes tumour of the breast. Biomed Imaging Interv J (2006) 2:e33

35. Liberman L, Bonaccio E, Hamele-Bena D, et al. Benign and malignant phyllodes tumours: mammographic and sonographic findings. Radiology (1996.)198:121-124.

36. Lifshitz OH, Whitman GJ, Sahin AA, et al. Radiologic-pathologic conferences of the University of Texas M.D. Anderson Cancer Center. Phyllodes tumor of the breast. AJR Am J Roentgenol (2003.) 180:332.

37. Bloom HJG, Richardson WW. Histological grading and prognosis in breast cancer A study of 1409 cases of which 359 have been followed for 15 years. British Journal of Cancer (1957.) 11:359-377.

38. Frkovic-Grazio S, Bracko M. Long term prognostic value of Nottingham histological grade and its components in early (pT1N0M0) breast carcinoma. Journal of Clinical Pathology (2002.) 55:88-92.

39. Galea MH, Blamey RW, Elston CH, Ellis IO. The Nottingham prognostic index in primary breast cancer. Breast Cancer Research and Treatment (1992.) 22:207-219.

40. Bentzon N, Düring M Bruun-Rasmussen B, Mouriden H, Kroman N. Prognostic eddect of estogen receptor status across age in primary breast cancer. International Journal of Cancer (2008.) 122:1089-1094.

41. Mohsin AK, Weiss H, Havighurst T, Clark GM, Berardo M, Roanh LD, T TV, Zho Q, Love RL, Allred DC. Progesterone receptor by immunohistochemistry and clinical outcome in breast cancer: a validation study. Modern Pathology (2004.) 17:1545-1554.

42. Early Breast Cancer Trialist's Collaborative group. Tamoxifen for early breast cancer: an overview of the randomised trials. The Lancet (1998) 351:1451-1467.

43.. Olayioye MA. Update on Her-2 as a target for cancer therapy intracellular signalling pathways of ErB2/HER-2 and family members. Breast Cancer Research (2001.) 3:385-389.

44. Slamon DJ et al. Clark GM, Wong SG, Levin WJ, Ullrich A, and McGuire WL. Human Breast Cancer: Correlation of relapse and survival with amplification of the HER2/neu oncogene. Science (1987.) 235:177-182.

45. Yerushalmi R, Woods R, Ravdin PM, and Hayes MH. Ki67 in Breast Cancer: prognostic and predictive potential. The Lancet (2010.) 11:174-183.

46. Harria L, Fritsche H, Mennel R, et al. American Society of Clnical Oncology 2007 update of recommendations for the use of tumour markers in breast cancer. Journal of Clinical Oncology (2007.) 25:5287-5312.

47. Lazo JS et al. Novel benzofuran inhibitors of human mitogen activated protein kinase phosphatase 1. Bioorganic and Medicinal Chemistry (2006.) 14:5643-5650.

48. Dent R, Trudeau M, Pritchard KI, Hanna WM, Kahn HK, Sawka CA, Lickley LA, Rawlinson E, Sun P Narod SA. Triple-Negative Breast Cancer: Clinical Features and Patterns of Recurrence. Clin Cancer Res (2007) 13:4429-4434.

48. Minn AJ, Gupta GP, Siegel PM et al. Genes that mediate breast cancer metastasis to lung. Nature (2005.) 436:518-24.

49. Rodriguez-Pinilla SM, Sarrio D, Honrado E, et al. Prognostic significance of basal-like phenotype and fascin expression in node-negative invasive breast carcinomas. Clin Cancer Res (2006.) 12:1533-1539.

50. Banerjee S, Reis-Filho JS, Ashley S et al. Basal-like breast carcinomas: clinical outcome and response to chemotherapy. J Clin Pathol (2006) 59:729-735.

51. McPherson K, Steel CM, Dixon JM. Breast cancer-epidemiology, risk factors, and genetics. BMJ (1994.) 309:1003-1006.

52. Brose MS, Rebbeck TR, Calzone KA, Stopfer JE, Nathanson BL. Cancer Risk Estimates for BRCA1 Mutation Carriers Identified in a Risk Evaluation Program. Weber Journal of the National Cancer Institute (2002.) 94:1365-1372.

53. Wang Y, Cortez D, Yazdi P, Neff N, Elledge SJ, and Qin J. BASC, a super complex of BRCA1-associated proteins involved in the recognition and repair of aberrant DNA structures. (2000) Genes Dev. 2000 14: 927-939.

54. Struewing JP, Abeliovich D, Peretz T, Avishai N, Kaback MM, Collins FS, Brody LC. The carrier frequency of the BRCA1 185delAG mutation is approximately 1 percent in Ashkenazi Jewish individuals. (1995) Nature Genetics. 11, 198-200.

55. Tonin P, Serova O, Lenoir G, Lynch H, Durocher F, Simard J, Morgan K, Narod S. BRCA1 mutations in Ashkenazi Jewish women (1995.) American Journal of Human Genetics. 57:189.

56. Howlett NG, Taniguchi T, Olson S, Cox B, Waisfisz Q, Die-Smulders C, Persky N, Grompe M, Joenje H, pals G, Ikeda H, Fox EA and D'Andrea AD. Biallelic inactivation of BRCA2 in Fanconi anemia. Science (2002.) 297:606-609.

57. Söderlund K, Skoog L, Fornander T and Askmalm MS. The BRCA1/BRCA2/Rad51 complex is a prognostic and predictive factor in early breast cancer. Radiotherapy and Oncology (2007.) 84:242–251.

58. Santibáñez-Koref, Birch JM, Harltey AL, Morris-Jones PH, Craft AW, Eden T, Crowther D, Kelsey AM, Harris M. p53 germline mutations in Li-Fraumeni. The Lancet (1991.) 338:1490-1491.

59. Eng C. Genetics of Cowden Syndrome: through the looking glass of oncology. International Journal of Oncology (1998.) 12:701-710.

60. Beral V, Bull D, Doll R, Peto R, Reeves G. Breast cancer and breastfeeding: collaborative reanalysis of individual data from 47 epidemiological studies in 30 countries, including 50 302 women with breast cancer and 96 973 women without the disease. The Lancet (2002) 360: 187-195.

61. Olson JS. Bathsheba's breast: women, cancer and history. Baltimore: the Johns Hopkins University Press. (2002.) 32–33. 62

62. Million Women Study Collaborators. Breast cancer and hormone-replacement therapy in the Million Women Study. The Lancet (2003.) 3629382:419-427.

63. Collaborative Group on Hormonal Factors in Breast Cancer Breast cancer and hormone replacement therapy: collaborative reanalysis of data from 51 epidemiological studies of 52 705 women with breast cancer and 108 411 women without breast cancer. The Lancet (1997.) 350:1047-1059.

64. Collaborative Group on Hormonal Factors in Breast Cancer. Breast cancer and hormonal contraceptives: collaborative reanalysis of individual data on 53 297 women with breast cancer and 100 239 women without breast cancer from 54 epidemiological studies. The Lancet (1996.). 347: 1713-1727.

65. Boyd NF, Martin LJ, Yaffe M, Minkin S. Mammographic density. Breast Cancer Research (2009.) 11:1-5.

66. Million Women Study Collaboration: Reeves GK, Pirie K, Beral V, Green J, Spencer E, and Bull D. Cancer incidence and mortality in relation to body mass index in the Million Women Study: cohort study. British Medical Journal (2007.). 335: 1134-1143.

67. Reeves GK, Pirie K, Beral V, Jane G, Spencer, Bull D. Cancer incidence and mortality in relation to body mass index in the million women study: a cohort study. British Medical Journal (2007). 335:1134-1144.

68. Million Women Study Collaborators: Allen NE, Beral V, Casabonne D, Wan Kan S , Reeves GK, Brown A, Green J. Moderate Alcohol Intake and Cancer Incidence in Women Journal of the National Cancer Institute (2009.). 101: 296-305.

69. Early Breast Cancer Trialists' Collaborative Group (EBCTCG.) Effects of radiotherapy and of differences in the extent of surgery for early breast cancer on local recurrence and 15-year survival: an overview of the randomised trials. The Lancet (2005.) 366:2087-2106.

70. Wong JS, Harris JR. Importance of local tumour control in breast cancer. The Lancet Oncology (2001.) 2:1-11.

71. Berveiller P, Mir O, Veyrie, Barranger E. The sentinel-node concept: a dramatic improvement in breast-cancer surgery. Lancet Oncology (2010.) 11:906.

72. Nelson LR and Bulun SE. Estogen production and action. J Am Acad Dermatol (2007). 45:s116-S124.

73. Jensen EV and Jacobsen HO. Basic Guides to the mechanism of estogen action Rev Prog Horm Res (1962.). 18:387-414.

74. Nilsson S, Mäkelä S, Treuter E, Tujague M, Thomsen J, Andersson G, Enmark E, Pettersson K, Warner M, Gustafsson JA. Mechanisms of oestrogen action Physiol Rev (2001.) 81:1535-65.

75. Pilarsky C, Wenzig M, Specht T, Saeger HD and Grütsmann R. Identification and Validation of Commonly Overexpressed Genes in Solid Tumours by Comparison of Microarray Data. Neoplasia (2004). 6:744-750.

76. Millour J, Constantinidou D, Stravopoulou AV, Wilson MSC, Myatt SS, Kwok JM-M, Sivanandan K, Coombes RC, Medema RH, Hartman J, Lykkesfeldt AE and Lam EW-F. FOXM1 is a transcriptional target of ER and has a critical role in breast cancer endocrine sensitivity and resistance. Oncogene (2010). 29: 2083:2995.

77. van Leeuwen FE, Klokman WJ, Stovall M, Dahler EC, van't Veer MB, Noordijk EM, Crommelin Ma, Aleman BMP, Broeks A, Gospodarowicz M, Travis LB, Russel NS. Roles of radiation dose, chemotherapy, and hormonal factors in breast cancer following Hodgkin's disease. Journal of the National Cancer Institute (2003.). 95:971-980.

78. Buchanan, R.B., Blamey, R.W., Durrant, K.R. & 6 others. A randomised comparison of tamoxifen with surgical oophorectomy in premenopausal patients with advanced breast cancer. J. Clin. Oncol (1986,) 4:1326–1330.

79. Fugh-Berman A, Epstein S. Tamoxifen: disease prevention or disease substitution? Lancet (1992.) 340:1143–11455

80. Jordan VC, editor. Long-term tamoxifen treatment for breast cancer. Madison (WI): University of Wisconsin Press (1994.) 289.

81. van Leeuwen FE, van den Belt-Dusebout AW, van Leeuwen FE, Benraadt J, Diepenhorst FW, van Tinteren H, Coebergh JWW, K1iemeney LALM, Gimbrère F, Otter R, Schouten LJ, Damhuis RAM, Benraadt M, Bontenbal M. Risk of endometrial cancer after tamoxifen treatment of breast cancer. The Lancet (1994.) 343:448-452.

82. Knabbe C, Lippman ME, Wakefield LM. *et al*. Evidence that TGF-β is a hormonally regulated negative growth factor in human breast cancer cells. Cell (1987.) 48:417–428.

83. Butta A, MacLennan K, Flanders KC. et al. Induction of transforming growth factor β1 in human breast cancer in vivo following tamoxifen treatment. Cancer Res. (1992) 52:4261-4264.

84. Nolvadex Adjuvant Trial Organization. Controlled trial of tamoxifen as a single adjuvant agent in the management of early breast cancer. Br J Cancer. (1988.) 57:608–611.

85. Early Breast Cancer Trialists' Collaborative Group (EBCTCG). Effects of chemotherapy and hormonal therapy for early breast cancer on recurrence and 15-year survival: an overview of the randomised trials. The Lancet (2005). 365: 1687-1717.

86. Vogel, Victor; Joseph Constantino, Lawrence Wickerman et al.. Effects of Tamoxifen vs. Raloxifene on the Risk of Developing Invasive Breast Cancer and Other Disease Outcomes". The Journal of the American Medical Association (2006.) 295: 2727–2741.

87. The Arimidex Tamoxifen, Alone or in Combination (ATAC) Trialists' Group Effect of anastrozole and tamoxifen as adjuvant treatment for early-stage breast cancer: 100-month analysis of the ATAC trial. The Lancet Oncology (2008) 9:45-53.

88. Crivellari D, Sun Z, Coates SA, Price KN, Thürlimann B, Mouridsen H, Mauriac L, Forbes JF, Paridaens RJ, Castiglione-Gertsch M, Gelber RD, Colleoni M, Láng I, Del Mastro L, Gladieff L, Rabaglio M, Smith IE, Chirgwin JH, and Goldhirsch A. Letrozole Compared with Tamoxifen for Elderly Patients with Endocrine Responsive Early Breast Cancer: The BIG 1-98 Trial Journal of Clinical Oncology (2008.) 26:1972-1979.

89. Coombes RC, Kilburn LS, Snowdon CF, Paridaens R, Coleman RE, Jones SE, Jassem J, Van de Velde CJH, Delozier T, Alvarez I, Del Mastro L, Ortmann O, Diedrich K, Coates AS, Bajetta A, Holmberg SB, Dodwell D, Mickiewicz E, Andersen J, Lønning PE, et al. Survival and safety of exemestane versus tamoxifen after 2–3 years' tamoxifen treatment (Intergroup Exemestane Study): a randomised controlled trial The Lancet (2007.). 369:559-570.

90. Goss PE, Ingle JN, Pater JL, Martino S, Robert NJ, Muss HB, Piccart MJ, Castiglione M, Shepherd LE, Pritchard KI, Livingston RB, Davidson NE, Norton L, Perez EA, Abrams JS, Cameron DA, Palmer MJ, and Tu D. Late Extended Adjuvant Treatment With Letrozole Improves Outcome in Women With Early-Stage Breast Cancer Who Complete 5 Years of Tamoxifen Journal of Clinical Oncology (2008.). 26:1948-1955.

91. Howell A and the attack trialist's group. Results of the ATAC (Arimidex, Tamoxifen, Alone or in Combination) trial after completion of 5 years' adjuvant Treatment for breast cancer. The Lancet (2005) 365:60-62,

92. Rejnmark L, Vestergaard P, Mosekilde L. Statin but not nonstatin lipid-lowering drugs decrease fracture risk: a nationwide case-control study. Calcif Tissue Int (2006) 79:27–36.

93. Ewer M, Glück, and S. "A woman's heart: the impact of adjuvant endocrine therapy on cardiovascular health". Cancer (2009) 115:1813–1826.

94. Lehrer, S). "Statin use to prevent aromatase inhibitor-induced fracture and cardiovascular complications". Medical hypotheses (2007) 68:1417.

95. Goel S, Sharma R, Hamilton A, Beith J.LHRH agonists for adjuvant therapy of early breast cancer in premenopausal women (Review.) Cochrane Database of Systematic Reviews (2009), 4:1-33.

96. Valabrega G, Montemurro F, Aglietta M. Trastuzumab: mechanism of action, resistance and future perspectives in HER2-overexpressing breast cancer. Ann Oncol (2007.) 18: 977–84.

97. Cho HS, Mason K, Ramyar KX, et al. Structure of the extracellular region of HER2 alone and in complex with the Herceptin Fab. Nature (2003) 421: 756–60.

98. Metro G, Mottolese M, Fabi A. HER-2-positive metastatic breast cancer: Trastuzumab and beyond. Expert Opin Pharmacother (2008.) 9: 2583–601.

99. Ménard S, Pupa S,M, Campiglio M, Tagliabue E. Biologic and therapeutic role of HER2 in cancer. Oncogene (2003.) 22:657-6578.

100. Kerbel RS, Viloria-Petit, Rak K J. "Accidental" antiangiogenic drugs: anti-oncogene directed signal transduction inhibitors and conventional chemotherapeutic agents as examples. European Journal of Cancer (2000.) 36: 1248-1257.

101. Picart-Gebhart MJ, Procter M, Leyland-Jones B, Goldhirsch A, Untuch M, Smith I, Gianni L, Baselga J, Bell R, Jackisch C, Cameron D, Dowsett M, Barrios CH, Steger G, Huang C-S, Andersson M, Inbar M, Lichinitser M, Láng I, Nitz U, Iwata H, Thomssen C, Lohrisch C, Suter TM, Rüschoff J, Sütő T, Greatorex V, Ward C, Straehle C, MdFadden E, Dolci S, Gelber RD for the Herceptin Adjuvant (HERA) trial study team. Trastuzumab after adjuvant chemotherapy in HER2-positive breast cancer. The New England Journal of Medicine (2005.) 353:1659-1672.

102. Baselga J, Perez EA, Pienkowski T, Bell R. Adjuvant trastuzumab: a milestone in the treatment of HER-2 positive early breast cancer. The Oncologist (2006.) 11:4-12.

103. Joy AA, Mackey JR. Adjuvant trastuzumab: progress, controversies and the steps ahead. Current Oncology (2006.) 13:8-13.

104. Nahta R and Esteva FJ. HER-2 target therapy: lessons learned and future directions. Clinical Cancer Research (2003.) 9:5078-5084.

105. Marty M, Cognetti F, Maraninchi D et al. Randomised phase II trial of the efficacy and safety of trastuzumab combined with docetaxel in patients with human epidermal growth factor 2-positive metastatic breast cancer administered as first line treatment: the M77001 study group. Journal of Clinical Oncology (2005.)23:4265-4374.

106. Osoba D, Slamon DJ, Burchmore M et al. Effects on quality of life combined trastuzumab and chemotherapy in women with metastatic breast cancer. Journal of Clinical Oncology (2002.) 20:3106-3113.

107. Slamon DJ, Leyland-Jones B, Shak S et al. Use of chemotherapy plus a monoclonal antibody against HER2 for metastatic breast cancer that overexpresses HER2. New England Journal of Medicine (2001.) 344:783-792.

108. Nelson MH and Dolder CR. Lapatinib: A Novel Dual Tyrosine Kinase Inhibitor with Activity in Solid Tumors. Ann Pharmacother 40 (2):261-269, 2006.

109. Chow LQ, Eckhardt SG. Sunitinib: from rational design to clinical efficacy. Journal Clinical Oncology (2007.) 25:88-96.

110. Valachis A, Polyzos NP, Patsopoulos NA, Georgoulias V, Mavroudis D, Mauri D. Bevacizumab in metastatic breast cancer: a meta-analysis of randomized controlled trials. Breast Cancer Res Treat (2010) 122:1–7.

111. Ashworth A. A Synthetic Lethal therapeutic approach: Poly (ADP) Ribose Polymerase inhibitors for the treatment of Cancer deficient in DNA double stand break repair Journal of Clinical Oncology (2008). 26:3785-3790.

112. Tutt A, Robson M, Garber JE, Domchek SM, Audeh MW, Weitzel JN, Friedlander M, Arun B, Loman N, Schmutzler RK, Wardley A, Mitchell G, Earl H, Wickens M, Carmichael J. Oral poly(ADP-Ribose) polymerase inhibitor olaparib in patients with BRCA1 or BRCA2 mutations and advanced breast cancer: a proof of concept trial. The Lancet (2010.) 376:235-244.

113. Abe O, Abe R, Enomoto K, Kikuchi K, Koyama H, Masuda H et al for Early Breast Cancer Trialists' Collaborative Group (EBCTCG.) Effects of chemotherapy and hormonal therapy for early breast cancer on recurrence and 15 year survival: an overview of the randomised trials. The Lancet (2005.) 365: 1687-1717.

114. Abe O, Abe R, Enomoto K, Kikuchi K, Koyama H, Nomura, Y. Early Breast Cancer Trialists' Collaborative Group. Polychemotherpy for early breast cancer: an overview of the randomised trials. The Lancet (1998.) 352:930-942.

115. Munro AF, Cameron DA and Bartlett JMS. Targeting anthracyclines in early breast cancer: new candidate predictive biomarkers emerge. Oncogene (2010.) 29:5231-5240.

116. Smith LA, Cornelius VR, Plummer CJ, Levitt G, Verrill M, Canney P and Jones Alison. Cardiotoxicity of anthracycline agents for the treatment of cancer: Systematic review and meta-analysis of randomised controlled trials. BMC Cancer (2010.) 10:337-350.

117. Ellis P, Barrett Lee P, Johnson L, Cameron DA, Wardley A, O'Reilly S, Verill M, Smith I, Yarnol J, Coleman R, Earl H, Canney P, Twelves C, Poole C, Bloomfield D, Hopwood P, Johnston S, Dowsett M, Bartlett JMS, Ellis I, Peckitt C, Hall E, Bliss JM for the TACT trial management group and the TACT trialists. Sequential Docetaxel as adjucant Chemotherapy for Early Breast cancer (TACT): an open label, phase III, randomised controlled trial. The Lancet (2009.) 373:1681-1691.

118. Moinpour C, Wu J, Donaldson G, Liepa A, Melemed A, Oshaughnessy J, Rappold E, Albain K, Gemcitabine plus paclitaxel (GT) versus paclitaxel (T) as First-line treatment for anthracycline pre-treated metastatic breast cancer (MBC): Quality of life (QoL) and pain palliation results from the global phase III study. ASCO Meeting Abstracts (2004) 22 (14S).

119. Wani MC, Taylor HL, Wall ME, Coggon P, McPhail AT. Plant antitumor agents. VI. The isolation and structure of Taxol, a novel antileukaemic and antitumor agent from Taxus brevifolia. J Am Chem Soc. (1971) 93:2325-2327.

120. Gueritte F. General and recent aspects of the chemistry and structure activity relationships of taxoids. Current Pharmacological Design. (2001.) 7:1229-1249.

121. Nicolaou KC, Yang Z, Liu JJ, Ueno H, Nantermet PG, guy RK, Claiborne SF, Renaud J, Couladouros EA, Paulvannan K, Sorensen EJ. Total Synthesis of Taxol. Nature (1994.) 367:630-634.

122. Lee E-K, Jin Y-W, Park JH,Yoo YM, Hong SM, Amir R, Yan Z, Kwon E, Alfick A, Tomlinson S, Halbritter F, Waibel T, Yun BW, Loake GJ. Cultured cambial meristematic cells as a source of plant natural products. Nature Biotechnology (2010.) 28:1213-1217.

123. Fitzpatrick FA, Wheeler R. The immunopharmacology of paclitaxel (Taxol(R)), docetaxel (Taxotere(R)), and related agents, International Immunopharmacology (2003) 3:1699–1714.

124. Laurentiis M, Cancello G, D'Agostino D, Giuliano M, Giordano A, Montagna E, Lauria R, Forestieri V, Esposito A, Silvestro L, Pennacchio R, Criscitiello C, Montanino A, Limite G, Bianco AR, and De Placido S. Taxane-Based Combinations As Adjuvant Chemotherapy of Early Breast Cancer: A Meta-Analysis of Randomized Trials. J Clin Oncol (2008) 26:44-53.

125. Ring E, Taxanes in the treatment of early breast cancer, Cancer Treat Rev. 31 (2005.) 618–627.

126. Paridaens R, Biganzoli L, Bruning P, Klijn JGM, Gamucci T, Houston S, Coleman R, Schachter J, Van Vreckem A, Sylvester R, Awada A, Wildiers J, Piccart M, Paclitaxel versus doxorubicin as first-line single-agent chemotherapy for metastatic breast cancer: a *European Organization for Research and Treatment of Cancer Randomized Study. Journal of Clinical Oncology. (2000) 18: 724.*

127. Crown J, O'Leary M and Ooi WS. Docetaxel and Paclitaxel in the Treatment of Breast Cancer: A Review of Clinical Experience The Oncologist (2004.) 9:24-32.

128. Orr G.A, Verdoer-Pinard P. McDaid H, Horowitz SB, Mechanisms of Taxol resistance related to microtubule Oncogene (2003.), 22:7280-7295.

129. Kienitz A, Vogel C, Morales I, Muller R, and Bastians H. Partial downregulation of MAD1 causes regulation of MAD2 causes spindle checkpoint inactivation and anueploidy, but does not confer resistance towards Taxol. Oncogene. (2005) 24: 4301: 4310.

130. Kelling J Sullivan K Wilson L Jordan MA. Suppression of centromere dynamics by Taxol in living osteosarcoma cells. Cancer Research (2003) 63:2794-2801.

131. Gligorov J, Lotz JP. Preclinical pharmacology of the taxanes: implications of the differences. The Oncologist (2004) 9:3-8.

132. Nogales E. Structural Insights into microtubule function Annual review Of Biophysics and Biomolecular Structure (2001). 30: 397-420.

133. Zhao J. Kim J.E. Reed E and Li Q.Q. Molecular mechanism of Antitumour activity of taxanes in lung cancer (2005) International Journal of Oncology. 27: 247-256.

134. Muggia FM, Braly PS, Brady MF, Sutton G, Niemann T, Lentz S, Alvarez RD, Kucera PR, Small JM. Phase III randomised study of cisplatin versus paclitaxel versus cisplatin and paclitaxel in patients with suboptimal III or IV ovarian cancer: a gynaecologic oncology group study. Journal of Clinical Oncology (2000.) 18:106-115.

135. Kornblith P, Wells A, Garbin MJ, Piwowar J, Chattopadhyay A, George LD, Ochs RL, Burholt D. In vitro responses of ovarian cancers to platinums and taxanes. Anticancer Research (2003.) 23:543-548.

136. Kornblith P, Wells A, Gabrin MJ, Piwowar J, George LD, Ochs RL, Burholt D. Breast cancer – response rates to chemotherapeutic agents studied in vitro. Anticancer Research (2003.) 23:3405-3411.

137. Sève P, Mackey J, Isaac S, Tredan O, Souquet PJ, Perol M et al. Class III-β tubulin in tumour cells predicts response and outcome in patients with non-small cell lung cancer receiving paclitaxel. Molecular Cancer Therapeutics (2005.) 4:2002-2007.

138. Monzó M, Rosell R, Sánchez JJ, Lee JS, O'Brate A, González-Larriba JL, Alberola V, Lorenzo JC, Núñez L, Ro JY, Martín C. Paclitaxel Resistance in Non–Small-Cell Lung Cancer Associated With Beta-Tubulin Gene Mutations. Journal of Clinical Oncology (1999.) 17:1786-1793.

139. Gonzalez-Garay ML, Chang L, Blade K, Menick DR, Cabral F. A β-Tubulin Leucine Cluster Involved in Microtubule Assembly and Paclitaxel Resistance. Journal of Biological Chemistry (1999.) 274:23875-23882.

140. Giannakakou P, Sackett DL, Kang YK, Zhan Z, Buters JTM, Fojo T, Poruchynsky MZ. Paclitaxel-resistant Human Ovarian Cancer Cells Have Mutant β-Tubulins That Exhibit Impaired Paclitaxel-driven Polymerization Journal of Biological Chemistry(1997.) 272: 17118-17125

141. Kavallaris M, Kuo DY, Burkhart CA, Regl DL, Norris MD, Haber M, and Horwitz SB. Taxol-resistant epithelial ovarian tumours are associated with altered expression of specific beta-tubulin isotypes. Journal of Clinical Investigation (1997.). 100:1282-1293.

142. Blade K, Menick DR, Cabral F. Overexpression of class I, II or IVb beta-tubulin isotypes in CHO cells is insufficient to confer resistance to paclitaxel Journal of Cell Science (1999.). 112:2213-2221.

143. Wagner P, Wang B, Clark E, Lee H, Rouzier R, Pusztai L. Microtubule associated protein (MAP)-Tau: A Novel mediator of paclitaxel sensitivity in vitro and in vivo. Cell Cycle (2005) 4: 1149-1152.

144. Makrides V, Maisc MR, Feinstein SC, Lew J. Evidence for two distinct binding sites for tau on microtubules PNAS (2004.) 101:6746-6751.

145. Andre F, Hatzis C, Anderson K, Sotiriou C, Mazouni C, Meija J, Wang B, Hortobagi GN, Symmans WF, Pusztai L. Microtubule-associated protein-tau is a bifunctional predictor of endocrine sensitivity and chemotherapy resistance in oestrogen receptor – positive breast cancer. Clinical Cancer Research (2007.). 13:2061-2067.

146. Tutt A, Gillet C, Pinder S, A'Hern RA, Dowsett M, Ellis I, Bartlett JMS, Bliss J, Johnston S, Ellis P and the TACT trial trialists. Microtubules associated protein tau as a predictive and prognostic marker in a trial assessing sequential docetaxel as adjuvant chemotherapy for early breast cancer (TACT) Cancer Research (2009.) 69 (meeting abstract supplement):607.

147. Alli E, Yang JM, Ford JM, Hait WN. Reversal of stathmin-mediated resistance to paclitaxel and vinblastine in human breast carcinoma cells. Molecular Pharmacology (2007.) 71:1233-40.

148. Zhang CC, Yang J-M, White E, Murphy M, Levine A and Hair WN. The role of MAP4 expression in the sensitivity to paclitaxel and resistance to vinca alkaloid in mutant p53 cells (1998). Oncogene. 16: 1617-1624.

149. Ramachandra M, Ambudkar SV, Chen D, Hyrcyna Cam Dey S, Gottesman MN, Pastana I. Human P-glycoprotein exhibits reduced affinity for substrates during a catalytic transition state. Biochemistry (1998) 37: 5010-5019.

150. Alvarez M, Paull K, Monks A, Hose C, Lee JS, Weinstein J, Grever M, Bates S, Fojo T. Generation of a drug resistance profile by quantification of mdr-1/P-glycoprotein in the cell lines of the National Cancer Institute Anticancer Drug Screen Journal of Clinical Investigation (1995.) 95:2205-2214.

151. HY Yang, Dudoit S, Luu P, Lin DM, Peng V, Ngai J, Speed TP. Normalization for cDNA microarray data: a robust composite method addressing single and multiple slide systematic variation. Nucleic Acids Research (2002.) 30:1-10.

152. Tan M, Jing T, Lan K-H, Neal CL, Li P, Lee S, F D, Nagata Y, Liu J, Arlinghaus R et al. Phosphorylation of tyrosine-15 of p34 Cdc2 by ErbB2 inhibits p24Cdc2 acitvation and is involved in resistance to Taxol induced apoptosis. Molecular Cell (2002.) 9:993-1004.

153. Knuefermann C, Lu Y, Liu B, Jin W, Lian K, Wu L, Scmidt M, Mills GB, Medelsohn J, Fan Z. HER2/PI-3K/Akt activation leads to a multidrug resistance in human breast adenocarcinoma cells. Oncogene (2003.) 22:3205-3212.

154. Woods-Ignatoski K M, Maehama T, Markwart SM, Dixon JE, Livant DL Ethier SP. ERBB-2 overexpression confers PI-3 kinase-dependent invasion capacity on human mammary epithelial cells. British Journal of Cancer (2000.) 82: 666–674.

155. Poznak CV, Tan L, Panageas KS, Arroyo CD, Hudis C, Norton L, Seidman AD. Assessment of molecular markers of clinical sensitivity to single-agent taxane therapy for metastatic breast cancer. Journal of Clinical Oncology (2002.) 20:2319-2326.

156. McGorgan BT, Gilmartin B, Carney SN, McCann. Taxanes Microtubules and chemoresistant breast cancer. Biochemica et Biophysica Acta: Reviews on Cancer (2008.) 1785:96-132

157. Cahill DP, Lengauer C, Yu J, Riggins GJ, Wilson JK, Morkowitz SD, Kinzler KW, Vogelstein B. Mutations of the spindle assembly checkpoint genes in human cancers. Nature (1998.) 392:300-303.

158. Sudo T, Nitta M, Saya H, Ueono NT. Dependence of paclitaxel sensititvity on a functional spindle assembly checkpoint. Cancer Research (2004.) 64:2502-2508.

159. Anand S, Pnrhyn-Lowe S, Venkitaraman. Aurora-A amplification overrides the mitotic spindle assembly checkpoint, including resistance to Taxol. Cancer Cell (2003.) 3:51-62.

160. van Amerongen R and Berns A. TXR-mediated thrombospondin repression: a novel mechanism of resistance to taxane? Genes Dev (2006). 20: 1975-1981.

161. Haldar S, Basu A, Croce CM. Bcl-2 is the guardian of microtubule integrity. Cancer Research (1997.) 57:229-233.

162. Hennenquin C, Giocanti N, Facaudon V. S phase specificity of cell killing by docetaxel (Taxotere) in synchronised HeLa cells. Br J Cancer (1995) 71:1195-1198.

163. Mullan PB, Quinn JE, Gilmore PM, McWilliams S, Andrews H, Gervin C, McCabe N, McKenna S, White P, Song Y-H, Maheswaran S, Liu E, Haber DA, Johnstone PG, Harkin DP. BRCA1 and GADD45 mediated G2/M cell cycle arrest in resposne to antimicrotubule agents. Oncogene (2001.) 20:6123-6131.

164. Quinn JE, Kennedy RD, Mullan PB, Gilmore PM, Carty M, Johnston PG, Harkin P. BRCA1 functions as a differential modulator of chemotherapy-induced apoptosis. Cancer Research (2001) 63:6221-6228.

165. Pharaoh PD, Day NE, Caldas C: Somatic mutations in the p53 gene and prognosis in breast cancer: a meta-analysis. Br J Cancer (1999) 80:1968-1973.

166. De Cremoux P, Salomon AV, Liva S, Dendale R, Bouchind'homme B, Martin E, Sastre-Garau X, Magdelenat H, Fourquet A, Soussi T: p53 mutation as a genetic trait of typical medullary breast carcinoma. J Natl Cancer Inst (1999) , 91:641-643

167. Esteller M, Silva JM, Domingue G, Bonilla F, Matias-Guiu X, Lerma E, Bussaglia E, Prat J, Harkes IC, Repasky EA, Gabrielson E, Schutte M, Baylin SB, Herman JG: Promoter hypermethylation and BRCA1 inactivation in sporadic breast and ovarian tumours. J Natl Cancer Inst (2001), 92:564-569.

168. Kandioler-Eckersberger D, Ludwig C, Rudas M, Kappel S, Janschek E, Wenzel C, Schlagbauer-Wadl H, Mittlböck M, Gnant M, Steger G, and Jakesz R. TP53 Mutation and

p53 Overexpression for Prediction of Response to Neoadjuvant Treatment in Breast Cancer Patients. Clin Cancer Res (2000) 6:50-56.

169. Hawkins D, Demers G, Galloway DA, Inactivation of p53 enhances sensitivity to multiple chemotherapeutic agents. Cancer Research (1996.) 56:892-898.

170. Vikhanskaya F, Vignati S, Beccaglia P, Ottoboni C, Russo P, D'incaci M, Broggini M. Inactivation of p53 in a human ovarian cancer cell line increases the sensitivity to paclitaxel by inducing G2/M arrest and apoptosis. Experimental Cell Research (1998.) 241:96-101.

171. Woods CM, Zhu J, McQueeny PA, Bollag D, Lazarides E. Taxol induced mitotic block triggers rapid onset of a p53-independent apoptotic pathway. Molecular Medicine (1995.) 5:506-526.

172. Debernardis D, Sire EG, De Feudis P, Vikhanskaya F, Valenti M, Russo P, Parodi S, D'incalci M, Broggini M. p53 status does not affect sensitivity of human ovarian cancer cell lines to paclitaxel. Cancer Research (1997.) 57:870-874.

173. Zhang CC, Yang JM, White E, Murphy M, Levine A, Hait WN. The role of MAP4 expression in the sensitivity to paclitaxel and resistance to vinca alkaloids in p53 mutant cells. Oncogene (1998.) 16:1617-1624.

174. Murphy M, Hinman A, Levine AJ. Wild type p53 negatively regulates the expression of a microtubule associated protein. Genes and Development (1996.) 10:2971-2980.)

175. Wang TH, Wang HS, Soong YK. Paclitaxel induced cell death: where the cell cycle and apoptosis come together. Cancer (2000.) 88:2619-2628.

176. Strobel T, Kraeft S-K, Chen LB, Cannistra SA. Bax Expression is associated with enhance accumulation of paclitaxel: A novel role for BAX during chemotherapy-induced cell death. Cancer Research (1998.) 58:4776-4781.

177. Gualberto A, Aldape K, Kozakiewicz K, Tlsty TD. An oncogenic for of p53 confers a dominant, gain of function phenotype that disrupts spindle checkpoint control. PNAS (1998.) 95:5166-5171.

178. Hu L, Hofmann J, Lu Y, Mills GB, Jaffe RB. Experimental Therapeutics: Inhibition of Phosphatidylinositol 3' –Kinase increases efficacy of paclitaxel in in vitro and in vivo Ovarian Models. Cancer Research (2002.) 62:1087-1092.

179. Shingu T, Yamada K, Hara N, Moritake K, Osago H, Terashima M, Uemura T, Yamasaki T, Tsuchiya M. Experimental therapeutics: Synergistic augmentation of antimicrotubule agents-induced cytotoxicity by a phosphoinositide 3-Kinase inhibitor in human Malignant glioma cells. Cancer Research (2003.) 63:4044-4047.

180. Cheng JQ, Lindsley CW, Cheng GZ, Yang H, Nicosia SV. The Akt/PKB pathway: molecular target for cancer drug discovery. Oncogene (2005.) 24:7482-7492.

181. Rodi DJ, Janes RW, Sanganee HJ, Holton RA, Wallace BA, Makowski L. Screening of a library of phage displayed peptides identifies human Bcl-2 as a Taxol binding protein. Journal of Molecular Biology (1999.) 285:197-203.

182. Shitashige M, Toi M, Yano T, Shibata M, Matsuo Y, Shibaski F. Dissociation of Bax from a Bcl-2/Bax heterodimer triggered by phosphorylation of serine 70 of Bcl-2. Journal of Biochemistry (2001.) 130:741-748.

183. Ferlini C, Raspaglio G, Mozzetti S, Distefano M, Fillepetti F, Martinelli E, Ferrabdina G,Gallo D, Ranelletti FO, and Scambia G. Bcl-2 Down-Regulation Is a Novel Mechanism of Paclitaxel Resistance. Mol Pharmacol (2003.) 64:51–58.

184. Cortes JE, Pazdur R Docetaxel. J Clin Oncol (1995) 13:2643–2655.

185. Rowinsky EK, Donehower RC Paclitaxel (Taxol). N Engl J Med (1995.) 332:1004–1014.

186.. Markham M, Managing Taxane Toxicities. Supportive Cancer Care (2003). 11:144-147.

187. Francis P, Schneider J, Hann L, Balmaceda C, Barakat R, Phillips M, and Hakes T. Phase II trial of docetaxel in patients with platinum-refractory advanced ovarian cancer. J Clin Oncol (1994) 12:2301–2308

188. Piccart MJ, Gore M, ten Bokkel Huinink W, Van Oosterom A, Verweij J, Wanders J, Franklin H, Bayssas M, Kaye S Docetaxel: an active new drug for treatment of advanced epithelial ovarian cancer. J Natl Cancer Inst (1995) 87:676–681

189. Gianni L, Muzone E, Capri G et al. Paclitaxel by 3 hour infusion in combination with bolus doxorubicin in women with untreated breast cancer: high anti-tumour efficacy and cardiac effects in a dose finding and sequence finding study Journal of Clinical Oncology (1995.). 13:2688-2699.

190. Biganzoli L, Cufer T, Bruning P et al. Doxorubicin (A)/Taxol(T) versus doxorubicin/ cyclophophamise (C) as first line chemotherapy in metastatic breast cancer (MBC): a phase III study (2000.) Proceeding of the American Society of Clinical Oncology. 19:73.

191. Rowinsky EK. The taxanes: dosing and scheduling considerations. Oncology (Williston Park) (1997.) 11:7-19.

192. Slamon, D. J, Godolphin, W, Jones, L. A, Holt, J. A., Wong, S. G, Keith, D. E, Levin, W. J, Stuart, S. G, Udove, J, Ullrich, A, *et al*. Studies of the HER-2/neu proto-oncogene in human breast and ovarian cancer. Science (1989) 244, 707–712.

193. Borresen, A. L, Andersen, T. I, Eyfjord, J. E, Cornelis, R. S., Thorlacius, S, Borg, A, Johansson, U, Theillet, C, Scherneck, S & Hartman, S TP53 mutations and breast cancer prognosis: particularly poor survival rates for cases with mutations in the zinc-binding domains. Genes Chromosomes Cancer (1995) 14, 71–75.

194. Bergh, J, Norberg, T, Sjogren, S, Lindgren, A. & Holmberg, L. Nature Medicine (1995). 1, 1029–1034.

195. Foekens, J. A, Look, M. P, Bolt-de Vries, J, Meijer-van Gelder, M. E, van Putten, W. L & Klijn, J. G. Cathepsin-D in primary breast cancer: prognostic evaluation involving 2810 patients. Br. J. Cancer (1999) 79, 300–307.

196. Torregrosa, D, Bolufer, P, Lluch, A, Lopez, J. A, Barragan, E, Ruiz, A, Guillem, V, Munarriz, B & Garcia Conde, J Specific oncological contribution of cathepsin D and pS2 in human breast cancer: their relationship with TNM status, estradiol receptors, epidermal growth factor receptor and neu amplification. Clin. Chim. Acta (1997), 262, 99–119.

197. Vollenweider-Zerargui, L, Barrelet, L, Wong, Y, Lemarchand-Beraud, T. & Gomez, F. The predictive value of estrogen and progesterone receptors' concentrations on the clinical behaviour of breast cancer in women. Clinical correlation on 547 patients. Cancer (1986), 57, 1171–1180.

198. Perou CM, Sørlie T, Eisen MB, van de Rijn M, Jeffey SS Rees CA, Pollack JR, Ross DT, Johnsen H, Akslen et al. Nature (2000.) 406:747-752.

199. Neve RM, Chin K, Fridlyand J, Yeh J, Baehner FL, Fever T, Clark L, Bayani N, Coppe J-P, Tong, Speed T, Spellman PT, De Vries S, Lapuk A, Wang NK, Kuo W-L, Stilwell JL, Pinkel D, Albertson DG, Waldman FM, McCormick F, Dickson RB, Johnson MD, Lippman M, Ethier S, Gazdar A, Gray JW. A collection of breast cancer cell lines for the study of functionally distinct cancer subtypes. Cancer Cell (2006.) 10-515-527.

200. Sørlie T, Perou CM, Tibshirani R, Aas T, Geisler S, Johnsen H, Hastie T, Eisen MB, van de Rijn M, Jeffrey SS, Thorsen T, Quist H, Matese JC, Browm P, Botstein D, Lønning PE, and Børresen-Dale A-L Gene expression patterns of breast carcinomas distinguish tumor subclasses with clinical implications. PNAS (2001.) 98:10869-0874.

201. Sørlie T, Tibshirani, Parker J, Hastie T, Marron JS, Nobel A, Deng S, Johnsen h, Pesich R, Geisler S, Demeter J, Perou CM, Lønning PE, Brown PA, Børresen-Dale A-L, Botstein D. Repeated observation of breast tumour subtypes in independent gene expression data sets. PNAS (2003.) 100:8418-8423.

202. Sotiriou C, Neo AY, McShane LM, Korn EL, Long PM, Jazaeri A, Martiat P, Fox SB, Harris AL, Liu ET. Breast cancer classification and prognosis based on gene expression profiles from population-based study. PNAS (2003.) 100:10393-10398.

203. Eisen, M. B, Spellman, P. T., Brown, P. O. & Botstein, D. PNAS (1998) 95, 14863–14868.

204. Sørlie T, Tibshirani R, Parker J, Hastie T, Marron JS, Nobel A, Deng S, Johnsen H, Pesich R, Geisler S, Demeter J, Perou CM, Lønning PE, Brown PO, Børresen-Dale A-L, and Botstein D. Repeated observation of breast tumor subtypes in independent gene expression data sets PNAS (2003). 100, 8418-8423.

205. Potti Anil Dressman HK, Bild A, Riedel RF, Chan G, Sayer R, Cragun J, Cottril H, Kelley MJ, Petersen R et al. Nature Medicine (2006.) 12:1294-1300.

206. Charafe-Jauffret,E.; Ginestier,C.; Monville,F.; Finetti,P.; Adelaide,J.; Cervera,N.; Fekairi,S.; Xerri,L.; Jacquemier,J.; Birnbaum,D.; Bertucci,F. Gene expression profiling of breast cell lines identifies potential new basal markers. Oncogene (2006.). 25: 2273-2284

207. Vindelov et al. A detergent-trypsin method for the preparation of nuclei for flow cytometric DNA analysis. Cytometry (1983.) 3:5:323-327.

208. Fisher, E. R., Costantino, J., Fisher, B. & Redmond, C. Pathologic Findings from the National Surgical Adjuvant Breast Project (Protocol 4) Cancer (1993) 71, 2141–2150

209. Tan DSP, Lambros MBK, Natrajan R and Reis-Filho JS. Getting it right: designing microarray (and not 'microawry') comparative genomic hybridisation studies for cancer research. Laboratory Investigation (2007) 87, 737-754.

210. Bao P, Frutos A G, Greef C, Lahiri J, Muller U, Peterson T C. Warden L, Xie X. High-sensitiveity detection of DNA hybridisation on microarrays using resonance light scattering. Anal Chem (2002) 74:1792-1799.

211. Tang Y M, Wo Y Y, Stewart J. Hawkins A L, Griffin C A, Sutter T R, Greenlee W F. Isolation and characterisation of the human cytochrome p450 CYP1B1 gene. J Biol Chem (1996) 271: 28324-28534

212. Little SE, Vuononvirta R, Reis-Filho JS, Natarajan R, Iravani M, Fenwick K, Mackay A, Ashworth A , Pritchard-Jones K, Jones. Array CGH using whole genome amplification of fresh-frozen and formalin-fixed, paraffin-embedded tumor DNA Genomics (2006.) 87:298–306.

213. Marchi C, Iravani M, Natrajan R, Lambros MBK, Savage K, Tamber N, Fenwick K, Mackay A, Senetta R, Di Palma S, Schmitt FC, Bussolati G, Ellis IO, Ashworth A, Sapino A, and Reis-Filho JS. Genomic and immunophenotypical characterization of pure micropapillary carcinomas of the breast. Journal of Pathology (2008.). 215:398-410.

214. Cameron DA, Marreud S, Zaman K, Bodmer A, Pierga J, Brain E, Veyret C, Bartlett JM, Bogaerts J, Bonnefoi HR. LAPATAX: A randomised phase II trial of the FEC-docetaxel combined with lapatinib and/or trastuzumab as neoadjuvant therapy of HER2-positive breast cancer-EORTC 10054 trial. J Clinical Oncol (2010.) 28:15s (suppl;abstrTPS116.)

215. Bedard PL, Di Leo A and Piccart-Gebhart MJ. Taxanes: optimising adjuvant chemotherapy for early stage breast cancer. Nat. Rev. Clin. Oncol. (2010.) 7:22-3

216. Vaishampayan U, Parchment RE, Jasti BR, Hussain M. Taxanes: An overview of the pharmacokinetics and pharmacodynamics. Urology (1999.) 54 (Suppl 6A) 22-29.

217. Rowinsky EK and Donehower RC: Antimicrotubule agents, in Chabner BA, Longon DL eds: Cancer Chemotherapy and Biotherapy, 2nd ed, Philadelphia, Lippincott Raven Publishers (1996.) 263-296.

218. Mullen P. Flow cytometric DNA analysis of human cancer cell lines. Methods of Molecular Medicine (2004.) 88:247-255.

219. Steel GG, Courtenay VD, Peckham MJ. The response to chemotherapy of a variety of human tumour xenografts. British Journal of Cancer (1983.) 47:1-13.

220. Fiebig HH, Maler A, Burger AM. Clonogenic assay with established human tumour xenografts: correlation of *in vitro* to *in vivo* activity as a basis for anticancer drug discovery. European Journal of Cancer (2004.) 40:802-820.

221. Scholtz CC, Berger DP, Winerhalter BR, Henss H, Fiebig HH. Correlation of drug response in patients and in the clonogenic assay with solid human tumour xenografts. European Journal of Cancer (1990.) 26:901-905.

222. Mullen P. The use of matrigel to facilitate the establishment of human cancer cell-lines as xenografts. Methods of Molecular Medicine (2004.) 88:287-292

223. Huang H, Sossey-Alaoui K, Beachy SH, Geradts J. The tetraspanin superfamily member NET-6 is a new tumour suppressor gene. Journal Cancer Research Clinical Oncology (2007.) 133:761-769.

224. Forozan F, Mahlamäki EH, Monni O, Chen Y, Veldman R, Jiang Y, Gooden GC. Comparative Genomic Hybridisation analysis of 38 breast cancer cell lines: A basis for interpreting complementary DNA microarray data. Cancer Research (2000.) 60:4519-4525.

225. Burdall SE, Hanby AM, Landsdown MRJ, and Speirs V. Breast cancer cell lines friend or foe? Breast Cancer Research (2003.) 5:89-95.

226. Schultze J L and Eggle D, IlluminaGUI: Graphical User Interface for analyzing gene expression data generated on the Illumina platform (2007.) Bioinformatics 23: 1431-1433.

227. Miyoshi N, Ishii H, Sekimoto M, Doki Y, and Mori M. RGS16 Is a Marker for Prognosis in Colorectal Cancer. Annals of Surgical Oncology. (2009.) 16:3501-3514.

228. Liang G, Bansal G, Xie Z and Druey KM. RGS16 Inhibits Breast Cancer Cell Growth by Mitigating Phosphatidylinositol 3-Kinase Signalling. Journal of Biological Chemistry (2009). 284:21719-21727.

229. Wiechec E,Overgaard J,Hansen LL. A Fragile Site Within the HPC1 Region at 1q25.3 Affecting RGS16, RGSL1, and RGSL2 in Human Breast Carcinomas. Genes Chromosomes and Cancer (2008.) 47: 776-780.

230. Blanchard AA, Skliris GP, Watson PH, Murphy LC, Penner C, Tomes L,Young TL, Leygue E, Myal Y. Claudins 1, 3, and 4 protein expression in ER negative breast cancer correlates with markers of the basal phenotype Virchows Arch (2009.). 454:647-656.

231. Wenzel K, Daskalow K, Herse F, Seitz S, Zacharias U, Schenk JA, Schulz H, Hubner N, Michell B, Schlag PM, Osteziel KJ, Ozcelik, Scherneck S, Janrig. Biological Chemistry (2007.) 388:489-495.

232. Lucas B, Grigo K, Erdmann S, Lausen J, Kelin-Hitpass L and Ryffel GU. HNF4α reduces proliferation of kidney cells and affects genes deregulated in renal cell carcinoma. Oncogene (2005.). 24:6418-6413.

233. Jover R, Bort R, Gómez-Lechón M J, Castell J V. (2001) Hepatology Cytochrome p450 regulation by hepatocyte nuclear factor in human hepatocytes: A study using adenovirus mediated antisense targetting. Hepatology (2001.). 33:668-675.

234. Baker SD, Verweji K, Cusatis GA, van Schaik RH, Marsh S, Orwick SJ, Franke RM, Hui S, Schuetz EG, Lamba V, Messersmith WA, Wolff AC, Carducci MA and Sparrebroom A. Pharmacogenetic pathway analysis of docetaxel elimination. Clinical Pharmacology and Therapeutics (2009.) 85:155-163

235 Baker, S.D, Sparreboom, A. & Verweij, J. Clinical pharmacokinetics of docetaxel: recent developments. Clin. Pharmacokinet (2006). 45: 235–252.

236. Bruno, R. et al. Population pharmacokinetics/pharmacodynamics of docetaxel in phase II studies in patients with cancer. J. Clin. Oncol (1998). 16: 187–196.

237. Veyrat-Follet, C., Bruno, R., Olivares, R., Rhodes, G.R. & Chaikin, P. Clinical trial simulation of docetaxel in patients with cancer as a tool for dosage optimization. Clin. Pharmacol. Ther (2000.) 68: 677–687.

238. Marsh S Somlo G, Li X, Frankel P, King CR, Shannon WD, Mcleaod HL, Synold TW. Pharmacogenetic analysis of paclitaxel transport and metabolism genes in breast cancer. Pharmacologenomics J (2007.) 7:362-365.

239. Allesandri-Haber N, Dina OA, Joseph EK, Reichling DB, Levine JD. Interaction of transient receptor potential vanilloid 4, integrin, and SRC tyrosine kinase in mechanical hyperalgesia. J Neuroscience (2008) 28:1046-1057.

240. Garnache-Outtou F, Chaperot L, Biichle S, Ferrand C, Remy-Martin J-P, Deconinck E, Darode de Tailly P, Bulabois B, Poulet J, Kuhlein E, Jacob M-C, Salaun V, Aroch M, Drenou B, Schillinger F, Seilles E, Tiberghien P, Bensa J-C, Plumas J, Saas P. Expression of the myeloid-associated marker CD33 is not an exclusive factor for leukemic plasmacytoid dendritic cells. Blood (2005.) 105:1256-1264.

241. Petrilli V, Papin S and Tschopp J. The inflammasome. Curr Biol (2005). 15:581.

242. Zhang M, Zou Z, Maass N, Sager R. Differential expression of elafin in human normal mammary epithelial cells and carcinomas is regulated at the transcriptional level. Cancer Research (1995.) 55:2537-2541.

243. Fletcher JI, Haber M, Henderson MJ, and Norris MD. ABC transporters in cancer: more than just efflux pumps. Nature Reviews Cancer (2010.) 10:147-156.

244. Dumontet C Sikic BI. Mechanisms of action of and resistance to antitubulin agents: microtubule dynamics, drug transport, and cell death. Journal of Clinical Oncology (1999). 17:1061-1070.

245. Schinkel AH, Mayer U, Wagenaar E, Mol CA, Van Deemter L, Smit JJ, Van Der Valk MA, Voorouw AC, Spits H, Van Tellingen A, Zijlmans JM, Fibbe WE, dorst P. Normal viability and altered pharmacokinetics in mice lacking Mdr-1-Type (drug transporting) P glycoproteins. PNAS (1997.) 94:4028-4033.

246. Alli E, Bash-Babula J, Jang JM, and Hait WN. Effect of stathmin on the sensitivity to antimicrotubule drugs in human breast cancer. Cancer Research (2002.) 62:6894-6869.

247. Matsumara N, Huang Z, Baba T, Lee PS, Barnett JC, Mori, Chang JT, Kuo WL, Gusberg AH, Whitaker RS, Gray J, Fujii S, Berchuck A, Murphy SK. Ying Yang 1 modulates taxane response in epithelial ovarian cancer. Molecular Cancer Research (2009.) 7:210-220.

248. Tabuchi Y, Matsuoka J, Gunduz M, Imada T, Ono R, Ito M, Motoki T, Yamatsuki T, Shirakawa Y, Takaoka M, Haisa M, Tanaka N, Kurebayashi J, Jordan VC, Noamoto Y. Resistance to paclitaxel is related with Bcl-2 expression through an oestrogen receptor mediated pathway in breast cancer. Int J Oncol. (2009.) 34:313-9.

249. Miller WR. Identification and mechanisms of endocrine resistance. Breast Cancer Research (2008.) 10:519.

250. Hari Kishore A, Vedamurthy BM, Mantelingu K, Agrawal S, Ashok BA, Siddharta R, Rangappa KS, Tapas K. Specific small-molecule activator of Aurora Kinase A induces autophosphorylation in a cell-free system. Journal of Medicinal Chemistry (2008.) 51:792-797

251. Balachadran R, Welsh MJ, Day BW Altered levels and regulation of stathmin in paclitaxel-resistant ovarian cancer cells. Oncogene (2003) 22:8924-8930.

252. Kitchen R, Sabine VS, Sims AH, Macaskill EJ, Renshaw L, Thomas JS. Van Hemert JI, Dixon M. Bartlett JMS. Correcting for intra-experiment variation in illumina BeadChip data is necessary to generate robust gene-expression profiles. BMC Genomics (2010.) 11:134-147.

253. Usher VG, Tibshirani R, Chu G. Significance analysis of microarrays applied to the ionizing radiation response. PNAS (2001.) 98 5116-5121

254. Zang S, Guo R, et al. Integration of statistical interference methods and a novel control measure to improve sensitivity and specificity of data analysis in expression profiling studies. Journal of Biomedical Informatics (2007.) 40:552-560.

255. Zhang S. A comprehensive evaluation of SAM, the SAM R-package and a simple modification to improve its performance. BMC Bioinformatics (2007.) 8:230-241.

256. Huang DW Sherman BT, Lemoicki AR. Systematic and Integrative analysis of large gene lists using DAVID bioinformatics. Nature Protocols (2009.) 4:44-57.

257. Eferl R, Wagner EF. AP-1: A double-edged sword in tumourigenesis. Nature Reviews Cancer (2003.) 3:859-868

258. Angel P, Imagawa M, Chiu R, Stein B, Imbra RJ, Rahmsdorf HJ, Jonat C, Herrlich P, Karin M. Phorbol ester-inducible genes contain a common cis element recognised by a TPA-modulated trans-acting factor. Cell (1987.) 49: 729-739.

259. van Straaten F, Muller R, Curran T, VanBeveren C and Verma IM. Complete nucleotide sequence of a human c-onc gene: deduced amino acid sequence of the human c-fos protein. PNAS (1983.) 80:3183-3187.

260. Wang Z-Q, Grigoriadis AE, Möhle-Steinlein U, Wagner EF. A Novel Target cell for c-fos induced oncogenesis: development of chrondrogenic tumours in embryonic stem cell chimeras. EMBO J (1991) 10:2437-2450.

261. Grigoriadis A, Scellander K, Wang Z-Q, Wagner EF. Osteoblasts are target cells for transformation in c-fos transgenic mice. The Journal of Cell Biology (1993.) 122:685-701.

262. Reaichmann, E et al. Activation of an inducible c-FosER fusion protein causes loss of epithelial polarity and triggers epithelial-fribroblastoid cell conversion. Cell (1992) 71:1103-1116.

263. Saez E, et al. c-Fos is required for malignant progression of skin tumours. Cell (1995) 82:721-732.

264. Edwards J, Krishna NS, Mukherjee R, and JMS Bartlett. The role of c-Jun and c-Fos expression in androgen-independent prostate cancer. Journal of Pathology (2004.) 204:153-158.

265. Sato N, Sadar MD, Bruchovsky N, et al. Androgenic induction of prostate-specific antigen gene is repressed by protein-protein interaction between the androgen receptor and AP-1/c-Jun in the human prostate cancer cell line LNCaP. Journal of Biochemistry (1997.) 272:17,485-17,494.

266. Bubulya A, Chen SY, Fisher CJ, Zheng Z, Shen XQ, Shemshedini L. c-Jun potentiates the functional interaction between the amino and carboxyl termini of the androgen receptor. Journal of Biology Chemistry (2001.) 276:44,704–44,711.

267. Lubahn DB, Brown TR, Simental JA, et al. Sequence of the introns exon junctions of the coding region of the human androgen receptor gene and identification of a point mutation in a family with complete androgen insensitivity. Proc Nat Acad Sci USA (1989.) 86:9,534–9,538.

268. Behrens A, Jochum W, Sibilia M, Wagner EF. Oncogenic transformation by Ras and Fos is mediated by c-Jun N-terminal phosphorylation. Oncogene (2000) 19:2657–2663.

269. Shimada K, Nakamura M, Ishida E, Kishi M, Konishi N. Requirement of c-Jun for testosterone-induced sensitization to N -(4-hydroxyphenyl)retinamide-induced apoptosis. Mol Carcin (2003.) 36: 115–122.

270. Kurt RA, Urba WJ, Smith JW, Schoof DD. Peripheral D lymphocytes from women with breast cancer exhibit abnormal protein expression of several signalling molecules. Int, J, Cancer (1998.) 78:16-20.

271. Loda M, Capodiedci P, Mishra R, et al . Expression of mitogen-activated protein kinase phosphatase-1 in the early phases of human epithelial carcinogenesis. Am. J Pathol (1996.) 149:1553-64.

272. Small GW, Shi YY, Higgins LS, Orlowski RZ. Mitogen-activated protein kinase phosphatase-1 is a mediator of breast cancer chemoresistance. Cancer Research (2007.) 67:4459-4466.

273. Wu W, Pew T, Zou M, Pang D, Conzen SD. Glucocorticoid receptor-induced MAPK Phosphatase-1 (MPK-1) expression inhibits paclitaxel-associated MAPK activation and contributes to breast cancer cell survival. The Journal of Biological Chemistry (2005.) 280:4117-4124.

274. Wagner EF, Nebreda AR. Signal integration by JNK and p38 MAPK pathways in cancer development. Nature Reviews Cancer (2009). 9:537-549.

275. Bulavin DV, Fornace Jr AJ. P38 MAP kinase's emerging role as a tumour suppressor . Advances in Cancer Research (2004.) 92:95-118.

276. Dolado I, Nebreda AR. Regulation of tumourigenesis by p38α MAP Kinase. Topics in Current Genetics: Stress activated protein kinases (2010.) 20:99-128.

277. Hui L, Stepinak E, Wagner E. p38α: A suppressor of cell proliferation and tumourigenesis. Cell cycle (2007.) 6:2429-2433.

278. Moncho-Amor V, Ibañez de Cácerces I, Bandres E, Martínez-Poveda B, Orgaz JL, Sánchez-Pérez I, Zazo S, Rovira A, Albanel J, Jíminez B, Rojo F, Belda-Iniesta C, Garcia-Foncillas J, Perona R. DUSP1/MKP1 promotes angiogenesis, invasion and metastasis in non-small-cell-lung-carcinoma. Oncogene (2010) AOP, doi:10.1038.

279. Burris III HA. Dual Kinase inhibition in the treatment of breast cancer: initial experience with the EGFR/ErbB-2 inhibitor Lapatinib. The Oncologist (2004.) 9 (Suppl 3):10-15.

280. Hanahan D and Weinburg RA. The hallmarks of Cancer. Cell (1999) 100:57-70

281. Vogelstein B and Kinzier KW. The multistep nature of cancer. Trends in Genetics (1993) 9: 138-141.

282. Blagosklonny MV. Oncogenic resistance to growth limiting conditions. Nature Reviews Cancer (2002.) 2:221-225.

283. Amarante-Mendes GP et al. BCR-ABL, exerts its antiapoptotic effect against diverse apoptotic stimuli through blockage of mitochondrial release of cytochrome c and activation of caspase 3. Blood (1998.) 91:1700-1705.

284. Greenhalgh DA, Wang XJ, Donehower LA, Roop DR. Paradoxical tumour inhibitory effect of p53 loss in transgenic mice expressing epidermal targeted v-Hras or v-FOS or human transforming growth factor-α. Cancer Research (1996) 56:4413-4423.

285. Jordan MA Wilson L. Microtubules as a target for anticancer drugs. Nature Reviews Cancer (2004) 4:253-265.

286. Martello LA, Verdier-Pinard P, Shen HJ, He L, Torres K, Orr GA, Horowitz SB. Elevated tubulin levels of microtubule destabilising factors in a Taxol resistant/dependent A549 cell lines with an α-tubulin mutation. Cancer Research (2003.) 63:1207-1213.

287. Zhang CC, Yang JM, White E, Murphy M, Levine A, Hait WN. The role of MAP4 expression in the sensitivity to paclitaxel and resistance to vinca alkaloids in p53 mutant cells. Oncogene (1998) 16:1617-1624.

288. Dumontet C, Dran GE, Steger KA, Beketoc-Oreskovic L and Sikic B. Resistance mechanisms in human sarcoma mutants derived by single-step exposre to paclitaxel (Taxol.) Cancer Research (1996.) 56:1091-1097

289. Ranganathan S, Benetatos CA, Colarusso PJ, Dexter DW and Hudes GR. Altered β-tubulin isotype expression in paclitaxelresistant human prostate carcinoma cells. British Journal of Cancer (1998). 77:562-566.

290. Hernández-Vargas H, Palalcio J, Moreno-Bueno. Telling cells how to die: Docetaxel therapy in cancer cell lines. Cell cycle (2007.) 6:780-783.

291. Torres K, Horowitz S. Mechanisms of Taxol induced cell death are concentration dependent. Cancer Research (1998.) 58:3620-3626

292. Jordan MA, Toso, RJ, Thrower D, Wilson L. Mechanisms of Mitotic block and inhibition of cell proliferation by Taxol at low concentration. PNAS (1993.) 90:9552-9556.

293. Jordan MA, Wendel K, Gardiner S, Derry WB, Copp H and Wilson L. Mitotic block induced in HeLa cells by low concentrations of paclitaxel (Taxol) results in abnormal mitotic exit and apoptotic cell death. Cancer Research (1996.) 56:816-825.

294. Kerbel RS. Human tumour xenografts as predictive models for anticancer drug activity in humans: better than commonly perceived but they can be improved. Cancer Biological Therapy (2003.) 2:S134-139.

295. Richmond A Yingjun Su. Mouse xenograft models vs. GEM models for human cancer therapeutics. Disease Models and Mechanisms (2008.) 1:78-82.

296. Sui M, Ho Park B, Davidson NE, Fan W. Estrogen receptor α mediates breast cancer cell resistance to paclitaxel through inhibition of apoptotic cell death. Cancer Research (2007) 67:5337-5344.

297. Lippman ME, Allegra JC, Thompson EB et al. The relation between oestrogen receptors and response rate to cytotoxic chemotherapy in metastatic breast cancer. New England Journal of Medicine (1978.) 298:1223-1238.

298. Henderson IC, Berry DA, Demetri CD et al. Improved outcomes from adding sequential paclitaxel, but not from escalating doxorubicin doses, in an adjuvant chemotherapy regimen for patients with node positive breast cancer. Journal of Clinical Oncology (2003.) 21:976-983.

299. Razandi M, Pedram A Levin ER. Plasma membrane oestrogen receptors sifnal to antiapoptotic in breast cancer. Molecular Endocrinology (2000.) 14:1434-1437.

300. Jeffrey KL, Camps M, Rommel C, Mackay C. Targeting dual-specificity phosphatises: manipulating MAP kinase signalling and immune responses. Nature Reviews Drug Discovery (2007.) 6: 391-403.

301. Vogt, A et al. The benzo-phenanthridine alkaloid sanguinarine, is a selective, cell active inhibitor of mitogen activated protein kinase phosphatase 1. Journal of Biological Chemistry (2005.) 208:19078-19086.

302. Scharer CD, Laycock N, Osinkoya AO, Logani S, McDonald JF, Beningo B and Morena CS. Aurora Kinase inhibitors synergise with paclitaxel to induce apoptosis in ovarian cancer cells. Journal of Translation Medicine (2008.) 6:79-91. (

303. Moos PJ, Fitzpatrick FA. Taxanes propagate apoptosis vis two cell population with distinctive cytological and molecular traits. Cell growth and differentiation (1998.) 9:687-697,.

304. Yu D, Jing T, Yao J, Tan M, McDonnell TJ, Hung M-C.Overexpression of ErB2 blocks Taxol-induced apoptosis by upregulation of $p21^{Cip1}$ which inhibits $p34^{Cdc2}$ Kinase. Molecular Cell (1998.) 2:581-591

305. Poole CJ, Earl HM, Hiller L, Dunn JA, Bathers S, Grieve RJ, Spooner DA, Agrawal RK, Fernando IN, Brunt AM, O'Reilly SM, Crawford M, Rea DW, Simmonds P, Mansi JL, Stanley A, Harvey P, McAdam K, Foster L, Leonard RCF, and Twelves CJ for the NEAT Investigators and the SCTBG. Epirubicin and Cyclophosphamide, Methotrexate, and Fluorouracil as Adjuvant Therapy for Early Breast Cancer. N Engl J Med (2006) 355:1851-1862.

306. Elston, C. W. & Ellis, I. O. Pathological prognostic factors in breast cancer. I. The value of histological grade in breast cancer: experience from a large study with long-term follow-up. Histopathology (1991) 19, 403–410.

307. Lokich J, Anderson N. Paclitaxel hypersensitivity reactions; a case for docetaxel substitution. Annals of Oncology (1998.), 9:5;573.

308. Ferlay J, Shin HR, Bray F, Forman D, Mathers C and Parkin DM. GLOBOCAN 2009, Cancer Incidence and Mortality Worldwide: IARC Cancerase No 10 Lyon France: International Agency for Research on Cancer, (2010.).

309. Wenzel K, Daskalow K, Herse Florian, Seitz S, Zacharias Ute, SchenkJ A, Schulz H, 1, Hubner N, Micheel B, Schlag PM, Osterziel KJ, Ozcelik C, Scherneck S and Jandrig B. Expression of the protein phosphatase 1 inhibitor KEPI is downregulated in breast

cancer cell lines and tissues and involved in the regulation of the tumor suppressor EGR1 via the MEK-ERK pathway. Biol Chem (2007.). 388: 489-495.

310. Tham LS, Holford NHG, Hor S-Y, Tan T, Wang L, Lim R-C, Lee H-S, Lee S-C, and Goh B-C. Lack of Association of Single-Nucleotide Polymorphisms in Pregnane X Receptor, Hepatic Nuclear Factor 4α, and Constitutive Androstane Receptor with Docetaxel Pharmacokinetics. Clinical Cancer Research (2007.). 13: 7126-7132.
311. McCormack VA and dos Santos Silva I. Breast Density and Parenchymal Patterns as Markers of Breast Cancer Risk: A Meta-analysis. Cancer Epidemiol Biomarkers Prev (2006) 5:1159-1169.
312. Rumsey D. Statistics II for Dummies. (2009.)
313. Marsh S Paul Jm King CR, Gifforf G, McLeod HL, Brown R. Pharmacogenetic assessment of toxicity and outcome after platinum plus taxane chemotherapy in ovarian cancer: the Scottish randomised trial in ovarian cancer. J Clinical Oncology (2007.) 10:4528-4535.
314. Cahill DP, Kinzier KW, Vogelstein B and Lengauer C. Genetic instability and Darwinian selection in tumours. Trends Cell Biology (1999.) 9:M57-M60.
315. Duesberg P, Stindl R and Hehlmann R. Explaining the high mutation rates of cancer cells to drug and multidrug resistance by chromosome reassortments that are catalysed by aneuploidy PNAS (2000.) 97:14295-14300.
316. Judah DJ, Legg RF and Neal GE. Development of resistance to cytotoxicity during aflatoxin carcinogenesis. Nature (1977.) 265:343-345.
317. Evan GI, and Vousden KH. Proliferation, cell cycle and apoptosis in cancer. Nature (2001.) 411:342-348.
318. Matsumoto Y, Takano H and Fojo T. Cellular adaptation to drug exposure: evolution of the drug resistant phenontype. Cancer Research (1997.) 57: 5086- 5092.
319. Ringel I, Horowitz SB. Studies with RP 56976 (Taxotere). A new semisynthetic analogue of Taxol. Journal of the National Institute (1989.) 83:288-291.
320. Vega M I, Jazirehi AR, Huerta-Yepez S and Bonvida B. Rituxiamb induced inhibition of YY1 and Bcl-xL expression in Ramos non Hodgkin's lymphoma cell line via induction of NF-κB activity: role of YY1 and Bcl-xL in Fas resistance and chemoresistance respectively. The Journal of Immunology (2005.) 175:2174-2183.

# Websites


- www.breastcancerabout.com
- www.cancerhelp.org.uk
- www.cancer.org
- www.nice.org.uk
- www.gene.cards.org
- www.ihop-net.org
- www.genome.jp/kegg/
- www.mathworks.com
- www.millionwomenstudy.org
- www.pid.nci.nih.gov

# Attendance at Meetings.

- NCRI Birmingham 2008: Presented Abstract

- NCRI Birmingham 2009: Presented Abstract entitled "A transcriptomic and genomic investigation into taxane resistant breast cancer."
- In 2009 I was invited to present my data at a proffered paper session as part of the "high throughput sequencing and cancer genomes" parallel session. My presentation and poster garnered much interest and I was pleased to be given the opportunity to bring my work to a much wider audience. Subsequently I was awarded the NCRI BOA Pfizer Young Investigator prize for my abstract and poster.

- SABCS San Antonio 2009: Presented Abstract.

# Published Papers.

- M Spears, J Kenicer, A F Munro, JMS Bartlett. Type I receptor tyrosine kinases as predictive or prognostic markers in early breast cancer. Biomarkers in Medicine (2008.) 2: 397-407.